JOURNAL OF BIOLOGICAL REGULATORS & HOMEOSTATIC AGENTS
Volume 28, No. 2, April - June, 2014

CONTENTS

EDITORIAL

OBESITY, INFLAMMATION AND ENDOTHELIAL DYSFUNCTION

M. IANTORNO[1], U. CAMPIA[2], N. DI DANIELE[3], S. NISTICÒ[4], G.B. FORLEO[3], C. CARDILLO[5] and M. TESAURO[3]

[1]Critical Care Medicine Department, National Institutes of Health, Bethesda, MD, USA; [2]MedStar Cardiovascular Research Network Washington, DC, USA; [3]Department of Systems Medicine, University of Rome Tor Vergata, Rome, Italy; [4]Department of Health Sciences, University of Catanzaro "Magna Grecia", Catanzaro, Italy; [5]Internal Medicine, Catholic University, Rome, Italy

Received February 11, 2014 – Accepted March 13, 2014

Cardiovascular disease is the leading cause of morbidity and mortality in obese individuals. Obesity dramatically increases the risk of development of metabolic and cardiovascular disease. This risk appears to originate from disruption in adipose tissue function leading to a chronic inflammatory state and to dysregulation of the endocrine and paracrine actions of adipocyte-derived factors. These, in turn, impair vascular homeostasis and lead to endothelial dysfunction. An altered endothelial cell phenotype and endothelial dysfunction are common among all obesity-related complications. A crucial aspect of endothelial dysfunction is reduced nitric oxide (NO) bioavailability. A systemic pro-inflammatory state in combination with hyperglycemia, insulin resistance, oxidative stress and activation of the renin angiotensin system are systemic disturbances in obese individuals that contribute independently and synergistically to decreasing NO bioavailability. On the other hand, pro-inflammatory cytokines are locally produced by perivascular fat and act through a paracrine mechanism to independently contribute to endothelial dysfunction and smooth muscle cell dysfunction and to the pathogenesis of vascular disease in obese individuals. The promising discovery that obesity-induced vascular dysfunction is, at least in part, reversible, with weight loss strategies and drugs that promote vascular health, has not been sufficiently proved to prevent the cardiovascular complication of obesity on a large scale. In this review we discuss the pathophysiological mechanisms underlying inflammation and vascular damage in obese patients.

Obesity has reached epidemic proportions worldwide, with approximately one-half billion people (12% of the world's population) considered obese (1). In the United States alone, the prevalence of obesity has increased by about 50% in the past 30 years, with 70% of all adults being classified as either overweight or obese (2). Central fat distribution in obese individuals has been associated to increased cardiovascular risk (3). In fact, specific localization of the fat in the trunk has been included in the deadly pentad called metabolic syndrome (3). The adipose regions drained by the portal circulation (omental and mesenteric) appear, in fact, to exert the most pronounced metabolic effects being sensitive to stimuli that mobilize free fatty acids (FFA) due to a high number of beta-adrenergic receptors and a relatively weak alpha-adrenergic inhibition (4). This sensitivity leads to high portal FFA concentrations,

Key words: obesity, inflammation, atherosclerosis, endothelial dysfunction

Mailing address:
Prof. Steven Paul Nistico
Dept of Health Sciences
University of Catanzaro
Viale Europa, Germaneto,
88100 Catanzaro, Italy
e-mail: steven.nistico@gmail.com

0393-974X (2014)

DISCLOSURE: ALL AUTHORS REPORT NO CONFLICTS OF INTEREST RELEVANT TO THIS ARTICLE.

which, in turn, exert a stimulus to increase synthesis and secretion of very-low-density lipoprotein (VLDL), stimulation of gluconeogenesis (5), hepatic insulin resistance and reduce hepatic clearance of insulin (6). Obesity is characterized by the confluence of key risk factors for coronary heart disease (e.g., dyslipidemia, hypertension, insulin resistant states) with a pro-inflammatory environment that appears to worsen cardiovascular outcomes. In particular, obesity is known to be closely related to impaired endothelial function, a well-known marker of pre-atherosclerotic disease (7). The mechanisms linking obesity-related vascular disorders and inflammation are the focus of this review.

The endothelium

The vascular endothelium, the inner cellular lining of blood vessels, is not inert but is instead highly metabolically and physiologically active. In fact, endothelial cells have been for years described as a dynamic organ that regulates vascular tone by balancing the production of vasodilators and vasoconstrictors in response to a variety of stimuli (7). The endothelium plays a central role in the maintenance of vascular health (8), and, as a dynamic organ, controls vasomotor tone, hemostatic balance, vascular permeability, and innate and adaptive immunity and trafficking blood cells while also inhibiting vascular smooth muscle cell proliferation and apoptosis (9). In addition to acting as a functional and structural barrier between blood and vessel wall preventing platelet and leukocyte adhesion and aggregation, the endothelium behaves as a receptor-effector structure sensing physical and chemical stimuli and/or releasing products to maintain homeostasis. Nitric Oxide (NO), the predominant mediator of normal vascular function, is released by healthy endothelium and diffuses within the vessel wall, causing smooth muscle dilation in response to stimulation by endogenous factors such as bradykinin, acetylcholine, and catecholamines, as well as ischemia, temperature change, and mechanical stimuli, including shear stress (8). The endothelium regulates vascular tone also by releasing vasoconstrictors such as endothelin-1 (ET-1), and by converting angiotensin I to II. ET-1 and angiotensin II have roles not only in vasoconstriction, but also in stimulation of smooth muscle cell proliferation, vascular remodeling, and inflammatory cell adhesion (10, 11). Given the fundamental role of NO in mediating endothelial function, impairment of vasodilation in response to stressors that increase endothelium-derived NO is often used as a measure of endothelial dysfunction (12). The term "endothelial dysfunction" refers to a maladapted endothelial phenotype characterized by reduced NO bioavailability, increased oxidative stress, elevated expression of pro-inflammatory and pro-thrombotic factors, and abnormal vasoreactivity to endothelial-dependent stressor (8) (Table I).

Endothelial dysfunction in obesity

There is clear evidence that obesity is associated with endothelial dysfunction characterized by decreased availability of NO and imbalance between the NO pathway and the ET-1 system. In the vessels of obese patients, a shift of the normal prevalence of NO-mediated vasodilator tone towards an enhanced ET-1- mediated vasoconstriction has, in fact, been observed. The presence of endothelial dysfunction in patients with obesity and insulin resistance was first reported by Steinberg et al. over a decade ago. These authors demonstrated a blunted increase of leg blood flow in response to graded intra-arterial doses of the muscarinic receptor agonist methacholine in patients with elevated BMI or type 2 diabetes compared with lean controls (13). These observations have been followed by exploration of the cellular and molecular action of insulin on the vasculature. Quon and colleagues demonstrated that the molecular signaling pathways mediating insulin stimulation of nitric oxide production in endothelial cells are similar to signaling pathways mediating insulin activation of glucose transport in classical target tissues (i.e., the PI 3-kinase pathway) (14) Their findings were subsequently replicated by other investigators (15) and by our group in a study showing that patients with the metabolic syndrome secondary to central obesity have impaired forearm vasodilator response to Ach (16). Furthermore, flow-mediated dilation of the brachial artery (FMD), an ultrasound-based non-invasive endothelial function test is impaired in obese patients and weight loss leads to an improvement of endothelial function and metabolic parameters in these individuals (17). Taken together, the findings of these studies suggest that interventions aimed at

Table I. *Adipokines and their effects on vascular function.*

Adipokine	Effect on Vascular Function
Leptin	Direct Vasodilatory effect ↑ VSMC proliferation and migration ↑ Vascular permeability ↑ Oxidative stress
Adiponectin	Direct Vasodilatory effect ↓ VSMC proliferation Anti-inflammatory effect Antioxidative effect
Resistin	Reduced eNOS expression ↑ Endothelial cell activation ↑VSMC proliferation ↑VSMC migration
TNF-alpha	↓Endothelium dependent vasodilation ↓eNOS expression Induces ET-1 and PAI-1 Oxidative stress
Ghrelin	Vasodilation ↑ NO production
MCP-1	Proinflammatory
PAI-1	↑VSMC proliferation
ROS	eNOS uncoupling Proinflammatory effect
NO	Vasodilation
ET-1	Vasoconstriction VSMC Proliferation Cell adhesion
Angiotensinogen	Vasoconstrictor Proinflammatory ↓NO bioavailability
FFA	↓Endothelium-dependent vasodilation

reducing weight may lead to a reversal of endothelial dysfunction in obese individuals, thus potentially reducing the risk of developing diabetes and CVD. In patients with obesity an increased activity of the ET-1 system may significantly contribute to the abnormal vascular homeostasis. Endothelin1 (ET-1), is the most potent vasoconstrictor peptide synthesized by the endothelial cells and is known to play a central role in the pathophysiology of the vasomotor abnormalities associated with endothelial dysfunction and in the formation and progression of the atherosclerotic plaque (10). Our group has indeed demonstrated an increased ET-1-dependent vasoconstrictor activity in the forearm circulation of overweight and obese individuals, but not in lean controls, with a linear relationship between the degree of vasodilation induced by ET-1 receptor blockade with BQ-123 and BMI (18). Furthermore, we have observed that patients with central adiposity and metabolic syndrome, in addition to enhanced intravascular ET-1 activity, also have impaired vasoconstrictor response to the inhibition of NO synthesis by NG-monomethyl-Larginine (L-NMMA), indicating a concomitant decrease of NO-dependent vasodilator capacity (16).

Inflammation in obesity as cause of endothelial dysfunction

It is well known that inflammation plays an important role in causing both insulin resistance and vascular dysfunction in obese individuals. The circulating levels of inflammatory cytokines are elevated in obesity and are associated with endothelial activation and a blunted response to the infusion of the NO precursor L-arginine (19). Furthermore, the increase of adipose tissue mass in obesity is accompanied by macrophage infiltration, secondary to the production of monocyte chemoattractant protein-1 (MCP-1) and other pro-inflammatory cytokines, such as Tumor Necrosis Factor-alpha (TNF-α and IL-6, by preadipocytes and endothelial cells (20). In keeping with these observations, Rask-Madsen and colleagues (21) have shown that infusion of TNF-α in healthy humans inhibits the stimulatory effects of insulin on glucose uptake and reduces endothelium-dependent vasodilation. *In vitro* studies show that incubation of human vascular endothelial cells with TNF-α produces a marked down-regulation of eNOS expression and induces the synthesis of ET-1 and plasminogen activator inhibitor 1 (22). In addition to these direct effects, TNF-α may also induce vascular dysfunction indirectly by stimulating lipolysis and FFA release (23). In our laboratory, we investigated the role of TNF-α in the vascular dysfunction associated with metabolic syndrome and by using the TNF-α

neutralizing antibody infliximab. We observed that TNF-α blockade enhances the stimulatory effects of insulin not only on endothelium-dependent, but also on endothelium-independent vasodilator reactivity. The effect of infliximab on vascular function was not additive to that observed following the administration of the antioxidant vitamin C, suggesting that TNF-α-related vasculopathy in these patients is likely related to increased oxidative stress (24).

Perivascular adipose tissue and adipokines

Perivascular adipose tissue (PVAT), the adipose tissue surrounding blood vessels, was considered for years as only a passive structural support for the vasculature. In obesity, the expanded PVAT significantly contributes to atherosclerosis. In fact, PVAT dysfunction triggers inflammation, oxidative stress, and hypoxic processes to promote vascular dysfunction (25). Greenstein et al. demonstrated that, in healthy individuals, PVAT around small arteries promote vasodilation by increasing NO bioavailability. In these experiments adiponectin appeared to be the mediator of these effects, since the anticontractile responses were completely abolished when arteries with PVAT from healthy individuals were incubated with an adiponectin type 1 receptor-blocking fragment (26). The dilator effect of PVAT was lost in the obese patients with metabolic syndrome, and was accompanied by higher expression of TNF-α receptor 1. Of note, the 'obese' phenotype could be reproduced by adding TNF-α or IL-6 to the PVAT around healthy blood vessels. Adipose tissue secretes a number of cytokines, also termed adipokines, involved in the regulation of several biological processes. The epidemic of obesity and cardiovascular diseases during the last century has led to intense research on the role of adipokines in obesity and atherosclerosis and their use as potential therapeutic targets to reduce cardiovascular morbidity and mortality. During recent years, in fact, adipose tissue has been acknowledged as a major endocrine and paracrine organ that produces hundreds of proteins e.g. adiponectin, leptin, resistin, TNF-α, interleukin-6 (IL-6), plasminogen activator inhibitor-1 (PAI-1), atrial natriuretic peptide and angiotensinogen (25). These molecules contribute to the modulation of insulin activity and resistance, and metabolism of fat and glucose indirectly determining atherosclerosis. In addition, they also exert direct actions on endothelial function, vascular homeostasis and atherogenesis (27). Leptin, a 16 kDa peptide, modulates energy intake and expenditure, lipid metabolism, hematopoiesis, thermogenesis and the function of pancreatic B cells and ovaries (28). Leptin acts on receptors of the endothelium and the vascular smooth muscle cells, influences vascular tone and promotes endothelial and smooth vascular muscle proliferation and migration by stimulating phosphorylation and activation of MAP kinases, and upregulating PI3-kinase activity (29). Despite its NO-dependent vasodilatory effect, leptin was shown to decrease bioavailable NO by endothelial cells when they were exposed to this adipokine for 12 h. This is thought to be caused by increased oxidative stress which leads to depletion of endothelial NO and increase of cytotoxic ONOO(-) (30). Interestingly, the majority of obese individuals have elevated circulating leptin levels, likely secondary to leptin resistance (31). High leptin concentrations correlate with adverse cardiovascular outcomes in obese patients (32). Human endothelial cells, indeed, express leptin receptors, and hyperleptinaemia has been shown to be an independent risk factor for coronary artery disease and a strong predictor of acute myocardial infarction (33). Adiponectin is an adipocyte-derived peptide involved in enhancement of insulin-mediated glucose uptake in skeletal muscle, suppression of hepatic glucose production and amelioration of insulin resistance (34). Adiponectin concentrations are reduced in obese and diabetic patients and inversely correlated with BMI and visceral fat (35). Studies have shown that adiponectin may exert beneficial vascular effects by stimulating NO production by endothelial cells via PI3K-dependent pathways (36). Furthermore, adiponectin may decrease TNF-α-induced production of asymmetric dimethylarginine (ADMA) (37) and improve the redox state of the endothelium by suppressing reduced nicotinamide adenine dinucleotide phosphate (NADPH) oxidase-derived superoxide generation (38). Resistin, is produced mainly by macrophages and may contribute to vascular disease through endothelial dysfunction mediated by reduced eNOS expression via oxidative stress and activation of JNK MAPK (39). In addition, resistin increases the levels of

VCAM-1 and MCP-1, whereas it downregulates TNF receptor-associated factor (TRAF- 3), which is a powerful inhibitor of CD40 ligand-mediated endothelial cell activation (40). In 26,490 middle-aged subjects from the European Investigation into Cancer and Nutrition-Potsdam Study without past history of myocardial infarction or stroke, higher levels of resistin were independent predictors of myocardial infarction (41). Ghrelin is a peptide hormone produced by the stomach that plays a relevant role in the central regulation of food intake (42). Ghrelin levels are decreased in obese individuals (42). Studies conducted by our group have shown that, in patients with obesity-related metabolic syndrome, ghrelin improves endothelial function (16) by restoring the NO/ET-1 balance (42). Furthermore, we have demonstrated that ghrelin acutely stimulates production of NO in endothelial cells through a signalling pathway that involves PI3K, Akt and eNOS (43, 44). Angiotensinogen is mainly produced by the liver but also by adipocytes and is considered to play a determinant role in obesity-related disorders and in the pathophysiology of metabolic syndrome (45). Renin cleaves the leucine-valine peptidic bond in angiotensinogen and transforms it into angiotensin I, which is then converted to angiotensin II by the angiotensin-converting enzyme. Angiotensin II, the most potent circulating vasoconstrictor, was shown to promote vascular inflammation in apolipoprotein-E-deficient mice and accelerate the atherosclerotic process by activating NF-αB-mediated proinflammatory genes. These effects are mediated by an increase in transcription of MCP-1, macrophage-colony stimulating factor (MCSF), E-selectin, ICAM-1, VCAM-1, iNOS and COX-2 (46). Furthermore, angiotensinogen reduces the bioavailability of NO, thus impairing endothelial function (47). Abdominally obese individuals manifest altered expression and/or secretion patterns of key cytokines or adipokines such as TNF-α, plasminogen activator inhibitor-1, and interleukin-6 that perpetuate and promote endothelial dysfunction in a vicious circle.

Oxidative stress and inflammation

In obesity, endothelial cell generation of reactive oxygen species (ROS) is triggered by high circulating levels of pro-inflammatory cytokines generated in the visceral adipose tissue through the action of the local renin–angiotensin system (47) and by low adiponectin levels. Excessive oxidative stress decreases NO bioavailability through multiple mechanisms as shown in a recent publication (48).

Insulin resistance and inflammation

Systemic inflammation and insulin resistance in obese individuals are mutually amplifying processes that increase the risk of cardiovascular morbidity and mortality (49). Proinflammatory cytokines produced by adipocytes contribute, at least in part, to insulin resistance by interfering with normal insulin receptor intracellular signaling (50). On the other hand, obesity-related insulin resistance is well-known to promote inflammation through diverse mechanisms including oxidative stress, stimulation of pro-inflammatory adipokines, advanced glycation end products, and free fatty acids (FFA) (4, 5). Several mechanisms may account for the detrimental effects of circulating FFA on vascular function, including, but not limited to, enhanced oxidative stress due to activation of the renin–angiotensin system (45) and ET-1 release (10), also shown in dermatological conditions (51-56).

CONCLUSION

Obesity and metabolic syndrome are important risk factors for metabolic and cardiovascular disease. Despite a well-known strong genetic component (57), this risk appears to originate from several abnormalities in adipose tissue function associated with a chronic inflammatory state. These conditions disrupt vascular homeostasis by causing an imbalance between the NO pathway and the ET-1 system, with impaired insulin-stimulated endothelium-dependent vasodilation. A better understanding of the pathophysiology of obesity-related vascular dysfunction may be of great importance to lead to new therapeutic approaches.

REFERENCES

1. Flegal KM, Kit BK, Orpana H, Graubard BI. Association of all-cause mortality with overweight and obesity using standard body mass index categories: a systematic review and meta-analysis.

JAMA 2013; 309:71-82.
2. Flegal KM, Carroll MD, Ogden CL, Curtin LR. Prevalence and trends in obesity among US adults, 1999-2008. JAMA 2010; 20:235-41.
3. Campia U, Tesauro M, Cardillo C. Human obesity and endothelium-dependent responsiveness. Br J Pharmacol 2012; 165:561-73.
4. Bjorntorp P. Metabolic implications of body fat distribution. Diabetes care 1991; 14:1132-43.
5. Ferrannini E, Barrett EJ, Bevilacqua S, DeFronzo RA. Effect of fatty acids on glucose production and utilization in man. J Clin Invest 1983; 72:1737-47.
6. Bevilacqua S, Bonadonna R, Buzzigoli G, Boni C, Ciociaro D, Maccari F, Giorico MA, Ferrannini E. Acute elevation of free fatty acid levels leads to hepatic insulin resistance in obese subjects. Metab Clin Exp 1987; 36:502-6.
7. Vita JA, Keaney JF, Jr. Endothelial function: a barometer for cardiovascular risk? Circulation 2002; 6:106:640-2.
8. Deanfield JE, Halcox JP, Rabelink TJ. Endothelial function and dysfunction: testing and clinical relevance. Circulation 2007; 13:1285-95.
9. Herman AG, Moncada S. Therapeutic potential of nitric oxide donors in the prevention and treatment of atherosclerosis. Eur Heart J 2005; 26:1945-55.
10. Kelly JJ, Whitworth JA. Endothelin-1 as a mediator in cardiovascular disease. Clin Exp Pharmacol Physiol 1999; 26:158-61.
11. Ferrario CM, Strawn WB. Role of the renin-angiotensin-aldosterone system and proinflammatory mediators in cardiovascular disease. Am J Cardiol 2006; 98:121-8.
12. Corretti MC, Anderson TJ, Benjamin EJ, et al. Guidelines for the ultrasound assessment of endothelial-dependent flow-mediated vasodilation of the brachial artery: a report of the International Brachial Artery Reactivity Task Force. J Am Coll Cardiol 2002; 39:257-65.
13. Steinberg HO, Chaker H, Leaming R, Johnson A, Brechtel G, Baron AD. Obesity/insulin resistance is associated with endothelial dysfunction. Implications for the syndrome of insulin resistance. J Clin Invest 1996; 97:2601-10.
14. Muniyappa R, Montagnani M, Koh KK, Quon MJ. Cardiovascular actions of insulin. Endocr Rev 2007; 28:463-91.
15. Perticone F, Ceravolo R, Candigliota M, et al. Obesity and body fat distribution induce endothelial dysfunction by oxidative stress: protective effect of vitamin C. Diabetes 2001; 50:159-65.
16. Tesauro M, Schinzari F, Iantorno M, Rizza S, Melina D, Lauro D. Ghrelin improves endothelial function in patients with metabolic syndrome. Circulation 2005; 112:2986-92.
17. Woo KS, Chook P, Yu CW, et al. Effects of diet and exercise on obesity-related vascular dysfunction in children. Circulation 2004; 27:109:1981-6.
18. Cardillo C, Campia U, Iantorno M, Panza JA. Enhanced vascular activity of endogenous endothelin-1 in obese hypertensive patients. Hypertension 2004; 43:36-40.
19. Ziccardi P, Nappo F, Giugliano G, et al. Reduction of inflammatory cytokine concentrations and improvement of endothelial functions in obese women after weight loss over one year. Circulation 2002; 105:804-9.
20. Wellen KE, Hotamisligil GS. Obesity-induced inflammatory changes in adipose tissue. J Clin Invest 2003; 112:1785-8.
21. Rask-Madsen C, Dominguez H, Ihlemann N, Hermann T, Kober L, Torp-Pedersen C. Tumor necrosis factor-alpha inhibits insulin's stimulating effect on glucose uptake and endothelium-dependent vasodilation in humans. Circulation 2003; 108:1815-21.
22. Mohamed F, Monge JC, Gordon A, Cernacek P, Blais D, Stewart DJ. Lack of role for nitric oxide (NO) in the selective destabilization of endothelial NO synthase mRNA by tumor necrosis factor-alpha. Arterioscl Thromb Vasc Biol 1995; 15:52-57.
23. Pittas AG, Joseph NA, Greenberg AS. Adipocytokines and insulin resistance. The J Clin Endocr Metab 2004; 89:447-52.
24. Tesauro M, Schinzari F, Rovella V, et al. Tumor necrosis factor-alpha antagonism improves vasodilation during hyperinsulinemia in metabolic syndrome. Diabetes Care 2008; 31:1439-41.
25. Kershaw EE, Flier JS. Adipose tissue as an endocrine organ. J Clin Endocr Metab 2004; 89:2548-56.
26. Greenstein AS, Khavandi K, Withers SB, et al. Local inflammation and hypoxia abolish the protective anticontractile properties of perivascular fat in obese

patients. Circulation 2009; 119:1661-70.
27. Tesauro M, Canale MP, Rodia G, Di Daniele N, Lauro D, Scuteri A, Cardillo C. Metabolic syndrome, chronic kidney, and cardiovascular diseases: role of adipokines. Cardiol Res 2011; 2011:653182.
28. Pelleymounter MA, Cullen MJ, Baker MB, Hecht R, Winters D, Boone T, Collins F. Effects of the obese gene product on body weight regulation in ob/ob mice. Science 1995; 269:540-43.
29. Vecchione C, Maffei A, Colella S, et al. Leptin effect on endothelial nitric oxide is mediated through Akt-endothelial nitric oxide synthase phosphorylation pathway. Diabetes 2002; 51:168-73.
30. Korda M, Kubant R, Patton S, Malinski T. Leptin-induced endothelial dysfunction in obesity. Am J Physiol 2008; 295:1514-21.
31. Martin SS, Qasim A, Reilly MP. Leptin resistance: a possible interface of inflammation and metabolism in obesity-related cardiovascular disease. J Am Coll Cardiol 2008; 52:1201-10.
32. Schinzari F, Tesauro M, Rovella V, et al. Leptin stimulates both endothelin-1 and nitric oxide activity in lean subjects but not in patients with obesity-related metabolic syndrome. J Clin Endocr Metab 2013; 98:1235-41.
33. Soderberg S, Ahren B, Jansson JH, Johnson O, Hallmans G, Asplund K, Olsson T. Leptin is associated with increased risk of myocardial infarction. J Int Med 1999; 246:409-18.
34. Chiarugi P, Fiaschi T. Adiponectin in health and diseases: from metabolic syndrome to tissue regeneration. Exp Op Ther Targ 2010; 14:193-206.
35. Lara-Castro C, Luo N, Wallace P, Klein RL, Garvey WT. Adiponectin multimeric complexes and the metabolic syndrome trait cluster. Diabetes 2006; 55:249-59.
36. Chen H, Montagnani M, Funahashi T, Shimomura I, Quon MJ. Adiponectin stimulates production of nitric oxide in vascular endothelial cells. J Biol Chem 2003; 278:45021-6.
37. Eid HM, Lyberg T, Arnesen H, Seljeflot I. Insulin and adiponectin inhibit the TNF-α-induced ADMA accumulation in human endothelial cells: the role of DDAH. Atherosclerosis 2007; 194:e1-8.
38. Motoshima H, Wu X, Mahadev K, Goldstein BJ. Adiponectin suppresses proliferation and superoxide generation and enhances eNOS activity in endothelial cells treated with oxidized LDL. BBRC 2004; 315:264-71.
39. Chen C, Jiang J, Lu JM, Chai H, Wang X, Lin PH, Yao Q. Resistin decreases expression of endothelial nitric oxide synthase through oxidative stress in human coronary artery endothelial cells. Am J Physiol 2010; 299:193-201.
40. Verma S, Li SH, Wang CH, Fedak PW, Li RK, Weisel RD, Mickle DA. Resistin promotes endothelial cell activation: further evidence of adipokine-endothelial interaction. Circulation 2003; 12:736-40.
41. Weikert C, Westphal S, Berger K, et al. Plasma resistin levels and risk of myocardial infarction and ischemic stroke. J Clin Endocr Metabol 2008; 93:2647-53.
42. Tesauro M, Schinzari F, Rovella V, Di Daniele N, Lauro D, Mores N, Veneziani A, Cardillo C. Ghrelin restores the endothelin 1/nitric oxide balance in patients with obesity-related metabolic syndrome. Hypertension 2009; 54:995-1000.
43. Iantorno M, Chen H, Kim JA, Tesauro M, Lauro D, Cardillo C, Quon MJ. Ghrelin has novel vascular actions that mimic PI 3-kinase-dependent actions of insulin to stimulate production of NO from endothelial cells. Am J Physiol 2007; 292:E756-64.
44. Tesauro M, Schinzari F, Caramanti M, Lauro R, Cardillo C. Metabolic and cardiovascular effects of ghrelin. Int J Peptides 2010; pii 864342.
45. Engeli S, Schling P, Gorzelniak K, et al. The adipose-tissue renin-angiotensin-aldosterone system: role in the metabolic syndrome? Int J Biochem Cell Biol 2003; 35:807-25.
46. Tham DM, Martin-McNulty B, Wang YX, et al. Angiotensin II is associated with activation of NF-kappaB-mediated genes and downregulation of PPARs. Physiolog Genom 2002; 11:21-30.
47. Dandona P, Dhindsa S, Ghanim H, Chaudhuri A. Angiotensin II and inflammation: the effect of angiotensin-converting enzyme inhibition and angiotensin II receptor blockade. J Human Hyperten 2007; 21:20-7.
48. Bendall JK, Alp NJ, Warrick N, et al. Stoichiometric relationships between endothelialtetrahydrobiopterin, endothelial NO synthase (eNOS) activity, and eNOS coupling *in*

vivo: insights from transgenic mice with endothelial-targeted GTP cyclohydrolase 1 and eNOS overexpression. Circ Res 2005; 97:864-71.

49. Schinzari F, Tesauro M, Rovella V, Galli A, Mores N, Porzio O, Lauro D, Cardillo C. Generalized impairment of vasodilator reactivity during hyperinsulinemia in patients with obesity-related metabolic syndrome. Am J Physiol Endocrinol Metab 2010; 299:E947-52.
50. Kim JA, Montagnani M, Koh KK, Quon MJ. Reciprocal relationships between insulin resistance and endothelial dysfunction: molecular and pathophysiological mechanisms. Circulation 2006; 113:1888-904.
51. Chiricozzi A, Zhang S, Dattola A, Gabellini S, Chimenti S, Nisticò S. Role of Th17 in the pathogenesis of cutaneous inflammatory diseases J Biol Regul Homeost Agents 2012; 26:313-8.
52. Chiricozzi A, Zhang S, Dattola A, Cannizzaro MV, Gabellini M, Chimenti S, Nisticò S. New insights in the pathogenesis of cutaneous autoimmune disorders. J Biol Regul Homeost Agents 2012; 26:165-70.
53. Nisticò S, Chiricozzi A, Saraceno R, Schipani C, Chimenti S. Vitiligo treatment with monochromatic excimer light and tacrolimus: Results of an open randomized controlled study. Photomed Laser Surg 2012; 30:26-30.
54. Specchio F, Carboni I, Chimenti S, Tamburi F, Nisticò S. Cutaneous manifestations in patients with chronic renal failure on hemodialysis. Int J Immunopath Pharmacol 2014; 27(1):1-4.
55. Chiricozzi A, Pitocco R, Saraceno R, Nistico SP, Giunta A, Chimenti S. New topical treatments for psoriasis. Exp Op Pharmacother 2014; 15(4):461-70.
56. Nisticò SP, Saraceno R, Chiricozzi A, Giunta A, Di Stefani A, Zerbinati N. UVA-1 Laser in the treatment of palmoplantar pustular psoriasis. Photomed Laser Surg 2013; 31:434-38.
57. Scuteri A, Tesauro M, Rizza S, et al. Endothelial function and arterial stiffness in normotensive normoglycemic first-degree relatives of diabetic patients are independent of the metabolic syndrome. Nutr Metab Cardiovasc Dis 2008; 18:349-56.

EDITORIAL

TITOLO NEUROPEPTIDE NGF MEDIATES NEURO-IMMUNE RESPONSE AND INFLAMMATION THROUGH MAST CELL ACTIVATION

S.K. KRITAS[1], A. SAGGINI[2], G. CERULLI[3], A. CARAFFA[4], P. ANTINOLFI[4], A. PANTALONE[5], S. FRYDAS[6], M. ROSATI[7], M. TEI[3], A. SPEZIALI[3], R. SAGGINI[8], F. PANDOLFI[9] and P. CONTI[10]

[1]Department of Microbiology and Infectious Diseases, School of Veterinary Medicine, Aristotle University of Thessaloniki, Macedonia, Greece; [2]Department of Dermatology, University of Rome Tor Vergata, Rome, Italy; [3]Nicola's Foundation, Onlus, Arezzo, Italy; [4]Orthopedic Division, University of Perugia, Perugia, Italy; [5]Orthopedic Division, University of Chieti-Pescara, Chieti, Italy; [6]Department of Parasitology, School of Veterinary Medicine, University of Thessaloniki, Macedonia, Greece; [7]Gynecology Clinic, Pescara Hospital, Pescara, Italy; [8]Department of Neurosciences and Imaging, Faculty of Medicine and Surgery, G. d'Annunzio University Chieti-Pescara, Chieti, Italy; [9]Department of Internal Medicine, Catholic University of the Sacred Heart, Rome, Italy; [10]Immunology Division, Medical School, University of Chieti-Pescara, Chieti, Italy

Received March 6, 2014 – June 15, 2014

Human mast cells (first described in 1879 by Paul Ehrlich) develop from committed precursors in the bone marrow expressing the differentiation marker CD34+ and distinct from the three other myeloid cells. Mast cells are present in various tissues especially near blood vessels, epithelia and nerves and they are activated by cross-linking of FcεRI, but also by a number of neuropeptides. NGF mediates a number of inflammatory and autoimmune states in conjunction with an increased accumulation of mast cells which appear to be involved in neuroimmune interactions and tissue inflammation. Here we report some relationships between mast cells and nerve growth factor (NGF).

Mast cells are derived from progenitors (Fig. 1) in the bone marrow, are not found in the circulation and produce certain cytokines (1). Cytokine proteins are produced by different cell types that mediate inflammatory and immune responses. Cytokines are heterogeneous peptide molecules, produced by a variety of cells of immune and non-immune origin. In addition, cytokines play a determinate role in the communication between cells of the immune system (2). After cytokine binding to a specific membrane receptor on target cells, a series of signal transduction pathways are stimulated. TH2 cytokines involved in allergic diseases have recently been implicated in several neurological diseases such as multiple sclerosis, brain metastases, allergic encephalomyelitis and allergic encephalomyelitis, all mediated by mast cell products. Mast cells are present in many epithelial and serosal cavities, and respond to microbes and various mediators by secreting molecules that stimulate inflammation (3).

Key words: mast cells, neuropeptides, nerve growth factor, peptides, inflammation

Mailing address: Spyridon K. Kritas,
DVM, PhD, Dipl. ECPHM Associate Professor,
Department of Microbiology and Infectious Diseases,
School of Veterinary Medicine, Aristotle University of Thessaloniki,
54124 Thessaloniki, Macedonia, Greece
Tel./Fax: +30 2310 999940
e-mail: skritas@vet.auth.gr

0393-974X (2014)

They are found throughout the body, especially near blood vessels, epithelia and nerves, and mast cells of central nervous system (CNS) origin are found intra-cranially, in the dura mater, leptomeninges and choroid plexus, and within the parenchyma of the brain, particularly in the thalamus and hypothalamus in many mammalian species, including humans. Ma st cells are activated by cross-linking of FcεRI molecules, which occurs by the binding of multivalent antigens to the attached IgE molecules but also by a number of neuropeptides such as neurotensin (NT), somatostatin or substance P (SP), to secrete numerous pro-inflammatory molecules that include histamine, cytokines and proteolytic enzymes. Cytokine production by activated mast cells is a consequence of newly-induced cytokine gene transcription which appears to be similar to the events that occur in T cells. Cytokines produced in the brain may influence its development, differentiation and function in normal and pathological circumstances. Mast cell mediators induce microvascular leakage and stimulate protease-activated receptors (PAR), leading to widespread inflammation (4). Brain diseases appear to worsen in response to acute stress that leads to the local release of cytokines such as tumor necrosis factor-alpha (TNF) alpha and vascular endothelial growth factor (VEGF) by mast cells, a phenomenon absent in W/W mast cell deficient mice (5).

Mast cells are also capable of secreting multiple cytokines including TNF-alpha, IL-1, IL-3, IL-4, IL-6, and GM-CSF. Mast cells also synthesize, store, and release nerve growth factor which accumulates in inflammatory sites or exudates. This suggests that alterations in normal mast cell behaviour can provoke maladaptive neuroimmune tissue responses, the consequences of which could have profound implications in inflammatory diseases (6).

It has been shown that neuropeptides are involved in the increase of synthesis of CC and CXC chemokines in inflammatory cells with chemotactic and inflammatory properties. In addition to being a mediator of pain, neuropeptides have been shown to play an important role in inflammatory states such as asthma, immune complex-mediated lung injury, experimental arthritis, and inflammatory bowel disease. Src family kinases (SFKs) are known to be involved in cytokine signaling. It has been reported that SFKs are involved in neuropeptide-induced

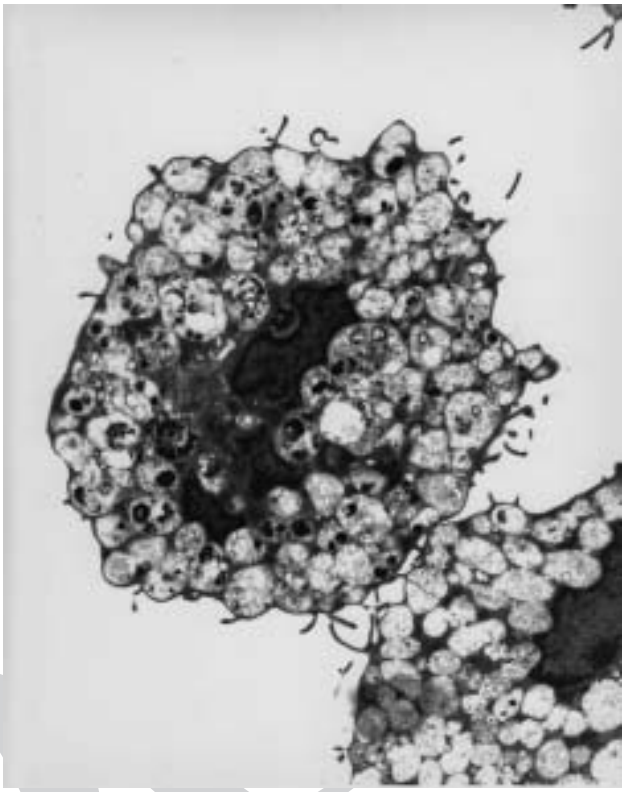

Fig. 1. *Human cord blood mast cells cultured for 15 weeks. Electron microscope magnification 11,200 X.*

chemokine production and inflammation. Inhibition of SFKs attenuates chemokine production and may prevent ischemia-reperfusion-induced injury, and attenuate sepsis, acute lung damage, and other injured organs (7).

We now know that secreted neuropeptides may mediate neuroinflammatory interactions by binding to and stimulating immune cells such as lymphoid cells and mast cells. In the past decade, considerable progress has been made towards a better understanding of the actions of nerve growth factor (NGF) in the nervous system. NGF is a neurotrophil molecule which acts on sympathetic and specific subsets of sensory neurones, and is present in the brain. Therefore, we believe that an accumulation of inflammatory exudates in the brain is also mediated by NGF released from resident tissue cells containing the stored protein, including mast cells (8). NGF is the prototype of target-derived neurotrophic factors critical for the development and maintenance of specific peripheral and central neuronal populations. NGF mediates a number of

inflammatory and autoimmune states in conjunction with an increased accumulation of mast cells which appear to be involved in neuroimmune interactions and tissue inflammation. Stress, which is modulated by mast cells, can induce intracranial mast-cell degranulation through the effect of corticotrophin-releasing hormone and sensory neuro-peptides. NGF may play an important role in cross-talk between cells of the nervous and the immune systems, demonstrating its function not only within the nervous system.

It has been reported that mast cells and NGF have the capacity to integrate neuro-endocrine immune responses in the patho-physiology of the CNS (6). The generation of NGF and the strong expression of mRNA TrkA by mast cells might provide a local and readily available source of this trophic factor that induces nociceptive C fibre sensitization and recruits and activates, together with cytokines, immune and inflammatory cells. Experimental animals treated with NGF *in vivo* increase the number and size of mast cells in several peripheral tissues (9), while the administration of anti-NGF antibodies cause cytological alterations of mast cells and decrease their numbers (9). Mast cells and cells of the inflammatory infiltrate such as lymphocytes, eosinophils and macrophages interact with neuronal cells, for example via neuropeptides and cytokines, mediating inflammation and allergic diseases. It has been reported that the neurotrophin NGF, brain-derived neurotrophic factor, neurokinins/neuropeptides (such as substance P), gastrin-releasing peptide, cytokines [such as interleukin(IL)-31, autotoxin] and the histamine H4 receptor mediate the pathophysiology of allergic reactions (10). Therefore, NGF and its receptor TrkA interact with nervous, endocrine and immune systems; however, the effect of NGF on mast cells does not activate degranulation (11).

TNF-alpha is also produced and regulated by mast cells and microglia which are involved in allergic inflammation and brain damage. TNF-releasing steps are regulated via the PKC alpha-dependent pathway. It has been found that in brain microglia, extracellular ATP triggers the release of TNF via the P2X7 receptor (12). The prototype of mitogen-activated protein (MAP) kinases, called extra cellular receptor-activated kinase (ERK), and c-Jun N-terminal kinase (JNK) (also called stress-activated protein) are also involved in ATP-induced TNF transcription, while p38, which is the third member of MAP kinase family, activates various transcription factors and regulates the transport of TNF mRNA from the nucleus to the cytosol (13). The transcription factors stimulate transcription of several cytokines such as TNF, IL-3, IL-4, IL-5, IL-6, IL-1, IL-13, IL-33, CSF, etc. along with several chemokines: MIP-1 alpha, MIP-1 beta, and others. IL-15 plays an important role in inflammatory diseases. In mast cells, IL-15 utilises a specific receptor IL-15RX and IL-15 gene is constitutively expressed in the nerve tissue and during differentiation of neurons. Recently, it has been shown that in the normal brain IL-15 is present only in neurons but glial cells contain this cytokine only when they are activated by inflammatory stimulus. These cytokines and chemokines are likely to be produced at the site of inflammation. Several neuropeptides, such as substance P, vasoactive peptides, somatostatin and others, induce mast cell release and may mediate neuroendocrine-linked mast cell activation (14). These mechanisms should be better clarified to offer further possible therapeutic targets for inflammatory diseases.

Chemokines are mediators of immunity and inflammation, acting through G-protein-coupled receptors. In the CNS, cytokines may play a relevant role in neurological diseases and pathogenesis of the brain and affect NGF synthesis.

Mast cell infiltration in inflammatory diseases and neurological dysfunctions are controlled by several chemokines and cytokines. NGF also is involved in neurogenic inflammation and may induce cytokines and chemokines, vasodilatation, plasma extravasation, and cellular adhesion molecule and may play a role in inducing also hyperalgesia trough the influence of 5-HT or histamine. In contrast, this neuropeptide has an important role in the repair of tissue injury. SP, which is an 11-amino acid neuropeptide released from nerve endings in many tissues, is also involved in immunity and inflammation and is capable of enhancing concanavalin A-activated mononuclear cells, resulting in a strong increase in the production of antibody IgA (15).

Substance P was first isolated by Leeman et al. (16) as an undecapeptide with important neurotransmitter-neuromodulator effects. In addition, substance P has been shown to induce and mediate inflammation,

angiogenesis, infections, intestinal mucosal immunity and stress. SP is generated by sensory ganglion cells, and it is transported to peripheral sites where it is stored and released on noxious stimulation and mediates an important biological role in inflammation and physiopathology of the brain. In addition, SP mediates both innate and adaptive immune system in SNS and lung. In fact, SP has an impact on lymphocyte activation and proliferation and increases the generation of the antibodies in IL-5 or TGF-beta co-stimulated cultures of human T and B lymphocytes. The immunomodulation by substance P includes cell activation and proliferation of human cells, with cytokine and chemokine generation and release. SP is a potent modulator of monocyte/ macrophage function, and causes transcription and translation of several different cytokines/chemokines such as TNF-alpha, macrophage inflammatory protein-1 (MIP-1) and GM-CSF, RANTES, MCP-1, CXCL8 (17), along with other proinflammatory compounds, proteases (chymase and tryptase), histamine, leukotrienes and prostaglandin D2 (18).

These observations support an important pro-inflammatory role for NGF acting via mast cell receptor activation in acute inflammatory diseases and associated tissue injury.

We already know that mast cell knockout mice express less inflammatory reaction than normal mice. In future studies it would be interesting to see whether knockout mice, deficient in the NGF gene are protected against acute inflammation and tissue injury.

In conclusion, these studies are focused on the role of NGF and mast cells in playing and modulating inflammatory response, and considering the possibility of potential cross-talk between a product of the CNS and the immune system.

However, there is still a lot to clarify regarding the mechanisms utilized by the nervous system to regulate immune function, and understanding the interrelationship between the nervous system and the immune system will provide new information for future treatment of inflammatory and immunological diseases.

REFERENCES

1. Theoharides TC, Conti P. Mast cells: the Jekyll and Hyde of tumor growth. Trends Immunol 2004; 25(5):235-41.
2. Arpaia N, Campbell C, Fan X, et al. Metabolites produced by commensal bacteria promote peripheral regulatory T-cell generation. Nature 2013; 504(7480):451-5.
3. Barrett NA, Austen KF. Innate cells and T helper 2 cell immunity in airway inflammation. Immunity 2009; 31(3):425-37.
4. Theoharides TC, Donelan JM, Papadopoulou N, Cao J, Kempuraj D, Conti P. Mast cells as targets of corticotropin-releasing factor and related peptides. Trends Pharmacol Sci 2004; 25(11):563-8.
5. Theoharides TC, Konstantinidou AD. Corticotropin-releasing hormone and the blood-brain-barrier. Front Biosci 2007; 12:1615-28.
6. Levi-Montalcini R, Skaper SD, Dal Toso R, Petrelli L, Leon A. Nerve growth factor: from neurotrophin to neurokine. Trends Neurosci 1996; 19:514-20.
7. Nijnik A, Pistolic J, Filewod NC, Hancock RE. Signaling pathways mediating chemokine induction in keratinocytes by cathelicidin LL-37 and flagellin. J Innate Immun 2012; 4(4):377-86.
8. Ricci A, Mariotta S, Pompili E, et al. Neurotrophin system activation in pleural effusions. Growth Factors 2010; 28(4):221-31.
9. Aloe L, Skaper SD, Leon A, Levi-Montalcini R. Nerve growth factor and autoimmune diseases. Autoimmunity 1994; 19(2):141-50.
10. Raap U, Ständer S, Metz M. Pathophysiology of itch and new treatments. Curr Opin Allergy Clin Immunol 2011; 11(5):420-7.
11. Kulka M, Sheen CH, Tancowny BP, Grammer LC, Schleimer RP. Neuropeptides activate human mast cell degranulation and chemokine production, Immunology 2008; 123(3):398-410.
12. Hide I. Mechanism of production and release of tumor necrosis factor implicated in inflammatory diseases. Nihon Yakurigaku Zasshi 2003; 121(3):163-73.
13. Sagi-Eisenberg R. The mast cell: where endocytosis and regulated exocytosis meet. Immunol Rev 2007; 217:292-303.
14. Dinh QT, Cryer A, Dinh S, et al. Protease-activated receptor 2 expression in trigeminal neurons innervating the rat nasal mucosa. Neuropeptides 2005; 39(5):461-6.
15. Serra MC, Bazzoni F, Della Bianca V, Greskowiak M,

Rossi F. Activation of human neutrophils by substance P. Effect on oxidative metabolism, exocytosis, cytosolic Ca2+ concentration and inositol phosphate formation. J Immunol 1988; 141(6):2118-24.

16. Oblas B, Boyd ND, Luber-Narod J, Reyes VE, Leeman SE. Isolation and identification of a polypeptide in the Hsp 70 family that binds substance P. Biochem Biophys Res Commun 1990; 166(2):978-83.
17. Katsanos GS, Anogeianaki A, Orso C, Tetè S, Salini V, Antinolfi PL, Sabatino G. Mast cells and chemokines. J Biol Regul Homeost Agents 2008; 22(3):145-51.
18. Ishimura M, Kataoka S, Suda M, Maeda T, Hiyama Y. Effects of KP-496, a novel dual antagonist for leukotriene D4 and thromboxane A2 receptors, on contractions induced by various agonists in the guinea pig trachea. Allergol Int 2006; 55(4):403-10.

ALLOGENEIC AND XENOGENEIC ANTI-TUMOR EFFECT OF *CALLITHRIX JACCHUS* NATURAL KILLER CELLS IS DEPENDENT ON NKp30 AND B7-H6 INTERACTION

T. MÜLLER, L. SCHLAHSA, H.J. ZHANG, S. VAHLSING, Y. SKAIK, B. EIZ-VESPER, S. IMMENSCHUH, R. BLASCZYK and C. FIGUEIREDO

Institute for Transfusion Medicine, Hannover Medical School, Hannover, Germany

Received March 20, 2013 – Accepted March 11, 2014

The first two authors contributed equally to this work

Natural Killer (NK) cells mount a fast and efficient immune response against tumor cells and are currently a major focus in the development of anti-cancer cell-based therapies. Due to major differences between the murine and human NK cell receptor system, a non-human primate model would be helpful to evaluate the efficiency of NK-cell based therapies prior to clinical applications. In humans, B7-H6 has been shown to facilitate the elimination of lymphoma cells through the interaction with its receptor NKp30. The common marmoset (*Callithrix jacchus*) is a new world monkey readily used in biomedical research due to its easy management and proximity to humans. In this study, we demonstrated the expression of B7-H6 antigen in marmoset B-lymphoblastoid cell lines. In addition, a method was established to isolate B- or NK-cells from peripheral blood of marmosets with purities of up to 97%. We detected the expression of B7-H6 in lymphoma cells and for the first time in leukemic blasts of human acute myeloid leukemia (AML). Marmoset NK cells were shown to lyse marmoset B lymphoblastoid cell line (B-LCL) cells by up to 28.4% and human B-LCL cells by up to 20%. This effect was abrogated when the NK cells were pre-treated with an anti-NKp30 specific antibody. Also, marmoset NK cells were able to lyse primary leukemic AML cells and lymphoma cells by up to 8.3 and 20.3%, respectively. Stimulation of marmoset NK cells with recombinant B7-H6 induced phosphorylation of ERK1/2 and proliferation rates. Furthermore, the secretion of IL-1β, IL-8, IFN-γ and TNF-α was significantly increased upon B7-H6 stimulation. In conclusion, we demonstrated that non-human primate NK cells have similar mechanisms for the lysis of tumor cells as human NK cells. Thus, this animal model constitutes a very promising tool for the development and evaluation of novel NK-cell based therapies.

Natural Killer (NK) cells are large granular lymphocytes that, besides their potent cytotoxic activity, secrete cytokines capable of modulating the innate and adaptive immune response. NK cells play a central role in host defence against a variety of tumor cells, virally infected cells and allogeneic cells (1). NK cells examine potential targets for the expression of MHC class I using inhibitory Killer-immunoglobulin-like receptors (KIR). Engagement of inhibitory KIR by MHC class I inhibits NK cell activation and target cell lysis. Although the effector activity of NK cells significantly depends on the recognition of "missing self", signals delivered by the NK cell activating receptors such as the natural

Key words: NK cells, NCR, NKp30, B7, B7-H6

Mailing address: Dr. Constanca Figueiredo,
Institute for Transfusion Medicine,
Hannover Medical School,
Carl-Neuberg-Str. 1,
D-30625 Hannover, Germany
Tel.: +49 511 532 9711 Fax: +49 511 532 2079
e-mail: figueiredo.constanca@mh-hannover.de

0393-974X (2014)

cytotoxicity receptor (NCR) family are required to trigger NK cell cytotoxic activity. The NCR family includes NKp46 (NCR1, CD335), NKp44 (NCR2, CD336), and NKp30 (NCR3, CD337). The NKp30 receptor has been demonstrated to play an important role in the antitumor effect in gastrointestinal stromal tumors and lymphoid leukemia (2, 3). NKp30 is a type I transmembrane (TM) protein containing a single Ig-like extracellular domain which is linked by a short stalk region to a TM segment and intracellular domain (4). For signal transduction in NK cells, the monomeric NKp30 receptor associates with CD3ζ and FcRγ for signal transduction. So far in humans, two ligands for NKp30 receptor have been identified: the HLA-B–associated transcript 3 (BAT3) and B7-H6. BAT3 is a nuclear protein that is involved in the interaction with p53 and induction of apoptosis after stress, such as DNA damage. BAT3 can also stimulate NK cells by being released by immature dendritic cells (DC) on the surfaces of exosomes (5-8). B7-H6 is a newly identified B7 family member. Unlike BAT3, B7-H6 is expressed on the surface of tumor cells but not on most normal cells (9-11). Several studies have demonstrated the potential of using NK cells as an efficient immunotherapy for cancer (12, 13). Therefore, reliable animal models are strongly desirable to evaluate safety and efficacy of new therapies prior to translation into clinical routine. The common marmoset (*Callithrix jacchus*), a small Brazilian non-human primate, is a readily used animal model in biomedical research, especially in neuroscience, reproductive medicine and stem cell research (14-16). This is mainly due to the genetic proximity and therefore associated cross-reactivity of most cytokines, growth factors, receptors and corresponding antibodies among marmosets and humans. In addition, the low body weight, high reproductivity in captivity and easy handling of the marmoset facilitate their use as valuable pre-clinical models for the validation of immunotherapeutic approaches (17, 18). Surprisingly, very little is known about the functional properties of the marmoset's NK cells. Therefore, we investigated the capacity of marmoset NK cells *in vitro* to eliminate cancer cells in an allogeneic and xenogeneic setting. For this purpose, we developed a method to isolate NK cells from peripheral blood of marmosets. The allogeneic and xenogeneic cytotoxic activity of the purified marmoset NK cells was tested using marmoset or human cells as targets. Moreover, the crosstalk between NK cells and primary healthy and tumor cells was investigated.

MATERIALS AND METHODS

Animal rights declaration

All animal work was strictly performed according to institutional guidelines and national regulations and was approved by the state office for protection of nature, environment, and consumers (LANUV) of North Rhine-Westphaelia, Germany. Retrieval of peripheral blood was performed in the Centre of Reproductive Medicine and Andrology (CeRA) Münster only in the context of other veterinary measures and was approved by the Institutional Animal Care.

Isolation of marmoset NK cells from peripheral blood and phenotypic analysis

Peripheral blood mononuclear cells (PBMCs) were isolated by centrifugation gradient of 3 to 5 mL fresh marmoset blood. Isolated PBMCs were labelled with the Phycoerythrin (PE)-conjugated anti-NKp30 mononuclear antibody (Beckmann Coulter, Krefeld, Germany) (clone Z25, 10µl/1x10^6 cells) for 30 min. Marmoset NK cells were isolated from 18 animals. B-cells were labelled with anti-CD20 (Genmab, Utrecht, The Netherlands) for 30 min followed by an incubation with a PE-conjugated anti-IgG (BD Biosciences) for 1 h at room temperature. Anti-PE microbeads (Miltenyi Biotech, Bergisch Gladbach, Germany) were used to isolate the labelled cells according to the manufacturer's instructions. Marmoset B-cells were isolated from 12 animals. The purity of the isolated cells was determined by flow cytometric analysis. For sequence comparison of B7-H6 between human and marmoset, MegAlign version 5.7 (DNASTAR Inc, Madison, WI, USA) and ClustalW2, NCBI were utilized.

Isolation of human NK and B-cells from healthy patients and leukemic blasts from patients

Human NK cells or B-cells were isolated from peripheral whole blood using the NK cell isolation kit II or B-cell isolation kit II (Miltenyi Biotec) respectively, according to the manufacturer's instructions. NK and B-cells were cultured in RPMI (Lonza, Cologne, Germany) supplemented with 2% AB serum (C.C. Pro, Oberdorla, Germany). Leukemic blasts from 2 B-cell lymphoma patients or 2 acute myeloid leukemia patients were isolated based on their CD138 expression (Miltenyi Biotec) by cell sorting (FACSAria, San Diego, CA).

Epstein-Barr virus immortalization of marmoset and human B-cells

Marmoset or human B-lymphoblastoid cell lines (B-LCL) were produced as previously described for human cells (19). Briefly, $1x10^8$ PBMCs cultured in RPMI supplemented with 10% FCS and Glutamin were incubated in 1 mL Epstein-Barr virus containing supernatant. The cell culture medium was changed once a week for a period of four weeks. We produced two B-LCLs named NASA and ZEO. Also the human B-LCLs 2151 and 1953 were produced.

Western blot

Cell extracts were prepared in lysis buffer (50 nM HEPES, 420 mM KCl, 1 mM ethylenediaminetetraacetate and 0.1% NP-40). The protein samples were separated on sodium dodecyl sulphate 10% to 20% gradient polyacrylamide gels (Life Technologies), electroblotted to polyvinylidene difluoride membranes (Life Technologies), and exposed to antibodies against B7-H6 or β-actin (abcam, Cambridge, UK). Secondary antibodies conjugated with horseradish peroxidase (DAKO) and 3,3',5,5'-tetramethylbenzidine, hydrogen peroxide substrate TMB (Kem-en-tec Diagnostic, Copenhagen, Denmark) were used for detection.

Real-Time PCR

Total RNA was isolated (RNAeasy kit, Qiagen) from NK cells after 48 h incubation with B7-H6-Fc (R&D Systems, Wiesbaden, Germany). A reverse transcription to complementary DNA was performed (High Capacity cDNA Reverse Transcription Kit, Life Technologies, Darmstadt, Germany). Fifty nanograms of total RNA were used in the reverse transcription for each reaction. To determine the levels of NKG2A, NKG2D and β-actin mRNA, specific Gene Expression Assays were used (Life Technologies). For the amplification of NKG2CE, specific primers described before (20) and an SYBR Green real-time PCR master mix (Life Technologies) were used. The thermal cycling settings on a Step Oneplus real-time PCR system (Life Technologies) were 95ºC for 10 min followed by 40 cycles at 95ºC for 15 sec and 60ºC for 1 min.

NK cell cytotoxic assays in presence or absence of NKp30 blocking antibody

Human or marmoset primary B-cells, B-LCL cells, or blasts of a human B-cell lymphoma or AML patients were labelled with CFSE (Molecular Probes, Eugene, OR), as previously described (21) and used as target cells. Freshly isolated NK cells were incubated with target cells in presence of 100 U/mL IL-2 (PeproTech) for 6 h at 10:1 and 5:1 Effector : Target (E:T) ratios *in vitro*. Target cell lysis was assessed by 7-aminoactinomycin D (7-AAD) staining (BD Biosciences, Heidelberg, Germany). For blocking of NKp30, freshly isolated NK cells were exposed for 2 h to an anti-NKp30 antibody (10µg/mL) (Beckman Coulter). NK cells were washed three times in PBS supplemented with 0.5% BSA and used in cytotoxic assays as described above. All experiments were performed in duplicate. To evaluate the NK-cell cytokine secretion profile, supernatant was collected and analyzed using a cytokine 14-plex panel and a Luminex 200 instrument (Invitrogen, Carlsbad, CA, USA).

Intracellular signaling assay

Marmoset NK cells treated with a Fc-blocking reagent (Sigma-Aldrich, Steinheim, Germany) were exposed to B7-H6-Fc (1µg/mL) for 5 min. An IgG protein was used as negative control. Also NK cells treated with an anti-NKp30 blocking antibody were stimulated with B7-H6-Fc protein. Activation of ERK1/2 was evaluated by FACS using BD Phosflow technologies. Stimulation was stopped using Cytofix buffer (BD Biosciences). Cells were permeabilized by incubation in 90% methanol for 15 min on ice and then washed with ice-cold PBS. A phospho-specific ERK1/2 (pT202/pY204) antibody (BD Biosciences) was used for the detection of phosphorylated ERK1/2.

NK cell proliferation assays

Freshly isolated marmoset NK cells were labelled with carboxyfluorescein diacetate succinimidyl ester (CFSE) [5- or 6-(Nsuccinimidyloxycarbonyl)-3′,6′-O,O′-diacetylfluorescein] from a CFDA SE cell tracer kit (Vybrant, Invitrogen, Carlsbad, CA, USA) at a final concentration of 4 mmol/L. CFSE-labelled NK cells were incubated with IL-2 (100U), B7-H6-Fc (1µg/mL) plus IL-2, B7-H6-Fc, IL-2 plus anti-NKp30 antibody. Proliferation of NK cells was assessed after 1 week by flow cytometry using a FACSCanto flow cytometer and FACSDiva software (BD Biosciences).

Statistical analysis

Statistical analysis was performed using the student *t* test for the comparison of two means or ANOVA when the means of more than two groups were compared. These analyses were performed using the GraphPad Prism v5.0 software (GraphPad Software Inc., La Jolla, CA, USA). Differences were considered statistically significant at $p<0.05$.

RESULTS

Homology between human and marmoset NCR3LG1

Sequence comparison of human (ENSEMBL ENSG00000188211) and marmoset (NCBI

Table I. *Cytokine secretion profile of marmoset NK cells upon B7-H6-Fc stimulation. Concentration means and standard deviation are shown for each analyte. Cytokine concentrations were measured in the supernatant of NK cells derived from four animals.*

Analyte pg/ml	IL-2	B7-H6-Fc + IL-2	IgG + IL-2 (NC)
IL-1β	21.3±15.6	133.1±95.6 (*)	29.9±12.6
IL-8	36.8±25.4	336.9±249.7 (**)	46.3±33.8
IFN-γ	20.3±16.2	422.9±226.6 (***)	18.6±33.6
TNF-α	8.2±3.4	98.5±51.4 (***)	7.5±3.6

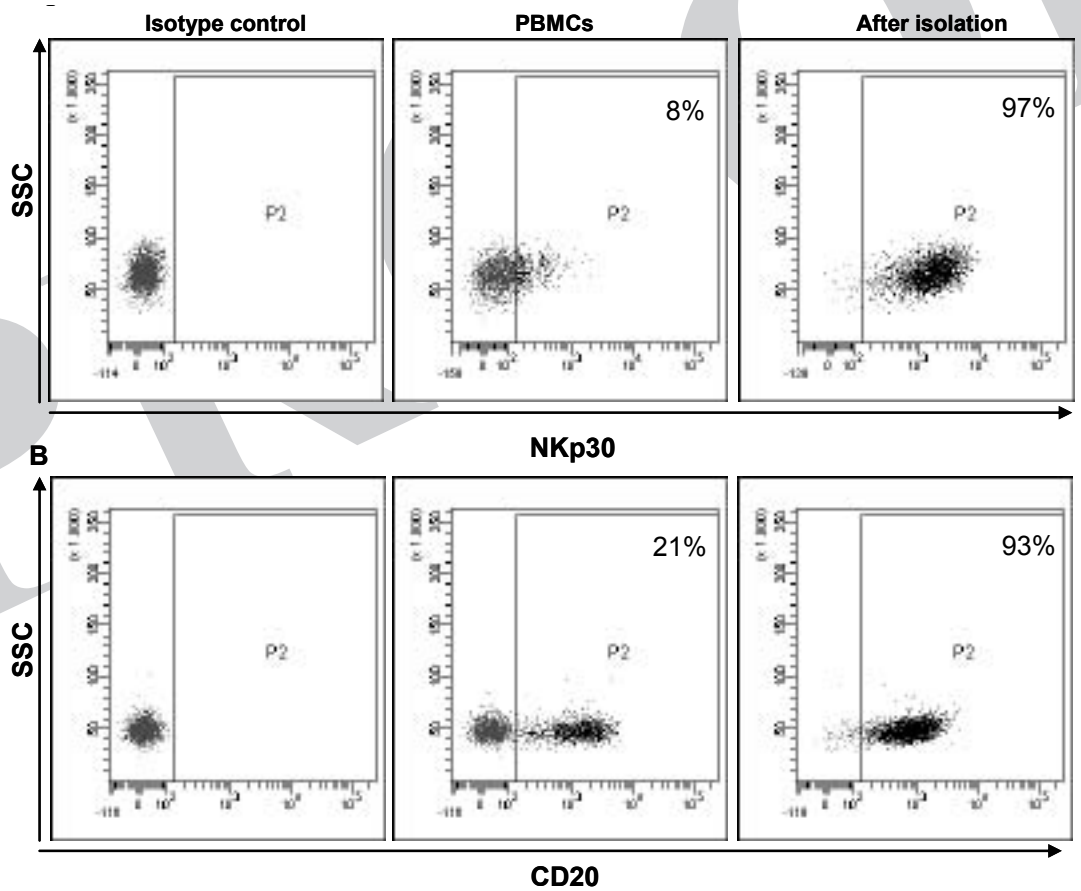

Fig. 1. *Isolation of NK-cell and B-cell subsets from marmoset peripheral whole blood. Peripheral blood mononuclear cells (PBMCs) were isolated using density gradient centrifugation. After washing, PBMCs were stained with Phycoerythrin (PE)-labelled antibodies specific for NKp30 or CD20. Labelled cells were incubated with anti-PE microbeads and sorted using MACS technology. The FACS dot plots display (A) NK or (B) B-cell populations before and after isolation.*

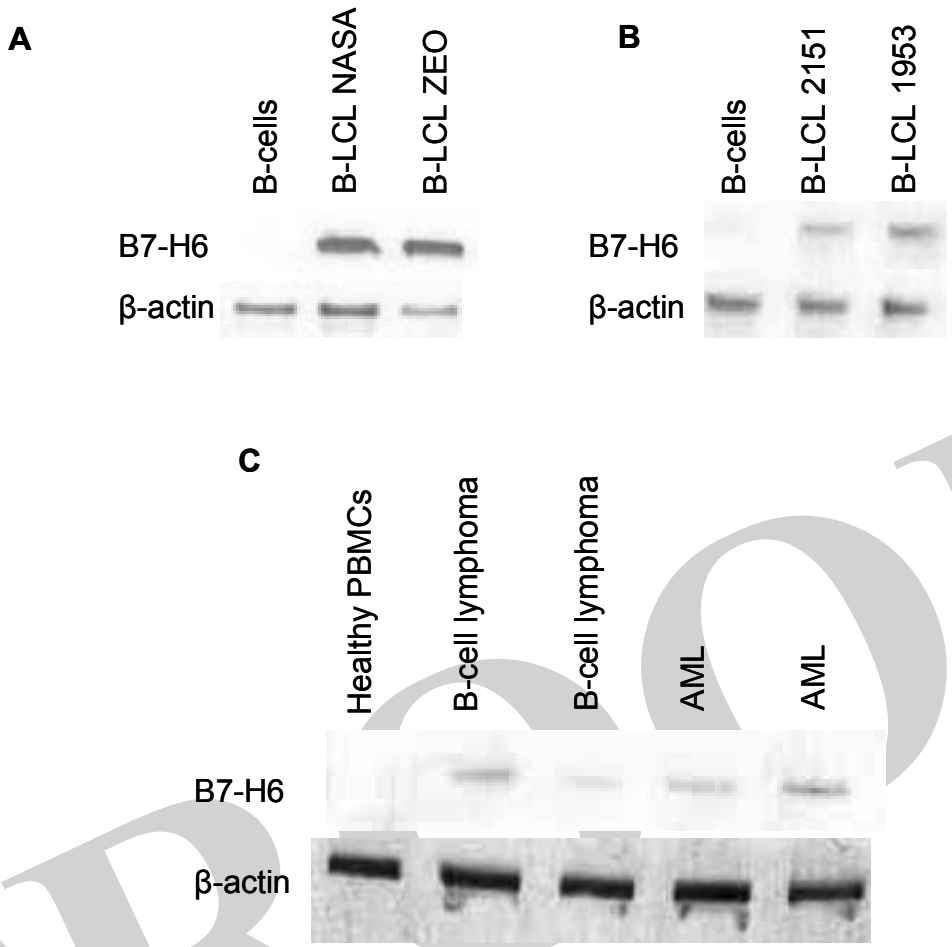

Fig. 2. *Expression of B7-H6 antigens in human or marmoset primary cells and cell lines. **A**) B7-H6 expression on marmoset-derived primary B-cells or B-lymphoblastoid cell lines (**B**) B7-H6 expression on human-derived primary B-cells or B-lymphoblastoid cell lines and (**C**) B7-H6 expression on healthy human peripheral blood mononuclear cells or native leukemia cells derived from B-cell lymphoma or acute myeloid leukemia.*

XM_003734221.1) NKp30 revealed 83% homology on nucleotide level and 70% on amino acid level as assessed by MegAlign and ClustalW2 (NCBI). Despite the relatively low overall homology, changes in functional elements are minimal. N-glycosylation sites at positions AA 43, 57, 174, and 242 were present, the other three sites were changed 208N-S, 216N-K and 260N-T. Furthermore, the important NCR3 interaction sites at positions AA 59-62 and 127-30 were preserved with two exchanges 61M-V and 129 L-K.

Isolation of marmoset NK cells and B-cells from marmoset peripheral blood

We have developed a strategy to isolate NK cells and B-cells subpopulations from peripheral whole blood of marmosets as described in the Materials and Methods section. NK cells or B-cells were separated from PBMCs based on their NKp30 or CD20 expression, respectively. NK cell subsets were isolated with average purity of 82%±15%. NK cell populations isolated with purities above 90% were used for further experiments. Primary B-cells were isolated from the PBMC population with a mean purity of 87±9% (Fig. 1).

Marmoset- and human-derived primary tumor cells and cell lines express B7-H6 antigens

B7-H6 was recently identified as a ligand for the activating receptor NKp30. Therefore, we evaluated

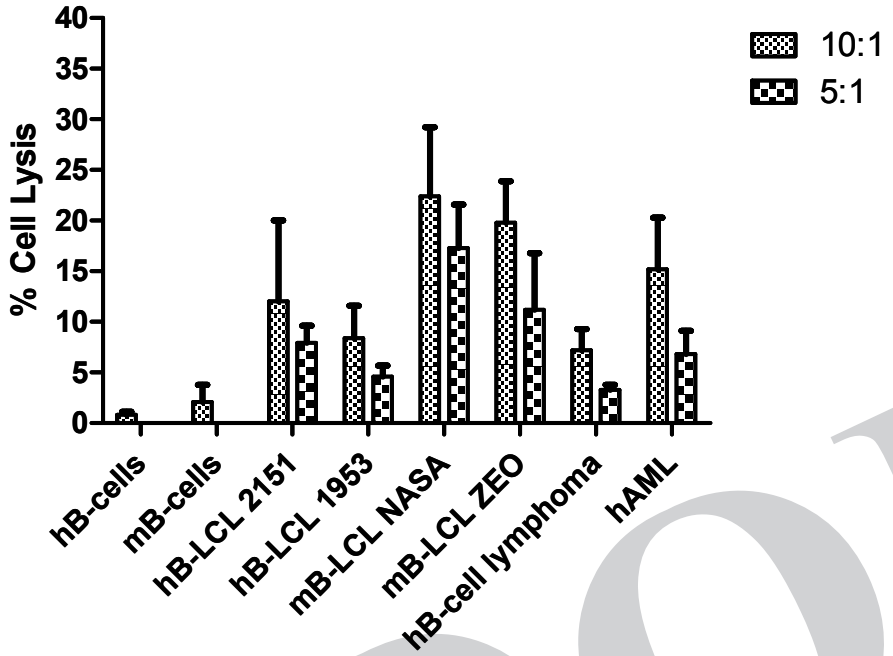

Fig. 3. *Allogeneic and xenogeneic cytotoxic activity of marmoset NK cells. Marmoset NK cells were incubated in the presence of human or marmoset-derived primary B-cells, human or marmoset-derived B-lymphoblastoid cell lines (B-LCL) or blasts of human B-cell lymphoma or acute myeloid leukemia patients at effector: target ratio 10:1 and 5:1 for 6 h. Cell lysis was evaluated by flow cytometry after staining with 7-AAD. The graphs display the mean and standard deviation of four independent experiments performed in duplicate using four different animals.*

the expression of B7-H6 on marmoset and human-derived B-LCLs. In contrast to primary B-cells of marmoset or human origin, all B-LCLs showed high B7-H6 antigen expression. Also B-cells isolated from a B-cell lymphoma or native blast of an acute myeloid leukemia patient (M2) showed to express B7-H6 antigen (Fig. 2).

Allogeneic and xenogeneic NK cell cytotoxic activity

Isolated marmoset NK cells were incubated with human or marmoset target cells to determine their cytotoxic potential. At an E:T cell ratio 10:1, marmoset NK cells were able to lyse 0.8±0.3% of primary human B-cells. 2.1±1.7% of primary marmoset B-cells were lysed by allogeneic NK cells. The cytotoxic activity of marmoset NK cells showed to be significantly higher when B-LCL cells of human or marmoset origin were used as target cells. 22±6.4% of NASA and 19.8±4.1% ZEO cells were lysed upon exposure to allogeneic NK cells. Interestingly, lysis rates by up to 20% were observed when the human B-LCL 2151 was used. Additionally, marmoset NK cells were capable of lysing 7.2±2.1% of primary tumor B-cells isolated from a human B-cell lymphoma. Similarly, acute myeloid leukemia cells were lysed by up to 20.3% by marmoset NK cells (Fig. 3). These results suggest the capacity of marmoset NK cells to lyse normal and tumor cells in an allogeneic and xenogeneic setting.

Blocking B7-H6 receptor inhibits NK cell cytotoxicity

To evaluate whether marmoset NK cell cytotoxicity is dependent on the interaction with B7-H6 expressed on tumor cells, an NKp30 blocking antibody was used. Marmoset NK cell cytotoxic activity was not affected by blocking NKp30 when using primary human or marmoset target cells. However, a significant inhibition of the capacity of marmoset NK cells to lyse human B-LCL cells

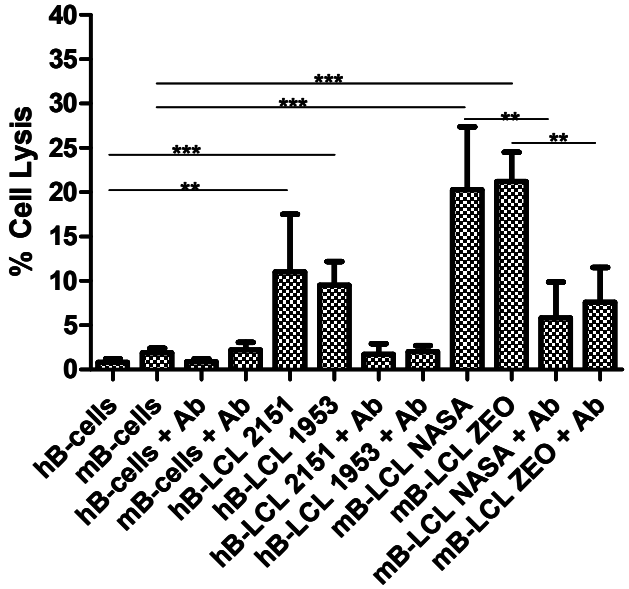

Fig. 4. *Marmoset NK cell cytotoxic activity against tumor cell lines is dependent on B7-H6 engagement with NKp30. NK cells were treated with an NKp30 blocking antibody. Non-treated NK cells were used as control. Cytotoxic assays were performed by incubation of marmoset NK cells (treated and non-treated) with primary human or marmoset B-cells (lacking B7-H6 expression) or B-LCL cells (expressing B7-H6 antigens). NK cells were incubated with the target cells at effector: target ratios of 10:1. Cell lysis was evaluated by flow cytometry after staining with 7-AAD. The graphs display the mean and standard deviation of three independent experiments using three animals as cell donors. Each experiment was performed in duplicate. Statistical significance is indicated by asterisks (* $p<0.05$, ** $p<0.01$, *** $p<0.001$).*

(2151: 1.7±1.2%; 1953: 2±0.7%, both $p<0.001$) was observed in comparison to non-blocked NK cells (2151: 11±6.5%; 1953: 9.5±2.7%). Similarly, significant decreases in the NK cell lysis rates were detected for marmoset cells (NASA: 5.8±4.1%; ZEO: 7.6±3.9%, $p<0.001$) (Fig. 4). These data indicate that the allogeneic and xenogeneic cytotoxic activity of marmoset NK cells against B-LCL target cells is dependent on B7-H6 interaction.

B7-H6-Fc stimulation of marmoset NK cells trigger ERK1/2 activation

To investigate whether the engagement of B7-H6 antigen with NKp30 receptor was able to trigger activation of marmoset NK cells independently of other factors, we used a chimeric B7-H6-Fc protein to stimulate NK cells. Exposure of NK cells to B7-H6-Fc resulted in a significant increase in ERK1/2 phosphorylation (MFI: 1540±960, $p<0.01$) in comparison to non-stimulated (MFI: 37±51) or IL-2-stimulated NK cells (MFI: 130±282). In addition, ERK1/2 phosphorylation levels induced by stimulation with B7-H6-Fc were significantly reduced by the pre-treatment of NK cells with an anti-NKp30 antibody (MFI: 455±218; $p<0.01$) (Fig. 5A). These data suggest that B7-H6 directly interacts with marmoset NKp30.

Marmoset NK cell proliferation is significantly increased by B7-H6-Fc

As ERK1/2 is a major regulator of proliferation, we investigated whether B7-H6 might trigger NK cell proliferation. IL-2-stimulated NK cells showed a mean proliferation of 6.2±3.6%. A combination of B7-H6-Fc with IL-2 caused a significant increase in NK cell proliferation (66.9±18.7%, $p<0.001$). Pre-incubation of NK cells with an anti-NKp30 antibody significantly abrogated the effect of B7-H6-Fc in NK cell proliferation (15.6±10.2%, $p<0.01$) (Fig. 5B). These results indicate that B7-H6 strongly induces NK cell proliferation after engagement with its receptor NKp30.

B7-H6-Fc binding alters the cytokine secretion profile of marmoset NK cells

Alterations in the cytokine secretion profile of NK cells may indicate a change in their regulatory and effector activity. Therefore, we evaluated the effect of B7-H6 in the regulation of cytokine secretion of marmoset NK cells. A significant increase in the secretion of IL-1b (133.1±95.6 pg/ml, $p<0.05$) was observed upon stimulation of NK cells with B7-H6-Fc in combination with IL-2 as compared to the stimulation with IL-2 alone (21.3±15.6 pg/ml) or in combination with a control protein (IgG) (29.9±12.6 pg/ml). Furthermore, a strong increase in IL-8 levels (336.9±249.7 pg/ml, $p<0.01$) was induced by the presence of B7-H6-Fc in comparison to IL-2 alone (36.8±25.4 pg/ml) or when IgG was used (46.3±33.8 pg/ml). Moreover, a significant increase in effector cytokines such as IFN-γ (422.9±226.6

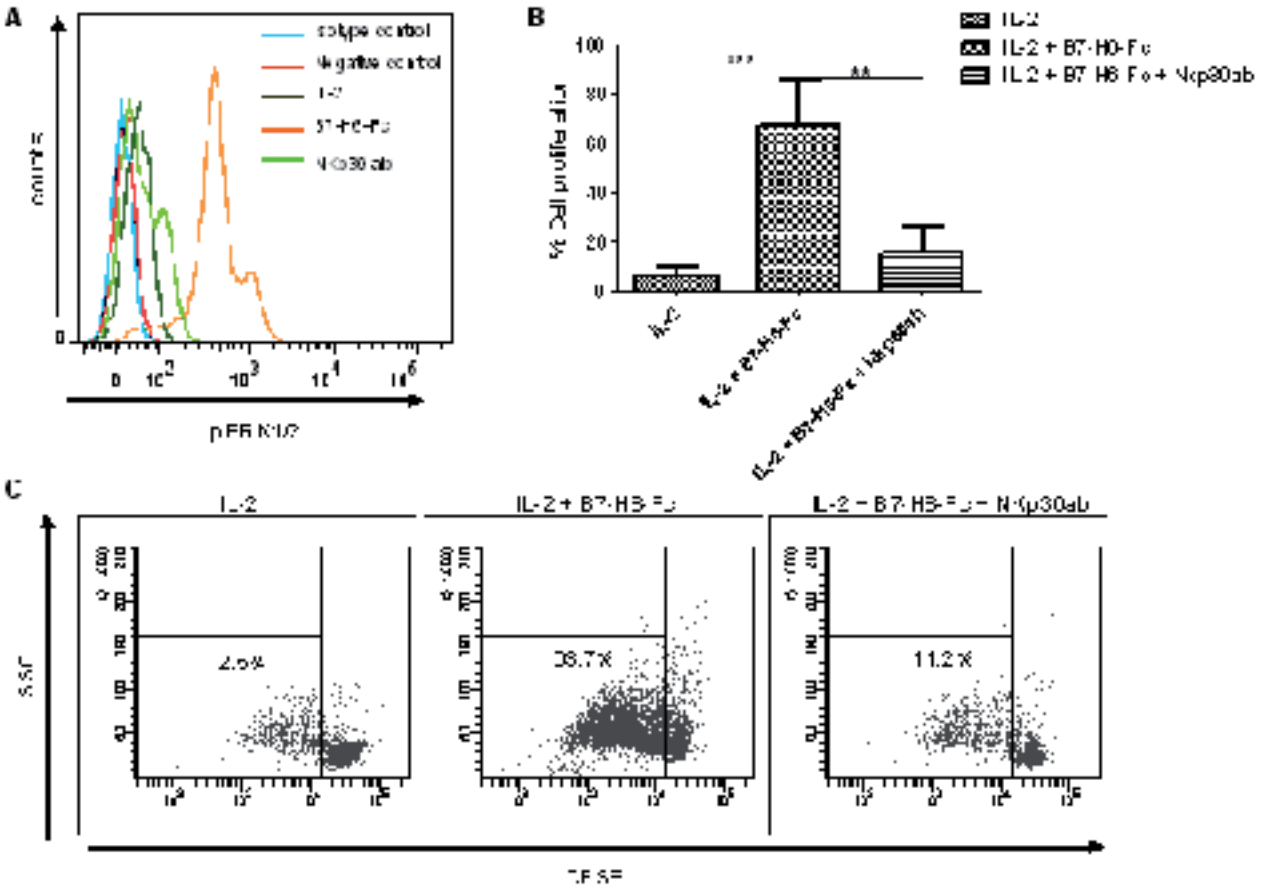

Fig. 5. *Stimulation of marmoset NK cells with B7-H6-Fc induces ERK1/2 activation and cell proliferation. Marmoset NK cells were exposed to recombinant B7-H6-Fc proteins in presence or absence of an anti-NKp30 antibody.* ***A****) ERK1/2 phosphorylation was detected after 5 min of stimulation of NK cells with B7-H6-Fc protein.* ***B****) NK cell proliferation assays were performed by incubating CFSE-labelled NK cells blocked or non-blocked for NKp30 with IL-2 alone or in combination with B7-H6-Fc protein. NK cell proliferation was analyzed by flow cytometry. The graphs display mean and standard deviations of four independent experiments using four animals as cell donors. Statistical significance is indicated by asterisks (* p<0.05, ** p<0.01,*** p<0.001). (C) The dot plots depict a representative NK cell proliferation experiment.*

pg/ml) and TNF-α (98.5±51.4 pg/ml) were detected upon stimulation with B7-H7-Fc in comparison to the levels produced by NK cells stimulated with IL-2 alone (IFN-γ:20.3±16.2; TNF-α: 8.2±3.4 pg/ml) or in presence of IgG (IFN-γ:18.6±33.6; TNF-α: 7.5±3.6 pg/ml) (Table I). These data suggest that the engagement of NKp30 with its ligand B7-H6 alters the cytokine secretion profile of NK cells.

B7-H6-Fc modulates the receptor repertoire of NK cells

Furthermore, we investigated whether the interaction of B7-H6-Fc might modulate the NK cell receptor repertoire. Therefore, we investigated the transcript levels of the inhibitory receptor NKG2A and the activating receptors NKG2CE and NKG2D. A minor increase in the levels of NKG2A transcripts (2.7±1.5) were detected upon B7-H6-Fc NK cell stimulation in comparison to IL-2 alone or IL-2 in combination with IgG (1.3±0.5). Interestingly, a significant increase in transcript levels of the activating receptors NKG2CE and NKG2D (NKG2CE: 7.5±4.2, $p<0.05$; NKG2D: 8.2±3.3) were observed upon NK cell stimulation with B7-

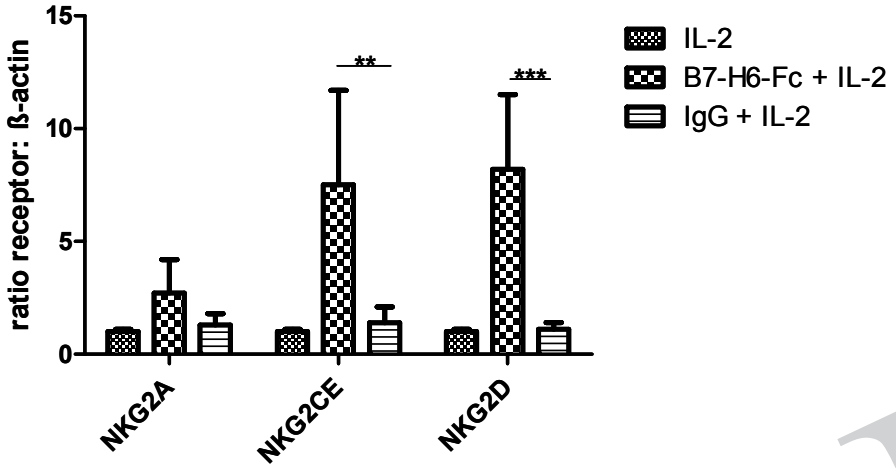

Fig. 6. *B7-H6 protein alters NK cell receptors transcript levels. Marmoset NK cells were stimulated with IL-2 alone, IL-2 plus B7-H6-Fc or IL-2 plus IgG for 48 h. Transcript levels of NKG2A, NKG2CE and NKG2D were assessed by real-time PCR. The graph shows mean and standard deviation of four independent experiments using four animals as cell donors. Statistical significance is indicated by asterisks (* $p<0.05$, ** $p<0.01$, *** $p<0.001$).*

H6-Fc (Fig. 6). These results demonstrate that B7-H6 has the capacity to modulate the marmoset NK cell phenotype to a more activated state.

DISCUSSION

Several preclinical studies have been published that demonstrate potential for utilizing NK cells as an effective immunotherapy for various type of cancers. Design and selection of appropriate animal models is crucial for the evaluation of the effectiveness and safety of those therapies (22). Marmosets exhibit an NK cell phenotype more similar to humans than rats or mice, and therefore represent a potentially useful animal model (20). In this report, we describe a method to isolate NK cells from marmoset peripheral whole blood. The isolation of blood cell subpopulations is essential for the evaluation and monitoring of immune responses *in vitro*. Furthermore, we assessed the capacity of marmoset NK cells to lyse tumor cells in an allogeneic and xenogeneic setting based on the interaction of the NKp30 receptor and the B7-H6 protein expressed on target cells. In contrast to mice, in which NKp30 is a pseudogene and therefore not expressed (23), marmosets express a functional NKp30 receptor. Recently, B7-H6 was described as a novel ligand for NKp30. In marmosets, we could detect the expression of B7-H6 antigen in tumor cells. A direct protein sequence comparison between human and marmoset B7-H6 retrieved a homology of 72%. In contrast to other members of the B7 family, such as B7-H1, 4IgB7-H3, and B7-H4, which were shown to inhibit the immune response against tumors, B7-H6 engagement with NKp30 strongly enhances NK cell activity. B7-H6 has been shown to be expressed in primary tumors and cell lines, but not in normal tissues. Previous studies have reported the expression of B7-H6 antigens in cell lines and in primary lymphoma cells (9). We detected B7-H6 antigen not only in primary lymphoma cells but also in blasts of an acute myeloid leukemia (M2) patient. Thus, this protein might constitute a potential candidate for the development of therapeutic approaches against cancer. In this study, we demonstrated that marmoset NK cell capacity of lysing B7-H6 expressing marmoset B-LCL cells is also dependent on NKp30 interaction. Interestingly, we also observed that xenogeneic cytolytic activity of marmoset NK cells against human B-LCL cells is strongly dependent on the interaction of B7-H6 with NKp30. These findings demonstrate that the elimination of cancer

cells through the interaction between NKp30 and B7-H6 is an evolutionary conserved mechanism. Recent studies have demonstrated that NK cell cytotoxicity is strongly dependent on the engagement of activating receptors (24, 25). We observed that the allogeneic and xenogeneic activity of marmoset NK cells against their B7-H6 positive targets is less dependent on the absence of MHC class I molecules but strongly relies on the interaction of B7-H6 with it receptor NKp30, as the increased NK cell lysis rates were abrogated through pre-treatment with a NKp30-specific antibody. Novel NK cell-based therapeutic approaches focus on the reduction of inhibitory signalling or the enhancement of activating signals. Although inhibitory ligand-receptor interactions are well characterized, less is known about activating ligand-receptor interactions in NK cells. The current study suggests that natural cytotoxic receptor–ligand system may also offer the possibility to develop efficient and specific therapeutic strategies against tumor cells. In addition, NK cells are able to secrete a large panel of cytokines involved in their immunomodulatory and effector functions (26). B7-H6 interaction with NKp30 triggered the secretion of the pro-inflammatory cytokine IL-1b, which is capable of activating and polarizing other immune cells, such as Th17 subsets, and of inducing the release of immunomodulatory molecules such as the NKG2D-ligand MICA (27). In addition, the secretion of IL-8, TNF-α and IFN-γ was shown to be increased by B7-H6 stimulation, indicating its contribution for the amplification and regulation of the immune response. In addition, we observed that B7-H6 causes a significant augmentation of NKG2D transcripts. Also, the transcript levels of NKG2CE, an ancestral form of the NKG2C- and NKG2E-activating receptor genes of humans and great apes, were shown to be upregulated by B7-H6. NKG2D ligands, human ULBP and MICs proteins are often expressed by a wide range of tumor cell lines of different tissue origins (28, 29). Thus, B7-H6 also increases the potential of NK cells to recognize other danger signals through the upregulation of activating receptorIn conclusion, given the similarity between the mechanisms used by the marmoset to eliminate tumor cells, they might constitute a privileged model to evaluate the efficiency of novel anti-tumor NK cell-based therapies.

ACKNOWLEDGEMENTS

We thank Michael Engelmann and Kirsten Elger for excellent technical support. Our gratitude also includes Prof. Stefan Schlatt from the Centre for Reproductive Biology and Andrology (CeRA) for donation of blood from the common marmoset. This work was supported by funding from the German Research Foundation (DFG) for the Cluster of Excellence REBIRTH (From Regenerative Biology to Reconstructive Therapy) and from the Institute for Transfusion Medicine of the Hannover Medical School.

REFERENCES

1. Vivier E, Raulet DH, Moretta A, et al. Innate or adaptive immunity? The example of natural killer cells. Science 2011; 331:44-49.
2. Correia DV, Fogli M, Hudspeth K, et al. Differentiation of human peripheral blood Vdelta1+ T cells expressing the natural cytotoxicity receptor NKp30 for recognition of lymphoid leukemia cells. Blood 2011; 118:992-1001.
3. Delahaye NF, Rusakiewicz S, Martins I, et al. Alternatively spliced NKp30 isoforms affect the prognosis of gastrointestinal stromal tumors. Nat Med 2011; 17:700-707.
4. Pende D, Parolini S, Pessino A, et al. Identification and molecular characterization of NKp30, a novel triggering receptor involved in natural cytotoxicity mediated by human natural killer cells. J Exp Med 1999; 190:1505-16.
5. Hartmann J, Tran TV, Kaudeer J, et al. The stalk domain and the glycosylation status of the activating natural killer cell receptor NKp30 are important for ligand binding. J Biol Chem 2012; 287:31527-39.
6. Joyce MG, Tran P, Zhuravleva MA, et al. Crystal structure of human natural cytotoxicity receptor NKp30 and identification of its ligand binding site. Proc Natl Acad Sci U S A 2011; 108:6223-28.
7. Pogge von Strandmann E, Simhadri VR, von Tresckow B, et al. Human leukocyte antigen-B-associated transcript 3 is released from tumor cells and engages the NKp30 receptor on natural killer cells. Immunity 2007; 27:965974.
8. Simhadri VR, Reiners KS, Hansen HP, et al. Dendritic

cells release HLA-B-associated transcript-3 positive exosomes to regulate natural killer function. PLoS One 2008; 3:e3377.
9. Brandt CS, Baratin M, Yi EC, et al. The B7 family member B7-H6 is a tumor cell ligand for the activating natural killer cell receptor NKp30 in humans. J Exp Med 2009; 206:1495-503.
10. Li Y, Wang Q, Mariuzza RA. Structure of the human activating natural cytotoxicity receptor NKp30 bound to its tumor cell ligand B7-H6. J Exp Med 2011; 208:703-14.
11. Kaifu T, Escaliere B, Gastinel LN, et al. B7-H6/NKp30 interaction: a mechanism of alerting NK cells against tumors. Cell Mol Life Sci 2011; 68:3531-39.
12. Brehm C, Huenecke S, Quaiser A, et al. IL-2 stimulated but not unstimulated NK cells induce selective disappearance of peripheral blood cells: concomitant results to a phase I/II study. PLoS One 2011; 6:e27351.
13. Tallerico R, Todaro M, Di Franco S, et al. Human NK Cells Selective Targeting of Colon Cancer-Initiating Cells: A Role for Natural Cytotoxicity Receptors and MHC Class I Molecules. J Immunol 2013; 190:2381-90.
14. Okano H, Hikishima K, Iriki A, et al. The common marmoset as a novel animal model system for biomedical and neuroscience research applications. Semin Fetal Neonatal Med 2012; 17:336-40.
15. Leibovitch E, Wohler JE, Cummings Macri SM, et al. Novel Marmoset (Callithrix jacchus) Model of Human Herpesvirus 6A and 6B Infections: Immunologic, Virologic and Radiologic Characterization. PLoS Pathog 2013; 9:e1003138.
16. Wiedemann A, Hemmer K, Bernemann I, et al. Induced pluripotent stem cells generated from adult bone marrow-derived cells of the nonhuman primate (Callithrix jacchus) using a novel quad-cistronic and excisable lentiviral vector. Cell Reprogram 2012; 14:485-96.
17. Ward JM, Vallender EJ. The resurgence and genetic implications of New World primates in biomedical research. Trends Genet 2012; 28:586-91.
18. Tardif SD, Mansfield KG, Ratnam R, et al. The marmoset as a model of aging and age-related diseases. Ilar J 2011; 52:54-65.
19. Hinrichs J, Foll D, Bade-Doding C, et al. The nature of peptides presented by an HLA class I low expression allele. Haematologica 2010; 95:1373-80.
20. Averdam A, Kuhl H, Sontag M, et al. Genomics and diversity of the common marmoset monkey NK complex. J Immunol 2007; 178:7151-61.
21. Figueiredo C, Wittmann M, Wang D, et al. Heat shock protein 70 (HSP70) induces cytotoxicity of T-helper cells. Blood 2009; 113:3008-16.
22. Ostrand-Rosenberg S. Animal models of tumor immunity, immunotherapy and cancer vaccines. Curr Opin Immunol 2004; 16:143-50.
23. Hollyoake M, Campbell RD, Aguado B. NKp30 (NCR3) is a pseudogene in 12 inbred and wild mouse strains, but an expressed gene in Mus caroli. Mol Biol Evol 2005; 22:1661-72.
24. Meinke S, Watzl C. NK cell cytotoxicity mediated by 2B4 and NTB-A is dependent on SAP acting downstream of receptor phosphorylation. Front Immunol 2013; 4:3.
25. Pende D, Marcenaro S, Falco M, et al. Anti-leukemia activity of alloreactive NK cells in KIR ligand-mismatched haploidentical HSCT for pediatric patients: evaluation of the functional role of activating KIR and redefinition of inhibitory KIR specificity. Blood 2009; 113:3119-29.
26. Lunemann A, Lunemann JD, Munz C. Regulatory NK-cell functions in inflammation and autoimmunity. Mol Med 2009; 15:352-58.
27. Kohga K, Tatsumi T, Tsunematsu H, et al. Interleukin-1beta enhances the production of soluble MICA in human hepatocellular carcinoma. Cancer Immunol Immunother 2012; 61:1425-32.
28. Pende D, Cantoni C, Rivera P, et al. Role of NKG2D in tumor cell lysis mediated by human NK cells: cooperation with natural cytotoxicity receptors and capability of recognizing tumors of nonepithelial origin. Eur J Immunol 2001; 31:1076-86.
29. Friese MA, Platten M, Lutz SZ, et al. MICA/NKG2D-mediated immunogene therapy of experimental gliomas. Cancer Res 2003; 63:8996-9006.

IF YOU HAVE AN ACTIVE VAGUS NERVE, CANCER STAGE MAY NO LONGER BE IMPORTANT

Y. GIDRON[1], M. DE COUCK[1] and J. DE GREVE[1,2]

[1]Faculty of Medicine and Pharmacy, Free University of Brussels (VUB), Belgium; [2]Department of Medical Oncology, Oncological Center UZ, Brussels, Belgium

Received March 8, 2013 – Accepted March 6, 2014

The parasympathetic system, and primarily the vagus nerve, informs the brain about multiple signals and returns the body to homeostasis. Recent studies have shown that vagal nerve activity independently predicts prognosis in cancer. Here, we take this one step further and show that when vagal nerve activity is high, cancer stage no longer predicts tumor burden. We examined whether vagal nerve activity, indexed by Heart Rate Variability (HRV), moderated the effects of initial tumor stage on tumor burden at follow-up. Patients' HRVs were derived from ECGs near diagnosis in colorectal cancer (CRC) and in prostate cancer (PC) patients. Outcomes included the tumor markers carcinoembryonic antigen (CEA) at 12 months for CRC and prostate-specific antigen (PSA) at 6 months for PC. As would be expected, initially advanced tumor stages of CRC or PC predicted higher tumor marker levels at follow-up than did early stages. However, this occurred only in patients with low, not high, vagal activity (HRV). Furthermore, in patients with advanced tumor stage at diagnosis, high HRV predicted lower tumor marker levels than did low HRV, in both cancers. Estimating a cancer patient's prognosis by determining his tumor stage needs to also consider the vagal nerve activity. This activity is easily measurable, and it determines in which subjects the tumor stage is prognostic. Importantly, higher vagal activity may even protect against the adverse effects of advanced cancer stage. These findings, observed in two distinct cancers, support the hypothesized neuroimmunomodulatory effects of vagal nerve activity on tumors.

A major task in clinical research is to identify prognostic factors that enable the clinician to estimate a patient's prognosis. This process is crucial in determining an evidence-based and personalized treatment for improving the patient's specific prognosis. Identifying prognostic factors that can be therapeutically changed helps to develop new treatments that target such factors. In oncology, a main prognostic factor is tumor stage, which reflects disease severity. Numerous other prognostic factors exist, including general background variables such as age, certain proteins or expressed genes, tumor markers, inflammatory parameters (e.g., C-reactive protein) (1), and organ functioning (e.g., forced expiratory volume in 1 second - FEV1, in lung cancer) (2), some of which are amenable to change. However, at times, some routinely used factors (e.g., stage or CRP) can predict prognosis, only in certain subgroups (e.g., in women but not in men, or in people over the age of 60 years). Such classifying variables (e.g., age) are statistically termed "moderators", and determine when another factor has prognostic value. Identifying such moderating factors helps clinicians to more precisely estimate prognosis and can assist in developing

Key words: vagal nerve activity, cancer prognosis, cancer stage, moderation, homeostasis

Mailing address: Yori Gidron, PhD.,
Faculty of Medicine and Pharmacy,
Free University of Brussels (VUB),
103, Laarbeeklaan, Jette,
1090, Brussels, Belgium
Tel.: +32 2 477 41 02 Fax: +32 2 477 41 59
e-mail: yori.gidron@vub.ac.be

0393-974X (2014)

DISCLOSURE: ALL AUTHORS REPORT NO CONFLICTS OF INTEREST RELEVANT TO THIS ARTICLE.

more tailored treatments. This study proposes a new important moderating factor, namely the extent of vagal nerve activity, which may determine in which patients cancer stage predicts prognosis. Furthermore, high vagal nerve activity may even have protective and prognostic roles on its own.

The vagus nerve is a main component of the parasympathetic nerve system. It mainly has afferent fibers which inform the brain about multiple peripheral signals from different systems, which in return it also modulates (3). Vagal nerve activity can be non-invasively measured by Heart Rate Variability (HRV), the variation in normal consecutive beat-to-beat (R-R peaks) intervals, obtained from an electrocardiogram (ECG) (4). Analysis of the differences between successive heart beats can be accomplished with reference to time (time domain analysis) or frequency (frequency domain analysis). In this study, we focus on one main time domain parameter, namely 'standard deviation of normal beat to beat intervals', SDNN (in msec) (4). HRV is highly correlated with vagal nerve activity (r = 0.88) (5) and is mainly under the control of and reflects efferent cardiac vagal nerve activity. HRV has been found to predict onset, short and long-term prognosis in multiple health conditions including cardiovascular diseases, emergency medicine, cancer, dementia, and mental health, to name but a few examples (6-9).

Vagal nerve activity is also relevant to cancer. Recent studies have shown that signals which normally emanate from the sympathetic nervous system,\ including norepinephrine, influence tumor invasiveness, metastasis and angiogenesis (10). In contrast, it has been hypothesized that high vagal nerve activity could slow down tumor progression since it inhibits three mechanisms contributing to tumor progression, namely excessive inflammation, oxidative stress and excessive sympathetic activity (8, 11). The vagus nerve also innervates multiple organs where severe cancers develop (e.g., colon, pancreas, lungs). High HRV was found to predict longer cancer survival and reduced tumor burden, and in some studies, these relationships were independent of confounders including cancer stage and treatment (6, 12-14). One important study also found that people with relatively high vagal nerve activity, upon exposure to acute stress, returned faster to baseline levels on endocrine, cardiovascular and inflammatory parameters, compared to those with low vagal activity (15). Together, these findings clearly show the modulatory and homeostatic roles of the vagus nerve in health and disease.

If the vagus nerve functions as a neuromodulatory and protective system in cancer, could it perhaps act as a protector against the adverse effects of known prognostic factors? This study examined in two different cancers whether the effects of initial cancer stage on tumor burden were weakened by high vagal nerve activity. Similarly to Weber et al. (15), we examined the relationship between cancer stage and tumor burden, separately in low and high HRV groups.

MATERIALS AND METHODS

Design

This study used a "historical prospective" design. Though it appears as a retrospective design, formally it is not since the measurement of the predictor variables (stage, HRV) preceded in time the measurement of the outcome variable (tumor markers at follow-up). In a historical prospective design, archival data are analyzed. ECGs were obtained near cancer diagnosis, and the prospective relationships between initial cancer stage and HRV, with tumor markers at follow-up, were tested. This design is commonly used in the reanalysis of existing datasets (e.g. 16).

Participants

After approval of the Medical Ethics Committee, medical records of 246 colorectal cancer (CRC) patients with electrocardiograms (ECG) treated at the Jules Bordet Hospital, Brussels, between March 2001 and December 2006, were reviewed. The same procedure was carried out at the University Hospital of Brussels (UZ), where the medical records of 620 patients with prostate cancer (PC) treated between January 2005 and December 2009, were reviewed. Exclusion criteria included conditions known to alter HRV or influence inflammation such as heart diseases, treatments with anti-arrhythmic drugs or beta-blockers, having a pacemaker, chronic inflammatory disease and thyroid disease. Following these strict exclusion criteria, we finally analyzed the data of N = 72 CRC patients and of N = 113 PC patients. The highest number of patients was excluded due to missing ECGs.

Measures

Background and prognostic data. For each cancer,

background information included age, gender, cancer stage, and treatments.

Vagus nerve activity

This was indexed by deriving Heart Rate Variability (HRV) from patients' 10 second- ECG near diagnosis. HRV is highly correlated with vagal nerve activity (r = 0.88) (5) and is mainly under the control of and reflects efferent cardiac vagal nerve activity. Concerning certain HRV parameters, such short ECGs have been found to correlate with ECGs of longer durations (5 and 10 min) (17). The time domain parameter 'standard deviation of normal beat to beat intervals', named SDNN (in msec), was derived. SDNN measured during 10 sec has been shown to predict tumor marker levels in colon cancer (13). A cut-off of 20 msec was used, as in past studies on cancer (13, 18, 19), to distinguish between patients with high and low HRV.

Tumor burden at follow-up

We examined the tumor markers Prostate Specific Antigen (PSA) at 6 months for PC and Carcinoembryonic antigen (CEA) at 1 year for CRC, obtained from medical files.

Statistical analysis

We examined whether vagal nerve activity (indexed by HRV) moderated (modified) the relationship between stage and tumor marker levels at follow-up. We first examined with an analysis of variance the relationship between stage and tumor markers. The 20 msec cut-off was used to classify patients into low and high HRV (18, 19). We then examined the relationships between stage and tumor marker levels at follow-up, separately for patients with low and high HRV. This enabled us to test whether HRV moderated the stage - tumor marker relationship. Finally, we also examined whether HRV (low versus high) predicted tumor marker levels, at each cancer stage group. This enabled us to test whether vagal nerve activity protected against the effects of advanced cancer stage on tumor marker levels, if HRV was prognostic in more advanced tumor stages.

RESULTS

Descriptive statistics of the two patient samples are presented in Table I. The distribution of patients as a function of cancer stage was slightly different

Table I. *General patient characteristics in prostate cancer and colorectal cancer.*

	Prostate cancer (N=113)	Colorectal cancer (N=72)
Variable	Mean (or %) SD	Mean (or %) SD
Age	65.1 (8.9)	63.7 (10.8)
Gender (% men)	100%	37.5%
Baseline tumor marker	130.0 (520.7)	68.1 (151.7)
Follow-up tumor marker	9.4 (36.2) (6-mo)	87.9 (291.6) (1 year)
% Stage I, II, III, IV	0, 60.0, 14.5, 25.5	20.0, 12.5, 27.5, 40.0
HRV (SDNN)	39.9 (57.9)	23.4 (21.0)
Chemotherapy (%)	2.0	32.5
Surgery (%)	62.2	97.5
Radiotherapy (%)	47.5	—
Hormonal (%)	43.3	—

SD: Standard deviation; HRV: Heart rate variability; SDNN: standard deviation of normal beat to beat intervals

between the two cancers, reflecting the more severe nature of CRC. In PC, as expected, the cancer stage significantly predicted PSA levels at 6 months in the total sample, with metastatic stages associated with higher PSA levels at follow-up [$F(2,49) = 7.42$, $p = 0.002$].

We then examined whether HRV influenced (moderated) this relationship by testing it separately in patients' high and low HRV [SDNN = 20 msec as cut-off; (Fig. 1)].

We found that cancer stage significantly predicted PSA levels 6 months later, however, only in patients with low HRV [$F(2,16) = 8.72$, $p = 0.003$], but not in patients with high HRV [$F(2,30) = 1.8$, $p > 0.05$]. These results remained similar when controlling for confounders such as age and treatment. Specific contrasts revealed that patients with stage 4 had significantly higher PSA levels at 6 months than those with stage 2, only in patients with low HRV ($p < 0.005$) and not in patients with high HRV ($p > 0.05$). One can look at the co-influence of stage and HRV another way. As seen in Fig. 1, stage also determined when HRV influenced PSA levels. Only among patients with stage 4 PC, those with high HRV had significantly lower PSA at follow-up than those with low HRV ($p = 0.001$), however, this did not occur in patients with stage 2 ($p = 0.06$) or stage 3 ($p = 0.77$) PC. This demonstrated stronger relationships between vagal nerve activity and PSA levels in the metastatic stage compared to other earlier stages of PC, which suggests vagal protection against the negative effects of stage 4 cancer on PSA levels.

In patients with CRC, as expected, stage significantly predicted CEA levels at follow-up, again with more advanced stage associated with high CEA levels than less advanced stages, in the full sample [$F(3, 38) = 6.71$, $p = 0.001$]. As with PC, we then examined whether HRV influenced (moderated) this relationship by testing it separately in patients' high and low HRV. Indeed, cancer stage significantly predicted levels of CEA at 1 year, only in patients with low HRV [$F(3,22) = 7.63$, $p = 0.001$], not in those with high HRV [$F(3,12) = 1.92$, $p > 0.05$], similar to PC. These results remained similar when controlling for confounders such as age and treatment. Specific contrasts revealed that patients with stage 4 had significantly higher CEA levels at 1 year than those with stage 1, only in low HRV ($p < 0.001$) and not in high HRV ($p > 0.05$). Furthermore, as found in PC patients, in CRC patients with

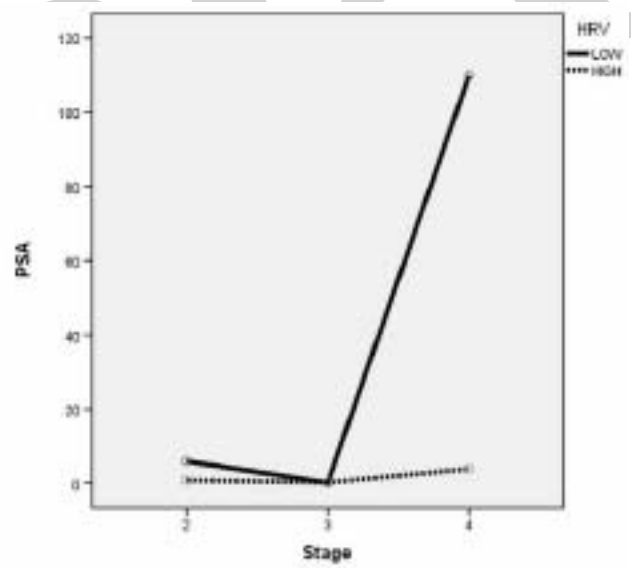

Fig. 1. *The relationship between baseline cancer stage and prostate specific antigen (PSA) at 6 months for low and high HRV (cut-off: SDNN = 20 msec), in prostate cancer patients. Patients with stage 4 had significantly higher PSA levels at 6 months than those with stage 2, only in low HRV ($p < 0.005$) but not in high HRV ($p > 0.05$).*

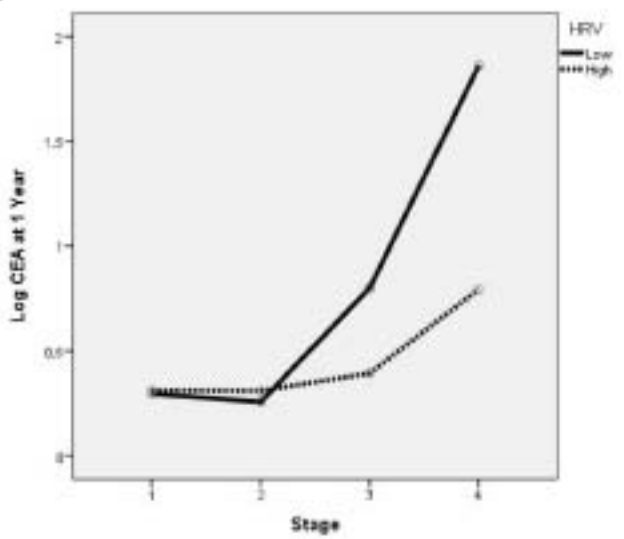

Fig. 2. *The relationship between colorectal cancer stage and Carcinoembryonic antigen (CEA) at 1 year, separately in colorectal cancer patients with high and low HRV (cut-off: SDNN = 20 msec). Cancer stage significantly predicted levels of CEA at 1 year, only in patients with low HRV ($p = 0.001$), but not in those with high HRV ($p > 0.05$).*

metastatic cancer (stage 4), those with high HRV had significantly lower CEA than those with low HRV, at follow-up [$F(1,14) = 7.8$, $p = 0.014$], but this did not occur in patients with stages 1, 2 and 3 of CRC (all p's > 0.05). Again, this result demonstrated that higher vagal nerve activity was related to lower tumor burden, only in metastatic CRC. Similar to PC, such vagal nerve activity may protect against the effects of metastatic CRC stages on CEA levels (Fig. 2).

DISCUSSION

In clinical practice, cancer stage is among the most important factors used to estimate patients' prognosis. This may be the first study demonstrating that vagal nerve activity (indexed by HRV) determines (moderates) the prognostic value of cancer stage in relation to tumor burden, in two different cancers. Specifically, in prostate cancer (PC) and in colorectal cancer (CRC), tumor stage predicted tumor marker levels at follow-up, but only in patients with low, not high, vagal nerve activity. Importantly, in both cancers we found that vagal nerve activity (inversely) predicted tumor marker levels, but only in patients with metastatic cancer (stage 4). In those patients, one would expect a high tumor burden at follow-up. Yet both CEA and PSA levels at follow-up were lower in patients with initially high HRV compared to those with low HRV, despite having metastatic cancers. This pattern of results (Figs. 1 and 2) remained also when statistically controlling for age and treatment. Together, these new findings suggest that vagal nerve activity protects against the adverse effects of advanced (metastatic) cancer stage on markers of tumor burden, in two different cancers. Furthermore, it informs us when cancer stage may be of prognostic value – only when vagal nerve activity is low. Fig. 3 depicts a clinical decision tree derived from these results. It shows how to consider patients' HRV when making clinical decisions about diagnosis and treatment of cancer.

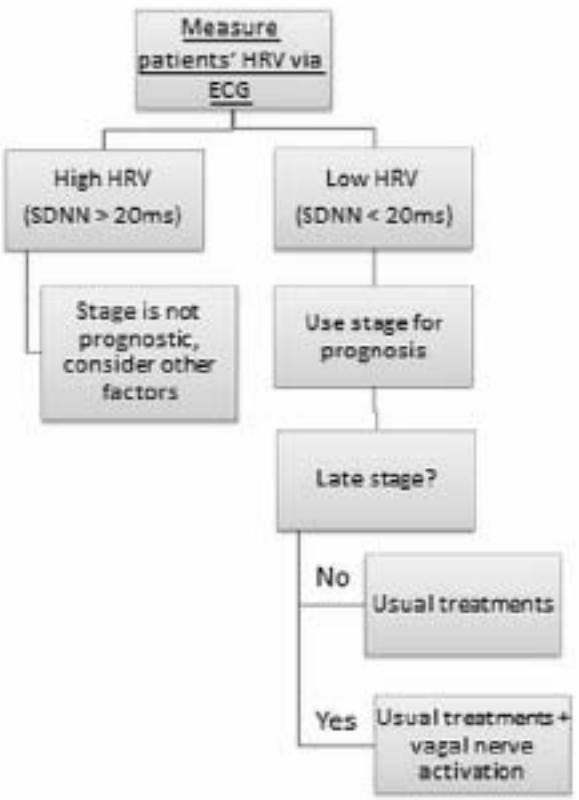

Fig. 3. *Clinical decision tree considering Heart Rate Variability (HRV), cancer stage and treatments.*

These results are in line with the emerging neuromodulatory role of the vagus nerve in cancer and other chronic diseases (3, 8, 11). This neuromodulation is thought to occur since the vagal nerve inhibits inflammation, oxidative stress and excessive sympathetic activity (3, 19), factors that promote tumor progression (10, 21). This modulatory role is mainly known for inflammation. The vagus nerve informs the brain about inflammation and inhibits peripheral inflammation via several negative feedback loops (3). Thus, the vagus nerve may "inform" the brain about and modulate tumor-associated inflammation, possibly improving prognosis (11). Though we did not measure such mechanisms, it is possible that high vagal nerve activity, via inhibiting these processes, could partly compensate for and protect patients from the adverse effects of advanced tumor stage on tumor burden, as shown here in our results. Though vagal activity may also be affected by cancer (19), two experimental studies on animals showed that vagotomy enhanced cancer metastasis (22, 23). Furthermore, a recent study showed that an anti-inflammatory drug which activates the vagus (CNI-1493) reduced tumor volume and metastasis (24). These findings demonstrate causally the protective effects of an intact vagus and of its activation on cancer progression. Moreover, Weber et al. (15) showed that people with higher vagal nerve activity return faster

to homeostasis after stress, in 3 systems - endocrine, immune and cardiac. Together, these results support the notion that this nerve plays a pivotal homeostatic role whose function may be disease prevention or protection against poor prognosis (8, 11), as shown here.

How may we explain that vagal nerve activity, indexed by HRV, predicted tumor burden specifically in the metastatic stage of PC and CRC? First of all, estimating survival time and disclosing the prognosis to patients with advanced disease is among the most difficult tasks that physicians face (25). Prognostic factors in patients with advanced cancer may be very different from those in patients with early cancers. Thus, finding additional prognostic factors in metastatic cancer is clinically and scientifically important. Furthermore, it is possible that in earlier tumor stages, treatments such as chemotherapy and radiotherapy are more successful in reducing tumor size and in impacting tumor markers. Such strong therapeutic effects may leave less of a margin for vagal nerve activity to contribute to the process. In contrast, local treatments may have less impact in later, advanced stages, while (systemic) vagal activity could possibly be of more importance in affecting prognosis. In addition, during the metastatic stage, all three mechanisms thought to underlie the effects of the vagus on tumors, namely, inflammation, oxidative stress and sympathetic activation (8, 20, 26, 27), may have a greater role in prognosis. This would then potentially enable to observe greater impact of the vagal nerve on these three processes, and on prognosis in the advanced stages of cancer specifically.

The main limitations of the present study are its sample sizes, the use of a "historical prospective" study design and the 10-second ECG taken near diagnosis. Due to the historical prospective design, an a-priori control over the confounders, patient sampling and ECG measures were lacking. Although several studies have suggested that certain HRV indices, obtained from 10-second ECGs, are correlated with 5- and 20-min ECGs (17, 28) and although such brief HRV data have also been shown to predict prognosis in cardiac disease (18) and in cancer (13), future formally prospective studies should measure HRV for longer periods. Future studies also need to measure inflammatory, oxidative and sympathetic biomarkers, to test our hypothesized mechanisms in vagal neuromodulation of cancer. These findings must also be replicated in other cancers.

Nevertheless, these results show in two diverse cancers that vagal nerve activity, indexed by HRV, needs to be considered when estimating the prognostic effects of basic variables such as tumor stage. Should these results be replicated in other cancers, our observations here may point at a general phenomenon. In addition, the protective findings may also suggest that activating the vagal nerve could improve the prognosis of patients, specifically in those with metastatic cancer. Other studies are currently planned to examine the prognostic and therapeutic value of vagal nerve activity in cancer outcomes.

ACKNOWLEDGEMENTS

The authors wish to thank "Anticancer Fund" and the Willy Gepts Scientific Foundation for funding this research project.

REFERENCES

1. Alifano M, Falcoz PE, Seegers V, et al. Preresection serum C-reactive protein measurement and survival among patients with resectable non-small cell lung cancer. J Thorac Cardiovasc Surg 2011; 142:1161-7.
2. Lee JH, Song EM, Sim YS, Ryu YJ, Chang JH. Forced expiratory volume in one second as a prognostic factor in advanced non-small cell lung cancer. J Thorac Oncol 2011; 6:305-9.
3. Tracey KJ. Reflex control of immunity. Nat Rev Immunol 2009; 9:418-28.
4. Task Force of the European Society of Cardiology and the North American Society of Pacing and Electrophysiology: Heart rate variability: standards of measurement, physiological interpretation and clinical use. Circulation 1996; 93:1043-65.
5. Kuo TB, Lai C J, Huang YT, Yang CC. Regression analysis between heart rate variability and baroreflex-related vagus nerve activity in rats. J Cardiovasc Electrophysiol 2005; 16:864-69.
6. Chiang JK, Koo M, Kuo TB, Fu CH. Association

between cardiovascular autonomic functions and time to death in patients with terminal hepatocellular carcinoma. J Pain Symptom Manage 2010; 39:673-9.
7. La Rovere, MT, Bigger, JT Jr, Marcus, FI, Mortara, A, Schwartz, PJ. Baroreflex sensitivity and heart-rate variability in prediction of total cardiac mortality after myocardial infarction. ATRAMI (Autonomic Tone and Reflexes After Myocardial Infarction) Investigators. Lancet 1998; 351:478-484.
8. De Couck M, Mravec B, Gidron Y. You may need the vagus nerve to understand pathophysiology and to treat diseases. Clin Sci (Lond) 2012; 122:323-8.
9. King DR, Ogilvie MP, Pereira BM, et al. Heart rate variability as a triage tool in patients with trauma during prehospital helicopter transport. J Trauma 2009; 67:436-40.
10. Entschladen F, Drell TL 4th, Lang K, Joseph J, Zaenker KS. Tumour-cell migration, invasion, and metastasis: navigation by neurotransmitters. Lancet Oncol 2004; 5:254-58.
11. Gidron Y, Perry H, Glennie M. The Vagus may inform the brain about sub-clinical tumors and modulate them: an hypothesis. Lancet Oncology 2005; 6:245-48.
12. Fadul N, Strasser F, Palmer LJ, Yusuf SW, Guo Y, Li Z, Allo J, Bruera E. The association between autonomic dysfunction and survival in male patients with advanced cancer: a preliminary report. J Pain Symptom Manage 2010; 39:283-90.
13. Mouton C, Ronson A, Razavi D, et al. The relationship between heart rate variability and time-course of carcinoembryonic antigen in colorectal cancer. Auton Neurosci 2012; 26:96-9.
14. De Couck, M, van Brummelen, D, Schallier, D, De Grève, J, Gidron, Y. The relationship between vagal nerve activity and clinical outcomes in prostate and non-small cell lung cancer patients. Oncol Rep 2013; 30(5):2435-41.
15. Weber CS, Thayer JF, Rudat M, et al. Low vagal tone is associated with impaired post stress recovery of cardiovascular, endocrine, and immune markers. Eur J Appl Physiol 2010; 109:201-11.
16. Pfleger CC, Flachs EM, Koch-Henriksen N. Social consequences of multiple sclerosis: clinical and demographic predictors - a historical prospective cohort study. Eur J Neurol 2010; 17:1346-51.
17. Nussinovitch U, Elishkevitz KP, Katz K, Nussinovitch M, Segev S, Volovitz B, Nussinovitch N. Reliability of ultra-short ECG indices for heart rate variability. Ann Noninvasive Electrocardiol 2011; 16:117-22.
18. Dekker JM, Schouten EG, Klootwijk P, Pool J, Swenne CA, Kromhout D. Heart rate variability from short electrocardiographic recordings predicts mortality from all causes in middle-aged and elderly men. The Zutphen Study. Am J Epidemiol 1997; 145:899-908.
19. De Couck M, Gidron Y. Norms of vagal nerve activity, indexed by Heart Rate Variability, in cancer patients. Cancer Epidemiol 2013; 37:737-41.
20. Tsutsumi T, Ide T, Yamato M, et al, K. Modulation of the myocardial redox state by vagal nerve stimulation after experimental myocardial infarction. Cardiovasc Res 2008; 77:713-21.
21. Voronov E, Shouval DS, Krelin Y, et al. IL-1 is required for tumor invasiveness and angiogenesis. Proc Natl Acad Sci USA 2003; 100:2645-50.
22. Erin N, Boyer PJ, Bonneau RH, Clawson GA, Welch DR. Capsaicin-mediated denervation of sensory neurons promotes mammary tumor metastasis to lung and heart. Anticancer Res 2004; 24:1003-9.
23. Erin N, Akdas Barkan G, Harms JF, Clawson GA. Vagotomy enhances experimental metastases of 4THMpc breast cancer cells and alters substance P level. Regul Pept 2008; 151:35-42.
24. Erin N, Duymuş O, Oztürk S, Demir N. Activation of vagus nerve by semapimod alters substance P levels and decreases breast cancer metastasis. Regul Pept 2012; 179:101-8.
25. Lamont EB, Christakis NA. Complexities in prognostication in advanced cancer. JAMA 2003; 290:98-104.
26. Mantovani A, Allavena P, Sica A, Balkwill F. Cancer-related inflammation. Nature 2008; 454:436-44.
27. Sloan EK, Priceman SJ, Cox BF, et al.The sympathetic nervous system induces a metastatic switch in primary breast cancer. Cancer Res 2010; 70:7042-52.
28. Hamilton RM, McKechnie PS, Macfarlane PW. Can cardiac vagal tone be estimated from the 10-second ECG? Int J Cardiol 2004; 95:109-15.

ENVIRONMENTAL RISK FACTORS FOR WOMEN WITH POLYCYSTIC OVARY SYNDROME IN CHINA: A POPULATION-BASED CASE-CONTROL STUDY

J. ZHANG[1], X.F. LIU[1], Y. LIU[1], L.Z. XU[1], L.L. ZHOU[1], L.L. TANG[1], J. ZHUANG[1], T.T. LI[1], W.Q. GUO[2], R. HU[3], D.S. QIU[3] and D.W. HAN[3]

[1]Department of Obstetrics and Gynecology, West China Second University Hospital, Sichuan University, Chengdu, Sichuan, People's Republic of China; [2]Department of Ultrasound, West China Second University Hospital, Sichuan University, Chengdu, Sichuan, People's Republic of China; [3]Clinical Laboratory center, West China Second University Hospital, Sichuan University, Chengdu, Sichuan, People's Republic of China

Received May 29, 2013 – Accepted March 7, 2014

Polycystic ovary syndrome (PCOS) is a common reproductive endocrinology disease with heterogeneous phenotype. Environmental factors are thought to be involved in the development of PCOS. The present study aimed to explore the potential environmental risk factors of PCOS. A cross-sectional study and stratified population-based case-control study were carried out. Pre-designed questionnaires were prepared, including questions about medication history, contact history of endocrine disruptors (EDs), environment and habituation. Fasting blood was collected for measurement of sex hormone, glucose and insulin. Matched logistic regression analysis was used to find the potential independent risk factor of PCOS. One thousand eight hundred fifty-four participants (aged 12-44 years) were analyzed in the cross-sectional investigation. One hundred sixty-nine PCOS patients and 338 matched controls were compared. PCOS patients were more frequent than controls in eating plastic-packaged food (p=0.001), contacting pesticide (p=0.021), eating fruit with pericarp (p=0.001), living beside a garbage heap (p=0.001), working at an acid plant (p=0.028), taking Chinese patent drugs (p=0.001), smoking (p=0.028) and drinking alcohol (p=0.001). However, PCOS patients were less likely to use kitchen ventilators (p=0.002), eat canned food (p=0.049), contact decorated materials, use skin care products (p=0.01) and cosmetics (p=0.027). No difference was found in taking antiepileptic drugs (p=0.93). Eating plastic-packaged food (p=0.001, OR=44.449), eating fruit with pericarp (p=0.03, OR=5.7) and drinking alcohol (p=0.001, OR=29.632) were found to be the independent risk factors for PCOS. The existence of an association between EDs and PCOS was proved. Plastic-packaged food, fruit with pericarp and drinking alcohol should be avoided as possible as we can. However, the causal relationships among these factors and PCOS should be proved by further research.

Polycystic ovary syndrome (PCOS) is a common reproductive endocrinology disease, affecting 5–10% of women of reproductive age (1). It involves reproductive, endocrinologic and metabolic systems, which are characterized by irregular menstrual cycle, infertility, hirsutism, acne, obesity, and insulin

Key words: population-based case-control study, endocrine disruptors, environment, polycystic ovary syndrome, risk factor

Mailing address: Dr Liangzhi Xu, Department of Obstetrics and Gynecology, West China Second University Hospital, Sichuan University, Chengdu 610041, Sichuan, People's Republic of China
Tel.: +86 28 85501979 Fax: +86-28 85559065
e-mail: liangzxu@126.com

0393-974X (2014)

DISCLOSURE: ALL AUTHORS REPORT NO CONFLICTS OF INTEREST RELEVANT TO THIS ARTICLE.

resistance. Because of these, PCOS patients are at higher risk of type 2 diabetes mellitus, dyslipidemia, cardiovascular disease, endometrial cancer and nonalcoholic fatty liver disease (2-4). However, its unclear causes makes treatment difficult. Because of this, people tend to focus on the risk factors which might increase the prevalent risk and try to control it. Genetic and environmental factors are thought to be involved in the development of PCOS (5). However, as genetic factors are difficult to be interfered with, potential environmental risk factors urgently need to be clarified to prevent or decrease PCOS.

Environmental endocrine disruptors (EDs) are chemicals which may interfere with hormone biosynthesis, metabolism, and action, resulting in deviation of reproductive, endocrinological, immunologic and nervous systems (6). Exogenously, EDs are currently explored as potential contributors to the pathogenesis of PCOS. These chemicals, mainly including bisphenol A (BPA), phthalic acid esters (PAEs), octylphenol (OP), dioxin and polychlorinated biphenyl, are widespread industrial compounds in the production of polycarbonate plastics, pesticides, detergents, cosmetics, decorated materials, sealing gum and canned food. Epigenetic modification of genes may be the pathophysiologic mechanism of environmental EDs on individuals susceptible to PCOS (7, 8).

However, the role of EDs in the pathogenesis of PCOS lacks clinical epidemiologic evidence. Etiology research on EDs and PCOS is also limited. We tested the hypothesis that environmental factors may be a pathogenetic factor in the development of PCOS. Therefore, a cross-sectional study and a stratified population-based case-control study were conducted to investigate the relationship between environmental EDs and PCOS.

MATERIALS AND METHODS

Study design and sample size

Five communities, two universities and three middle schools from nine districts of Chengdu city were randomly cluster sampled to collect participants. Pilot investigation was conducted on 105 adolescents and 506 reproductive-age women randomly recruited from a middle school and a community. Sample size of the cross-sectional study was calculated based on the PCOS prevalence of 0.95% for reproductive-age women and 3.56% for adolescents, resulting from our pilot investigation, with a margin of error of 1% and alpha error of 5%. The calculated sample size of 361 and 1,319 subjects was further increased to 396 and 1,451, respectively, in order to account for a drop-out rate of 10%. In total, 1,847 participants were recruited in the present study. The number of participants for each age group was calculated according to the population constituent ratio of Sichuan province.

Participants

One thousand eight hundred and fifty-four women, aged 12-44 years, who had lived in Chengdu for at least 6 months, who had had menses for at least 2 years and who agreed to answer the questionnaires, were included in the present study. Participants who had used hormones in the previous three months were excluded. Pregnant women were also excluded. The study was approved by the Human Ethics Committee of West China Second University Hospital. Information and consent forms were obtained from all the subjects or their guardians.

The diagnosis of PCOS was based on the Rotterdam criteria, with the association of at least two of the three following criteria: i) oligo-ovulation or anovulation evidenced by oligomenorrhea (8 or less menstrual cycles in the preceding year) or the serum progesterone level in the luteal phase (<5ng/ml); ii) clinical and/or biochemical signs of hyperandrogenism; iii) polycystic ovaries (9). Congenital adrenal hyperplasia, androgen-secreting tumors, Cushing's syndrome, thyroid disease and prolactinoma were excluded.

Controls matched for age and sampling cluster, were randomly chosen from the non-PCOS participants of cross-sectional investigation with the ratio of 1:2.

Questionnaire

Questionnaires based on related literature were specially compiled to collect general condition, menstrual history, family history, childbearing history, individual medication history, contact history of EDs, environmental situation and habituation (11). Participants were asked to recall whether they had obtained the above environmental items during the year previous to the investigation. If yes, the frequency had to be recorded.

The validity of the questionnaires was discussed and was identified as being eligible for investigation by specialists in clinical epidemiology, reproductive endocrinology and social medicine. Test-retest reliability was assessed by repeating the questionnaires one week after the first investigation on 100 random women. The completeness and clearness of the answered questionnaires were checked by two trained investigators. The data were input individually by two investigators and the consistency was tested to ensure the accuracy of the data.

Measurements

Body weight, height, body mass index, waist circumference, hip circumference, waist hip ratio, systolic and diastolic blood pressure were measured, and hirsutism, acne, acanthosis nigricans and baldness were evaluated individually by two trained investigators. Pelvic ultrasound was examined by a professional doctor to measure the endometrium and ovaries.

Overnight fasting blood samples were collected for detection from all the participants. All the samples were taken during the early follicular phase of the menstrual cycle (the 3-7 day), or after at least three months of amenorrhea. Blood samples were immediately centrifuged. The plasma was separated and stored at −20°C until assay. Estradiol, progesterone, testosterone, free testosterone, luteinizing hormone, follicle-stimulating hormone, fasting insulin and fasting glucose were measured by chemiluminescence method, glucose oxidase method and radioimmunoassay, respectively, with intra- and inter- assay coefficients of variation of <10% and <15%. All of above tests were performed by professional laboratorian in the clinical test center of our hospital.

Statistical assays

Student's *t*-test was used to compare continuous variables between the groups. Categorical variables were compared with the χ^2-test or rank-sum test as appropriate. Spearman's rank correlation coefficient was used. Odds ratios (OR) with 95% confidence intervals (95% CI) were calculated using matched logistic regression analysis. Analyses were performed using the Statistical Package for Social Science (SPSS16.0).

RESULTS

General results

Test-retest reliability tests were completed by 87 women of 100 participants. The consistency of test-retest results was moderated (p=0.001, Kappa=0.644). The validity and reliability of the questionnaire were eligible for the investigation. The study flow chart was illustrated as Fig. 1. Two thousand and fifty participants were recruited for the cross-sectional investigation from 5 communities, 3 middle schools and 2 universities in Chengdu city, China. Finally, 1,854 participants were included in the results analysis, with 398 adolescents (aged 12-17 years) and 1,456 reproductive-age women (aged 18-44 years). One hundred sixty-nine PCOS patients participated in the present study. The general baseline levels between the case and control groups were comparable except for birth weight (Table I). The birth weight of the PCOS patients was lower than that of controls (p=0.049).

Medication history

The results were stratified and analyzed according to birth weight to exclude the influence of confounders (Table II). PCOS patients were found to be more frequent than controls in taking Chinese patent drugs (p=0.001). No difference was found between groups in using intrauterine devices

Table I. *Background factors of the participants.*

	Cases (n= 169)	Controls (n= 338)	*P*
Age (years)	22.07±6.10	22.08±6.08	0.972
Menarche age (years)	12.76±1.25	12.84±1.41	0.525
SBP（mmHg）	104.38±10.65	100.48±12.16	0.224
DBP（mmHg）	67.60±10.50	66.37±9.90	0.571
Birth weight (kg)	2.85±1.07	3.02±0.81	0.049*

DBP: diastolic blood pressure; SBP: systolic blood pressure
**p <0.05*

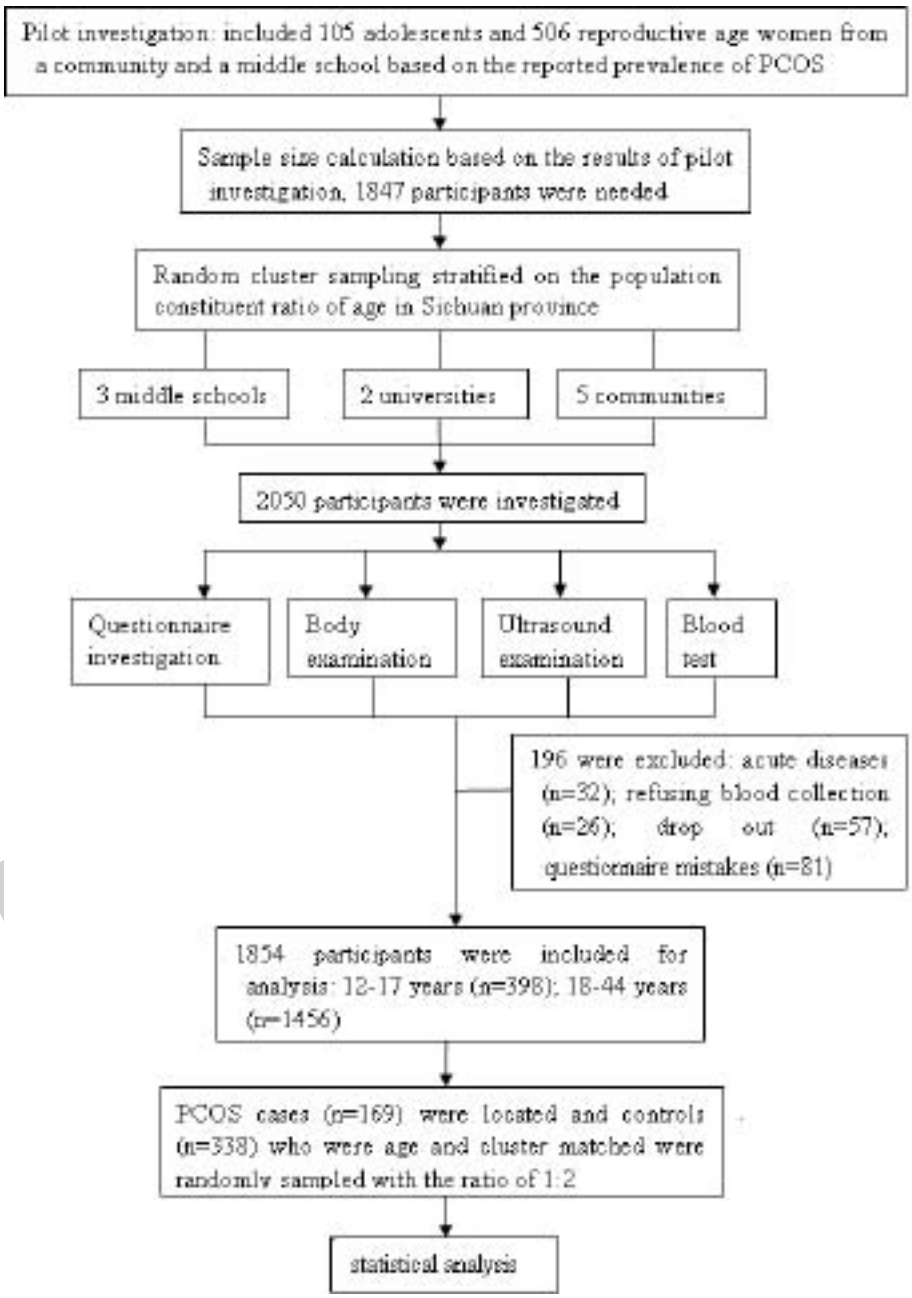

Fig. 1. *Flow chart of the study.*

(p=0.042, 95%CI 0.090, 1.035), taking antiepileptic drugs (p=0.93), hormones (p=0.765) and health products (p= 0.904).

Contact history of EDs

Contact history of endocrine disruptors was compared to investigate the association between endocrine disruptors and PCOS (Table II). Surprisingly, PCOS patients were less likely to eat canned food (p=0.049), contact decorated materials, use skincare products (p=0.01) and cosmetics (p=0.027) than controls. However, PCOS patients were more frequent than controls in eating plastic-packaged food (p=0.001), contacting pesticides (p=0.021) and eating fruit with pericarp (p=0.001). In particular, persons eating plastic-packaged food

Table II. *The medication history and contact history of endocrine disruptors between groups stratified by birth weight.*

Variables	Birth weight <3kg		Birth weight >3kg		χ^2	*P*	OR	95%CI
	Cases n(%)	Controls n(%)	Cases n(%)	Controls n(%)				
Medical drug								
Health care products	38(36.54)	71(37.77)	25(38.46)	57(38)	0.015	0.904	0.977	(0.667, 1.431)
Hormones	20(19.23)	34(18.09)	11(16.92)	24(16)	0.090	0.765	1.076	(0.665, 1.743)
Antiepileptic drugs	4(3.85)	6(3.19)	0(0)	2(1.33)	0.008	0.930	0.947	(0.278, 3.226)
Chinese patent drugs	51(49.04)	6(3.19)	27(41.54)	9(6.00)	103.6	0.001*	17.37	(9.582, 31.49)
Phthalic acid esters or Bisphenol A								
Skin care products	101(97.12)	184(97.87)	59(90.77)	143(95.33)	3.52	0.010*	0.066	(0.034, 0.127)
Cosmetics	45(43.27)	90(47.87)	25(38.46)	86(57.33)	4.885	0.027*	0.659	(0.454, 0.956)
Perfumes	44(42.31)	91(48.40)	27(41.54)	74(49.33)	2.079	0.149	0.766	(0.524, 1.104)
Plastic-packaged food	98(94.23)	16(8.51)	59(90.77)	25(16.67)	309.5	0.001*	84.65	(43.518, 164.65)
Canned food	25(24.04)	62(32.98)	19(29.23)	56(37.33)	3.876	0.049*	0.663	(0.440, 0.999)
Decorating materials	45(43.27)	103(54.79)	22(33.85)	68(45.33)	5.925	0.015*	0.627	(0.430, 0.914)
Moving into newly-decorated house	50(48.08)	121(64.36)	31(47.69)	94(62.67)	11.46	0.001*	0.525	(0.361, 0.764)
IUD	1(0.971)	13(6.91)	2(3.08)	6(4.00)	4.124	0.042*	0.360	(0.090, 1.035)
Tooth filling	32(30.77)	81(43.09)	22(33.85)	53(35.33)	1.521	0.217	0.784	(0.532, 1.155)
Polybrominated biphenyls								
Pesticides	23(22.12)	24(12.77)	13(20.00)	21(14.00)	5.348	0.021*	1.764	(1.087, 2.865)
Detergents	73(70.19)	146(77.66)	51(78.46)	124(82.67)	2.501	0.114	0.705	(0.457, 1.088)
Eating fruit with pericarp	25(24.04)	10(5.32)	9(13.85)	6(4.00)	29.06	0.001*	5.000	(2.666, 9.379)
Poisonous metal	11(10.58)	13(6.91)	6(9.23)	25(16.67)	0.090	0.764	0.911	(0.497, 1.672)

IUD: intrauterine device
**p<0.05*

and fruit with pericarp in PCOS patients were 85 (95%CI 43.5, 164.65) and 5 (95%CI 2.666, 9.379) times more than those in controls, respectively.

Environment and habituation

Living, working environment and lifestyle were compared between cases and controls (Table III). PCOS patients were more likely to live near to the garbage heap (p=0.001) and work at an acid plant (p=0.028), but less likely in inserting kitchen ventilators (p=0.002). Smokers in PCOS groups were 2.5 (participants themselves, 95%CI 1.077, 5.645) and 1.6 (participants' fathers, 95%CI 1.079, 2.256) times more than those in controls, respectively. PCOS patients were more frequent than controls in drinking alcohol (p=0.001), and the alcohol drinkers in PCOS patients were 7.557 times more than those in controls (95%CI 3.979, 14.35).

Independent environmental risk factors of PCOS

All of above variables with significant difference were included and analyzed in matched logistic regression analysis to find the potential risks of PCOS and exclude the influence of confounder. Eating plastic-packaged food (p=0.001, OR=44.449), drinking alcohol (p=0.001, OR=29.632) and eating

Table III. *Living, working environment and lifestyle between groups stratified by birth weight.*

Variables	Birth weight <3kg		Birth weight >3kg		χ^2	*P*	OR	95%CI
	Cases n(%)	Controls n(%)	Cases n(%)	Controls n(%)				
Living								
Garbage heap	15(14.42)	8(4.26)	10(15.38)	8(5.33)	15.47	0.001*	3.528	(1.824, 6.824)
Wooden furniture	102(98.08)	180(95.74)	61(93.85)	144(96.0)	0.084	0.772	1.151	(0.440, 3.012)
Kitchen ventilator	67(64.42)	116(61.70)	40(61.54)	102(68.0)	9.334	0.002*	2.020	(1.269, 3.215)
Working								
Acid plant	9(8.65)	6(3.19)	4(6.15)	5(3.33)	4.813	0.028*	2.466	(1.077, 5.645)
Insecticide factory	3(2.88)	6(3.19)	1(1.54)	4(2.67)	0.166	0.684	0.783	(0.241, 2.544)
Oil refinery	2(1.92)	5(2.66)	4(6.15)	4(2.67)	0.361	0.548	1.373	(0.483, 3.902)
Tannery	8(7.69)	18(9.57)	4(6.15)	11(7.33)	0.377	0.539	0.803	(0.399, 1.619)
Printing and dyeing mill	8(7.69)	11(5.85)	4(6.15)	11(7.33)	0.068	0.749	1.103	(0.531, 2.291)
Paper mill	11(10.58)	14(7.45)	5(7.69)	11(7.33)	0.616	0.4333	1.301	(0.674, 2.514)
Fiber mill	0(0.00)	5(2.66)	1(1.54)	7(4.67)	3.755	0.053	0.170	(0.022, 1.309)
Electrical variable capacitor factory	13(12.50)	16(8.51)	5(7.69)	18(12.0)	1.151	0.283	1.378	(0.760, 2.500)
Smoking								
Father	59(56.73)	54(62.23)	40(61.54)	96(64.0)	5.796	0.016*	1.560	(1.079, 2.256)
Mother	5(4.81)	5(2.66)	2(3.08)	3(2.0)	1.157	0.282	1.754	(0.023, 4.934)
Herself	9(8.65)	6(3.19)	4(6.15)	5(3.33)	4.813	0.028*	2.466	(1.077, 5.645)
Drinking								
Alcohol	30(28.85)	10(5.32)	12(18.46)	4(2.67)	47.86	0.001*	7.557	(3.979, 14.35)
Coffee	49(47.12)	84(44.68)	40(61.54)	81(54.0)	0.879	0.349	1.195	(0.823, 1.735)
Tea	63(60.58)	129(68.62)	51(78.46)	114(76.0)	0.827	0.363	0.829	(0.554, 1.241)

*$p<0.05$

Table IV. *Matched logistic regression analysis for the independent environmental factors of PCOS.*

	B	SE	Wald	*P*	Exp(B)	95% CI
Plastic-packaged food	3.794	0.629	36.414	0.001*	44.449	(12.961, 152.433)
Drinker (herself)	3.389	1.059	10.245	0.001*	29.632	(3.720, 236.030)
Eating fruit with pericarp	1.741	0.800	4.729	0.030*	5.700	(1.188, 27.363)

*$p<0.05$

fruit with pericarp (p=0.03, OR=5.7) were found to be potential independent risk factors of PCOS (Table IV).

DISCUSSION

Modern environmental insults on the reproductive and metabolic balance are thought to affect susceptible women. In addition, environmental factors may modulate the clinical severity of PCOS (5). Environmental exposure may start in uterus, persist postnatally until adolescence, and extend throughout life. The fetal programming hypothesis

of PCOS is based on the studies of prenatally androgenized female primates (11). However, the intrauterine environment of prenatal androgen excess has not been replicated in human (12, 13).

This study is the first to report the association between environmental factors and PCOS by a stratified population-based case-control study. Eating plastic-packaged food, drinking alcohol and eating fruit with pericarp were associated with the increased risk of PCOS, which indicates that EDs might relate to the development of PCOS.

An association of increased BPA levels with reproductive, endocrine and metabolic features of PCOS was suggested by recent studies (6). Rats exposed to BPA were associated with the development of reproductive and metabolic characteristics of PCOS (14). BPA appeared to act directly on the ovary and might affect both folliculogenesis and ovarian steroidogenesis (15, 16). Furthermore, BPA was associated with deregulation of glucose homeostasis through a direct affect on beta- and alpha- pancreatic cells (17, 18) or an indirect affect on glucose transport in adipocytes (19). Higher serum BPA levels were observed in women with ovulatory dysfunction compared to those of regularly ovulating women (20). In two previous studies serum BPA concentrations were found to be significantly higher in women with PCOS compared with normal women (21, 22). In the present study, eating plastic-packaged food was found to be more frequent in PCOS patients. This indirectly indicates that BPA which is commonly used in food and drink packaging might be involved in the development of PCOS.

The association between other EDs, such as Di 2-Ethyl Hexyl Phthalate, (DEHP) and PCOS had not been explored by previous studies. *In vivo*, DEHP decreased serum estradiol levels, prolonged estrous cycles, and suppressed ovulation in cycling adult rats. *In vitro*, monoethylhexyl phthalate (MEHP; the active metabolite of DEHP) decreased granulosa cell aromatase RNA message and protein levels and acted through a receptor-mediated signaling pathway to suppress ovulation (23, 24). Eating fruit with pericarp was found to be more frequent in PCOS patients by the present study, which indirectly suggests that pesticides might be involved in the risk of PCOS. To directly explore the association of EDs and PCOS, the plasma levels of different kinds of EDs in PCOS patients need to be further tested.

Intrauterine growth restriction, early postnatal catch-up growth and premature adrenarche and menarche might be the phenotypical evolution of PCOS (25). Lower birth weight of PCOS patients was found in the present study, which was in accordance with some previous studies (26, 27). However, the reason for lower birth weight was unclear. A meta-analysis suggested that low-level exposure to polychlorinated biphenyls or correlated exposures could impair fetal growth, but exposure to *p,p′*- dichlorodiphenyldichloroethylene (DDE) did not (28). Higher serum level of DEHP and MEHP were found in thelarche patients, which indicated a possible association between plasticizers with known estrogenic and antiandrogenic activity and the cause of premature breast development in a human female population (29). However, the presence and levels of pesticides in serum and adipose tissues were not related to precocious puberty (30).

No correlation was found between PCOS and antiepileptic drugs in the present study. Results of a meta-analysis suggested that PCOS might be associated with valproate-treated women with epilepsy. However, this result was PCOS criteria-dependent; valproate was not relative to PCOS patients who were diagnosed by NIH criteria (31). The discrepancy between these studies might result from the low prevalence of epilepsy in the present study, as the antiepileptic drugs were used by several women in both groups. PCOS patients were found to be more frequent than controls in taking Chinese patent drugs in the present study. In China, most women with irregular menstrual cycles prefer to try traditional Chinese medicine therapy first.

To date, standard environmental questionnaires for women of PCOS are unavailable throughout the world. For the credibility and authenticity of this study, we designed our own environmental questionnaire. The reliability of the questionnaire was proved to be eligible by test-retest consistency investigation. However, the face and content validity were subjectively evaluated by epidemiologic, social medicine and reproductive endocrinological specialists, and will require objective parameters in the future. The present study investigated the environmental factors of participants in the year previous to being enrolled in the study. The earlier

environmental factors might confuse the results. Meanwhile, the results of the present study might be influenced by some risks of the questionnaire, such as memory bias and information bias. These biases could not be completely avoided in the retrospective study. A cohort study with a larger sample size is called for.

Another important limitation of our study was the confusion in diagnosing PCOS in adolescent girls. Adult PCOS criteria was used for adolescents in the present study for a lack of detailed adolescent diagnostic criteria. It might overrate the prevalence of PCOS in adolescents, as insulin resistance, hyperandrogenism and polycystic ovary might physiologically exist in adolescent girls.

Eating plastic-packaged food, drinking alcohol and eating fruit with pericarp were found to be significantly associated with the development of PCOS. However, the presence of a significant association did not necessarily imply the existence of a causal relationship among the studied parameters, which should be proved by a cohort study in the future.

In conclusion, the present study shows that plastic-packaged food, alcohol intake and fruits with pericarp might relate with the increased risk of PCOS, possibly by the intake of EDs existing in these kinds of food. However, these relationships should be proved by further prospective studies with a larger cohort of subjects.

ACKNOWLEDGEMENTS

We thank professor Hongwei Liu and Lin Qiao for the guidance of clinical research, professor Taizhu Yang and Min He for their support of ultrasound measurement, Xiaoxian Liu, Wenjuan Li, Ying Hu and Qingyuan Zeng for their help in blood collection.

This research was supported by: National Natural Science Foundation of China (81270665); Scientific Research Foundation of Health Department of Sichuan province (100377, 060020, 090289), China; Science and Technology Basic platform foundation of Sichuan Province (2012JCPT009), China.

REFERENCES

1. Ehrmann DA. Polycystic ovary syndrome. N Engl J Med 2005; 352:1223-36.
2. Shaw LJ, Bairey Merz CN, Azziz R, et al. Postmenopausal women with a history of irregular menses and elevated androgen measurements at high risk for worsening cardiovascular event-free survival: results from the National Institutes of Health-National Heart, Lung, and Blood Institute sponsored Women's Ischemia Syndrome Evaluation. J Clin Endocrinol Metab 2008; 93:1276-84.
3. Pierpoint T, McKeigue PM, Isaacs AJ, Wild SH, Jacobs HS. Mortality of women with polycystic ovary syndrome at long-term follow-up. J Clin Epidemiol 1998; 51:581-6.
4. Gambarin-Gelwan M, Kinkhabwala SV, Schiano TD, Bodian C, Yeh HC, Futterweit W. Prevalence of nonalcoholic fatty liver disease in women with polycystic ovary syndrome. Clin Gastroenterol Hepatol 2007; 5:496-501.
5. Diamanti-Kandarakis E, Christakou C, Marinakis E. Phenotypes and environmental factors: their influence in PCOS. Curr Pharm Des 2012; 18:270-82.
6. Diamanti-Kandarakis E, Bourguignon JP, Giudice LC, Hauser R, Prins GS, Soto AM, Zoeller RT, Gore AC. Endocrine- disrupting chemicals: an endocrine society scientific statement. Endocr Rev 2009; 30:293-342.
7. Hickey TE, Legro RS, Norman RJ. Epigenetic modification of the X chromosome influences susceptibility to polycystic ovary syndrome. J Clin Endocrinol Metab 2006; 91:2789-91.
8. Junien C, Nathanielsz P. Report on the IASO Stock Conference 2006: early and lifelong environmental epigenomic programming of metabolic syndrome, obesity and type II diabetes. Obes Rev 2007; 8:487-502.
9. The Rotterdam ESHRE/ASRM-sponsored PCOS Consensus Workshop Group. Revised 2003 consensus on diagnostic criteria and long-term health risks related to polycystic ovary syndrome (PCOS). Hum Reprod 2004; 19:41-7.
10. Kenji Y, Takashi Y, Masahiro S. Reliability and validity of a comprehensive environmental questionnaire for community-living elderly with healthcare needs. Psychogeriatrics 2008; 8:66-72.
11. Dumesic DA, Abbott DH, Padmanabhan V. Polycystic ovary syndrome and its developmental origins. Rev Endocr Metab Disord 2007; 8:127-41.
12. Hickey M, Slooda DM, Atkinson HC, Doherty DA,

Franks S, Norman RJ, Newnham JP, Hart R. The relationship between maternal and umbilical cord androgen levels and polycystic ovary syndrome in adolescence: a prospective cohort study. J Clin Endocrinol Metab 2009; 94:3714-20.
13. Anderson H, Fogel N, Grebe SK, Singh RJ, Taylor RL, Dunaif A. Infants of women with polycystic ovary syndrome have lower cord blood androstenedione and estradiol levels. J Clin Endocrinol Metab 2010; 95:2180-6.
14. Fernández M, Bianchi M, Lux-Lantos V, Libertun C. Neonatal exposure to bisphenol A alters reproductive parameters and gonadotropin releasing hormone signaling in female rats. Environ Health Perspect 2009; 117:757-62.
15. Takeuchi T, Tsutsumi O, Ikezuki Y, et al. Elevated serum bisphenol A levels under hyperandrogenic conditions may be caused by decreased UDP-glucuronosyltransferase activity. Endocr J 2006; 53:485-91.
16. Zhou W, Liu J, Liao L, Han S, Liu J. Effect of bisphenol A on steroid hormone production in rat ovarian theca-interstitial and granulosa cells. Mol Cell Endocrinol 2008; 283:12-8.
17. Alonso-Magdalena P, Morimoto S, Ripoll C, Fuentes E, Nadal A. The estrogenic effect of bisphenol A disrupts pancreatic beta-cell function *in vivo* and induces insulin resistance. Environ Health Perspect 2006; 114:106-12.
18. Alonso-Magdalena P, Laribi O, Ropero AB, Fuentes E, Ripoll C, Soria B, Nadal A. Low doses of bisphenol A and diethylstilbestrol impair Ca2+ signals in pancreatic alpha-cells through a nonclassical membrane estrogen receptor within intact islets of Langerhans. Environ Health Perspect 2005; 113:969-77.
19. Sakurai K, Kawazuma M, Adachi T, Harigaya T, Saito Y, Hashimoto N, Mori C. Bisphenol A affects glucose transport in mouse 3T3-F442A adipocytes. Br J Pharmacol 2004; 141:209-14.
20. Takeuchi T, Tsutsumi O, Ikezuki Y, Takai Y, Taketani Y. Positive relationship between androgen and the endocrine disruptor, bisphenol A, in normal women and women with ovarian dysfunction. Endocr J 2004; 51:165-9.
21. Tsutsumi O. Assessment of human contamination of estrogenic endocrine- disrupting chemicals and their risk for human reproduction. J Steroid Biochem Mol Biol 2005; 93:325-30.
22. Kandaraki E, Chatzigeorgiou A, Livadas S, et al. Endocrine disruptors and polycystic ovary syndrome (PCOS): elevated serum levels of bisphenol A in women with PCOS. J Clin Endocrinol Metab 2011; 96:E480-4.
23. Lovekamp-Swan T, Davis BJ. Mechanisms of phthalate ester toxicity in the female reproductive system. Environ Health Perspect 2003; 111:139-45.
24. Yamasaki K, Okuda H, Takeuchi T, Minobe Y. Effects of in utero through lactational exposure to dicyclohexyl phthalate and p,p'-DDE in Sprague-Dawley rats. Toxicol Lett 2009; 189:14-20.
25. de Zegher F, Ibáñez L. Early Origins of polycystic ovary syndrome: hypotheses may change without notice. J Clin Endocrinol Metab 2009; 94:3682-5.
26. Ibáñez L, López-Bermejo A, Callejo J, Torres A, Cabré S, Dunger D, de Zegher F. Polycystic ovaries in nonobese adolescents and young women with ovarian androgen excess: relation to prenatal growth. J Clin Endocrinol Metab 2008; 93:196-9.
27. Melo A, Vieira C, Barbieri M, et al. High prevalence of polycystic ovary syndrome in women born small for gestational age. Hum Reprod 2010; 25:2124-31.
28. Govarts E, Nieuwenhuijsen M, Schoeters G, et al; OBELIX; ENRIECO. Birth weight and prenatal exposure to polychlorinated biphenyls (PCBs) and dichlorodiphenyldichloroethylene (DDE): a meta-analysis within 12 European Birth Cohorts. Environ Health Perspect 2012; 120:162-70.
29. Colón I, Caro D, Bourdony CJ, Rosario O. Identification of phthalate esters in the serum of young Puerto Rican girls with premature breast development. Environ Health Perspect 2000; 108:895-900.
30. Ozen S, Darcan S, Bayindir P, Karasulu E, Simsek DG, Gurler T. Effects of pesticides used in agriculture on the development of precocious puberty. Environ Monit Assess 2012; 184:4223-32.
31. Hu X, Wang J, Dong W, Fang Q, Hu L, Liu C. A meta-analysis of polycystic ovary syndrome in women taking valproate for epilepsy. Epilepsy Res 2011; 97:73-82.

ESTROGENS CONTROL INFLAMMATION IN EXPERIMENTAL COLITIS

I. HAJJ HUSSEIN[1,2], A. EID[1], R. MAKSOUD[1], S. JAMBART[1], T. BOU ASSI[1], Z. ZGHEIB[1], D. OUEIDAT[1], N. CHAMS[1], S. CHAMS[1], R. DIAB[1], K. BARADA[1], R. JURJUS[3], F. CAPPELLO[4], J. REIMUND[5], J. KREIKER[6], A. LEONE[4] and A. JURJUS[1]

[1]Department of Anatomy, Cell Biology and Physiology, Faculty of Medicine, American University of Beirut, Beirut, Lebanon; [2]Oakland University William Beaumont School of Medicine, USA; [3]George Washington University, Washington D.C., USA; [4]University of Palermo, Italy; [5]Strasbourg University, France; [6]Lebanese University, Beirut, Lebanon

Received February 27, 2014 – Accepted April 9, 2014

There is now a wealth of experimental evidence indicating that the deficit in endogenous estrogen facilitates the onset of inflammation that can be antagonized by estrogen replacement therapy. This work investigated the role of estrogen in the control of intestinal inflammation in a panel of colitis models, focusing on the morphological changes, the activity of mast cells, the expression of cytokines (IL-1β, IL-6, and TNF-α), fibronectin and reactive oxygen species. Two hundred adult male rats were divided into 4 groups: colitis was induced in Group I and Group II but only the latter was treated with estrogen; Group III received estrogen only, and Group IV saline. Colitis was induced in 4 models using: iodoacetamide; iodoacetamide + enteropathogenic *E. coli*; 2,4,6-Trinitrobenzene sulfonic acid; and dextran sulfate sodium salt. Macroscopic and microscopic evaluations of abdominal structures as well as molecular analysis were made on days 7, 14, 28 and 56. There was a significant improvement in the health condition of the estrogen-treated rats: the inflammation scores were reduced by at least 10-15%, the number of mast cells in the colon decreased by 30%, fibronectin expression was only 50% and reactive oxygen species decreased by 30%. In addition, there was a significant decrease in TNF-α, IL-6 and IL-1β expression by about 25%. In conclusion, there was an improvement in the inflammatory status in all estrogen-treated groups through the duration of the experiment at all-time points. In addition, there was less tissue necrosis as depicted by less fibronectin and a marked antioxidant effect.

Estrogens (Es) have been proven to modulate the immune system and to have anti-inflammatory as well as pro-inflammatory effects (1). In addition, it has been well documented that young females, in general, experience significantly lower rates of infection while women in menopause show enhanced production of the pro-inflammatory cytokines (1, 2). Es have also been known to possess a strong inhibitory effect on leukocyte migration in inflamed areas, particularly neutrophils and monocytes, leading to less severe inflammation (3).

At pregnancy levels or higher, Es inhibit pro-inflammatory pathways. They mediate the inhibition of TNF-α, decrease IL-2 production in mature dendritic cells, inhibit IL-1 and IL-6, decrease reactive oxygen species (ROS), and down-regulate

Key words: inflammatory bowel diseases, estrogen, colitis, TNF-α, IL-1β, fibronectin, mast cells

Mailing address: Dr Abdo Jurjus,
Department of Anatomy, Cell Biology & Physiology,
Faculty of Medicine, American University of Beirut,
P.O.Box 11-0236 / (Department of Anatomy, Cell Biology & Physiology), Riad El-Solh / Beirut 1107 2020, Lebanon
Tel.: +961 3 308716 Fax: +961 1 4806 87
e-mail: aj00@aub.edu.lb

0393-974X (2014)

adhesion molecules (4-7). On the other hand, post-menopausal levels of Es increase the expression of adhesion molecules (5), and render women to a more pro-inflammatory situation, thus contributing to the manifestation of chronic inflammatory diseases after menopause (1).

The role of Es in human inflammatory bowel diseases (IBDs), both Crohn's disease (CD) and ulcerative colitis (UC) has not been fully investigated. Some experimental studies using dinitrobenzene sulfonic acid colitis (DNCB) showed that Es, at pregnancy level, reduced macroscopic and histological alterations, as well as myeloperoxidase levels and ICAM-1 expression (8). In another model of chronic inflammation in HLA-27 transgenic rats, Es treatment also improved the histological scores, decreased inflammatory cell infiltration, fibrosis, and mast cell proteases 1, 3 and 4 (9-11). On the other hand, Es treatment of the dextran sodium sulfate (DSS) colitis increased the macroscopic and histological scores (9). In brief, earliest studies demonstrated anti-inflammatory and pro-inflammatory effects of Es in 3 different models out of more than sixty reported models of inducible colitis (10-12).

This article reexamined the anti-inflammatory effect of Es on a panel of induced colitis including: trinitrobenzene sulfonic acid (TNBS), dextran sodium sulfate (DSS), as well as iodoacetamide (IA) alone or plus enteropathogenic *E. coli* bacteria (IA+B). The parameters assessed included: clinical signs and symptoms, microscopic alterations, TNF-α, interleukins IL-1β, IL-6, fibronectin, and ROS.

MATERIALS AND METHODS

Experimental animals

A total of 200 adult male Sprague-Dawley rats, weighing 250-300 g, were used in accordance with the criteria set for care and use of animals by the Institutional Animal Care and Use Committee (IACUC) at the American University of Beirut. The animals were housed in rack mounted cages, 5 rats per cage, and kept on a 12-h light/dark cycle in a controlled temperature and humidity room. Standard laboratory pelleted formula and tap water were provided *ad libitum*.

Colitis induction

The rats were divided into 4 groups: 2 major groups, GI and GII, of 80 rats each, and 2 minor groups, GIII and GIV of 20 rats each. Colitis was induced in GI and GII but only GII was treated by weekly interscapular injections of estrogen (250 µg) starting one week before the induction. The rats in GIII received subcutaneous injections with estrogen (E) at the same dose and schedule as in GII (17ß-estradiol, Sigma-Aldrich, E8875); while the rats in GIV served as control (C), they were neither induced with colitis nor received estrogen (13).

Groups I and II were further subdivided into 4 subgroups of 20 rats each. Colitis was induced in 40 rats according to previously established procedures using rectal injection with 100 µl of 4% Iodoacetamide in 1% methyl cellulose (IA) (Sigma Aldrich, St. Louis, MO, USA), according to Satoh et al. (14). Another 40 rats received IA plus 200 µl containing 4×10^8 colony factor unit of Enteropathogenic *E.coli* (EPEC) according to Hajj Hussein et al. (11). In addition, another 40 rats were subjected to 100 µl TNBS solution (Sigma-Aldrich, 92822-1ML) according to Morris et al. (15), and Fan et al. (16), and 40 rats used drinking water mixed with 2% Dextran Sulfate Sodium Salt (DSS) (Sigma-Aldrich, D4911-1G), 5 ml per rat per day, according to Writz et al. (17).

Daily observations

Rats were weighed and their health condition was checked daily. Signs and symptoms of colitis (weight loss, diarrhea, mucus and/or blood in stools) were monitored. Scores were given by two different observers and averages of the two scores of each category were calculated (18, 19).

Macroscopic assessment

The rats were sacrificed on days 7, 14, 28 and 56. Abdominal viscera were checked for inflammatory parameters, and biopsies were removed and fixed in 10% formaldehyde for routine microscopy, or frozen at -80°C for immunohistochemistry and RNA testing. The tissues included the descending colon, the jejunum, the kidney and the liver. Parameters, such as the size of the affected area due to inoculation, the descending colon morphology, number of mushroom-like structures in the serosa, vasodilatations, the presence of adhesions, were observed and scored by two different observers (11).

Histological evaluations

The H&E stained slides of jejunum and descending colon biopsies were examined under a light microscope at different magnifications. A previously reported scheme was used to determine the extent of inflammatory reaction and included: interruption of intestinal epithelium, dilation of glandular crypts, depletion and loss of goblet cells, inflammatory cells infiltration, edema, crypt abscesses and dysplasia (11). Slides were evaluated and scored by

two different observers for each time point (days 7, 14, 28 and 56).

Analysis of cytokine expression

Molecular parameters, also assessed at various time points by qRTPCR, included TNF-α, IL-1β, IL-6, and Fibronectin. RNA extraction was performed from the scrap tissues collected on sacrifice days using Trizol reagent (Bio-Rad) according to the supplier's protocol. After following the protocol and having diluted 1 µl of RNA with 25 µl of DEPC water, the final RNA concentrations were determined with the Nanodrop knowing that A260/A280 should be between 1.8-2.0. Next, Genomic DNA elimination mixture was prepared using 2 µl of GE (5x genomic DNA elimination buffer) for every µg of RNA. To that, RNase free water was added to reach a volume of 10 µl. 10 µl of reverse transcriptase cocktail was added to each sample (4 µl of BC3, 1 µl of P2, 2 µl of RE, 3 µl of RNAse free water). The plates were prepared using 23 µl of the RTPCR mixture (12.5 µl RT2qPCR Master Mix, 1 µl of forward primer, 1 µl of reverse primer and 8.5 µl of RNAse free water) with 2 µl of cDNA, then sealed. All tests were performed according to procedures previously reported (22).

Dihydroethidine staining

Dihydroethidine (DHE) for ROS was carried out on 10 µm frozen sections using confocal microscopy (20, 21). DHE is a cell-permeable compound which, due its ability to freely penetrate cell membranes, is used extensively to monitor superoxide production (20, 21). Reactive oxygen species (ROS) are chemically reactive molecules containing superoxide anion O2−. They are biologically toxic and deployed by the immune system to kill invading microorganisms (23). They increase during time of stress. DHE is oxidized by reaction with O2- to ethidium bromide, or oxyethidium (24), which binds to DNA in the nucleus and fluoresces in red, detectable qualitatively by a fluorescent microscopy.

Statistical analysis

The histological scores were computed and represented with matching standard error of the mean using PRISMS software. Statistical significance comparing the treatment with estrogen versus no treatment was evaluated by Student's *t*-test and ANOVA test. P value of less than 0.05 indicates a statistically significant difference.

RESULTS

Estrogens improved the clinical picture in the rats

Animals in GI showed to various degrees, all signs and symptoms of an induced active ulcerative colitis (UC), more severe in the IA+B treated rats compared to the others. On the other hand, GII rats, treated with estrogen, showed lower clinical scores, thus less inflammation compared to GI. In general, the subgroups in GII showed a significantly reduced spectrum of total scores, compared to their corresponding subgroups in Group I, $p < 0.05$ (Fig. 1).

The total clinical score of the IA+B induced colitis was the highest, the most severe inflammation (7.6/10), followed by the TNBS (6.5/10), the IA (5.5/10) then the DSS (3/10). The colitis score increased after each intra-rectal induction with IA+B, IA, and TNBS, and after each cycle of DSS. For the IA+B, IA and TNBS, after day 28, the clinical scores gradually decreased till day 56 but never reached the control baseline levels. However, it is important to note that on day 36, when the last induction of colitis took place, the inflammation peaked but it was 30% lower than the previous peaks. Therefore, the inflammation was present after one month and it was maintained at a lower scale till the end of the experiment time; and estrogen decreased inflammation significantly as depicted in Fig. 1.

Estrogens decreased inflammation in the abdominal structures at inspection

The IA+B model had the highest scores of alterations in abdominal viscera on each sacrifice day (day 7=15/18, day 14=17/18, day 28=14/18, and day 56=7/18) (Fig. 1). Comparing the models to their treatment subgroups, a statistically significant difference was present at each end point for the IA, IA+B and TNBS models, decreasing by approximately 20% compared to the non-treated group. A similar trend was observed with the DSS but the difference was not significant on days 7 and 56.

On the other hand, the estrogen treated rats and the non-treated controls showed low and similar inflammatory scores all along the experiment (Fig. 1).

Histological alterations

The IA+B, IA and TNBS-treated groups showed higher colonic histological scores than the controls or those treated with estrogen alone. However, the

DSS group showed a higher histological score in the jejunum than in the colon, probably because the DSS was provided orally to the rats. All four models exhibited inflammatory changes to various extents in the colon and jejunum. They were most severe in IA+B-treated groups at all time points, while relatively less in IA, TNBS, and DSS, respectively (Figs. 1 and 2).

The estrogen treatment decreased significantly all these changes, in all groups and at all time points. However, these alterations were never completely resolved by estrogen to reach the normal non treated or estrogen alone treated groups (Fig. 3).

Estrogens decreased the activity of mast cells in the colon

Mast cells responded to the induction of colitis by increasing significantly in number in all models compared to controls. The highest numbers were in the IA+B group at all time points and the lowest were in the DSS group (Figs. 1 and 4). The number of mast cells increased with the duration of the inflammation in each group, particularly in the IA+B group from an average of 73.2 on day 7, to 80 on day 14, to 91 on day 28 and 120 on day 56 compared with 8.3 and 7.5 in the group that received only estrogen and the non-treated group. In brief, estrogen treatment did show a

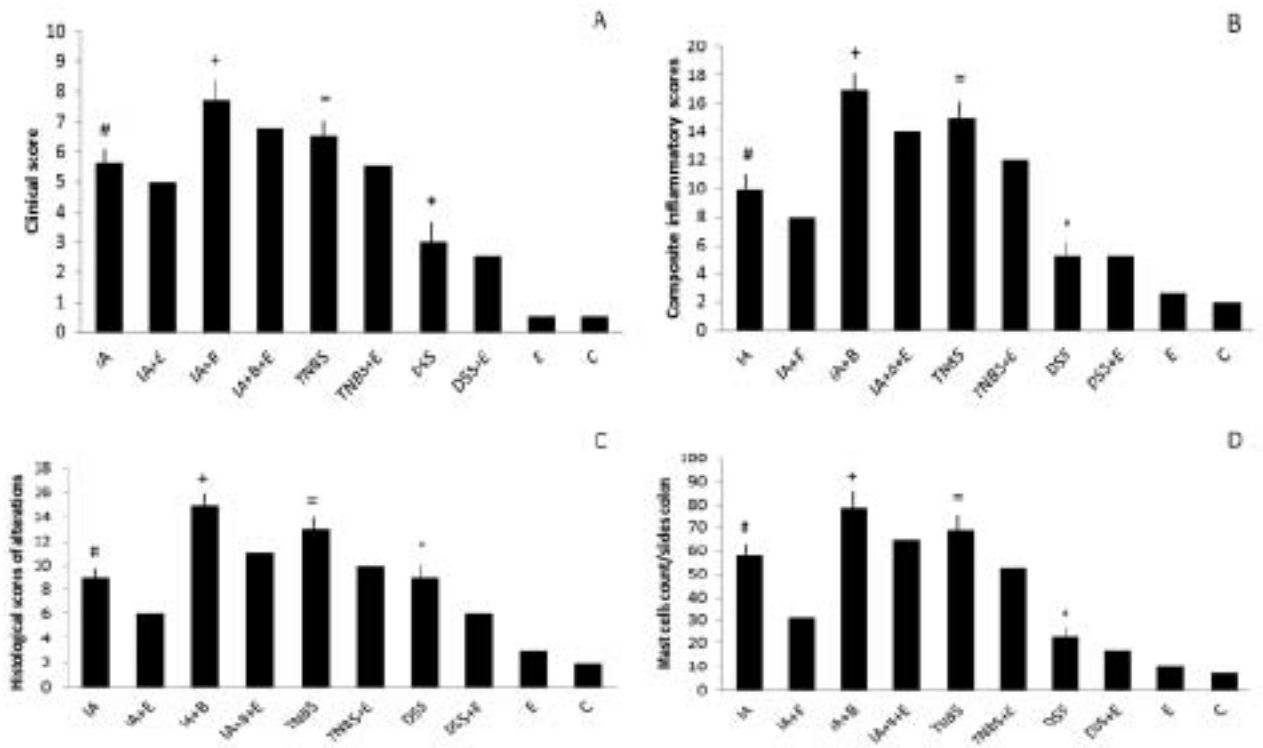

Fig. 1. *Clinical, macroscopic and histological assessment.* ***A)*** *Total clinical score on day 14. Note that in estrogen-treated rats, the scores were markedly lower.* ***B)*** *Composite inflammatory scores of abdominal viscera on day 14. Values represented the average scores of parameters including: damage site, morphology of Descending Colon (DC), mushroom-like structures per 10 cm, adhesions, vasodilatations and thickness of DC. The scores of the IA, IA+B, and TNBS subgroup were statistically significant when compared to their concordant treatment subgroups.* ***C)*** *Average composite histological scores of alterations in colon on day 14. The improvement of inflammatory reaction parameters was approximately 20%. Each score represents the average of total changes in mucosal architecture, in crypts, goblet cells, inflammatory cells infiltrate and edema. These alterations decreased significantly with estrogen.* ***D)*** *Mast cell count in the colon on day 14. Note that the count increased throughout the experiment in the IA, IA+B, and TNBS subgroups while in the DSS subgroups, the counts were much lower and constant; however, they were relatively two-fold more than the estrogen alone or normal. Similar results were seen on days 7, 28 and 56 but to a lesser extent (data not shown). T-test $p<0.05$; #$p<0.05$: IA vs IA+E groups; +$p<0.05$: IA+B vs IA+B+E groups; =$p<0.05$: TNBS vs TNBS+E groups; *$p<0.05$: DSS vs DSS+E groups.*

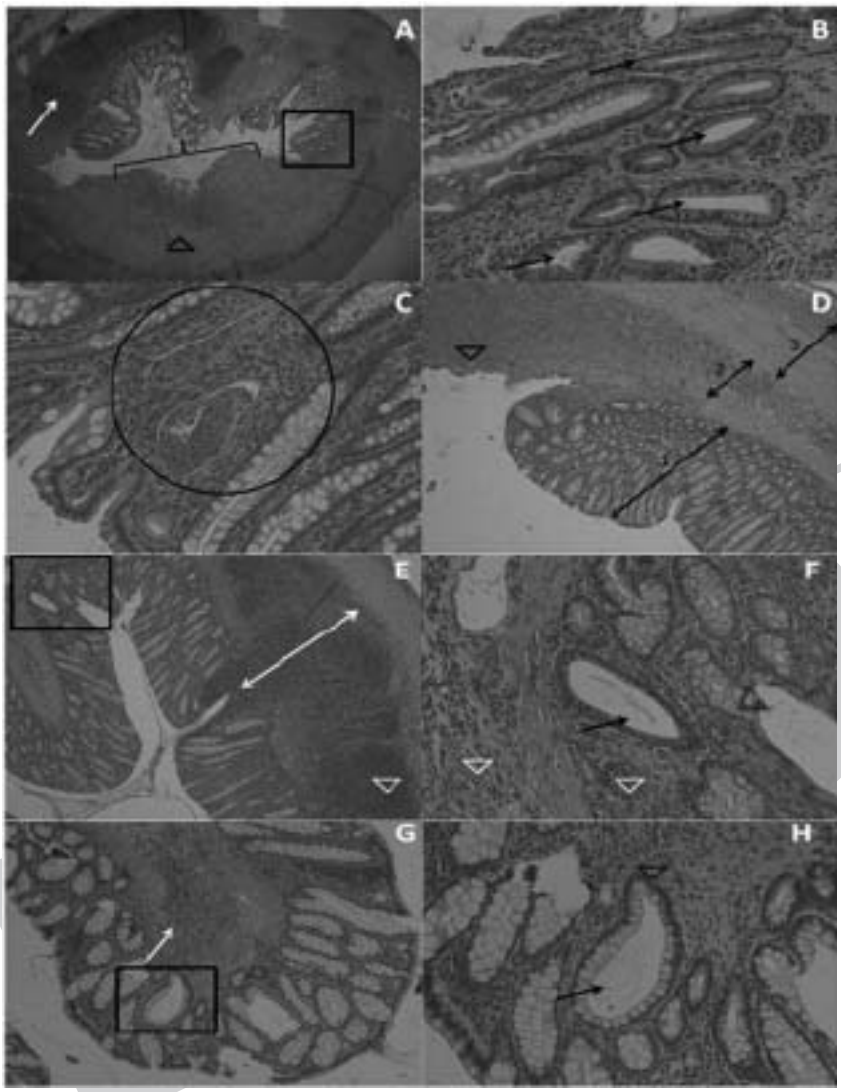

Fig. 2. *Induction of colitis led to microscopic changes in colonic structures.* ***A****) Disruption of colonic mucosal epithelium (parenthesis 100X) and Colonic Payer's patch (A-white arrow).* ***B****) Dilated crypts, circular and less loaded goblet cells (B-black arrow).* ***C****) Abscess in the mucosa crypts (C-black circle 400X) with invasion of the mucosa by inflammatory cells (A-D: black triangle 400X).* ***D****) Altered architecture of the colon layers in colon of rats treated with IA+EPEC (D-1: mucosa, 2: submucosa and 3: musculosa 100X).* ***E****) Altered architecture of the colon layers of the IA-treated rats (E-two headed white arrow 100X) with lymphoid tissue expansion.* ***F****) Dilated crypts, circular and less loaded goblet cells (F-black arrow 400X). Note the invasion of mucosa by inflammatory cells (E-F-white triangle).* ***G****) Cellular mucosal infiltration of the colon of DSS-treated rats (G-white arrow 100X).* ***H****) Dilated lumen of crypt (H-black arrow) with inflammatory aggregations (H-black triangle 400X).*

marked reduction in the number of mast cells across the board in all groups and at all time points. These reductions were significant in all models $p < 0.05$, except the DSS model (Figs. 1 and 4).

Modulation of TNF-α, IL-1β and IL-6 by estrogen

All 3 parameters showed a similar trend of expression. They all increased to various extents as a result of colitis induction throughout the experiment. The highest relative increase was in the IA+B, followed by TNBS and IA. This increase in expression in the colon was relatively the least with the DSS model.

As expected, TNF-α increased significantly

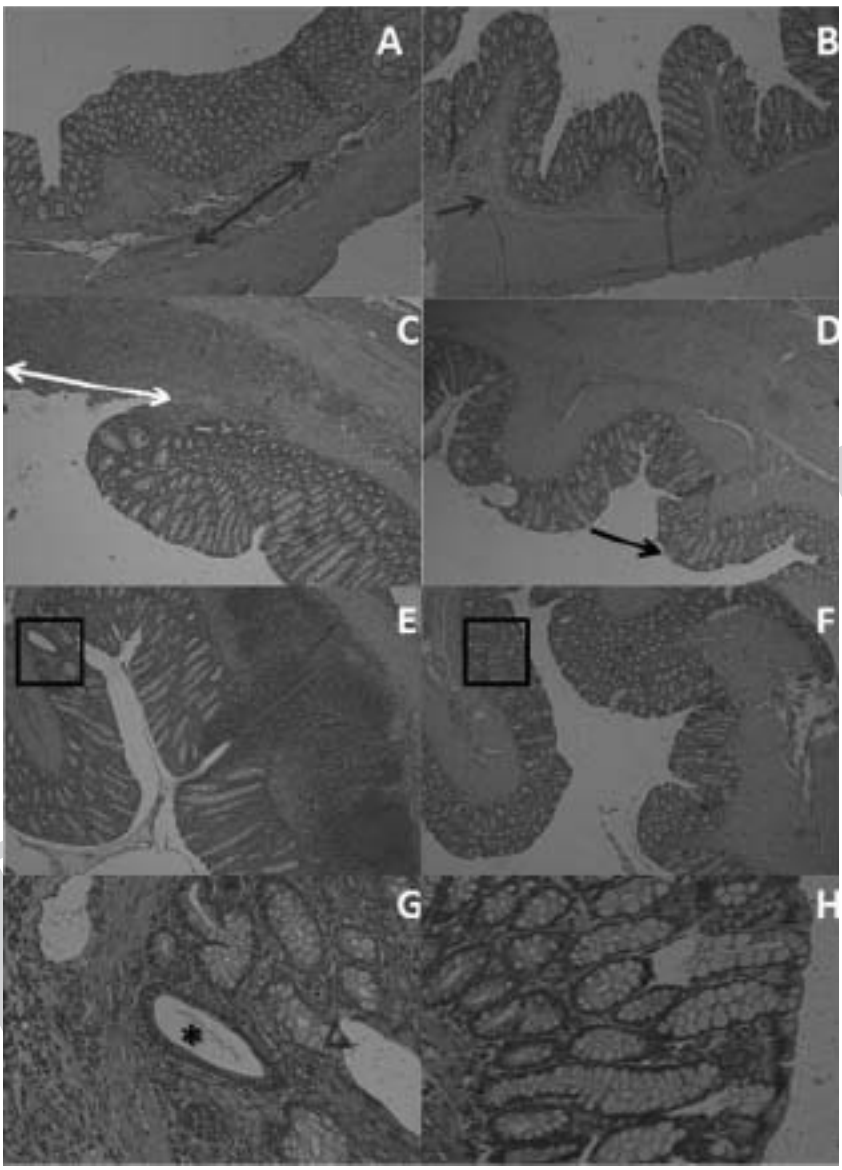

Fig. 3. *Microscopic alteration in the colon decreases upon treatment with estrogen. **A)** Note decreased edema in the colonic submucosa of estrogen-treated rats (gray doubled-headed arrow, 100X), compared to non-treated rats in (**B**). **C)** The sloughed epithelium in colitis animals (white double-headed arrow) is significant compared to (**D**) where estrogen was used (100X). **E)** Note the infiltration of inflammatory cells and extensive lymphoid follicles in non-treated colons compared to those of treated in (**F**) whereby the alterations were less. **G)** Higher magnification of the changes (400 X) compared to treated animals in (**H**) whereby alterations were less.*

compared to control levels in all models and at all time points. However, such increases were much lower on day 56 when the inflammatory reaction was sustained, and it was significantly higher than the controls in all groups except in the DSS (Fig. 5 A).

The high expressions of TNF-α, IL-1β and IL-6 were significantly reduced to various extents ($p < 0.05$) in the estrogen-treated groups at all time points (Fig. 5 B).

IL-B gene expression was similar to that of IL-6. Rats treated with estrogen showed marked and significant decreases in the levels of expression at all

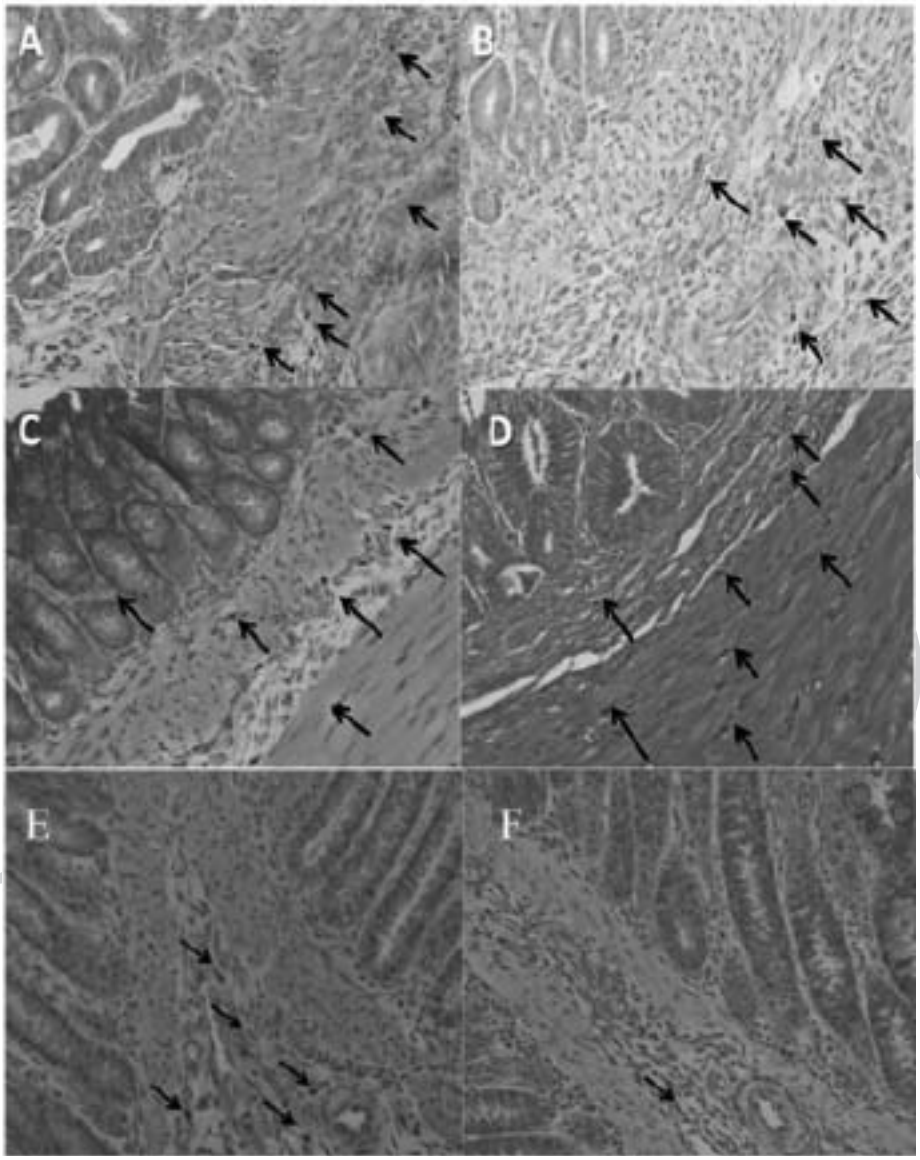

Fig. 4. *Number of mast cells infiltrating the colonic layer increases with the progression of inflammation and decreases with estrogen treatment. **A)** Microscopic observation of mast cells (black arrows) in colon of rats treated with IA+B at 400 X. The number of mast cells increases along with the progression of colitis from day 7 (**A**), day 14 (**B**), day 28 (**C**) and day 56 (**D**). In exacerbated cases, mast cells were diffused throughout the colonic layers (C-D). Animals treated with estrogen (**F**) had a decreased number of infiltrating mast cells in the colon compared with non-treated (**E**).*

time points (Fig. 5 C).

Fibronectin decreased by estrogen treatment

Fibronectin RNA expression increased significantly as a result of the induction of inflammation. Such an increase was maintained in the various groups compared to controls throughout the experiment. However, it decreased significantly in the tissues removed from the estrogen-treated rats at all time points (Fig. 5 D).

Dihydroethidine staining

Using DHE staining, the fluorescence was detected mostly in the IA + B model at day 14

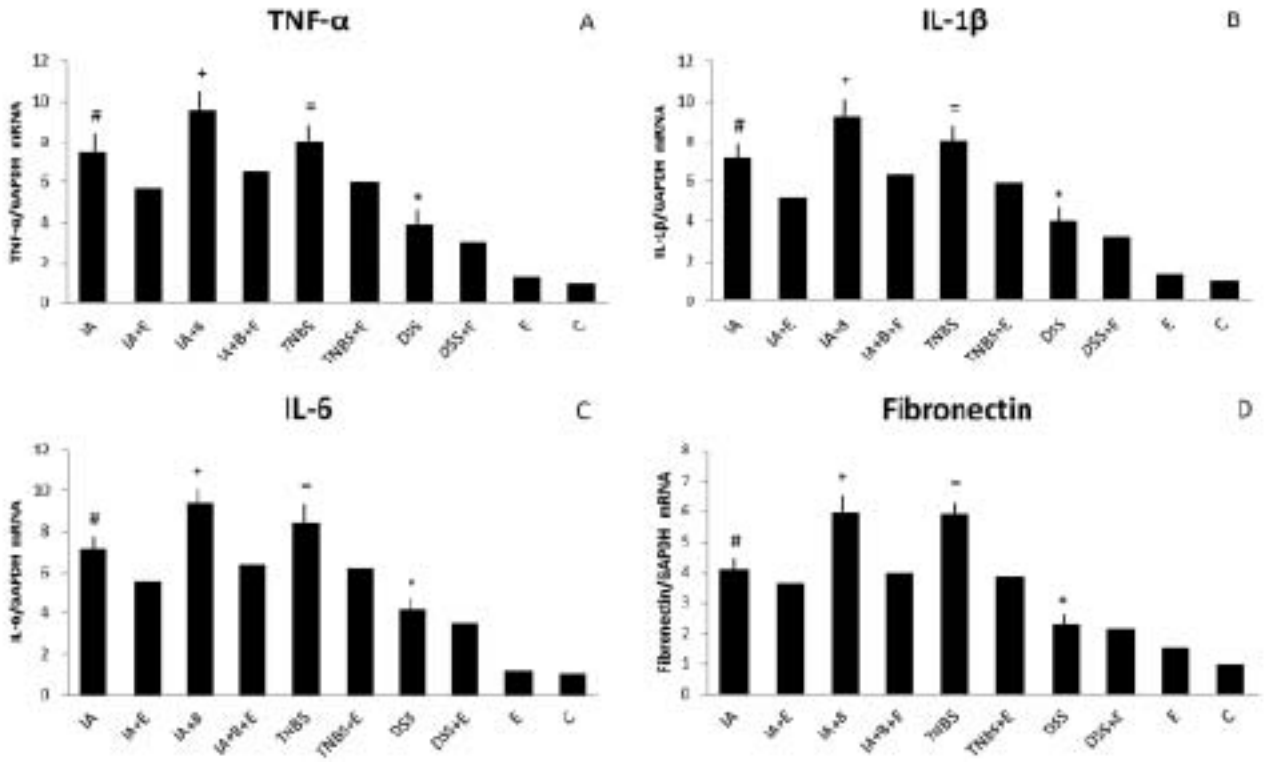

Fig. 5. *TNF-α, IL-1β, IL-6 and fibronectin expression on day 14. **A)** TNF-α gene expression decreased with estrogen treatment. The values represent amplification of TNF-α relative to GAPDH mRNA levels. The values on days 7, 14, and 28 were mostly equal, and then they decreased by more than half on day 56. The highest value was always found on the IA+B model at the 4 time points. They decreased significantly when the rats were treated with estrogen, except for DSS. **B)** IL-1β gene expression decreased with estrogen treatment. **C)** IL-1β gene expression decreased with estrogen treatment. **D)** Fibronectin gene expression decreased with estrogen treatment. In all these figures, the highest value was always found on the IA+B model at the 4 time points (data not shown). They decreased significantly when the rats were treated with estrogen. Similar results were seen on days 7, 28 and 56 but to a lower extent (data not shown). T-test $p<0.05$; #$p<0.05$: IA vs IA+E groups; +$p<0.05$: IA+B vs IA+B+E groups; =$p<0.05$: TNBS vs TNBS+E groups; *$p<0.05$: DSS vs DSS+E groups.*

(Relative mean of intensity= 27 for jejunum, 19 for the kidney and 24 for the liver). Such expressions decreased significantly by more than 30% ($P<0.05$) following estrogen treatment (Figs. 6, 7). There was a positive correlation between the fluorescence intensity and the duration of the inflammation. The DSS model showed fluorescence intensity that was very close to normal (average of 5 for the intensity in the control and 5.5 in the DSS model).

DISCUSSION

The beneficial effects of estrogen treatment in experimental models of inflammatory bowel disease are well documented (3, 8, 9, 25). A significant reduction of colonic TNF-α level in rats with experimentally-induced colitis was previously reported (9, 10). The ability of estrogen to improve disease progression has been attributed to its interference with NF-KB activity. This interference is mediated by the ER receptors, and is not a direct antioxidant effect of estrogen (26). In addition, mast cells numbers and degranulation decreased in the estrogen-treated rat colons compared with non-treated rats. This fact suggests that estrogen may exert its effect partly through modulation of mast cell activity (22, 27). Understanding the basic mechanism of estrogen action in the various colitis models might provide new pathways for the treatment of inflammatory bowel disease.

To date, no consensus has been reached regarding

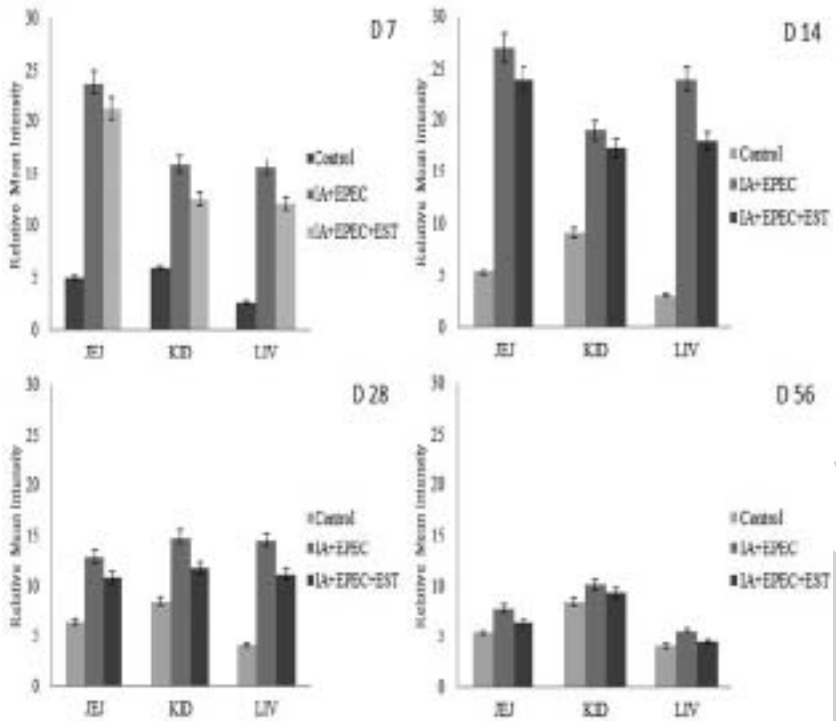

Fig. 6. *Relative mean intensity of the red fluorescence in the jejunum, kidney, and liver of the IA+B-treated rat models on days 7, 14, 28, 56. It is more intense on day 14 followed by days 7, 28 then 56. The estrogen treatment reduces this intensity significantly. T-test p<0.05; + p<0.05: IA+B vs IA+B+E groups.*

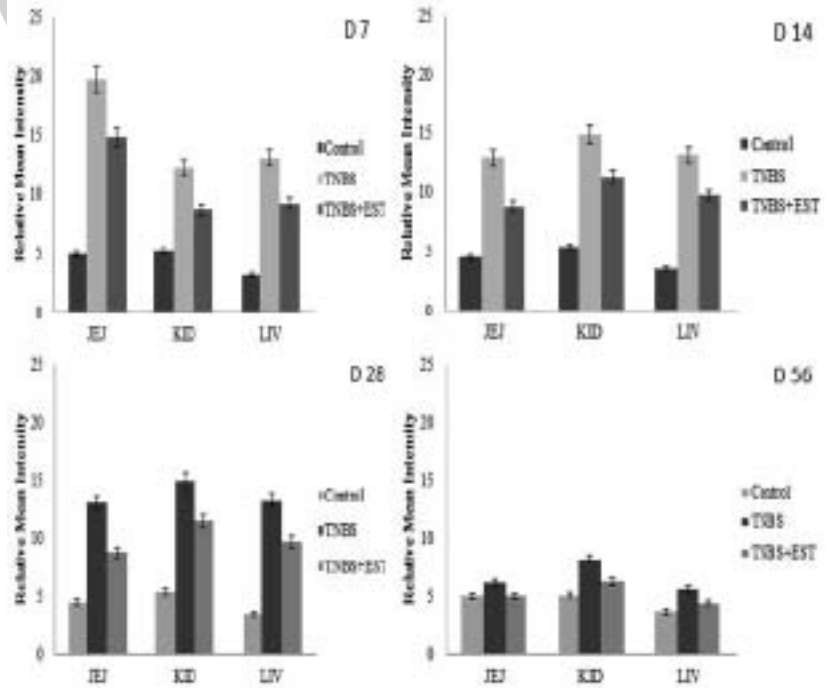

Fig. 7. *Relative mean intensity of the red fluorescence in the jejunum, kidney, and liver of the TNBS-treated rats model on days 7, 14, 28, 56. It is more intense on day 7 followed by days 14, 28 then 56. The estrogen treatment reduced this intensity significantly.T-test p<0.05; = p<0.05: TNBS vs TNBS+E groups.*

the role of estrogen in IBD. Multiple studies have shown that estrogen suppresses chronic inflammation in several animal models of chronic inflammatory diseases. On the other hand, other studies have reported that estrogen has a pro-inflammatory effect in some chronic autoimmune diseases in humans as an initiating or perpetuating factor.

The present data show that estrogen possesses an anti-inflammatory role in experimental colitis. Estrogen improved experimental colitis both clinically and histologically. The subgroup that showed the least expression of such parameters and the lowest scores was the DSS, while the one that showed the most and the highest inflammation scores was the iodacetamide plus bacteria, seconded by the iodoacetamide alone and TNBS groups. Such results go in concordance with findings reported by Verdu et al. (9). Such an effect of estrogen was expressed across the board; however, where the inflammation was more severe the effect of estrogen was more significant (Fig. 1). In addition, treatment with estrogen significantly attenuated the damage in morphology associated with all the panel models of induced colitis (Figs. 2, 3).

The mast cells, which are important players in this inflammatory process, have been affected. Data showed that the number of mast cells increased markedly in the various IBD models upon induction compared to controls. Previous data, reported by Harnish et al. (8), as well as our own, showed that such an increase of mast cells correlated significantly with the severity and duration of the disease found in rat models of experimental colitis (22). In our experiment, the numbers were highest in the IA+B group seconded by the IA and TNBS then the DSS (Figs. 1, 4). It is important also to note that the numbers were associated with the chronicity of the inflammation in each group and not only the total number of mast cells increased but also the number of degranulating (activated) cells. It seems as if the estrogen is inhibiting the activity of mast cells or even their proliferation through the decreased expression of cytokines from nearby cells. Thus, leading to a decrease in the secretion of TNF-α, IL-1β and other factors or through the ERβ down regulation (1, 28).

Previous work from our group (11, 22) also reported increased levels of mucosal proinflammatory cytokines in IBD's, such as Il-1β, IL-6, TNF-α and others, which have been shown to play an important role in sustained inflammatory responses. It was also reported that expression of these immunomodulatory agents seems to be regulated mainly by the transcription factor NFkB. Preventing NFkB activation and cytokine production might result in the prevention of mucosal inflammation (28). Compounds like estrogen which down regulate the production of cytokines as IL-1β, IL-6 and TNF-α, might be acting through the deactivation or prevention of activation of NFkB, thus proving to be beneficial in the treatment of IBD. The use of estrogen as a treatment for IBD has alleviated inflammation and reduced symptoms but has not provided a cure or completely prevented complications. In brief, estrogen shows the potential as a proper effective molecule which might induce protective responses by inhibition of the production of proinflammatory cytokines. Estrogen has also decreased intestinal fibrosis, a dynamic multifactorial process which results from the reaction of intestinal tissue to the damage inflicted by chronic inflammation. Intestinal fibrosis can occur in both forms of IBD and is a common complication that follows inflammation. Estrogen treatment decreased fibronectin significantly in all tested models of colitis. Consequently, the process of fibrosis which is commonly recognized as unidirectional and irreversible could be improved in light of the data emanating from these experiments (29, 30). The effect is probably through decreasing the proliferation and activity of fibroblasts secreting such extracellular matrix molecules.

In conclusion, rats with IBD improved clinically and histologically with the use of estrogen. Based on this observation, further studies are needed to elucidate estrogen mechanism of action and possible side effects. The results we present suggest that this protective effect is mediated by limiting the inflammatory reaction, decreasing mucosal mast cell activity as well as the secretion of pro-inflammatory cytokines TNFα, IL-1β, and IL-6 and decreased necrosis through its effect on fibronectin and ROS.

ACKNOWLEDGEMENTS

This research was supported by the Lebanese National Council for Scientific Research.

REFERENCES

1. Straub RH. The complex role of estrogens in inflammation. Endocr rev 2007; 28:521-74.
2. Olsen NJ, Kovacs WJ. Gonadal steroids and immunity. Endocr rev 1996; 17:369-84.
3. Yamada K, Hayashi T, Kuzuya M, Naito M, Asai K, Iguchi A. Physiological concentration of 17β-estradiol inhibits chemotaxis of human monocytes in response to monocyte chemotactic protein 1. Artery 1996; 22:24-35.
4. Ralston SH, Russell RG, Gowen M. Estrogen inhibits release of tumor necrosis factor from peripheral blood mononuclear cells in postmenopausal women. J Bone Miner Res 1990; 5:983-88.
5. Sato T, Ito A, Mori Y, Yamashita K, Hayakawa T, Nagase H. Hormonal regulation of collagenolysis in uterine cervical fibroblasts. Modulation of synthesis of procollagenase, prostromelysin and tissue inhibitor of metalloproteinases (TIMP) by progesterone and oestradiol-17 beta. Bio Chem J 1991; 275:645-50.
6. Barth A, Landmann G, Liepold K, Zapf H, Müller D, Karge E, Klinger W. Influence of oestrogens on formation of reactive oxygen species in liver microsomes of differently aged male Wistar rats. Exp Toxico Pathol 1999; 51:282-88.
7. Kawasaki T, Ushiyama T, Inoue K, Hukuda S. Effects of estrogen on interleukin-6 production in rheumatoid fibroblast-like synoviocytes. Clin Exp Rheumatol 2000; 18:743-45.
8. Harnish DC, Albert LM, Leathurby Y, Eckert AM, Ciarletta A, Kasaian M, Keith JC Jr. Beneficial effects of estrogen treatment in the HLA-B27 transgenic rat model of inflammatory bowel disease. Am J Physiol Gastrointest Liver Physiol 2004; 286:G118-25.
9. Verdú EF, Deng Y, Bercik P, Collins SM. Modulatory effects of estrogen in two murine models of experimental colitis. Am J Physiol Gastrointest Liver Physiol 2002; 283:G27-36.
10. Jurjus AR, Khoury NN, Reimund JM. Animal models of inflammatory bowel disease. J Pharmacol Toxicol Methods 2004; 50:81-92.
11. Hajj Hussein IA, Tohme R, Barada K, Mostafa MH, Freund JN, Jurjus RA, Karam W, Jurjus A. Inflammatory bowel disease in rats: bacterial and chemical interaction. World J Gastroenterol 2008; 14:4028-39.
12. Borm M, Bouma G. Animal models of inflammatory bowel diseases. Drug Discovery Today: Dis Mod 2004; 1:437-43.
13. Imaoka M, Kato M, Tago S, Gotoh M, Satoh H, Manabe S. Effects of estradiol treatment and/or ovariectomy on spontaneous hemorrhagic lesions in the pancreatic islets of Sprague-Dawley rats. Toxicol Pathol 2009; 37:218-26.
14. Satoh H, Sato F, Takami K, Szabo S. New ulcerative colitis model induced by sulfhydryl blockers in rats and the effects of antiinflammatory drugs on the colitis. Jpn J Pharmacol 1997; 73:299-309.
15. Morris GP, Beck PL, Herridge MS, Depew WT, Szewczuk MR, Wallace JL. Hapten-induced model of chronic inflammation and ulceration in the rat colon. Gastroenterology 1989; 96:795-803.
16. Fan J, Yu LH, Zhang Y, Ni X, Ma B, Burnstock G. Estrogen altered visceromotor reflex and P2X(3) mRNA expression in a rat model of colitis. Steroids 2009; 74:956-62.
17. Wirtz S, Neufert C, Weigmann B, Neurath MF. Chemically induced mouse models of intestinal inflammation. Nat Protoc 2007; 2:541546.
18. Chung HL, Yue GG, To KF, Su YL, Huang Y, Ko WH. Effect of Scutellariae Radix extract on experimental dextran-sulfate sodium-induced colitis in rats. World J Gastroenterol 2007; 13:5605-11.
19. Azuma YT, Nishiyama K, Matsuo Y, Kuwamura M, Morioka A, Nakajima H, Takeuchi T. PPARα contributes to colonic protection in mice with DSS-induced colitis. Int Immunopharmacolm 2010; 10:1261-67.
20. Bindokas VP, Jordán J, Lee CC, Miller RJ. Superoxide production in rat hippocampal neurons: selective imaging with hydroethidine. J Neurosci 1996; 16:1324-36.
21. Rivera A, Maxwell SA. The p53-induced gene-6 (proline oxidase) mediates apoptosis through a calcineurin-dependent pathway. J Biol Chem 2005; 280:29346-54.
22. Hajj Hussein AI, Freund JN, Reimund JM, Shams A, Yamine M, Leone A, Jurjus AR. Enteropathogenic *E. coli* sustains iodoacetamide-induced ulcerative colitis-like colitis in rats: modulation of IL-1beta, IL-6, TNF-alpha, COX-2, and apoptosisi. J Biol Regul

Homeost Agents 2012; 26:515-26.

23. Miller FJ Jr, Gutterman DD, Rios CD, Heistad DD, Davidson BL. Superoxide production in vascular smooth muscle contributes to oxidative stress and impaired relaxation in atherosclerosis. Circ Res 1998; 82:1298-305.
24. Zhao H, Kalivendi S, Zhang H, Joseph J, Nithipatikom K, Vásquez-Vivar J, Kalyanaraman B. Superoxide reacts with hydroethidine but forms a fluorescent product that is distinctly different from ethidium: potential implications in intracellular fluorescence detection of superoxide. Free Radic Biol Med 2003; 34:1359-68.
25. Motavallian-Naeini A., Minaiyan M, Rabbani M, Mahzuni P. Anti-inflammatory effect of ondansetron through 5HT3 receptors on TNBS-induced coloitis in rat. EXCLI J 2012; 11:30-44.
26. Zhou YH, Yu JP, Liu YF, et al. Effects of ginkgo biloba extract on inflammatory mediators (SOD, MDA, TNF-α, NF-κ Bp65, IL-6) in TNBS-induced colitis in rats. Mediators Inflamm 2006; 2006:92642.
27. La JH, Kim TW, Sung TS, Kim HJ, Kim JY, Yang IS. Role of mucosal mast cells in visceral hypersensitivity in a rat model of irritable bowel syndrome. J Vet Sci 2004; 5:319-24.
28. Ukil A, Maity S, Das PK. Protection from experimental colitis by theaflavin-3, 3′-digallate correlates with inhibition of IKK and NF-κB activation. Br J Pharmacol 2006; 149:121-31.
29. Rieder F, Fiocchi C. Intestinal fibrosis in IBD - a dynamic, multifactorial process. Nat Rev Gastroenterol Hepatol 2009; 6:228-35.
30. Hamamoto N, Maemura K, Hirata I, Murano M, Sasaki S, Katsu K. Inhibition of dextran sulphate sodium (DSS)-induced colitis in mice by intracolonically administered antibodies against adhesion molecules endothelial leucocyte adhesion molecule-1 (ELAM-1) or intracellular adhesion molecule-1 (ICAM-1)) Clin Exp Immunol 1999; 117:462-68.

CLINICAL ASSOCIATION OF CIRCULATING VEGF-B LEVELS WITH HYPERLIPIDEMIA AND TARGET ORGAN DAMAGE IN TYPE 2 DIABETIC PATIENTS

C.Y. SUN[1], C.C. LEE[1], M.F. HSIEH[1], C.H. CHEN[2] and K.M. CHOU[2]

[1]Department of Nephrology, [2]Department of Endocrinology and Metabolism, Chang Gung Memorial Hospital, Keelung, Taiwan

Received September 8, 2013 – Accepted April 9, 2014

Vascular endothelial growth factor-B (VEGF-B is an important member of the VEGF protein family. Recent animal studies indicated that VEGF-B signaling had determinant roles in insulin resistance, lipid distribution and metabolism in type 2 diabetes. The clinical significance of VEGF-B in type 2 diabetes is still not clear. This study aimed to correlate VEGF-B levels with biochemistry characteristics and target organ damage in type 2 diabetic patients. Serum VEGF-B levels were measured using ELISA. A cross-sectional control study, which included 180 type 2 diabetic patients and 62 healthy subjects, was carried out. Diabetic patients who were undergoing insulin therapy were not included. This results showed that serum VEGF-B levels did not differ between the type 2 diabetic patients and the healthy controls (169.2±118.8 *vs* 163.5±115.2 pg/mL; P=0.734). VEGF-B levels in type 2 diabetic patients were significantly associated with the levels of c-peptide, total cholesterol and triglyceride. *T*-test analysis showed that the associations of serum VEGF-B levels with insulin resistance, pancreatic reserve, HDL and LDL were not significant. Regression analysis showed that VEGF-B levels were significantly correlated with diabetic retinopathy and nephropathy. No significant association between VEGF-B and macro-vasculopathy was found. In conclusion, our study findings suggested that VEGF-B levels did not differ between the type 2 diabetic patients and the normal controls. High VEGF-B levels might correlate with the presence of hyperlipidemia and target organ damage in type 2 diabetic patients.

Type 2 diabetes melllitus (DM) has a high prevalence worldwide and a serious impact on public health (1). Type 2 DM is typically associated with a shorter life expectancy due to its related complications (2). Insulin resistance, which is the inability of cells to respond adequately to normal levels of insulin, is considered to be the major pathological mechanism in the development of type 2 DM. In addition to the effect on the glucose disposal, insulin resistance is also associated with dysregulated protein and lipid metabolism (3, 4).

Vascular endothelial growth factors (VEGFs) are a family of signal proteins similar to that of platelet-derived growth factors. Vascular endothelial growth factor-B (VEGF-B) is an important member of the VEGF protein family, and is abundantly expressed in most tissues and organs (5-8). The biological function of VEGF-B is not fully understood currently. Studies with VEGF-B transgenic mice suggested that VEGF-B has no significant activities under normal conditions (9). A recent study suggested that VEGF-B plays an important role in regulating lipid

Key words: Type 2 diabetes mellitus, vascular endothelial growth factor-B, target organ damage

Mailing address:
Kuei-Mei Chou, M.D.,
Department of Endocrinology and Metabolism,
Chang Gung Memorial Hospital,
No. 222, Mai-Jin Road,
Keelung, Taiwan
e-mail: sylvia@ms32.url.com.tw

0393-974X (2014)

DISCLOSURE: ALL AUTHORS REPORT NO CONFLICTS OF INTEREST RELEVANT TO THIS ARTICLE.

and glucose metabolism. An animal study indicated that increased ceramide and decreased triglyceride levels were found in VEGF-B transgenic hearts (10). It was also reported that VEGF-B knock-out mice showed less uptake and accumulation of lipids in muscle, heart and brown adipose tissue, and instead shunted lipids to white adipose tissue (11). VEGF-B has been suggested recently to be a therapeutic target for insulin resistance and type 2 diabetes. The vascular endothelium can function as an efficient barrier to excess muscle lipid uptake even under conditions of severe obesity and type 2 diabetes by antagonizing VEGF-B signaling (12). However, clinical data related to the pathological roles of VEGF-B in type 2 diabetic patients are scarce, so the clinical significance of VEGF-B is still unclear.

This study aimed to compare the serum VEGF-B levels of type 2 diabetes patients and a non-diabetic population. The putative associations of VEGF-B levels with insulin resistance characteristics and target organ damage in type 2 diabetic patients were examined.

MATERIALS AND METHODS

Study subjects

A cross-sectional control study, which included 180 prevalent type 2 diabetic patients and 62 non-diabetic controls, was carried out. Type 2 diabetes was diagnosed using the World Health Organization (WHO) criteria (13). Data on the administration of hypoglycemic drugs, and anti-hypertension and lipid-lowering medications during the most recent months were obtained from the clinical records of each patient. All type 2 diabetic patients included in this study received oral regimens of sulfonylurea/metformin with or without thiazolidinediones (TZD) as anti-diabetes therapy, and multi-discipline diabetic care according to the ADA's clinical practice recommendations (14).

Cerebral vascular accidents (CVA) and coronary vascular disease (CAD) were defined as the documented major events that required hospitalization during the previous 3 years. Diabetic retinopathy was diagnosed based on the findings of the fundus examination (15). Peripheral arterial occlusion disease (PAOD) was diagnosed by the ankle brachial index (ABI $\leq$0.9) (16). Diabetic peripheral neuropathy was diagnosed by decreasing vibration perception (17).

The study was approved by the Human Ethics Review Committee, Chang Gung Memorial Hospital, Taiwan, and performed in accordance with the Declaration of Helsinki.

Biochemical analysis

Blood samples were collected from all subjects after overnight fasting for at least 10 hours. Albuminuria was measured with the urine albumin-to-creatinine ratio (18). The indexes of the homeostatic model assessment for insulin resistance (HOMA-IR) and beta cell function (HOMA-beta) were calculated as in a previous report (19). Another index for insulin resistance, the quantitative insulin sensitivity check index (QUICKI), was also calculated (20).

VEGF-B was measured by the ELISA method (ELISA kit for human VEGF-B; Uscn LifeScience Inc., Wuhan, P.R. China) using frozen stored serum (21). Each serum sample was analyzed in duplicate, and the average value was used for the statistical analysis that followed. The detection range of the VEGF-B ELISA test was 15.6 to 1000 pg/mL. The samples with a VEGF-B concentration greater than the upper detection limit were analyzed with a serial dilution. The intra- and inter-assay coefficients of variation for the test were less than 10% and 12%, respectively.

Statistical analysis

Descriptive statistics were expressed as means ± standard deviation or percentage frequency, as appropriate. Paired *t*-tests were used to compare means of continuous variables. The normal distribution of VEGF-B of the study subjects was examined with the Shapiro-Wilk W test, and plotted with the Gaussian distribution formula. Pearson correlation coefficients were used to test correlations between the VEGF-B levels and other biochemical variables. Multiple linear regression analysis was used to determine the independent association between the VEGF-B levels and other biochemical variables. Logistic regression analysis was used to test the independent association between VEGF-B and diabetic retinopathy. A P-value < 0.05 was considered significant (two-tailed). Data were analyzed using the commercially available SPSS 16.0 statistical software program (SPSS, Chicago, IL, USA).

RESULTS

Serum VEGF-B levels in diabetic patients and non-diabetic controls

In all, 180 diabetic patients and 62 non-diabetic controls were included in the study. There were no significant differences in age and gender between the two study groups. The serum VEGF-B levels of the diabetic patients and non-diabetic controls were 169.2±118.8 and 163.5±115.2 pg/mL, respectively; the difference between the two groups was not significant (P = 0.734) (Table I). Gaussian

distribution of the VEGF-B levels of the two study groups was tested, and the results revealed a normal distribution (Fig. 1).

Associations of VEGFB with c-peptide levels and PPAR agonist therapy in type 2 diabetic patients

Pearson correlation analysis revealed that serum VEGF-B levels were positively and significantly correlated with c-peptide levels (Pearson correlation: 0.230; P = 0.012) (Fig. 2A). In addition, diabetic patients without TZD therapy had significantly higher serum VEGF-B levels than those with TZD therapy (176.0±129.2 *vs* 140.2±45.9 pg/mL; P = 0.008) (Fig. 2B). No significant associations of VEGF-B with indexes of insulin resistance (HOMA-IR, QUICKI) and pancreatic reserve (HOMA-beta) were noted (Table IIA). After adjustment for age, gender, BMI, DM duration, HbA1C and TZD, multiple linear regression analysis demonstrated that VEGF-B was the significantly independent determinant variable for variance of serum c-peptide (standardized coefficients: 0.196; P = 0.020) (Table IIIA).

Associations of VEGF-B with total cholesterol and triglyceride levels in type 2 diabetic patients

In the diabetic patients, serum VEGF-B levels

Table I. *Demographic features of the study subjects.*

	DM (n=180)	non-DM (n=62)	P
Age (Y/O)	56.4±10.5	59.0±7.1	0.200
Gender (M/F)	96/84	24/38	1.000
DM duration (month)	81.6±64.6	0	0.000
SBP (mmHg)	135.0±13.6	123.5±13.3	0.004
DBP (mmHg)	75.9±8.6	69.3±8.5	0.022
BMI	27.3±4.3	23.9±3.9	0.000
Fasting sugar (mg/dL)	151.4±43.6	97.5±6.2	0.000
HbA1C (%)	7.6±1.3	5.6±0.3	0.000
Insulin (mU/L)	13.5±25.7	6.7±3.1	0.001
c-peptide (ng/mL)	3.3±2.1	1.6±0.7	0.000
Total cholesterol (mg/dL)	216.3±32.1	179.0±37.1	0.001
Triglyceride (mg/dL)	179.4±135.0	124.2±32.1	0.007
HDL (mg/dL)	42.1±12.3	60.5±15.4	0.000
LDL (mg/dL)	132.6±34.3	101.1±31.6	0.007
BUN (mg/dL)	15.9±7.4	12.1±3.1	0.000
Creatinine (mg/dL)	0.9±0.3	0.6±0.1	0.000
Albuminuria (mg)	183.8±530.4	3.3±2.7	0.000
HS-CRP (mg/dL)	2.8±5.7	1.3±1.1	0.006
VEGF-β (pg/mL)	169.2±118.8	163.5±115.2	0.734
ACEI/ARB (%)	60.0	3.5	0.000
Statin/ezetrol/fibrate (%)	64.4	0	0.000
TZD (%)	18.9	0	0.000

DM: diabetes mellitus; SBP: systolic blood pressure, DBP: diastolic blood pressure; BMI: body mass index; HbA1C: glycosylated hemoglobin; HDL: high-density lipoprotein; LDL: low-density lipoprotein; HS-CRP: high-sensitivity C-reactive protein VEGF-B: vascular endothelial growth factor-B: ACEI: angiotensin-converting-enzyme inhibitor; ARB: angiotensin receptor blocker; TZD: thiazolidinediones.

Table II. *Univariate analysis of the association of VEGF-B with general characteristics, biochemical parameters and medications of diabetic patients (n=180).*

A

VEGF-B	Pearson correlation (Beta)	P
Age	-0.116	0.121
DM duration	-0.036	0.633
SBP	0.029	0.695
DBP	0.073	0.333
BMI	-0.039	0.601
Fasting sugar	-0.028	0.708
Insulin	-0.013	0.862
c-peptide	0.23	0.012*
HOMA-IR	0.001	0.988
HOMA-beta	-0.039	0.602
QUICKI	-0.053	0.481
HbA1C	0.054	0.477
Total cholesterol	0.16	0.033*
Triglyceride	0.203	0.007*
HDL	-0.054	0.475
LDL	0.062	0.421
BUN	0.174	0.022*
Creatinine	0.145	0.036*
Albuminuria	0.169	0.024*
HS-CRP	-0.049	0.514

B

Gender	**Male (n=94)**	**Female (n=86)**	**P**
VEGF-B (pg/mL)	180.5±150.6	156.9±67.9	0.172
ACEI/ARB	**With (n=108)**	**Without (n=72)**	**P**
VEGF-B (pg/mL)	163.8±74.5	177.4±164.6	0.511
Statin/ezetrol/fibrate	**With (n=116)**	**Without (n=64)**	**P**
VEGF-B (pg/mL)	170.2±127.0	167.5±103.2	0.880
TZD	**With (n=34)**	**Without (n=146)**	**P**
VEGF-B (pg/mL)	140.2±45.9	176.0±129.2	0.008*

*A) Results of Pearson correlation analysis; **B**) results of independent-samples t test. (*: P< 0.05) DM: diabetes mellitus; SBP: systolic blood pressure; DBP: diastolic blood pressure; BMI: body mass index; HbA1C: glycosylated hemoglobin; HDL: high-density lipoprotein; LDL: low-density lipoprotein; HS-CRP: high-sensitivity C-reactive protein; VEGF-B: vascular endothelial growth factor–B; ACEI: angiotensin-converting-enzyme inhibitor; ARB: angiotensin receptor blocker; TZD: thiazolidinediones; HOMA-IR: Homeostasis Model of Assessment - Insulin Resistance; HOMA-Beta: Homeostasis Model of Assessment - Beta-cell Function; QUICKI: quantitative insulin sensitivity check index.*

Table III. *Multiple linear regression analysis for the correlations between the levels of serum VEGF-B and other clinical parameters in type 2 diabetic patients (n=180).*

A

c-peptide	Standardized Coefficients (Beta)	t	P
VEGF-B	0.196	2.537	0.020*
Age	-0.032	-0.362	0.718
Gender	-0.093	-1.096	0.267
BMI	0.394	4.633	0.000*
DM duration	0.058	0.631	0.529
HbA1C	0.063	0.727	0.469
TZD	-0.189	-2.233	0.028*

B

Total cholesterol	Standardized Coefficients (Beta)	t	P
VEGF-B	0.156	2.105	0.037*
Age	-0.025	-0.313	0.754
Gender	-0.145	-1.933	0.055
DM duraion	-0.129	-1.58	0.116
BMI	-0.069	-0.896	0.372
HbA1C	0.142	1.875	0.062
Statin/ezetrol/fibrate	0.155	2.088	0.038*
TZD	0.016	0.203	0.839

C

Triglyceride	Standardized Coefficients (Beta)	t	P
VEGF-B	0.158	2.213	0.028*
Age	-0.186	-2.392	0.018*
Gender	0.094	1.306	0.193
DM duraion	-0.036	-0.445	0.650
BMI	0.141	1.915	0.057
HbA1C	0.015	0.201	0.841
Statin/ezetrol/fibrate	0.181	2.543	0.012*
TZD	-0.131	-1.755	0.081

D

UACR	Standardized Coefficients (Beta)	t	P
VEGF-B	0.174	2.274	0.024*
Age	0.044	0.53	0.597
Gender	0.012	0.162	0.872
DM duraion	0.092	1.089	0.278
BMI	0.092	1.148	0.253
SBP	0.126	1.602	0.111
HbA1C	-0.005	-0.062	0.951
ACEI/ARB	-0.011	-0.146	0.881
Statin/ezetrol/fibrate	-0.017	-0.217	0.829
TZD	-0.012	-0.146	0.884

A) c-peptide: adjusted for age, gender, BMI, DM duration, and TZD. ***B****) total cholesterol: adjusted for age, gender, DM duration, BMI, HbA1C statin/ezetrol/fibrate and TZD.* ***C****) triglyceride: adjusted for age, gender, DM duration, BMI, HbA1C statin/ezetrol/fibrate and TZD.* ***D****) UACR: adjusted for age, gender, DM duration, BMI, SBP, HbA1C, ACEI/ARB, statin/ezetrol/fibrate and TZD. (*: P < 0.050) VEGF-B: vascular endothelial growth factor-B; DM: diabetic mellitus; BMI: body mass index; HbA1C: glycosylated hemoglobin; TZD: thiazolidinediones; UACR: urine albumin-to-creatinine ratio; SBP: systolic blood pressure; ACEI: angiotensin-converting-enzyme inhibitor; ARB: angiotensin receptor blocker.*

were positively and significantly correlated with the levels of total cholesterol (Pearson correlation: 0.160; P = 0.033) (Fig. 3A) and triglyceride (Pearson correlation: 0.203; P = 0.007) (Fig. 3B). Subgroup analysis with cutoff values of cholesterol ≥ 200 mg/dL and triglyceride ≥ 200mg/dL also showed that patients with higher cholesterol or triglyceride had higher VEGF-B levels (Fig. 3C, 3D). After adjustment for age, gender, DM duration, BMI, HbA1C statin/ezetrol/fibrate and TZD, multiple linear regression analysis demonstrated that VEGF-B was the significantly independent determinant variable for variance of serum total cholesterol (standardized coefficient: 0.156; P = 0.037) (Table IIIB) and triglyceride levels (standardized coefficient: 0.158; P = 0.028) (Table IIIC). No significant associations of VEGF-B with HDL, LDL or anti-hyperlipidemia therapy were found (Table IIB).

Associations of VEGF-B with diabetic nephropathy in type 2 diabetic patients

VEGF-B levels were significantly associated with serum BUN (standardized coefficient: 0.174; P = 0.022) (Fig. 4A), creatinine (standardized

Table IV. *T-test analysis of the association between VEGF-B and target organ damage in diabetic patients (n=180).*

CVA	**With (n=25)**	**Without (n=155)**	**P**
VEGF-B (pg/mL)	169.1±100.8	169.2±121.7	0.996
CAD	**With (n=17)**	**Without (n=163)**	**P**
VEGF-B (pg/mL)	149.8±50.9	171.3±123.6	0.179
PAOD	**With (n=10)**	**Without (n=170)**	**P**
VEGF-B (pg/mL)	134.7±47.2	171.3±121.4	0.053
Diabetic retinopathy	**With (n=32)**	**Without (n=148)**	**P**
VEGF-B (pg/mL)	236.4±124.7	154.7±112.7	0.001*
Diabetic neuropathy	**With (n=21)**	**Without (n=159)**	**P**
VEGF-B (pg/mL)	161.9±80.8	170.2±123.1	0.683

(: P< 0.05) VEGF-B: vascular endothelial growth factor B; CVA: cerebral vascular accidence; CAD: coronary artery disease; PAOD: peripheral artery occlusion disease.*

Table V. *Logistic regression analysis for the correlation between VEGF-B and diabetic retinopathy after adjustment for age, gender, DM duration, SBP, and HbA1C in diabetic patients (n=180).*

Diabetic retinopathy	**B**	**S.E.**	**P**
VEGF-B	0.004	0.002	0.018*
Age	0.051	0.023	0.026*
Gender	-0.01	0.414	0.980
DM duration	0.01	0.003	0.002*
SBP	0.004	0.015	0.794
HbA1C	-0.136	0.177	0.442

(: P < 0.050) VEGF-B: vascular endothelial growth factor-B; DM: diabetic mellitus; SBP: systolic blood pressure; HbA1C: glycosylated hemoglobin.*

coefficient: 0.145; P = 0.036) (Fig. 4B) and UACR (standardized coefficient: 0.169; P = 0.024) (Fig. 4C) in diabetic patients. Subgroup analysis also showed that patients with macro-albuminuria (UACR ≥300 mg/g) had higher VEGF-B levels than those with non-albuminuria (UACR < 30 mg/g) and micro-albuminuria (UACR: 30 – 300 mg/g) (Fig. 4D). After adjustment for age, gender, DM duration, BMI, SBP, HbA1C, ACEI/ARB, statin/ezetrol/fibrate and TZD, multiple linear regression analysis demonstrated that VEGF-B was the significantly independent determinant variable for variance of albuminuria (standardized coefficient: 0.174; P = 0.024) (Table IIID).

Associations of VEGF-B with diabetic retinopathy in type 2 diabetic patients

T-test analysis revealed that the association of VEGF-B with cerebral vascular disease, coronary

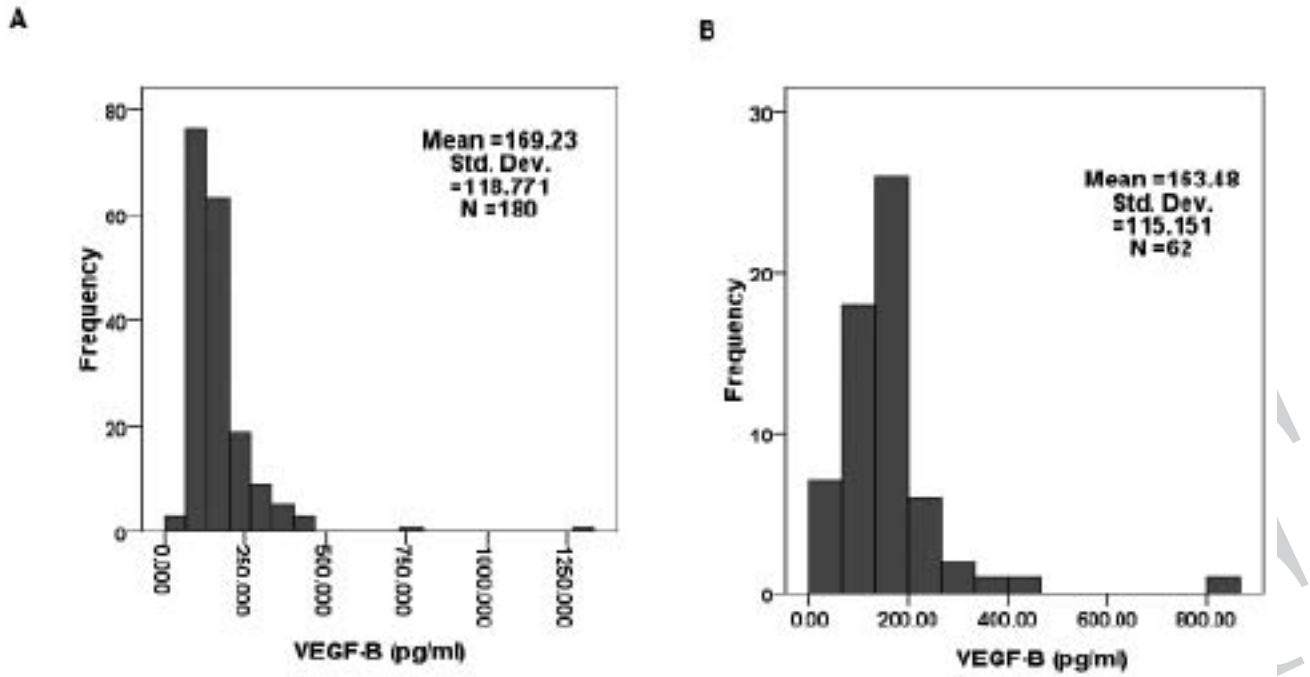

Fig. 1. *Normal distribution of serum VEGF-B levels in diabetic patients (Statistic: 0.574; df: 180; P = 0.000) (**A**), and non-diabetic controls (Statistic: 0.689; df: 62; P = 0.000) (**B**).*

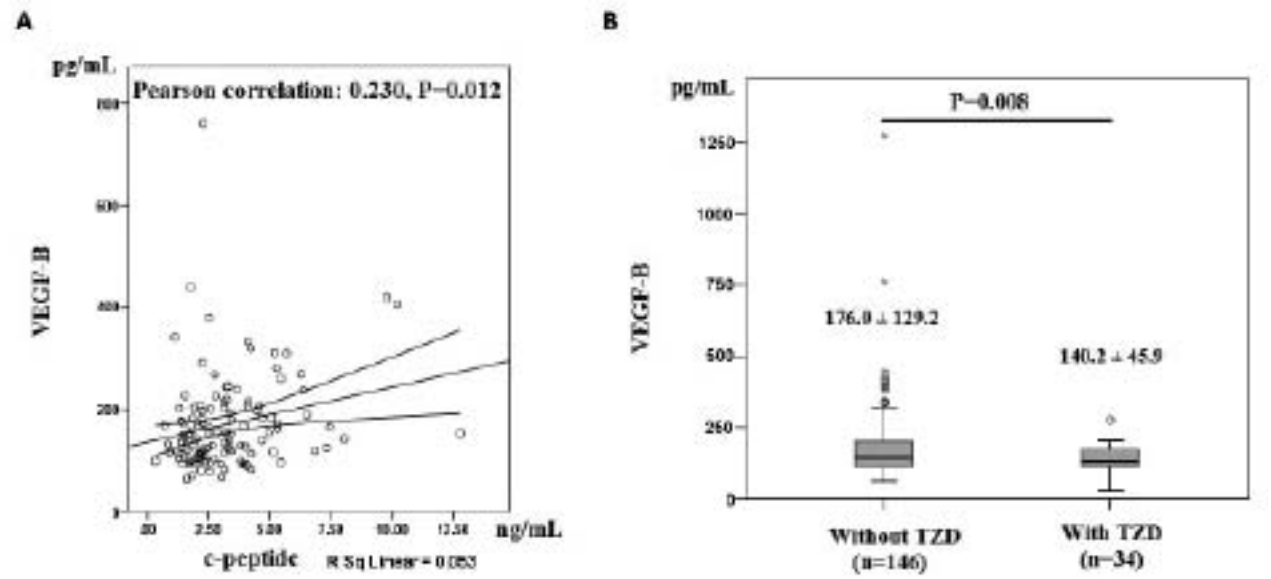

Fig. 2. *Plots for the associations of VEGF-B with c-peptide and TZD therapy in diabetic patients (n=180). **A**) plot for VEGF-B vs c-peptide; **B**) distribution boxplot for VEGF-B vs TZD. (*: extremes; o: outliers) (VEGF-B: vascular endothelial growth factor-B; TZD: thiazolidinediones).*

artery disease, peripheral arterial occlusive disease, and diabetic neuropathy was not significant (Table IV). Diabetic patients with diabetic retinopathy had significantly higher VEGF-B levels (236.4±124.7 pg/mL) than those without diabetic retinopathy (154.7±112.7 pg/mL) (P = 0.001) (Fig. 4E). After

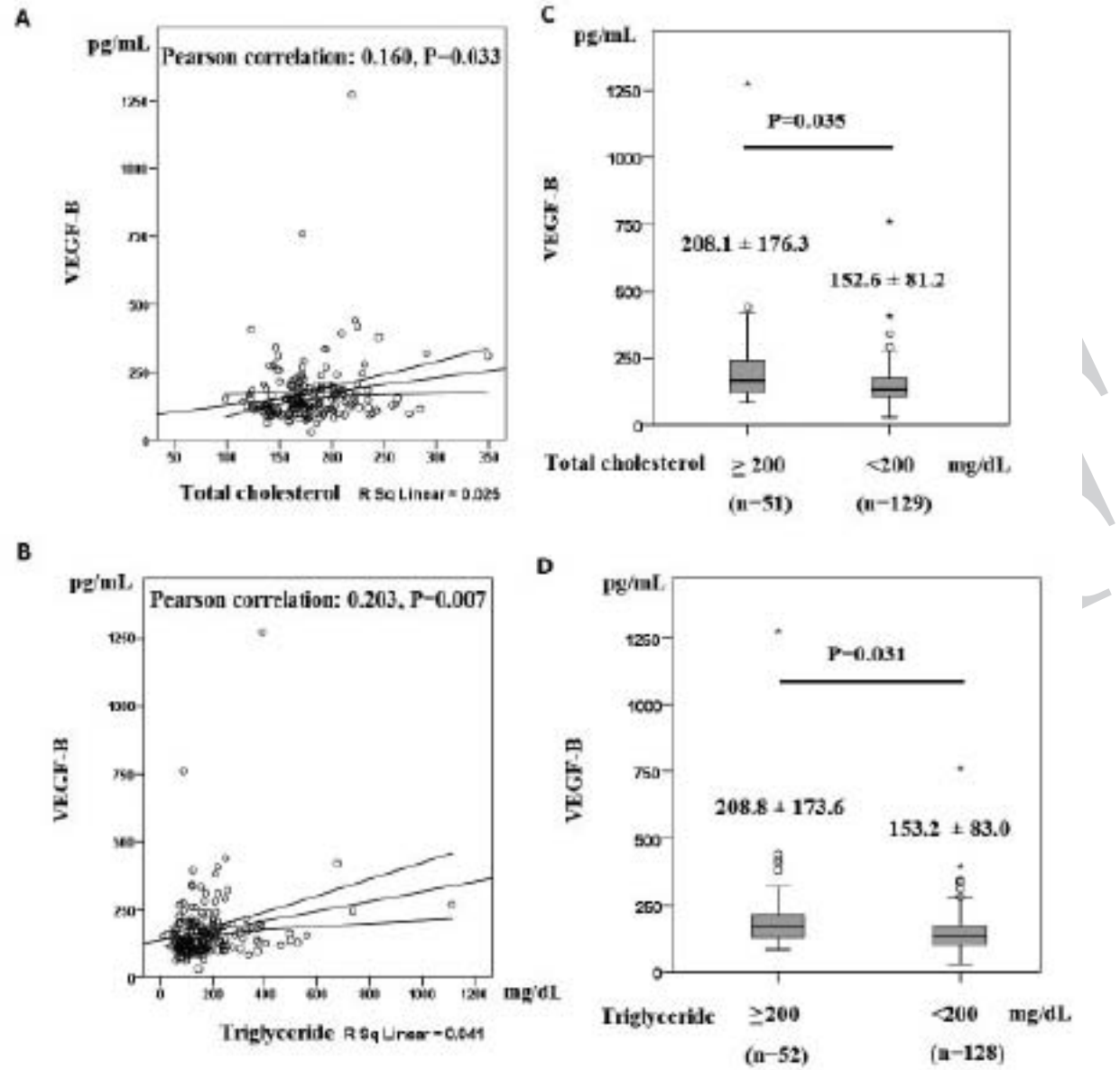

Fig. 3. *Plots for the associations of VEGF-B with total cholesterol and triglyceride in diabetic patients (n=180).* ***A****: plots for VEGF-B vs total cholesterol;* ***B****: plots for VEGF-B vs triglyceride. (*: extremes; o: outliers) (VEGF-B: vascular endothelial growth factor-B).*

adjustment for age, gender, DM duration, SBP, and HbA1C, logistic regression analysis demonstrated that VEGF-B was a significantly independent determinant variable for the presence of diabetic retinopathy (P = 0.018) (Table V).

DISCUSSION

The main finding of the present study is that circulating VEGF-B has a significant clinical association with the hyperlipidemia and micro-vasculopathy, diabetic nephropathy and retinopathy in type 2 diabetic patients. Type 2 diabetes is complicated with systemic co-morbidities, which impact the life quality and survival of type 2 diabetic patients (22). The identification of a new therapeutic target for treating insulin resistance and its related complications is an important and currently challenging clinical issue. Recent studies have found that inhibiting VEGF-B signaling could

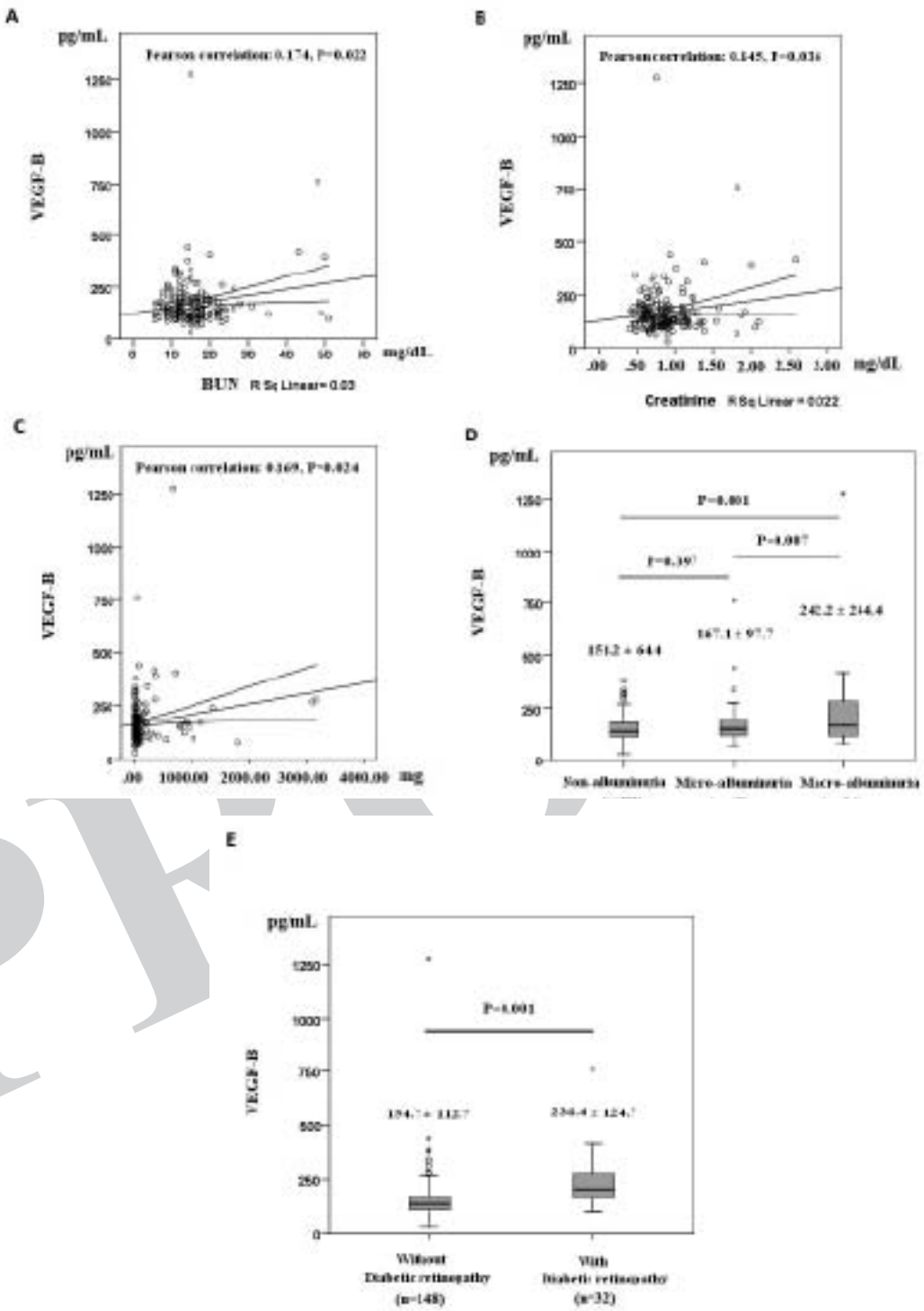

Fig. 4. *Plots for the correlation of VEGF-B with serum BUN, creatinine,* urine *UACR and diabetic retinopathy in diabetic patients (n=180).* ***A****) plot for the correlation between VEGF-B and BUN;* ***B****) plot for the correlation between VEGF-B and creatinine;* ***C****) plot for the correlation between VEGF-B and urine albumin excretion rate;* ***D****) boxplots for the VEGF-B levels in patients with non-albuminuria (UACR: <30 mg/g), micro-albuminuria (UACR: 30-300 mg/g) and macro-albuminuria (UACR: ≥300 mg/g);* ***E****) plot for the correlation between VEGF-B and diabetic retinopathy. (*: extremes; o: outliers) (VEGF-B: vascular endothelial growth factor B; UACR*: *urine albumin-to-creatinine ratio).*

ameliorate insulin resistance in diabetic mice. It has been proposed that antagonizing VEGF-B might be a promising pharmacological approach for treating type 2 diabetes (11). The findings of this study further reveal the clinical correlation of VEGF-B with the traits of insulin resistance in type 2 diabetic patients.

VEGF-B is a close relative of VEGF-A. VEGF-A has been considered to have important pathological roles in developing diabetic retinopathy and nephropathy. It was reported that the circulating VEGF-A level was significantly higher in diabetic patients 73.85 (57.32 - 119.00) pg/mL than in non-diabetic controls 43.20 (30.10 - 65.90) pg/mL (23). The results of this study revealed that the serum VEGF-B level of type 2 diabetic patients did not differ from those of non-diabetic controls.

The balance of lipid metabolism at the whole-body and tissue levels is exceedingly reliant on interorgan crosstalk. VEGF-B acts as a paracrine signal that regulates lipid delivery to fat-burning tissues. Studies showed that *Vegfb* knockout mice had decreased uptake and storage of fatty acid in heart, skeletal muscle, and brown adipose tissue (11, 26). *Vegfb* knockout was associated with a decrease in plasma triglyceride and LDL, and an increase in HDL levels in diabetic mice (12). That study suggested that high circulating VEGF-B levels were associated with hypercholesterolemia and hypertriglyceridemia in type 2 diabetic patients. However, no clinical correlations between VEGF-B and HDL and LDL were found in this study.

It has been proposed that inhibiting VEGF-B signalling could improve insulin resistance and beta-cell function in diabetic mice by targeting the lipid-transport properties of the endothelium to improve muscle insulin sensitivity and glucose disposal (11, 12). The results of this study indicated that circulating VEGF-B was significantly associated with serum c-peptide levels in type 2 diabetic patients. Treatment with TZDs, which decrease insulin resistance by inhibiting PPAR-γ activity, is associated with decreased circulating VEGF-B levels. But there was no correlation between VEGF-B and clinical indexes of insulin resistance and beta-cell function in this study. The type 2 diabetic patients included in this study all received oral hypoglycemic therapy, which might have confounded the test results of insulin resistance.

The association of circulating VEGF-B levels with the presence of diabetic nephropathy and retinopathy in type 2 diabetic patients has also been noted. Diabetes is one of the leading causes of end-stage renal disease and blindness worldwild. Histological hallmarks of diabetic glomerulopathy are glomerulus basement membrane thickening, mesangial matrix expansion, and podocyte foot process effacement (27). Diabetic retinopathy is the result of microvascular retinal damage, which changes the blood-retinal barrier and also makes the retinal blood vessels more permeable (15). Diabetic nephropathy and retinopathy are considered to be the alarm of micro-vascular injury in diabetes. A recent study showed that hyperexpression of VEGF-B in the retina could augment ischemia- and laser injury-induced retinal and choroidal neovascularization. Intraocular injection of adeno-associated virus encoding VEGF-B 186 has also been shown to potentiate retinal vascular permeability (28). Based on this evidence, it was proposed that VEGF-B might play important pathological roles in diabetic micro-vasculopathy. A recent clinical study reported that plasma levels of VEGF-B increased after acute myocardial infarction and were correlated with the preservation of cardiac function (29). However, current evidence for the association of VEGF-B with the development of macro-vasculopathy in diabetes is not adequate.

In summary, the findings of the present study suggest that circulating VEGF-B levels in type 2 diabetic patients may be associated with hyperlipidemia, diabetic nephropathy and retinopathy. Circulating VEGF-B may have clinical utility in the treatment of insulin resistance, and in the identification of type 2 diabetic patients at risk of target organ damage.

ACKNOWLEDGEMENTS

We would like to thank the colleagues of the Medical Research Center of Keelung Chang Gung Memorial Hospital for assistance in carrying out this study. This study was supported by a research grant of Chang Gung Memorial Hospital.

REFERENCES

1. Smyth S, Heron A. Diabetes and obesity: the twin

epidemics. Nat Med 2006; 12:75-80.
2. Campos C. Chronic hyperglycemia and glucose toxicity: pathology and clinical sequelae. Postgrad Med 2012; 124:90-97.
3. Welle S, Nair KS. Failure of glyburide and insulin treatment to decrease leucine flux in obese type II diabetic patients. Int J Obes 1990; 14:701-10.
4. Avramoglu RK, Qiu W, Adeli K. Mechanisms of metabolic dyslipidemia in insulin resistant states: deregulation of hepatic and intestinal lipoprotein secretion. Front Biosci 2003; 8:d464-d476.
5. Holmes DI, Zachary I. The vascular endothelial growth factor (VEGF) family: angiogenic factors in health and disease. Genome Biol 2005; 6:209.
6. Li X, Kumar A, Zhang F, Lee C, Tang Z. Complicated life, complicated VEGF-B. Trends Mol Med 2012; 18:119-127.
7. Li X, Aase K, Li H, von Euler G, Eriksson U. Isoform-specific expression of VEGF-B in normal tissues and tumors. Growth Factors 2001; 19:49-59.
8. Aase K, Lymboussaki A, Kaipainen A, Olofsson B, Alitalo K, Eriksson U. Localization of VEGF-B in the mouse embryo suggests a paracrine role of the growth factor in the developing vasculature. Dev Dyn 1999; 215:12-25.
9. Mould AW, Greco SA, Cahill MM, et al. Transgenic overexpression of vascular endothelial growth factor-B isoforms by endothelial cells potentiates postnatal vessel growth *in vivo* and *in vitro*. Circ Res 2005; 97:e60-e70.
10. Karpanen T, Bry M, Ollila HM, et al. Overexpression of vascular endothelial growth factor-B in mouse heart alters cardiac lipid metabolism and induces myocardial hypertrophy. Circ Res 2008; 103:1018-26.
11. Hagberg CE, Falkevall A, Wang X, et al. Vascular endothelial growth factor B controls endothelial fatty acid uptake. Nature 2010; 464:917-21.
12. Hagberg CE, Mehlem A, Falkevall A, et al. Targeting VEGF-B as a novel treatment for insulin resistance and type 2 diabetes. Nature 2012; 490:426-30.
13. Alberti KG, Zimmet PZ. Definition, diagnosis and classification of diabetes mellitus and its complications. Part 1: diagnosis and classification of diabetes mellitus provisional report of a WHO consultation. Diabet Med 1998; 15:539-53.
14. Standards of Medical Care in Diabetes. Diab Care 2012; 35:11-63.
15. Hudson C. The clinical features and classification of diabetic retinopathy. Ophthalmic Physiol Opt 1996; 16:43-48.
16. Kanji JN, Anglin RE, Hunt DL, Panju A. Does this patient with diabetes have large-fiber peripheral neuropathy? JAMA 2010; 303:1526-32.
17. Gaylis H. Diagnosis and treatment of peripheral arterial disease. JAMA 2002; 287:313.
18. Bakker AJ. Detection of microalbuminuria. Receiver operating characteristic curve analysis favors albumin-to-creatinine ratio over albumin concentration. Diabetes Care 1999; 22:307-13.
19. Matthews DR, Hosker JP, Rudenski AS, Naylor BA, Treacher DF, Turner RC. Homeostasis model assessment: insulin resistance and beta-cell function from fasting plasma glucose and insulin concentrations in man. Diabetologia 1985; 28:412-19.
20. Katz A, Nambi SS, Mather K, Baron AD, Follmann DA, Sullivan G, Quon MJ. Quantitative insulin sensitivity check index: a simple, accurate method for assessing insulin sensitivity in humans. J Clin Endocrinol Metab 2000; 85:2402-10.
21. Campbell DJ, Somaratne JB, Jenkins AJ, et al. Reduced microvascular density in non-ischemic myocardium of patients with recent non-ST-segment-elevation myocardial infarction. Int J Cardiol 2013; 167:1027-37.
22. Ripsin CM, Kang H, Urban RJ. Management of blood glucose in type 2 diabetes mellitus. Am Fam Physician 2009; 79:29-36.
23. Kacso IM, Bondor CI, Kacso G. Soluble serum Klotho in diabetic nephropathy: relationship to VEGF-A. Clin Biochem 2012; 45:1415-20.
24. Zhang X, Bao S, Hambly BD, Gillies MC. Vascular endothelial growth factor-A: a multifunctional molecular player in diabetic retinopathy. Int J Biochem Cell Biol 2009; 41:2368-71.
25. Tufro A, Veron D.VEGF and podocytes in diabetic nephropathy. Semin Nephrol 2012; 32:385-93.
26. Muoio DM. Metabolism and vascular fatty acid transport. N Engl J Med 2010; 363:291-93.
27. Gnudi L, Thomas SM, Viberti G. Mechanical forces in diabetic kidney disease: a trigger for impaired

glucose metabolism. J Am Soc Nephrol 2007; 18:2226-32.

28. Zhong X, Huang H, Shen J, Zacchigna S, Zentilin L, Giacca M, Vinores SA. Vascular endothelial growth factor-B gene transfer exacerbates retinal and choroidal neovascularization and vasopermeability without promoting inflammation. Mol Vis 2011; 17:492-507.
29. Devaux Y, Vausort M, Azuaje F, et al. Low levels of vascular endothelial growth factor B predict left ventricular remodeling after acute myocardial infarction. J Card Fail 2012; 18:330-37.

EDITORIAL

GROWTH FACTORS AND METABOLIC MARKERS IN CORD BLOOD: RELATIONSHIP TO BIRTH WEIGHT AND LENGTH

F. NAPOLI[1], N. DI IORGI[1], F. BAGNASCO[2], G. CANGEMI[3], B. D'AMICO[1], M. BOSCHETTI[4], A.E.M. ALLEGRI[1], I.A. BRUZZONE ICHIM[5], C. TRAGGIAI[6], A. ALLODI[7], P. POLO PERUCCHIN[1], M. GHEZZI[1], S. NOLI[1], M. GIACCARDI[1], B. ROVIGLIONE[1], L. DE MIGLIO[1], A. CALCAGNO[1], R. LORINI[1] and M. MAGHNIE[1]

[1]Pediatric Clinic, IRCCS G. Gaslini, University of Genova, Genova, Italy; [2]Epidemiology, Biostatistics and Committee Unit, Istituto G. Gaslini, Genova, Italy; [3]Clinical Pathology Laboratory Unit, Istituto G. Gaslini, Genova, Italy; [4]Department of Endocrinology and Medical Sciences, University of Genova, Genova, Italy; [5]Ob/Gym Department, Istituto G. Gaslini, Genova, Italy; [6]Neonatal Intensive Care Unit, Istituto G.Gaslini, Genova, Italy; [7]Neonatology, S. Martino Hospital, Genova, Italy

Received June 18, 2013 – Accepted March 11, 2014

Low birth weight and length for gestational age are associated with a high risk of short stature and metabolic syndrome in adulthood. The mechanisms that link prenatal growth to adult stature and metabolic syndrome have not yet been entirely clarified. The aim of our study was to evaluate the relationship between standardized anthropometric measures at birth and insulin-like growth factor (IGF)-I, IGF-II, insulin, adiponectin, and non-esterified fatty acid (NEFA) cord blood levels in the general population. One hundred fifty-eight random newborn subjects (77F, 81M) from Genoa, Italy, were analyzed. Anthropometric parameters were measured and standardized according to standard Italian tables. Insulin values were treated as categorical, since in several cases the results fell below detection cut-off. Mean birth weight was 3,214.23±488.99 gr and mean length was 49.82±2.17 cm. Females had higher mean IGF-I (p=0.04), and were more likely to have insulin values either <2 µU/ml or >4.5µU/ml (p= 0.04) compared to males. Weight and length SD scores (SDS) were higher in subjects with elevated insulin levels (p=0.002). A moderate correlation was found between weight and IGF-II (r=0.354). Multivariable analysis demonstrated that standardized birth weight was associated with IGF-II and insulin values. Our data highlight the importance of IGF-II in fetal growth and suggest that gender differences should be taken into consideration when evaluating prenatal growth.

Fetal growth is regulated by several factors such as fetus gender, genetics and epigenetics, insulin, and IGFs levels (1). A central role in this complex orchestration is played by vascularity which is intrinsically related to the most common definitions of pathological fetal growth pattern: indeed, any disruption of maternal-fetal system balance which reduces fetal intake of oxygen and nutrients can

Key words: birth weight, SDS, SGA, IGF-II, IGF-I, insulin

Mailing address: Flavia Napoli, M.D., Ph.D.
Department of Pediatrics,
G. Gaslini Institute, Largo Gaslini 5
16147 Genova, Italy
Tel.: +39 01056362365
Fax: +39 010388185
e-mail: flavianapoli@ospedale-gaslini.ge.it

0393-974X (2014)

cause a redistribution of blood flow in order to spare embryonic cerebral, cardiac and placental functions. If this condition persists, other organs are likely to receive inadequate nutrients, leading to the occurrence of Intrauterine Growth Restriction (IUGR) (2). IUGR may determine the birth of a Small for Gestational Age (SGA) newborn, defined by a weight and/or length of less than -2 SD from the mean of the reference population (3, 4); however, the exact definition of SGA varies according to different authors.

Impairment at different levels of the IGF system may cause both prenatal and postnatal growth impairment (5); indeed, mouse models have shown that deletion of either the IGF-I, IGF-II or IGF receptor genes reduces fetal body weight (6). These data have also been confirmed in humans, where low levels of plasmatic IGF-I at birth have been found in SGA children compared to adequate (AGA) or large for gestational age (LGA) infants at birth (7-8), and low levels of cord blood IGF-I have been detected in fetuses with IUGR (9). The role of IGF-II in fetal and placental growth is crucial (10), though still controversial. Studies on cord blood have reported low IGF-II in fetuses with IUGR (11) and higher levels in LGA newborns (15); other studies, however, have failed to demonstrate a significant impact of IGF-II on birth weight (9). In parallel with animal findings, human infants bearing mutations of the IGF-I receptor gene tend to be SGA and microcephalic at birth (12), and their stature as adults is usually compromised. Insulin is also known to influence fetal growth and metabolism (13), as shown by the finding of lower insulin levels in IUGR fetuses (10).

In adults, being born SGA has been associated with increased morbidity (14), mortality from coronary heart disease (CHD), stroke (15), insulin resistance and metabolic syndrome (16), independently from lifestyle factors. The latter condition is a well-known combination of metabolic disturbances characterized by the quartet core of obesity, hyperinsulinemia and insulin resistance, hypertension and dyslipidemia. A relatively new factor found to be involved in metabolic syndrome is adiponectin, a protein secreted by adipocytes that acts as a powerful regulator of insulin sensitivity and inflammation (17) and mediates an anti-atherogenic and insulin-sensitizing signal. Low adiponectin levels have been found in obese subjects and in type 2 diabetics, as well as in patients suffering from CHD. Interestingly, adiponectin levels have been reported to be low in SGA newborns compared to healthy controls and to be negatively correlated also with catch-up growth; however, a clear link between adiponectin levels and insulin resistance in these subjects has not yet been firmly established (18, 19).

Finally, high levels of non-esterified fatty acids (NEFA), expression of insulin resistance in all major insulin target organs, and thus considered a reliable metabolic syndrome marker (20), have been found in mothers' sera and in the cord blood of IUGR complicated pregnancies (21) and in cases of low Apgar score secondary to hypoxia (22), indicating that NEFA could be a very early marker of metabolic disruption.

In view of this multifaceted evidence, and since the definition of SGA varies across authors, often leading to results that are difficult to compare, the present study aims to evaluate the role of different cord blood growth factors and metabolic markers on standardized birth weight and length considered as continuous and not as categorical variables – i.e., by considering the impact of these factors on birth weight and length in the general population, not only in SGA or LGA infants.

MATERIALS AND METHODS

Subjects

Our study population is composed of subjects born at two birth centers - G. Gaslini Institute and S. Martino Hospital - in Genova (Italy), between July 1st, 2006 and November 30th, 2009. All newborns whose cord blood samples were available - and whose parents or legal guardians had given informed consent to the study - were considered eligible for the study.

Since the aim of the study was to evaluate a sample of general population, there were no clinical exclusion criteria; inability of parents or legal guardians to understand the aim of the study and inability or refusal to give written informed consent were the only exclusion criteria. For each neonate, birth weight and length, gestational age, delivery mode and Apgar score were recorded. Birth weight was measured within 2 hours of delivery with an electronic weighing scale and recorded to the nearest 10 g. Birth crown-heel length was measured within 1 day of delivery with a SECA neonatometer,

and recorded to the nearest 5 millimeters. Measurements were performed by trained personnel. For each subject, anthropometric measures at birth were evaluated and standard deviation scores were calculated by the classic method (value-mean)/standard deviation, using Bertino's centiles as reference standards (4), according to the latest consensus recommendations (3).

Laboratory methods

The umbilical venous blood samples collected from each neonate were divided into 3 tubes: one containing lithium heparin and two containing EDTA and then centrifuged; plasma and sera were aliquoted and immediately analyzed for NEFA and insulin, or stored at -20°C until assayed for other markers.

Adiponectin was measured with a TECO Adiponectin ELISA kit (total human adiponectin ELISA, TECO MEDICAL group, Switzerland) on a DSX automated ELISA processing system (Dynex technologies-Technogenetics-Milan-Italy) following the manufacturer's instructions. NEFA were analyzed by the colorimetric method (Free fatty acids, half micro test, Roche Diagnostics, Mannheim, Germany) according to the manufacturer's instructions. Insulin was measured by solid phase, two-site chemiluminescent immunometric assay (Immulite 1000 insulin, Siemens Diagnostics-Medicalsystems, Genova, Italy) on an IMMULITE 1000 (Siemens Diagnostics) analyzer following the manufacturer's instructions. In order to avoid interference from binding proteins, single plasma EDTA samples for IGF-I and IGF-II were treated with acid ethanol, according to Daughaday et al. (23). IGF-I was measured by radioimmunoassay using immunochemicals and tracers provided by Biosource (Nivelles, Belgium). The sensitivity of the assay is 1.54ng/mL; the intra-assay and inter-assay coefficients of variation are 6% and 7.5%, respectively. IGF-II was measured by radioimmunoassay using immunochemicals and tracers provided by Sera-Lab (Techno-genetics, Trezzano, Italy) and ^{125}I-IGF-II provided by Amersham (Aylesbury, Buckinghamshire, United Kingdom). The sensitivity of the assay is 0.9 ng/ml; the intra-assay and inter-assay coefficients of variation are 6% and 9%, respectively.

The study protocol was approved by the Gaslini Institute Ethics Committee according to Helsinki guidelines.

Statistical analysis

Descriptive statistics were reported in terms of absolute frequency and percentage for the qualitative variables, while mean and standard deviation (SD) were used for the quantitative variables, and the Shapiro-Wilk test was used to test their normal distribution. Insulin values were treated as categorical since in a relevant proportion of cases the results were below the laboratory detection cut-off (2 μU/ml); thus three groups were defined: i) undetectable values (<2 μU/ml); ii) below; and iii) above the observed median (4.5 μU/ml) of all of the detectable values. The distribution of some quantitative parameters was not symmetric, thus these values were transformed using their natural logarithms (ln).

The comparison of the frequency data was carried out by *chi*-square test or by Fisher's exact test in cases of expected frequencies less than five. The *t*-test and the analysis of variance (ANOVA) were used to compare the values of normally distributed variables, while the Mann-Whitney test, the Kruskall Wallis test and the non-parametric test for trend by Cuzick were carried out in cases of abnormal distribution.

Pearson correlation coefficient (r) and simple linear regression were used to investigate the correlation between quantitative variables. Correlation was defined as follows: weak for $r<0.3$, moderate for $r<0.7$ and strong for $r>0.7$ (24).

The variables associated with standardized weight were identified in univariate and multivariable analysis of covariance (ANCOVA). Gender, insulin category, gestational age, adiponectin, NEFA, and IGF-II were entered in the ANCOVA model. Neither birth length, since it was strictly correlated with birth weight, nor IGF-I, for its moderate correlation with IGF-II, were included in the ANCOVA model. To test the best-fit model, variables were sequentially eliminated in a stepwise backward selection procedure until all remaining variables were statistically significant. Regression coefficients with their confidence intervals were reported to express the independent effect of the analyzed variables.

All tests were two-sided and a P value of less than 0.05 was considered statistically significant. Statistical analyses were performed using STATA (STATA Statistical Software, Release 11.0 College Station, TX, STATA Corporation, 2009).

RESULTS

Characteristics of study subjects and biochemical parameters

The study population was composed of 158 subjects, 81 males (51%) and 77 females (49%) as reported in Table I. On average they were born 39.30 (±1.35) weeks after last menstrual period from a vaginal delivery in 73% of cases, caesarean section in 23% and operative delivery in 4% of cases. Apgar scores after 1' and 5' were in the normal range in the majority of subjects, with no differences between

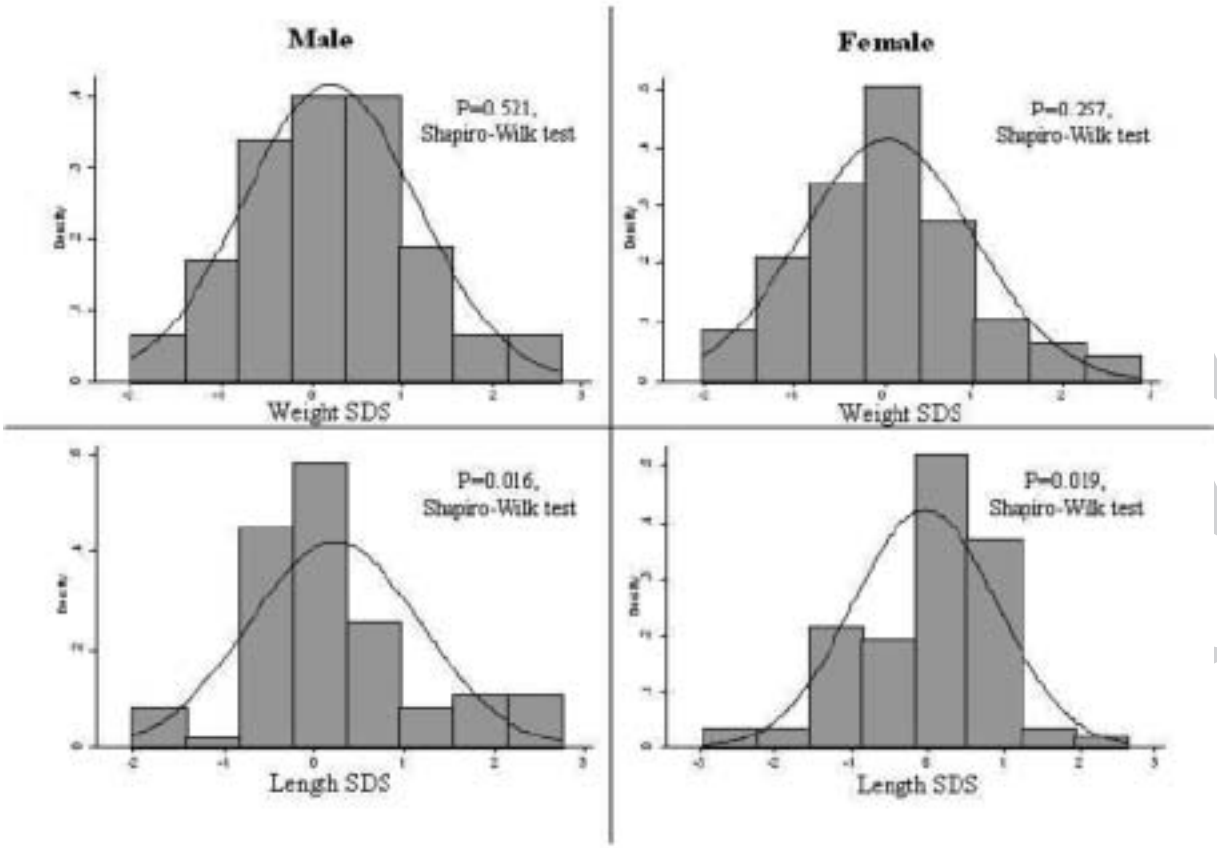

Fig. 1. *Distribution of weight SDS and length SDS by gender with normal curve estimate.*

males and females; only five male subjects had an Apgar score lower than 7 at 1 minute, but none were lower than 5.

Average birth weight and length were 3214.23±488.99 g and 49.82±2.17 cm respectively, with males being slightly - but significantly - heavier and longer than females. When birth weight and length were standardized, no differences were found between genders (Table I). As shown in Fig. 1, the weight of the males and females showed a normal distribution, while study males were slightly shorter (p=0.016) and females longer (p=0.019) than expected (non-normal distribution). Only five subjects (3%; 4 F, 1 M) were SGA, while 148 subjects (93%) were AGA and 5 subjects (3%, 2F, 3M) were LGA.

Because of some difficulties with the blood sampling, it was not possible to obtain complete biochemical data for all of the studied markers. Table II reports mean original and ln transformed values of the measured markers and insulin categories stratified by gender. There were no significant differences between males and females except for IGF-I and for insulin. In particular, females had higher IGF-I values (4.36 ng/ml *vs* 4.26, p=0.04) than males, and were more likely to have "extreme" insulin values (either <2 µU/ml or >4.5µU/ml, p= 0.04; Table II). Furthermore, the NEFA values found in newborns with low Apgar scores (mean: 0.10mmol/l) did not differ from those found in the rest of the subjects.

Distribution of anthropometric and biochemical parameters by insulin and gender

When anthropometric and laboratory values were stratified by insulin category, we observed a significant difference in the three insulin categories for the following variables: weight, length, IGF-I and IGF-II. Furthermore, all four parameters increased progressively with the increase of insulin and this increase was significant (non-parametric test for trend

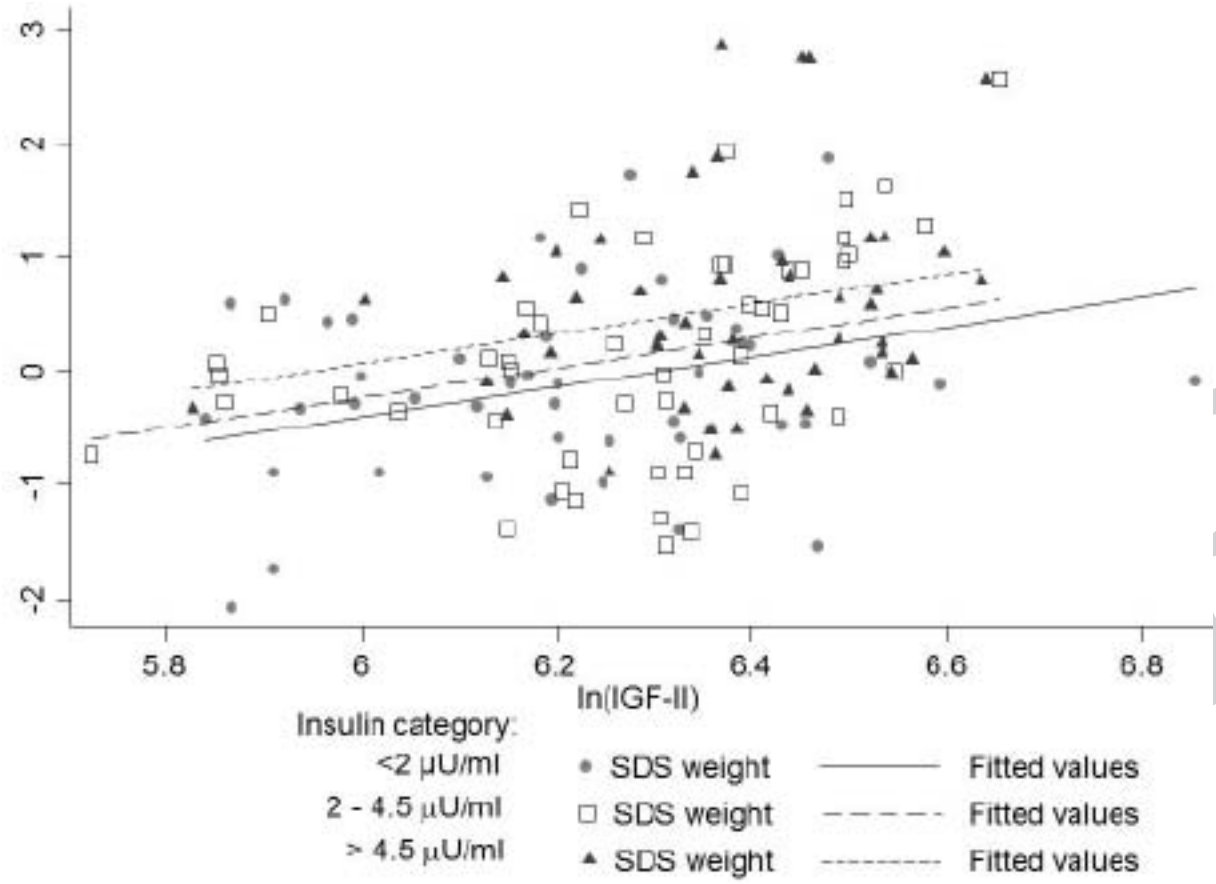

Fig. 2. *Graphical representation of the ANCOVA model for standardized weight. The three regression lines of weight SDS modifications by increase of IGF-II - stratified by the three insulin categories - are reported. The vertical distances between the lines represent the effect of insulin at any level of IGF-II. The estimated adjusted weight SDS was –0.02 (unadjusted weight was -0.12, Table III) for the group with undetectable insulin, 0.15 for insulin<4.5 µU/ml (unadjusted weight was 0.13, Table III) and 0.45 for insulin>4.5 µU/ml (unadjusted weight was 0.46, Table III).*

by Cuzick). NEFA tended to be lower in subjects with higher insulin, but the difference between groups was not significant. Gender distribution is shown in Table III. No effect was detected for adiponectin.

Correlation between quantitative variables

We performed a correlation analysis among all the continuous variables in the overall cohort (i.e., all markers except insulin) and the anthropometric data. The correlation was weak between most variables with the exception of a strong correlation between weight and length (r=0.723), a moderate correlation between weight and IGF-II (r=0.354) and between IGF-I and IGF-II (r=0.326). We did not find any correlation between birth weight SDS and cord blood IGF-I; moreover, no significant correlation was found between cord blood NEFA levels and other growth or metabolic factors, nor between adiponectin and other markers. A moderate negative correlation was observed between NEFA and weight (r=-0.386) in females.

Univariate and multivariable analysis

In the univariate analysis, only IGF-II and insulin were found to be significantly associated with birth weight SDS (Table IV), also confirmed by the multivariable analysis (Table IV, Fig. 2). In particular, at any given level of insulin, the standardized weight increased by 0.0131 SD ($p<0.001$) for each 1% increase of IGF-II. Similarly,

Table I. *Characteristics and anthropometric features of study subjects by gender.*

	Male, n=81	Female, n=77	Total, n=158	P
Gestational age (weeks), mean (SD)	39.37 (1.24)	39.22 (1.46)	39.30 (1.35)	0.57[b]
Mode of delivery, n (%)	81	77	158	
Vaginal	58 (72)	58 (75)	116 (73)	
Operative	3 (4)	3 (4)	6 (4)	0.86[c]
Caesarean section	20 (24)	16 (21)	36(23)	
Apgar at 1 min, n (%)	76	73	149	
0-6	5 (7)	0	5 (3)	0.06[c]
7-10	71 (93)	73 (100)	144 (97)	
Apgar at 5 min, n (%)	77	73	150	
0-6	0	0	0	-
7-10	77 (100)	73 (100)	150 (100)	
Weight SDS, mean (SD)	0.21 (0.96)	0.04 (0.96)	0.12 (0.96)	0.27[a]
Length SDS, mean (SD)	0.23 (0.95)	-0.03 (0.94)	0.11 (0.95)	0.47[b]
Weight (g), mean (SD)	3339.25 (456.41)	3084.35 (490.66)	3214.23 (488.99)	<0.01[a]
Length (cm), mean (SD)	50.47 (1.96)	49.13 (2.18)	49.82 (2.17)	<0.01[b]

[a] *t test*
[b] *Mann-Whitney test and* [c] *Fisher's exact test*

at any IGF-II level, only neonates with insulin >4.5 μU/ml had significantly higher (0.47%) birth weight SDS (p=0.011) compared to the reference group (< 2 μU/ml). No effect was found for insulin values between 2 and 4.5 μU/ml. However, on the whole, insulin had a significant effect on birth weight (p=0.036). These estimates are based on the model that performs a linear adjustment for IGF-II and assuming the same angular coefficient for the three insulin categories (parallel lines). The parallelism hypothesis was therefore tested and accepted (Fig. 2) by demonstrating that the interaction between insulin and IGF-II was equal to 0 (p=0.414, F-test).

More specifically, we estimated that the two predictors together can account for 16.7% of birth weight variability: IGF-II accounts for 12.7% and insulin for approximately 4%.

DISCUSSION

Studying the impact of metabolic and growth factors on fetal growth is of paramount importance, at first, for the approach to a neonate of abnormal weight and/or length and, secondarily, for understanding patho-physiological mechanisms underlying growth patterns during developmental age and metabolic outcomes throughout life.

Recognized growth parameters, such as IGF-I, are related to growth more than to chronological age, although both of these variables are obviously and intrinsically related. Seeing that birth weight in our study population showed a normal distribution,

Table II. *Distribution of original and ln transformed biochemical parameters by gender.*

	Male, n=81	Female, n=77	Total, n=158	P
Adiponectin (μg/ml), n	73	68	141	
original parameter, mean (SD)	27.13 (12.52)	31.08 (14.80)	29.04 (13.76)	
ln transformation, mean (SD)	3.20 (0.46)	3.32 (0.51)	3.26 (0.49)	0.09[a]
NEFA (mmol/l), n	60	56	116	
original parameter, mean (SD)	0.11 (0.05)	0.11 (0.06)	0.11 (0.06)	0.23[a]
IGF-I (ng/ml), n	78	74	152	
original parameter, mean (SD)	79.22 (45.84)	83.68 (28.03)	81.39 (38.16)	
ln transformation, mean (SD)	4.26 (0.43)	4.36 (0.37)	4.31 (0.41)	0.04[a]
IGF-II (ng/ml), n	80	72	152	
original parameter, mean (SD)	536.91 (109.23)	563.42 (103.01)	549.47 (107.18)	
ln transformation, mean (SD)	6.26 (0.21)	6.32 (0.19)	6.29 (0.21)	0.19[a]
Insulin category[c], n	77	73	150	
<2 μU/ml, n (%)	21 (27)	26 (36)	47 (31)	
2.1 - 4.5 μU/ml, n (%)	34 (44)	18 (24)	52 (35)	0.04[b]
>4.5 μU/ml, n (%)	22 (29)	29 (40)	51 (34)	

[a] *Mann-Whitney test and* [b] *chi-square test*

[c] *Since 47 insulin values were below the laboratory detection cut-off (<2 μU/ml), data were categorized into three groups: undetectable values (<2 μU/ml) and values below or above the median (4.5μU/ml) of detectable parameters (150-47=103).*

we standardized anthropometric parameters based on current Bertino's reference growth charts for the Italian population in order to remove the influence of gestational age; we therefore used standardized weight as a continuous and independent variable to evaluate the role of different growth factors and metabolic markers on physiological variability.

In previous studies, the analysis of predictors of anthropometric parameters at birth has always been somewhat inconsistent: some authors used standardization - and -2SDS - to define SGA; others compared AGA and SGA newborns, using the 5th or 10th percentile as a cut-off, or compared subjects born from IUGR and non-IUGR pregnancies without any definition of birth size. Comparisons between different study results are therefore problematic and somewhat imprecise since they are conditioned by the choice of reference tables from among a wide range available for diverse populations that have been compiled over the last 40 years using varied

Table III. *Distribution of anthropometric and biochemical parameters by insulin category and gender.*

	Insulin category				
	<2 μU/ml	≤ 4.5 μU/ml	>4.5μU/ml	P	P[c]
Weight SDS, mean (SD)					
Overall	-0.12 (0.81)	0.13 (0.93)	0.46 (0.96)	0.007[a]	0.002
Males	-0.12 (0.91)	0.27 (0.94)	0.48 (0.91)	0.102[a]	0.047
Females	-0.11 (0.74)	-0.12 (0.88)	0.45 (1.02)	0.033[a]	0.015
Length SDS, mean (SD)					
Overall	-0.10 (0.71)	0.15 (0.96)	0.37 (1.04)	0.009[b]	0.002
Males	-0.01(0.79)	0.28 (0.95)	0.46 (1.02)	0.113[b]	0.046
Females	-0.17 (0.63)	-0.09 (0.96)	0.30 (1.07)	0.035[b]	0.010
ln (Adiponectin) (μg/ml), mean (SD)					
Overall	3.26 (0.45)	3.33 (0.46)	3.21 (0.55)	0.708[b]	0.799
Males	3.14 (0.52)	3.32 (0.43)	3.09 (0.45)	0.273[b]	0.846
Females	3.36 (0.37)	3.35 (0.54)	3.28 (0.60)	0.988[b]	0.966
NEFA (mmol/l), mean (SD)					
Overall	0.12 (0.06)	0.11 (0.05)	0.10 (0.06)	0.071[b]	0.046
Males	0.10 (0.06)	0.11 (0.04)	0.09 (0.06)	0.061[b]	0.262
Females	0.14 (0.07)	0.11 (0.05)	0.10 (0.06)	0.154[b]	0.057
ln (IGF-I) (ng/ml), mean (SD)					
Overall	4.22 (0.41)	4.28 (0.33)	4.43 (0.44)	0.028[b]	0.014
Males	4.19 (0.41)	4.24 (0.37)	4.41 (0.51)	0.235[b]	0.122
Females	4.24 (0.41)	4.35 (0.22)	4.45 (0.39)	0.093[b]	0.033
ln (IGF-II) (ng/ml), mean (SD)					
Overall	6.22 (0.22)	6.29 (0.21)	6.37 (0.16)	<0.001[b]	<0.001
Males	6.17 (0.20)	6.28 (0.22)	6.34 (0.22)	0.042[b]	0.014
Females	6.25 (0.22)	6.31 (0.18)	6.39 (0.13)	0.008[b]	0.002

[a] *ANOVA test*
[b] *Non-parametric Kruskal-Wallis test*
[c] *Non-parametric test for trend by Cuzick*

criteria.

Cord blood insulin was evaluated in our study since it is a growth factor involved both in fetal growth and in abnormal metabolic outcomes later in life; indeed, increased visceral fat - a metabolic syndrome marker - has been observed in children born SGA compared to AGA controls (25), and metabolic syndrome has been reported in 2.3% of

Table IV. *Univariate and multivariable analysis for standardized weight.*

Variable	Coefficient	Standard error	P	Confidence Interval
Univariate analysis				
Gender			0.274[a]	
Male	ref	ref		
Female	-0.17	0.15	0.274[b]	-0.47; 0.13
Insulin category			0.007[a]	
<2 μU/ml	ref	ref		
2.1- 4.5 μU/ml	0.25	0.18	0.176[b]	-0.11; 0.61
>4.5 μU/ml	0.58	0.18	0.002[b]	0.22; 0.95
Gestational age	-0.04	0.06	0.947[b]	-0.17; 0.11
ln (Adiponectin)	-0.15	0.17	0.364[b]	-0.48; 0.18
Nefa	-1.91	1.63	0.246[b]	-5.14; 1.33
ln(IGF-II)	1.64	0.35	<0.001[b]	0.94; 2.34
Best-fitting multivariable model, n=145				
Intercept	-8.29	2.26	<0.001[b]	-12.75; -3.83
ln(IGF-II)	1.31[c]	0.36	<0.001[b]	0.59; 2.03
Insulin category			0.036[a]	
<2 μU/ml	ref	ref		
2.1- 4.5 μU/ml	0.17	0.17	0.325[b]	-0.17; 0.52
>4.5 μU/ml	0.47	0.18	0.011[b]	0.11; 0.83

[a] *F-test*
[b] *t-test*
[c] *the estimated modification by 1% increase of IGF-II is 0.0131 standardized weight*

young adults born SGA, but only in 0.4% of those who were AGA (17). No clear difference between metabolic syndrome markers has been detected between AGA and SGA subjects at birth to date; however, some metabolic parameter alterations in early childhood are significantly correlated with postnatal catch-up growth and metabolic risk. Several hypotheses have been proposed to explain the fetal programming of adult metabolism, including "thrifty phenotype", "fetal salvage hypothesis", "thrifty

Table V. *Univariate and multivariable analysis for standardized weight considering insulin as continuous variable.*

Variable	Coefficient	Standard error	P[a]	Confidence Interval
Univariate analysis				
Insulin	0.06	0.01	<0.001	0.03; 0.09
Best-fitting multivariable model				
Intercept	-8.45	2.18	<0.001	-12.76; -4.14
ln(IGF-II)	1.34[b]	0.35	<0.001	0.65; 2.02
Insulin	0.05	0.01	0.001	0.02; 0.08

[a] *t-test*

[b] *the estimated modification by 1% increase of IGF-II is 0.0134 standardized weight*

genotype" (2) and "catch-up growth hypothesis" (26); nevertheless, the mechanisms linking fetal and postnatal growth to obesity and insulin resistance – the main pathogenetic factors of metabolic syndrome – still have to be revealed.

We found a surprising gender difference in cord blood values for insulin in that female newborns exhibited significantly higher or lower extreme cord blood insulin levels than males. The cause of gender difference in insulin levels and of its duality in females is not clear and merits further investigation. Interestingly, IGF-I levels were also higher in females and positively related with insulin levels. These findings suggest that gender differences in growth factors and metabolic parameters should be taken into consideration right from birth. Insulin also varied with birth weight, being lower in lighter subjects; similarly, lower cord blood insulin levels were reported in newborns from IUGR pregnancies compared to normal controls (10).

Insulin levels were categorized because of the high frequency of undetectable values; nevertheless, the analysis was performed also considering insulin as a continuous variable - by attributing an arbitrary value of 1 μU/ml to values <2 μU/ml - and showed similar results (Table V). Nevertheless, considering the high frequency of undetectable values – 1/3 of all samples – we infer that the division into categories is more correct in this case. By performing this division, it is clearly visible that high insulin levels are associated with weight.

Insulin was also found to be reciprocally related with cord blood NEFA levels, thus underlining the role of this oxidative stress marker in fetal growth and metabolism, as previously reported (21). Since NEFA are usually correlated to hyperinsulinemia in adult life (27) and with body weight and BMI in children as well, it is possible to infer that, in contrast to older ages, fetal and perinatal hyperinsulinemia is not a marker of metabolic syndrome risk in later life, yet fetal hypoinsulinemia might be. This hypothesis is partially corroborated by the finding that cord blood NEFA levels tended to be higher in smaller children suggesting that these subjects are more likely to develop higher metabolic risk. Surprisingly, Apgar scores did not appear to influence cord blood NEFA in our subjects, yet most of them had normal Apgar, and no difference was found in the small group of newborns with relatively low Apgar scores. Further studies may focus on adipose tissue distribution differences (subcutaneous versus visceral) which might explain the higher NEFA levels in newborn subjects with undetectable insulin.

Adipose tissue clearly plays a major role in determining insulin resistance and metabolic syndrome in different groups of subjects, among whom SGA subjects can be included. Adiponectin has been shown to correlate negatively with weight

and BMI; our study, however, did not find any correlation of adiponectin levels with birth weight and length SDS, in contrast with previous reports (19, 20).

The multifaceted interactions underlying the complex trait of fetal growth are well supported by the finding that standardized birth weight was positively related to IGF-II in our study population, and that IGF-II and insulin had an independent and addictive significant effect on weight, together accounting for 16.7% of weight variability. Similar results have been published by Lee et al. (10) and Street et al. (12), who compared IUGR subjects to controls. Our data, by highlighting the role of IGF-II in fetal growth, in accordance with previously published data, suggest that more specific investigations on IGF-II and IGF-II expression in fetal life should be carried out. Epimutations of the IGF-II control region on chromosome 11p15 have been found in SGA subjects (28); our work seems to confirm the hypothesis that IGF-II deficiency can be identified as a major cause of fetal growth impairment. Further studies are needed in order to assess whether cord blood IGF-II levels can also predict catch-up growth in the first years of life. If this hypothesis is confirmed, cord blood IGF-II levels could represent an important tool for identifying clusters of subjects at higher risk for short stature.

Unlike previous published data (7-9), we did not find any correlation between birth weight and cord blood IGF-I; our results are, however, similar to those reported by others (12) that failed to demonstrate any difference in cord blood IGF-I between IUGR and non-IUGR subjects. Since there is clear evidence of the crucial role played by IGF-I in both human and animal prenatal growth, the interpretation of this finding is in some way ambiguous and requires further confirmation.

The limitation of our study was not taking into consideration other variables that are known to influence fetal growth, such as maternal nutrition, parity, maternal age, smoking, health status and parents' height and birth size, as well as maternal IGF system status; the relationship between these parameters and growth factors at birth should be evaluated in further studies. A further limitation of the present study was our choice of reference data which may be a source of bias in and of itself since the tables published by Bertino et al. (4) are more than ten years old and were created using Italian citizens only and considering maternal and/or fetal pathology exclusion criteria; while our study included immigrants and non-Caucasian subjects, and did not adopt exclusion criteria. Finally, pregnancy dating - by ultrasound or last menstrual period - is not always reliable and could influence the standardization.

The strengths of our study are the relatively large sample size, the multiple cord blood metabolic factors taken into consideration, and the novelty of using standardized birth weight as a continuous variable in order to study its determinants.

In conclusion, our study highlights the crucial role of gender, IGF II and insulin in fetal and neonatal growth. Further studies, however, need to be undertaken in order to unravel the complex interplay of growth factors and better understand their influence on both fetal growth and late metabolic effects.

ACKNOWLEDGEMENTS

Dr. Riccardo Haupt from Epidemiology and Biostatistics Section, G. Gaslini Institute, provided valuable support in data analysis and paper review; midwives from G. Gaslini Institute and S. Martino Hospital, Genova, Italy and Ob/Gyn department staff provided valuable support.

REFERENCES

1. Männik J, Vaas P, Rull K, Teesalu P, Rebane T, Laan M. Differential expression profile of growth hormone/chorionic somatomammotropin genes in placenta of small- and large-for-gestational-age newborns J Clin Endocrinol Metab 2010; 95(5):2433-42.
2. Saenger P, Czernichow P, Hughes I, Reiter OE. Small for gestational age: short stature and beyond. Endocr Rev 2007; 28:219-251.
3. Clayton P E, Cianfarani S, Czernichow P, Johannsson G, Rapaport R, Rogol A. Management of the child born small for gestational age through to adulthood: a consensus statement of the International Societies of Pediatric Endocrinology and the Growth Hormone Research Society. J Clin Endocrinol Metab 2007; 92:804-810.

4. Bertino E, Murru P, Bagna R, et al. Standard antropometrici neonatali dell'Italia nord-Occidentale Ital J Pediat 1999; 25:899-906.
5. Abuzzahab MJ, Schneider A, Goddard A, et al.: Intrauterine Growth Retardation (IUGR) Study Group. IGF-I Receptor mutations resulting in intrauterine and postnatal growth retardation. N Engl J Med 2003; 349(23):2211-22.
6. Baker J, Liu JP, Robertson EJ, Efstratiadis A. Role of insulin like growth factors in embryonic and postnatal growth. Cell 1993; 75:73-82.
7. Iñiguez G, Ong K, Bazaes R, Avila A, Salazar T, Dunger D, Mericq V. Longitudinal changes in insulin-like growth factor-I, insulin sensitivity, and secretion from birth to age three years in small- for-gestational-age children. J Clin Endocrinol Metab 2006; 91(11):4645-9.
8. Chiesa C, Osborn JF, Haass C, Natale F, Spinelli M, Scapillati E, Spinelli A, Pacifico L. Ghrelin, leptin, IGF-I, IGFBP-3, and insulin concentrations at birth: is there a relationship with fetal growth and neonatal anthropometry? Clin Chem 2008; 54(3):550-8.
9. Hung TY, Lin CC, Hwang YS, Lin SJ, Chou YY, Tsai WH. Relationship between umbilical cord blood insulin-like growth factors and anthropometry in term newborns. Acta Paediatr Taiwan 2008; 49(1):19-23.
10. Lee MH, Jeon YJ, Lee SM, Park MH, Jung SC, Kim YJ. Placental gene expression is related to glucose metabolism and fetal cord blood levels of insulin and insulin-like growth factors in intrauterine growth restriction. Early Hum Dev 2010; 86(1):45-50.
11. Fowden AL, Forhead AJ. Endocrine regulation of feto-placental growth. Horm Res 2009; 72(5):257-65.
12. Street ME, Seghini P, Fieni S, et al. Changes in interleukin-6 and IGF system and their relationships in placenta and cord blood in newborns with fetal growth restriction compared with controls. Eur J Endocrinol 2006; 155(4):567-74.
13. Ester WA, van Duyvenvoorde HA, de Wit CC, et al. Two short children born small for gestational age with insulin-like growth factor 1 receptor haploinsufficiency illustrate the heterogeneity of its phenotype. J Clin Endocrinol Metab 2009; 94(12):4717-27.
14. Kuo PL. Glucose gradients of maternal vein-umbilical vein and umbilical vein-umbilical artery in normally grown-retarded fetuses. J Perinatol Med 1991; 19(6):421-5.
15. Karlberg J, Albertsson-Wikland K. Growth in full-term small-for-gestational-age infants: from birth to final height Ped Res 1995; 38:733-39.
16. Barker DJ. Fetal origins of coronary heart disease. BMJ 1995; 311(6998):171-4.
17. Jaquet D, Deghmoun S, Chevenne D, Collin D, Czernichow P, Lévy-Marchal C. Dynamic change in adiposity from fetal to postnatal life is involved in the metabolic syndrome associated with reduced fetal growth. Diabetologia 2005; 48(5):849-55.
18. Whitehead JP, Richards AA, Hickman IJ, Macdonald GA, Prins JB. Adiponectin-a key adipokine in the metabolic syndrome. Diabetes Obes Metab 2006; 8(3):264-80.
19. Cianfarani S, Martinez C, Maiorana A, Scirè G, Spadoni GL, Boemi S. Adiponectin levels are reduced in children born small for gestational age and are inversely related to postnatal catch-up growth. J Clin Endocrinol Metab 2004; 89(3):1346-51.
20. Jaquet D, Deghmoun S, Chevenne D, Czernichow P, Lévy-Marchal C. Low serum adiponectin levels in subjects born small for gestational age: impact on insulin sensitivity. Int J Obes (Lond) 2006; 30(1):83-7.
21. Boden G. Obesity and free fatty acids. Endocrinol Metab Clin North Am 2008; 37(3):635-46, VIII-IX.
22. Ortega-Senovilla H, Alvino G, Taricco E, Cetin I, Herrera E. Enhanced circulating retinol and non-esterified fatty acids in pregnancies complicated with intrauterine growth restriction. Clin Sci (Lond) 2009; 118(5):351-8.
23. Yuvienco JM, Dizon ME, Kleinfeld A, Anwar M, Hiatt M, Hegyi T. Umbilical cord unbound free fatty acid concentration and low apgar score. Am J Perinatol 2005; 22(8):429-36.
24. Daughaday WH, Mariz IK, Blethen SL. Inhibition of access of bound somatomedin to membrane receptor and immunoglobin sites: a comparison of radioreceptor and radioimmunoassay of somatomedin in native and acid-ethanol extracted serum. J Clin Endocrinol Metab 1980; 51:781-88.
25. Swinscow TDV Revised by Campbell MJ. Statistics at Square One, Ninth Edition, University

of Southampton 1997; p 78.
26. Ibáñez L, Suárez L, Lopez-Bermejo A, Díaz M, Valls C, de Zegher F. Early development of visceral fat excess following spontaneous catch-up growth in children with low birthweight. J Clin Endocrinol Metab 2008; 93(3):925-8.
27. Cianfarani S, Germani D, Branca F. Low birthweight and adult insulin resistance: the "catch-up growth" hypothesis. Arch Dis Child Fetal Neonatal Ed 1999; 81(1):F71-3.
28. Balent B, Goswami G, Goodloe G, et al. Acute elevation of NEFA causes hyperinsulinemia without effect on insulin secretion rate in healthy human subjects. Ann N Y Acad Sci 2002; 967:535-43.
29. Gicquel C, Rossignol S, Cabrol S, et al. Epimutation of the telomeric imprinting center region on chromosome 11p15 in Silver-Russell syndrome. Nat Genet 2005; 37:1003-7.

LACTOBACILLUS CASEI AND *BIFIDOBACTERIUM LACTIS* SUPPLEMENTATION REDUCES TISSUE DAMAGE OF INTESTINAL MUCOSA AND LIVER AFTER 2,4,6-TRINITROBENZENESULFONIC ACID TREATMENT IN MICE

M. BELLAVIA[†1,*], F. RAPPA[1,2,*], M. LO BELLO[2], G. BRECCHIA[3], G. TOMASELLO[1,4], A. LEONE[2], G. SPATOLA[2], M.L. UZZO[2], G. BONAVENTURA[2], S. DAVID[2], P. DAMIANI[5], I. HAJJ-HUSSEIN[6], M.N. ZEENNY[2,7], A. JURJUS[7], P. SCHEMBRI-WISMAYER[8], M. COCCHI[9,10], G. ZUMMO[2], F. FARINA[2], A. GERBINO[2], F. CAPPELLO[1,2,8] and G. TRAINA[11,*]

[1]Euro-Mediterran Institute of Science and Technology, Palermo, Italy; [2]Department of Experimental Biomedicine and Clinical Neurosciences, University of Palermo, Palermo, Italy; [3]Department of Veterinary Medicine, University of Perugia, Perugia, Italy; [4]Department of Surgical, Oncologic and Stomatologic Disciplines, University of Palermo, Palermo, Italy; [5]Biomedical Department of Internal and Specialist Medicine, University of Palermo, Palermo, Italy; [6]Department of Biomedical Sciences, Oakland University William Beaumont School of Medicine, Rochester (MI) USA; [7]Department of Human Morphology, American University of Beirut, Beirut, Lebanon; [8]Department of Anatomy, University of Malta, Msida, Malta; [9]"Paolo Sotgiù" Institute, L.U.de.S. University, Lugano, Switzerland; [10]Department of Pharmaceutical Sciences, University of Bologna, Bologna, Italy; [11]Department of Pharmaceutical Sciences, University of Perugia, Perugia, Italy

Received December 2, 2013 – Accepted March 20, 2014

* These authors contributed equally to the present work
†This was one of the last works of Maurizio Bellavia and all the authors want to dedicate this work to him.

Probiotics (PB) are living microorganisms that act as a commensal population in normal intestines and confer numerous beneficial effects on the host. The introduction of probiotics in the treatment of inflammatory bowel disease (IBD) prolongs remission. The aim of this study was to investigate the intestinal and hepatic effects of PB supplementation in an experimental IBD model in mice induced by 2,4,6-trinitrobenzene sulfonic acid (TNBS). In the first step of the experimental procedure, CD-1 male mice, 5 to 6 weeks old, were randomly divided into 3 groups and inoculated intrarectally with, respectively, saline, alcohol, or TNBS to assess the experimental IBD model. In the second step, mice treated, or not, with TNBS inoculation, were treated with PB (*Lactobacillus Casei, Bifidobacterum Lactis)* for 1, 2 or 3 weeks, on a daily basis. Large bowel (colon and rectum) and liver were processed for histological alterations, according to a scoring system. Large bowel was also assessed for apoptosis by TUNEL assay. TNBS induced, as expected, severe damage and inflammation in the large bowel, including

Key words: intestinal inflammation, intestinal cancer, microbiota, probiotic supplementation, large bowel, liver, apoptosis

Mailing address: Prof. Francesco Cappello,
Sezione di Anatomia Umana,
Dipartimento di Biomedicina Sperimentale
e Neuroscienze Cliniche,
Università degli Studi di Palermo,
Via del Vespro 129 90127, Palermo, Italy
e-mail: francapp@hotmail.com.

0393-974X (2014)

nuclear alterations and apoptosis, and, to a lesser extent, to the liver. Administration of PB determined significant reduction of both histological alterations and apoptosis. PB administration in advance protects from inflammation. In conclusion, supplementation with *Lactobacillus casei, Bifidobacterum lactis* PB is able to ameliorate the colitis by reversing the histological changes caused by TNBS in mice. Experimentation in human subjects in needed to prove their efficacy in reducing histological alterations that may be present in subjects with IBD.

Probiotics (PB) are living microorganisms, usually bacteria, able to confer numerous beneficial effects on the host's health. These microorganisms are part of the normal intestinal microbiota acting as a commensal population and are capable of increasing resistance to disease. PB effects often depend on the interactions with the immune cells of the gut-associated lymphoid system (GALT) that is the largest immune-competent organ in the human body, and upon which depends the maturation and development of the immune system (1). PB participate in the onset and regulation of the mucosal immune response to bacteria by interacting with the immune cells of the GALT (2) and may reinforce innate immune functions such as phagocytic activity of neutrophils and cytotoxic activity of NK cells (3).

In the literature, persuasive results are reported on the use of PB in the treatment of different disorders (4). PB use has both direct and indirect effects. In particular, their use is beneficial for diarrheal diseases (5), necrotizing enterocolitis, bacterial and viral colitis (6, 7), and gastric and urogenital infections (8, 9). In the gastro-intestinal (GI) lumen, PB modulate the intestinal microbiota and exert their action directly with inhibition of colonization of the gut by potential pathogens, as well as translocation of pathogenic bacteria through the intestinal wall by competition for adhesion sites and nutrients, and possibly the production of H_2O_2, the acidification of the environment and production of antimicrobial substance (10). There are also indirect effects exerted by PB outside the GI lumen. In fact, they are involved in the down-regulation of inflammation in hypersensitivity reactions (4) and in serum-lipid reduction through their ability to take up cholesterol in the intestinal tract (11).

Many studies have shown positive effects of PB on the course of the Inflammatory Bowel Disease (IBD). The introduction of PB in the treatment of inflammatory bowel disease reduces remission. PB produce their beneficial effects by protecting the intestinal mucosa against invasive pathogenic bacteria, for example normalizing epithelial ion transport function (12). Moreover, PB balance the generation of pro- and anti-inflammatory cytokines in the gut, and then modulate the immune response. In particular, these bacteria can bind and activate T regulatory cells by the production of anti-inflammatory cytokines (e.g., IL-10) (13) and can also secrete small molecules that can enter intestinal epithelial cells to inhibit activation of nuclear factor kB and some cytokines, such as IL-8 and IL-6, that provide the basis for an acute innate inflammatory response to a pathogen (14). In addition, it has recently been reported that the interaction of bacterial molecules, such as peptidoglycans of membrane, with toll-like receptor 2 and 4 of dendritic cells, can activate intracellular negative regulators, which can lead to a reduction in the production of inflammatory cytokines and chemokines (12, 15).

It has also been reported that PB may help to fight cancer through multiple approaches that have varying degrees of efficacy. The antitumoral effects studied are various and different in relation to the type of tumor. For example, in breast cancer, the administration of PB with chemotherapeutic agents induces a regression of tumor size and an increase of lymphocyte proliferation by production of cytokines (16) Moreover, various scientific works suggest that colorectal cancer is very susceptible to PB treatment (4, 17-19). Indeed, PB lead to a reduction of tumor size induced by cellular apoptosis and suppression of proliferation, a decrease of pro-carcinogenic enzymes (20), and an enhancement of immune cell response (21).

The aim of the present study was to investigate the intestinal and hepatic effects of *Lactobacillus casei* and *Bifidobacterium lactis* supplementation in male mice treated with 2,4,6-trinitrobenzenesulfonic acid (TNBS). TNBS is a chemical compound that, administered to mice through rectal instillation, induces an IL-12-mediated TH1 T cell transmural

colitis, which resembles human IBD in regard to many features, both at histologic and immunologic levels. In fact, TNBS causes an intestinal dense transmural inflammatory cell infiltration with loss of normal crypt architecture and granuloma formation (22). The TNBS model is widely used for the study of the immunological mechanisms that have a role in the pathogenesis of IBD since it is easily induced and highly reproducible (23). Our results show an amelioration of histological damage induced by TNBS after PB supplementation, compared to controls. PB administration in advance protects from inflammation.

MATERIALS AND METHODS

Animals

Male mice (CD-1 strain, an outbred genetic background) 5- to 6-week-old (25-30 g weight) were purchased from Harlan Laboratoires S.r.l. (Correzzana D'Adda, Milan, Italy). They were kept in a room under a natural daylight rhythm at a constant temperature of 21±1°C and relative humidity of 55±10%. Access to food (standard pellets) and water was *ad libitum* throughout the experiment. All experiments conformed to the Guide for the Care and Use of Laboratory Animals published by the US National Institutes of Health (NIH publication No. 85-23, revised 1996). Animal care was in compliance with regulations in Italy (Ministerial Declaration 116/92), as well as with European Economic Community regulations (O.J. of European Commission L 358/1 12/18/1986), and the experimental design was approved by the Ethics Committee for Animal Experimentation at the University of Perugia, Italy. All efforts were made to minimize animal distress and to use only the number of animals necessary to produce reliable results.

Bacterial strains

Citogenex (*Lactobacillus Casei, Bifidobacterium Lactis*) kindly provided by Bromatech, S.p.A, Milan, Italy were used.

Induction of TNBS colitis in mice

We aimed first to establish the animal model of TNBS-induced colitis. For this purpose, we used n = 45 mice randomly divided into three groups of 15 and we inoculated intrarectally saline solution (control # 1), an ethanol 50% solution (control # 2) or TNBS solution (Sigma-Aldrich, Milan, Italy), respectively, under light anaesthesia with isoflurane (Merial, Milan Italy). In particular, to induce inflammation, mice were fasted for 24 h, lightly anesthetized, and a volume of 150 µl of TNBS solution per mouse [1.0 % in 50 % ethanol (v/v)] was injected via a 1-ml syringe fitted with a catheter (2 biological instruments, Basozzo, Varese, Italy), which was advanced to 3 cm proximal to the anus. The catheter end was lubricated beforehand (Luan, Molteni Farmaceutici, Firenze, Italy). In order to distribute the TNBS within the colon, the mouse was kept in a vertical position with the head downwards for 1 min after the injection. Control mice were treated with the same volume of saline or ethanol. Mice were euthanized 3 days after the induction of inflammation and large bowel was evaluated histologically. All mice were checked daily for loss of body weight, stool consistency, and the presence of gross bleeding.

Treatment with PB

To evaluate the effect of PB on the previously assessed model of TNBS-induced colitis, mice (n = 50) were randomly divided into eight groups (6 or 7 animals per group), four of which were treated with intrarectal TNBS injection. Six groups (three treated with TNBS and three not treated) were inoculated for different periods by gavage with PB solution for one, two and three weeks, respectively. In particular, the treated groups received daily 0.3 mL of a PB suspension (10^9 bacteria/ml, 10 ml/kg b.w.) for 7 (PB-1W or T+PB1W groups, respectively), 14 (PB-2W or T+PB2W groups, respectively) or 21 (PB-3W or T+PB3W groups, respectively) days. Saline solution inoculation by gavage and TNBS intrarectal injection groups were used as controls.

A routine plastic feeding tube for gavage (2 biological instruments, Basozzo, Varese, Italy) was used to introduce the saline solution or the suspension of PB into the stomachs of the mice. The animals were euthanized 3 days after the induction of inflammation. All mice were checked daily for loss of body weight, stool consistency, and the presence of gross bleeding.

Tissue processing

The mice were sacrificed by cervical dislocation. The abdominal cavity was opened and a gross evaluation of the digestive tract was made. The liver and the gastrointestinal tract, intact from anus to stomach, were immediately excised. The large intestine was subdivided into colon and rectum, and then opened longitudinally and cleaned with saline. Several samples were collected for the histological evaluation and fixed in a solution of 10% of formalin.

Histochemical analyses

Samples of colon, rectum and liver were processed for light microscopy examination. Each sample was routinely fixed in formalin and embedded in paraffin. Sections with a thickness of 5 µm were obtained from paraffin blocks,

and were deparaffinised with xylene for 10 min at 60°C and hydrated with a decreasing ethanol gradient. They were stained with haematoxylin for 4 min (Merck KGaA, Darmstadt, Germany), blocked for 15 min in tap water, treated with eosin (Merck KGaA) for 1 min and rinsed in water. The sections were dehydrated and mounted with a coverslip for histological examination using an automated Leica DM5000 B microscope (Leica, Milan, Italy) connected to a Leica DC300 F high-resolution camera (Leica, Milan, Italy).

All the histological evaluations were carried out by two different histopathologists on ten random fields at 200X magnification. For samples of colon and rectum, a quantitative analysis was performed to determine the extent of chronic inflammation in the mucosa, considering the inflammatory infiltration of the lamina propria and of the glands. Results were expressed in a semiquantitative scale (-: 0%; +: 1-33%; ++: 34-66%; +++: 67-100%). For histological analysis of the liver, the observers used a semiquantitative score (0-14) evaluating eight histological features of liver status: i) Nuclear change (score 0-3); ii) Necrosis (score 0: absent; 1: present); iii) Binucleation (score 0: absent; 1: present); iv) Hypereosinophilia (score 0: absent; 1: present); v) Intralobular inflammation (score 0-3); vi) Steatosis (score 0-3); vii) Haemorrhage (score 0: absent; 1: present); viii) Foreign body reaction (score 0: absent; 1: present).

Periodic acid of Schiff (PAS) (Sigma Aldrich, USA) staining was also performed to highlight goblet cells in the colon mucosa, in order to assess changes in the epithelial differentiation. After hydrating, paraffin sections were incubated in periodic acid for 5 min followed by staining with Schiff reagent for 15 min and finally haematoxylin staining. The sections were examined using an automated Leica DM5000 B microscope (Leica, Milan, Italy) connected to a high-resolution camera, Leica DC300 F (Leica, Milan, Italy). Morphological examination was performed on ten random fields at 400X magnification. The goblet cells were quantified in the epithelia of all samples from the colon and rectum, and the final value was expressed as a percentage of goblet cells for each case.

In situ detection of apoptosis

Detection of apoptosis was performed using an *In Situ* Cell Death Detection Kit, AP (Roche Cat. No 11684809910) on samples of paraffin-embedded colon tissue. Five µm thick sections were deparaffinised in a 60°C water bath, in two xylene baths and rehydrated in decreasing alcohol baths (absolute, 95%, 80%, 50%). Then, the slides were incubated with proteinase K at 37°C for 30 min to permeabilize the samples. Later, the labelling protocol of TUNEL reaction mixture addition for 60 min at 37°C was performed. The Converter AP was then added to the slides for 30 min at 37°C and the Substrate Solution for 10 min at room temperature in the dark. After a rinse with PBS, the slides were mounted with glass coverslips and observed using light automated Leica DM5000 B microscope (Leica, Milan, Italy) connected to a high-resolution camera, Leica DC300 F (Leica). Positive and negative controls were run concurrently, according to the manufacturer's instructions. The results were evaluated separately by two different observers who calculated the percentage of positive nuclei of epithelial cells in the colonic and rectal mucosae on ten random fields at 400X magnification. The mean of the two independent observations was considered as the result.

Statistical analyses

Standard statistical analyses were performed to calculate means and standard deviation, as well as to determine the presence of differences within the data obtained by histochemistry and TUNEL reactions. In particular, differences between groups were analysed using analysis of variance. Differences between the means were regarded as significant when a value of $p < 0.05$ was obtained**.** Data were plotted by graph pad.

RESULTS

Assessment of TNBS colitis in mice

We performed a histological evaluation of large bowel damage after induction of TNBS colitis in mice as described in the "Materials and Methods" section. These experiments were performed to assess the model and then were replicated to study the efficacy of the treatment of TNBS after treatment with PB. We found histological lesions resembling IBD. Data are not shown since they were very similar to those we found in the second round of experiments described in detail below.

Assessment of treatment with PB of TNBS-induced colitis

We examined the supplementation with PB in colon, rectum and liver, separately. At macroscopic examination, the distal tract of the colon of TNBS-treated mice was swollen, oedematous and thickened, with evidence of mucosal haemorrhage compared to the controls. At histological level, the exposure to TNBS caused a significantly higher degree of acute inflammation in the colonic mucosa when compared to controls ($p < 0.01$) (Fig. 1A). The inflammation

Table I. *Histological score results for liver evaluation.*

GROUPS	SCORE								
	Nuclear change	Necrosis	Binucleation	Hyper-eosinophilia	Intralobular Inflammation	Steatosis	Haemorrhage	Foreign body reaction	TOTAL
CTR	1	0	0.4	0	0.1	0	0.1	0.06	1.66
PB 1w	1.6	0	0.42	0	0.04	0	0	0	2.06
PB 2w	0.8	0.2	0.6	0.22	0.2	0	0	0	2.02
PB 3w	0.6	0.43	0.2	0	0.1	0	0	0	1.33
TNBS	1.5	1	0.5	0.5	1.5	1	0.15	0.6	6.75
T+PB 1w	2.8	1	1	1	0.8	0.36	0	0.2	7.16
T+PB 2w	1.6	0.8	1	1	1.2	0.8	0	0	6.4
T+PB 3w	2.2	0.5	0.8	0.6	1	0.3	0.15	0.01	5.56

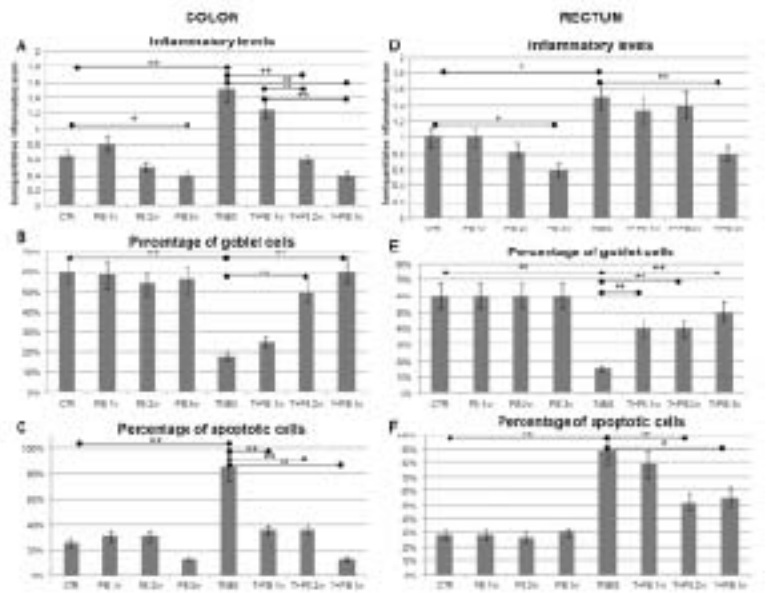

Fig. 1. *Statistical analyses of effects of treatments on colon and rectum.* ***A-C****) Evaluation of the colon.* ***D-F****) Evaluation of the rectum. A and D: Evaluation of the inflammatory status by H&E staining. B and E. Evaluation of percentage of goblet cells by PAS staining. C-F. Evaluation of apoptotic epithelial cell percentage by TUNEL assay. CTR: control animals group. PB 1w: control animals with PB for one week. PB 2w: control animals with PB for two weeks. PB 3w: control animals with PB for three weeks. TNBS: TNBS treated animals group. T+PB 1w: TNBS treated animals with PB for one week. T+PB 2w: TNBS treated animals with PB for two weeks. T+PB 3w: TNBS treated animals with PB for three weeks. * = $p < 0.05$; ** = $p < 0.01$.*

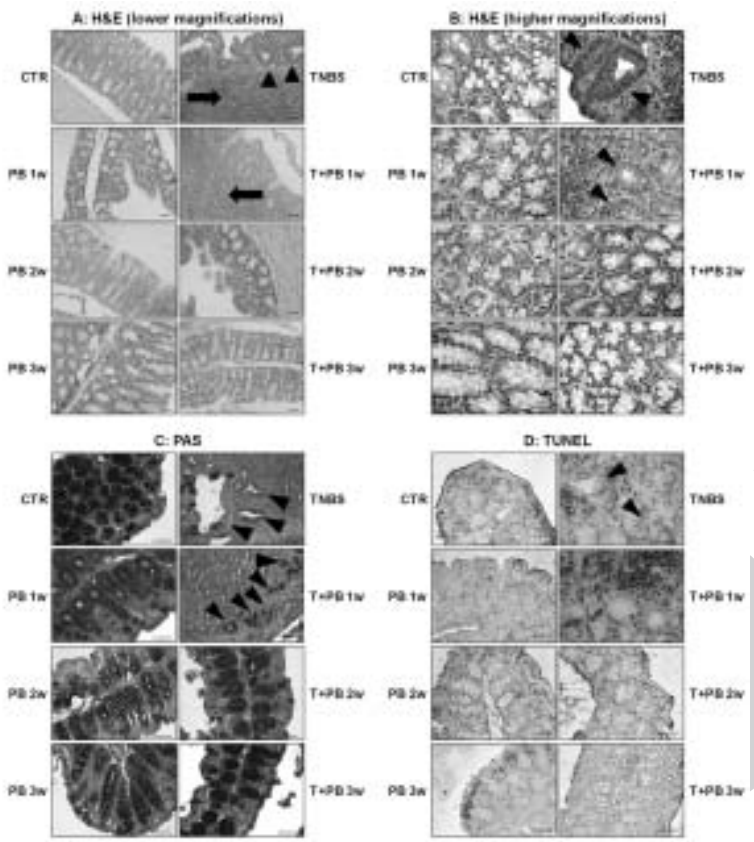

Fig. 2. *Morphological analyses of colon. This panel shows representative pictures of morphological evaluations on colon tissues. **A**) H&E, lower magnifications. **B**) H&E, higher magnifications. **C**) PAS reactions. **D**) TUNEL assays. Bar in A, C and D = 100 micra; Bar in B = 50 micra. CTR: control animals group. PB 1w: control animals with PB for one week. PB 2w: control animals with PB for two weeks. PB 3w: control animals with PB for three weeks. TNBS: TNBS treated animals group. T+PB 1w: TNBS treated animals with PB for one week. T+PB 2w: TNBS treated animals with PB for two weeks. T+PB 3w: TNBS treated animals with PB for three weeks. Inflammation was present in TNBS and T+PB 1w groups (A, arrows). Distortion of gland architecture is also visible in TNBS group (A, arrowheads). In addition, TNBS and T+PB 1w groups showed an altered nucleo-cytoplasmic ratio, due to an increase in nuclear dimension (B, arrowheads), and a reduced number of PAS positive cells (C, arrowheads) compared to the other groups. Finally, TNBS showed also an increased number of apoptotic epithelial cells (D, Arrowheads) compared to the other groups.*

was particularly present at lamina propria and submucosa levels in all specimens examined (Fig. 2A). Inflammation was reduced significantly after two weeks of PB treatment ($p < 0.01$) (Fig. 1A and Fig. 2A). Interestingly, changes were observed in the nucleo-cytoplasmic ratio (due to enlargement of nuclei) in the epithelial cells (Fig. 2B) and architectural distortion of glands (Fig. 2A) after treatment with TNBS. Such alterations remained well evident after one week of PB administration, started to decrease after two weeks and, most importantly, after three weeks of pre-treatment, PB administration resulted in advance to protect mucosa from inflammation and damage. The number of PAS positive epithelial cells was dramatically reduced after TNBS treatment ($p < 0.01$) and the normal number of goblet cells was restored only after two weeks of PB (Fig. 1B and Fig. 2C). Exposure to TNBS also showed a significant increase of apoptotic cells, compared to controls ($p < 0.01$), that returned to normal levels after one week of PB administration (Fig. 1C and Fig. 2D). Moreover, we found a significant reduction of inflammation after three weeks of PB compared with unsupplemented

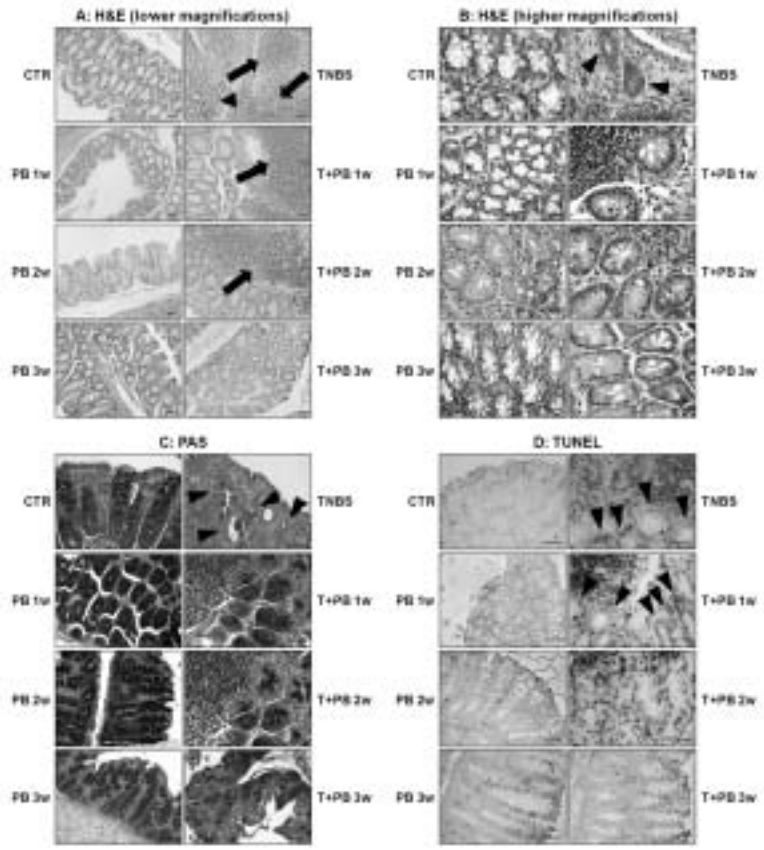

Fig. 3. *Morphological analyses of rectum. This panel shows representative pictures of morphological evaluations on rectal tissues. **A**) H&E, lower magnifications. **B**) H&E, higher magnifications. **C**) PAS reactions. **D**) TUNEL assays. Bar in A, C and D = 100 micra; Bar in B = 50 micra. CTR: control animals group. PB 1w: control animals with PB for one week. PB 2w: control animals with PB for two weeks. PB 3w: control animals with PB for three weeks. TNBS: TNBS treated animals group. T+PB 1w: TNBS treated animals with PB for one week. T+PB 2w: TNBS treated animals with PB for two weeks. T+PB 3w: TNBS treated animals with PB for three weeks. Inflammation was present in TNBS, T+PB 1w and T+PB 2w groups (A, arrows) while T+PB 3w group did not show differences to controls. Distortion of gland architecture is visible in TNBS group (A, arrowhead) but not in other groups. Moreover, TNBS group showed an altered nucleo-cytoplasmic ratio due to an increase in nuclear dimension (B, arrowheads) as well as a reduced number of PAS positive cells (C, arrowheads) compared to the other groups. Finally, TNBS and T+PB 1w showed an increased number of apoptotic epithelial cells (D, arrowheads) compared to the other groups.*

controls ($p < 0.05$) (Fig. 1A). Finally, treatment with both saline solution and alcohol did not induce any histological damage (not shown).

Exposure to TNBS induced a significantly higher degree of acute inflammation in the rectal mucosa as compared to controls ($p < 0.05$) (Fig. 1D). Inflammation was particularly visible in the lamina propria and submucosa of all specimens examined (Fig. 3A). Such inflammation was reduced significantly only after three weeks of PB treatment ($p < 0.01$) (Fig. 1D and Fig. 3A). As in colonic mucosa, we observed changes in the nucleo-cytoplasmic ratio and architectural distortion of glands (Fig. 3A and 3B) after treatment with TNBS which were reduced significantly after only one week of PB treatment. The number of PAS positive epithelial cells dropped dramatically after TNBS treatment but recovered significantly after only one week of PB treatment ($p < 0.01$) (Fig. 1E and Fig. 3C). TNBS exposure also caused a significant increase in apoptosis, compared to controls, that returned to normal levels after two weeks of PB treatment (Fig. 1F and Fig. 3D). In addition, a reduction of inflammation was observed in controls after three weeks of PB administration

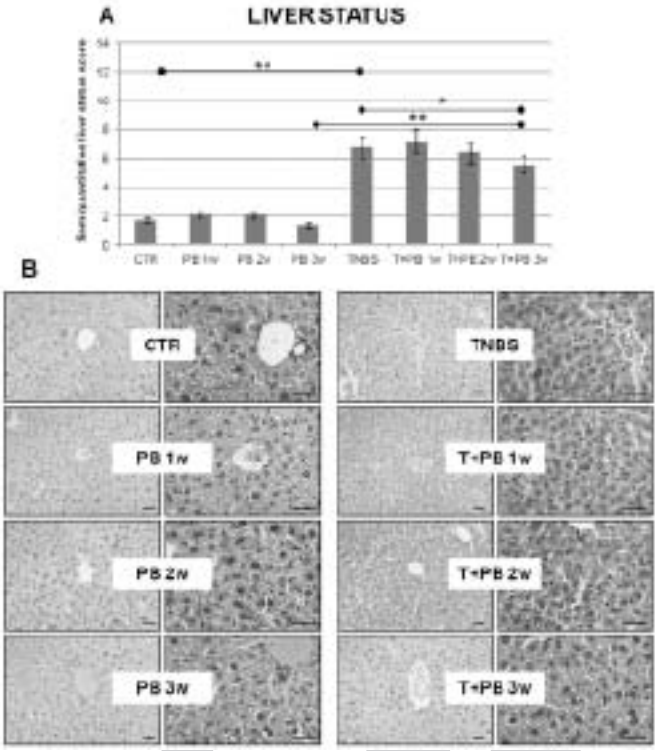

Fig. 4. *Liver status evaluation. This panel shows in **A** the statistical results of liver status and in **B** representative pictures of evaluations performed by H&E at 200 X and 400 X magnifications (Bar = 100 micra). CTR: control animals group. PB 1w: control animals with PB for one week. PB 2w: control animals with PB for two weeks. PB 3w: control animals with PB for three weeks. TNBS: TNBS treated animals group. T+PB 1w: TNBS treated animals with PB for one week. T+PB 2w: TNBS treated animals with PB for two weeks. T+PB 3w: TNBS treated animals with PB for three weeks. * = $p < 0.05$; ** = $p < 0.01$. In B, note that large nuclei, binucleation, hypereosinophilia and focal intralobular inflammation are visible in the pictures of the right panel (TNBS-treated groups, without and with PB), while very limited damage is present in the pictures of the left panel (control groups, without and with PB). See also Table I for histological scores.*

compared with unsupplemented controls ($p < 0.05$) (Fig. 1D). Finally, treatment with saline solution did not induce any histological damage at this level, while alcohol treatment induced small necrotic areas in one half of cases (not shown).

Histological score results of liver evaluation are summarized in Table I. Exposure to TNBS induced a higher degree of inflammation in the liver as compared to controls ($p < 0.01$) (Fig. 4A). However, after three weeks of PB treatment, liver damage appeared significantly reduced, although it remained higher than in controls ($p < 0.05$). Exposure to TNBS caused damage in liver parenchyma that consisted mainly in nuclear changes (large nuclei), increased binucleation, hypereosinophilia and focal intralobular inflammation (Fig. 4B) when compared to controls (Fig. 4A). Finally, treatment with saline solution and an alcohol did not induce any histological damage (not shown).

DISCUSSION

Evidence that PB can be used with therapeutic potential in IBD has emerged from clinical studies (24) and experimental models of colitis in animals (25). We carried out this study to analyze the effects of supplementation with a mixture of *Lactobacillus casei* and *Bifidobacterium lactis* on the large bowel and liver of mice exposed to TNBS as an inflammatory agent.

Our results have shown that exposure to TNBS induces severe damage both in the bowel wall and liver parenchyma. Both colon and rectum were characterized by an acute inflammation accompanied by an increased nuclear-cytoplasmic ratio, distortion of gland architecture and a reduction of goblet cells. Increased nuclear dimensions resulting in increased nucleo-cytoplasmic ratio and distortion of glands are morphological lesions highly suggestive for malignant transformation. In addition we detected an increased in apoptosis in intestinal cells after TNBS treatment.

Supplementation with a mixture of *Lactobacillus casei* and *Bifidobacterium lactis* (Citogenex) significantly reduced the inflammation in the colonic mucosa. Moreover, it showed efficacy in reversing malignant changes and in reducing apoptosis exerting a potential role in cancer prevention (26-28). Finally, it restored the normal number of goblet cells. These modifications, although with a different time-course, were seen both in colon and rectum. In our opinion, these results are important since they may indicate that the treatment with PB is not only effective in reducing inflammation, but also in decreasing the carcinogenic risk at colorectal level. However, other studies on larger samples are needed to confirm these results.

Beneficial effects of PB may be produced by various mechanisms (29, 30). For example: i) they compete with other luminal bacteria and prevent them from reaching the lamina propria and stimulating the mucosal immune system; ii) they modulate intestinal barrier properties, regulating expression of genes encoding adherence junction proteins; iii) they enhance mucous production and, thus, protect the mucosa against invasive bacteria; iv) they stimulate the mucosal immune system in the patient's intestinal tract to secrete protective immunoglobulins (Ig) such as secretory IgA and protective defensins; v) they produce bacteriocins in the lumen; vi) they stimulate apoptosis of mucosal immune cells, counteracting the excessive accumulation of these cells in the gut; vii) they alter the function of the mucosal immune system to make it more anti-inflammatory and less pro-inflammatory; viii) they prevent nuclear factor kappa B (NFkB) binding in murine epithelial gut cells and block the proteasome-dependent degradation of the NFkB inhibitor IkBa; ix) they have a role in regulating intestinal cell survival and growth, e.g. stimulating protein kinase B (PKB/Akt) activation, promoting cell growth, and inhibiting tumor necrosis factor (TNF)-induced epithelial cell apoptosis in cultured cells and in *ex-vivo* colon organ culture models; and x) they favour intestinal cell turnover, stimulating intestinal stem cells to differentiate.

In summary, PB treatment showed efficacy in reducing damage induced by TNBS in both large bowel segments. In the liver, TNBS induced damage seen as nuclear enlargement, more binucleation, hypereosinophilia and focal intralobular inflammation. This damage was reduced significantly after PB treatment although normal liver morphology was not completely restored. In our opinion, this could be due to the fact that the large bowel is able to repair and remodel itself more rapidly than liver. Administration of PB facilitates the recovery of inflammation of the mucosa and submucosa of the large bowel in mice exposed to TNBS. This beneficial effect could be ascribed to PB action. PB have probably beneficial effects thanks to their ability of restoring the intestinal microbiota balance. These effects are more important because the alteration of intestinal microbiota is often the first cause of mucosal inflammatory damage (31, 32). Previous studies reported that specific PB supplementation showed antigenotoxic properties, resulting useful for the protection of intestinal epithelia and liver cells in mice (33-35). Our observations are in agreement with the majority of data in the literature that confirm the important role of PB in the treatment of intestinal disease. Molecular mechanisms by which PB are able to exert their beneficial effect are currently under investigation.

REFERENCES

1. Guarner F, Malagelada JR. Bacterial flora of the digestive tract. Gastroenterol Hepatol 2003; 26:1-5.
2. Kagnoff MF, Eckmann L. Epithelial cells as sensor for microbial infection. J Clin Invest 1997; 100:6-10.
3. Takeda K, Suzuki T, Shimada SI, et al. Interleukin-12 is involved in the enhancement of human natural killer cell activity by *Lactobacillus casei Shirota*. Clin Exp Immunol 2006; 146:109-15.
4. Drisko JA, Giles CK, Bischoff BJ Probiotics in health maintenance and disease prevention. Altern

Med Rev 2003; 8:153-55.
5. Saavedra JM, Bauman NA, Oung I, Perman JA, Yolken RH. Feeding of *Bifidobacterium bifidum* and streptococcus thermophiles to infants in hospital for prevention of diarrhea and shedding of rotavirus. Lancet 1994; 344:1046-49.
6. Caplan MS, Jilling T. Neonatal necrotizing enterocolitis: possible role of probiotic supplementation. J Pediatr Gastroenterol Nutr 2000; 30:18-22.
7. Gorbach SL, Chang TW, Goldin B. Successful treatment of relapsing *Clostridium difficile* colitis with *Lactobacillus GG*. Lancet 1987; 2:1519.
8. Vanderhoof JA, Young RJ. Use of probiotics in childhood gastrointestinal disorders. J Pediatr Gastroenterol Nutr 1998; 27:323-32.
9. Aiba Y, Suzuki N, Kabir AM, Takagi A, Koga Y. Lactic acid-mediated suppression of *Helicobacter pylori* by the oral administration of *Lactobacillus salivarius* as a probiotic in a gnotobiotic murine model. Am J Gastroenterol 1998; 93:2097-101.
10. Gupta V, Garg R. Probiotics. Indian J Med Microbiol 2009; 27:202-9.
11. Sanders ME, Klaenhammer TR. Invited review: the scientific basis of *Lactobacillus acidophilus* NCFM functionality as a probiotic. J Dairy Sci 2001; 84:319-31.
12. Resta-Lenert SC, Barrett KE. Modulation of intestinal barrier properties by probiotics: role in reversing colitis molecular structure and function of the tight junction: Ann NY Acad Sci 2009; 1165:175-82.
13. Rachmilewitz D, Katakura K, Karmeli F, et al. Toll-like receptor 9 signaling mediates the anti-inflammatory effects of probiotics in murine experimental colitis. Gastroenterology 2004; 126:520-28.
14. Neish AS, Gewirtz AT, Zeng H, et al. Prokaryotic regulation of epithelial responses by inhibition of IkBa degradation. Science 2000; 289:1560-63.
15. Otte JM, Podolsky DK. Functional modulation of enterocytes by grampositive and gram-negative microorganisms. Am J Physiol Gastrointest Liver Physiol 2004; 286:G613-26.
16. Maroof H, Hassan ZM, Mobarez AM, Mohamadabadi MA. *Lactobacillus acidophilus* could modulate the immune response against breast cancer in murine model. J Clin Inmmunol 2012; 32:1353-59.
17. Ma EL, Choi J, Pothoulakis C, Rhee SH, Im E. The anticancer effect of probiotic *Bacillus polyfermenticus* on human colon cancer cell is mediated through ErbB2 and ErbB3 inhibition. Int J Cancer 2010; 127:780-90.
18. Lan A, Lagadie-Gossmann D, Lemaire C, Brenner C, Jan G. Acidic extracellular pH shifts colo-rectal cancer cell death from apoptosis to necrosis upon exposure to propionate and acetate, major end-products of the human probiotic proprioni-bacteria. Apoptosis 2007; 12:573-91.
19. Jan G, Belzacq AS, Haouzi D, et al. Propionibacteria induce apoptosis of colorectal carcinoma cells via short-chain fatty acids acting on mitochondria. Cell Death Differ 2002; 9:179-88.
20. De Moreno LA, Perdigon G. The application of probiotic fermented milks in cancer and intestinal inflammation. Proc Nutr Soc 2010; 69:421-28.
21. Bassaganya-Riera J, Viladomiu M, Pedragosa M, De Simone C, Hontecillas R. Immunoregulatory mechanisms underlying prevention of colitis-associated colorectal cancer by probioticbacteria. PLoS ONE 2012; 7:e34676.
22. Morris G, Beck P, Herridge M, et al. Hapten-induced model of colonic inflammation and ulceration in the rat colon. Gastroenterology 1989; 96:795-803.
23. Scheiffele F, Fuss IJ. Induction of TNBS Colitis in Mice. Curr Protocol Immunol 2002; Chapter 15: Unit 15.19. doi:10.1002/0471142735.
24. Tomasello G, Rodolico V, Zerilli M, et al. Changes in immunohistochemical levels and subcellular localization after therapy and correlation and colocalization with CD68 suggest a pathogenetic role of Hsp60 in ulcerative colitis. Appl Immunohistochem Mol Morphol 2011; 19:552-61.
25. Peran L, Camuesco D, Comalada M, et al. Preventative effects of a probiotic, *Lactobacillus salivarius ssp. salivarius*, in the TNBS model of rat colitis. World J Gastroenterol 2005; 11:5185-92.
26. Tang D, Lotze MT, Kang R, Zeh HJ. Apoptosis promotes early tumorigenesis. Oncogene 2011; 30:1851-4.
27. Cappello F, Bellafiore M, Palma A, Bucchieri F. Defective apoptosis and tumorigenesis: role of p53 mutation and Fas/FasL system dysregulation. Eur J Histochem 2002; 46:199-208.

28. Renehan AG, Bach SP, Potten CS. The relevance of apoptosis for cellular homeostasis and tumorigenesis in the intestine. Can J Gastroenterol 2001; 15:166-76.
29. Bellavia M, Tomasello G, Romeo M, et al. Gut microbiota imbalance and chaperoning system malfunction are central to ulcerative colitis pathogenesis and can be counteracted with specifically designed probiotics: a working hypothesis. Med Microbiol Immunol 2013; 202:393-406.
30. Sinagra E, Tomasello G, Cappello F, et al. Probiotics, probiotics and symbiotics in inflammatory bowel diseases: state-of-the-art and new insights. J Biol Regul Homeost Agents 2013; 27:919-33.
31. Bellavia M, Damiano G, Gioviale MC, et al. Abnormal expansion of segmented filamentous bacteria in the gut: a role in pathogenesis of chronic inflammatory intestinal diseases? Rev Med Microbiol 2011; 22:45-47.
32. Llopis M, Antolin M, Carol M, et al. *Lactobacillus casei* downregulates commensals inflammatory signals in Crohn's disease mucosa. Inflamm Bowel Dis 2009; 15:275-83.
33. Dominici L, Moretti M, Villarini M, et al. *In vivo* antigenotoxic properties of a commercial probiotic supplement containing Bifidobacteria. Int J Probiotics Prebiotics 2011; 6: 179-86.
34. Persichetti E, De Michele A, Codini M, Traina G. Antioxidative capacity of *Lactobacillus fermentum* evaluated *in vitro* by oxygen radical absorbance capacity assay. Nutrition 2014; in press; doi. org/10.1016/j.nut.2013.12.009.
35. Chong ES. A potential role of probiotics in colorectal cancer prevention: review of possible mechanisms of action. World J Microbiol Biotechnol 2014; 30:351-74.

DEGENERATIVE EVENTS IN RETINA AND OPTIC NERVE INDUCED BY INHIBITION OF CARNITINE TRANSPORT

N. PESCOSOLIDO[1], A. PASCARELLA[2], M. NEBBIOSO[3] and G. SCARSELLA[2]

[1]Department of Cardiovascular, Respiratory, Nephrology, Geriatric and Anesthetic Sciences, [2]Department of Biology and Biotechnology Charles Darwin, [3]Department of Sense Organs, Sapienza University of Rome, Italy

Received July 30, 2013 – Accepted February 28, 2014

Biochemical and pharmacological evidence supports the hypothesis that the mechanism of action of mildronate [3-(2,2,2-trimethylhydrazinium)propionate dihydrate] is based on its regulatory effect on carnitine concentration. The present study demonstrates that carnitine acts as a neuroprotective agent both in optic nerve head and in retinal ganglion cell (RGC) by means of antioxidant and antiradical activities. In fact, carnitine normalized the increase in caspase-3, cellular apoptosis susceptibility protein (CAS) and inducible nitric oxide synthase (iNOS) expression by stabilizing mitochondrial membranes, as assessed by quantitative and qualitative analysis. This research shows that the neuroprotective effects of carnitine result, at least partially, from anti-neurodegenerative (anti-apoptotic) and anti-inflammatory mechanisms. It is suggested that the molecular conformation of carnitine can facilitate its easy binding to mitochondria, and regulate the expression of different signal molecules, hence maintaining normal cellular signaling and survival by modulating caspase-3 activity.

L-carnitine (L-3-hydroxy-4-N-N-N-trimethyl-aminobutyrate) is a carrier for fatty acids across the inner mitochondrial membrane for subsequent β-oxidation (1). It is also an antioxidant that reduces metabolic stress in the cells by acting as scavenger for free radicals (2). In addition, L-carnitine treatment is able to elevate peroxisome proliferator-activated receptor-α (PPAR-α) activation and exerts an anti-apoptosis effect (3, 4). Cellular energy homeostasis relies on both fatty acid and carbohydrate metabolism. After transportation to the intracellular space, carbohydrates and fatty acids are gradually metabolized and transferred to mitochondria. The metabolic final step results in synthesis of adenosine triphosphate (ATP) molecules. It is known that mildronate decreases carnitine transport into mouse muscular cells by a noncompetitive mechanism (5). Moreover, mildronate influences activity of both high- and low-affinity transporters. Because carnitine concentration in tissues is 20 to 50 times higher than in plasma (6), the inhibition of carnitine transport through the plasma membrane is a powerful approach to controlling intracellular carnitine concentration. The links that exist between neurodegeneration and neuroinflammation and the importance of mitochondria as cellular targets are now recognized (7). The production of reactive oxygen species and reactive nitrogen species during oxidative stress initiates and promotes the damage of macromolecules, resulting in central nervous system (CNS) neurodegeneration. Furthermore, oxidative stress also promotes glia-mediated

Key words: antioxidant activity, carnitine, cytotoxicity, mildronate, neuroprotection, optic nerve, retina

Mailing address: Dr. Marcella Nebbioso,
Department of Sense Organs,
Centre of Ocular Electrophysiology,
viale del Policlinico 155,
00161 Rome, Italy
Tel.: +39 06 49975422 Fax: +39 06 49975425
e-mail: marcella.nebbioso@uniroma1.it

0393-974X (2014)

inflammation that, in turn, causes secondary neuronal damage (8). Consequently, a rational therapy for neurodegenerative diseases may potentially involve targeting mitochondria, leading to reductions in both inflammatory and neurodegenerative events.

Our aim was to study the effects of experimental murine mildronate and carnitine intraocular administration, focusing on the characterization of biomolecular mechanisms of apoptosis (9-11) and investigate the possibility of having the same cellular responses observed for stress pressure. For this reason, retinas and optic nerves obtained from mildronate and/or carnitine-treated animals were microscopically compared to specimens from an experimental ocular hypertension animal model, where apoptotic death of retinal cells is observed 24 hours after the induction of ocular hypertension (12). This latter model has been proved to reproduce both clinical and histopathological signs of acute human glaucoma.

MATERIALS AND METHODS

Animals, treatment and experimental procedures

All experimental procedures were in accordance with the ARVO Statement for the Use of Animal in Ophthalmic and Vision Research, the guidelines of the European Communities Council Directive of 24 November, 1986 (86/609/EU), Italian Health leading to ocular hypertension (12-14).

A group of 20 male Wistar rats, average weight 300-350 g, were housed in controlled light and temperature with unlimited access to food and water. The animals were submitted to intraocular injection of 0.5 mM, 2 mM, 3.5 mM, or 5 mM mildronate (Sigma-Tau, Italy) to standardize experimental conditions (data not shown). A group of 12 animals was submitted to intraocular injection of 2% methylcellulose [(MTC) Sigma-Aldrich]. MTC is a molecule capable of mechanically blocking the outflow of aqueous humor, (Sigma-Tau, Italy); all controlateral eyes were used as control. These animals were randomly separated into 3 experimental groups: rats from the first group received mildronate 5 mM; rats from the second group received mildronate 2 mM; rats from the third group received mildronate 2 mM + L-carnitine 0.6 mM Ministry guidelines, and EU directive 2010/63/EU for animal experiments. After systemic general anesthesia with ether to avoid movement, the animals were injected in the posterior chamber of the right eye with the solutions described above. The animal sufferance was evaluated by the behavioral Irwin test (14, 15). Ocular inflammation was evaluated with the Drize test (15) adapted to the rat. Successively, twenty-four hours after the intraocular injection, rats were given general anesthesia by intra-peritoneal injection of 500 µl sodium-thiopental solution (Farmotal, Pharmacia & Upjohn, USA) in saline. They were then sacrificed by carotid bleeding and the eyeballs were removed. Immunohistochemical techniques and Western blot were used to detect glial cell activation markers, alteration of the cell cycle, apoptotic cell damage in the retina and optic nerve head of the rats.

Induction of the intra-ocular hypertension

The intraocular pressure (IOP) was daily monitored in the animals, from time 0 to 7 days by tonometry (Tonopen XL, Automated Ophthalmics, Ellicott City, MD, USA) (14, 16). Then they were injected in the anterior chamber of the right eye with 15 µl of 2% (w/v) MTC in physiological solution. The IOP (normal value ~12 mmHg) sharply increased (~50 mmHg) 3 min after MTC injection, due to the progressive occlusion of trabeculate and Schlemm's canal. The controlateral eye was used as control and injected only with physiological solution.

Ocular inflammation was assessed by the Drize test adapted to the rat (15). The degree of animal sufferance was evaluated by the behavioral Irwin test and by the recovery of bodyweight (14, 15). The animals were finally sacrificed by hemorrhagic shock. No difference was observed after comparison between non-injected and operated animals.

Immunohistochemistry and sample preparation

The eyes were enucleated, the corneas were cut vertically, and the crystalline lenses and vitreous humor were removed. The residual tissues were fixed in paraformaldehyde 4% for 6 h at 4°C, followed by rapid wash with 1X PBS pH 7.4; immersion in a 30% sucrose solution in 1X PBS pH 7.4 at 4°C overnight; and embedded in Killik embedding medium (Bio-Optica, Milan, Italy). Ten µm cryostat sections were cut horizontally, to allow longitudinal observation of the optic nerve. Sections were placed on microscope slides and stored at -20°C.

Inducible nitric oxide synthase (iNOS) expression was detected with a rabbit polyclonal anti-iNOS antibody (Santa Cruz) (1:50), followed by a green fluorescent goat anti-rabbit IgG Alexa Fluor (Molecular Probes) secondary antibody. Caspase-3 expression was detected with a rabbit polyclonal anti-caspase-3 antibody (Santa Cruz) (1:100), followed by a green fluorescent goat anti-rabbit IgG Alexa Fluor (Molecular Probes) secondary antibody. The sections, left to dry at room temperature for 30 min, were subjected to various treatments: washes in 1X PBS for 5 min; post-fixated with alcohol at increasing volumes (70°, 95°, 100°) for 2 min; washed in 1X PBS for 5 min; blocked

with serum (NRS or NGS), 10% in PBS, 1 h in a moist chamber; incubation with the primary antibody diluted in 1X PBS + BSA 1% for 1 h; fast washed in 1X PBS; incubation with the secondary antibody (conjugated with phosfatase) diluted 1: 200 in1X PBS + 1% of the serum of the animal in which the antibody was produced, for 30 min at room temperature; washed in 1X PBS for 5 min; first to mounting of the slides with Eukitt. Tissue sections were counterstained by precipitation of tetrazolium salts by phosfatase to reveal antibody activity at visible light. In order to highlight morphology, the cytoplasms were stained with blue-eosin (C.I. 45400), the color of which is more apt to contrast tetrazolium precipitates than standard eosin.

Preparation of protein extracts

Rat retinas were immersed in lysis buffer, and test-tubes were kept for 10 min on ice, then centrifuged at 13,000 rpm for 5 sec and transferred back to the ice for another 10 min. Finally, they were centrifuged for 10 min, at 13,000 rpm. Subsequently, the supernatant was collected to be analyzed.

Western blotting and immunodetection

An equal amount of protein was loaded, separately, on a SDS PAGE gel and then iNOS and caspase-3 presence were identified by Western blotting. α-tubulin was used as loading control to normalize protein expression. The Bradford assay was used to estimate protein concentration.

TUNEL assay

Cellular DNA Fragmentation ELISA - Roche Dia (cat. 11 585) determination was made by incubation at 37° with TUNEL reagent, containing 1/10 in volume of terminal deoxynucleotidyl transferase and the remaining fraction of nucleotides. Readings were performed in optical density by a platelet photometer at wavelength of 450. One of the specimens was always used as the negative control.

Statistical analysis

All the experiments were repeated at least four times. Statistical analysis of the results was carried out using the ANOVA test. The significance of the results was determined by the Student's *t*-test. P-values <0.05 were considered significant.

RESULTS

DNA damage

Eyes from control animals showed no positivity either in optic nerve or retina after TUNEL assay. Eyes treated with mildronate 5 mM showed a strong fluorescence in the retinal ganglion cells (RGCs) and astrocyte cells of the optic nerve due to DNA fragmentation. Eyes from mildronate 2 mM-treated animals showed a slight positive fluorescence, and animals treated with both mildronate and carnitine were quite similar to controls, suggesting a cytoprotective effect for carnitine (Fig. 1).

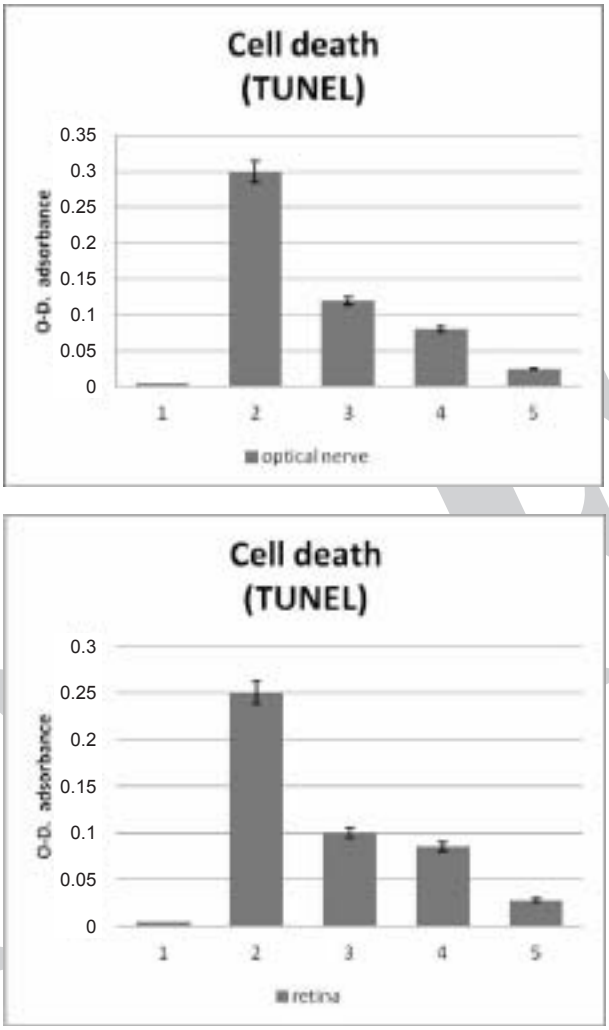

Fig. 1. *DNA damage. 1) Control. 2) Optic nerve (upper) and retina (lower) 5 mM mildronate-treated rats. 3) Optic nerve (upper) and retina (lower) 2% MTC-treated rats. 4) Optic nerve (upper) and retina (lower) from 5 mM mildronate+0.6 mM L-carnitine-treated rats. 5) Treated specimens with 2 mM mildronate+0.6 mM L-carnitine. All values represent mean and ± S.E.M. DNA damage was evaluated by a TUNEL colorimetric test.*

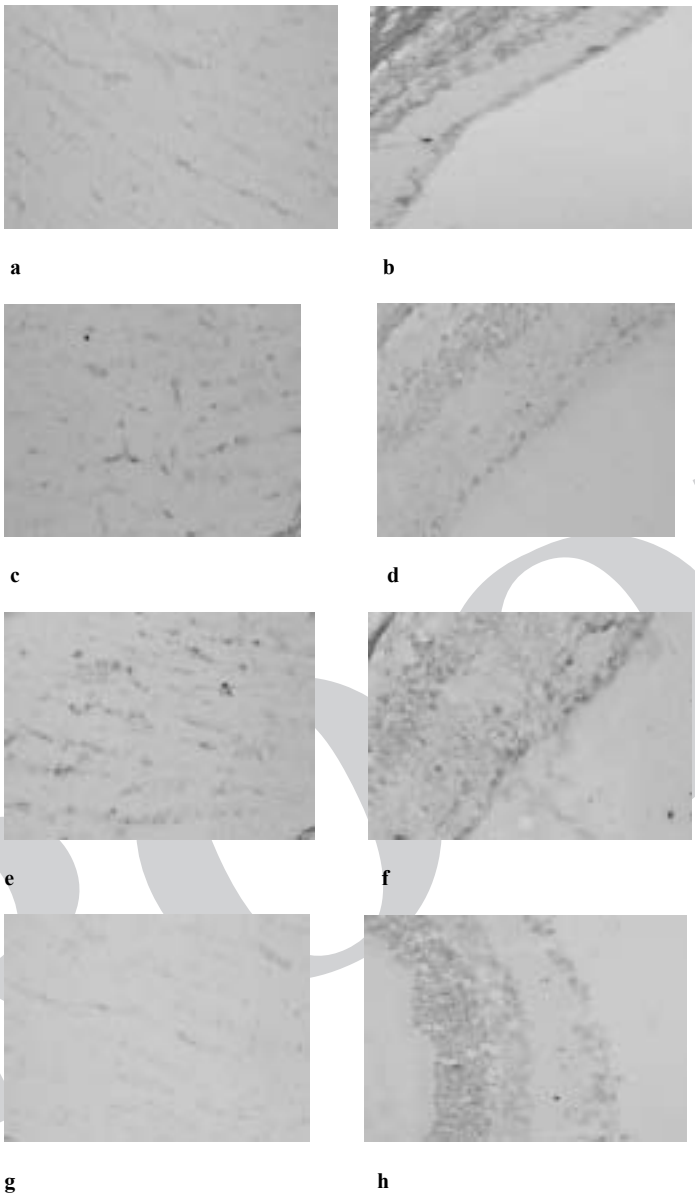

Fig. 2. *iNOS immunoreactivity.* ***a)*** *Section of optic nerve from control rats (500X).* ***b)*** *Section of retina from control rats (500X).* ***c)*** *Section of optic nerve from 5 mM mildronate-treated rats (500X).* ***d)*** *Section of retina from 5 mM mildronate-treated rats (500X).* ***e)*** *Section of optic nerve from 2% MTC-treated rats (500X).* ***f)*** *Section of retina from 2% MTC-treated rats (500X).* ***g)*** *Section of optic nerve from 2 mM mildronate + 0.6 mM L-carnitine-treated rats (500X).* ***h)*** *Section of retina from 2 mM mildronate + 0.6 mM L-carnitine-treated rats (500X).*

iNOS expression

iNOS immunolocalization was performed in order to verify cellular stress in the optic nerve and retina at different concentrations of mildronate (Fig. 2a-h).

Twenty-four hours after treatment with 5 mM mildronate, high levels of iNOS were expressed both in astrocytes of optic nerve (Fig. 2c) and glial retinal cells (Fig. 2d) as compared to controls (Fig. 2a/b), suggesting that treatment with mildronate and/or a decrease in the intracellular levels of L-carnitine causes mitochondrial damage and an oxidative stress

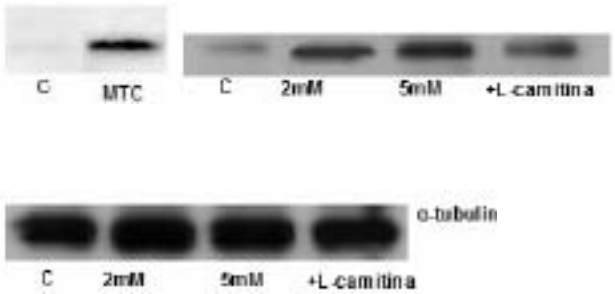

Fig. 3. *iNOS of retina Western blot analysis. C: control; MTC treated with meticellulosa; 2mM: treated with 2 mM mildronate; 5mM: treated with 5 mM mildronate; +L-carnitine: treated with 2 mM mildronate + 0.6 mM carnitine; α tubulin: standardization of Western blot with tubulin.*

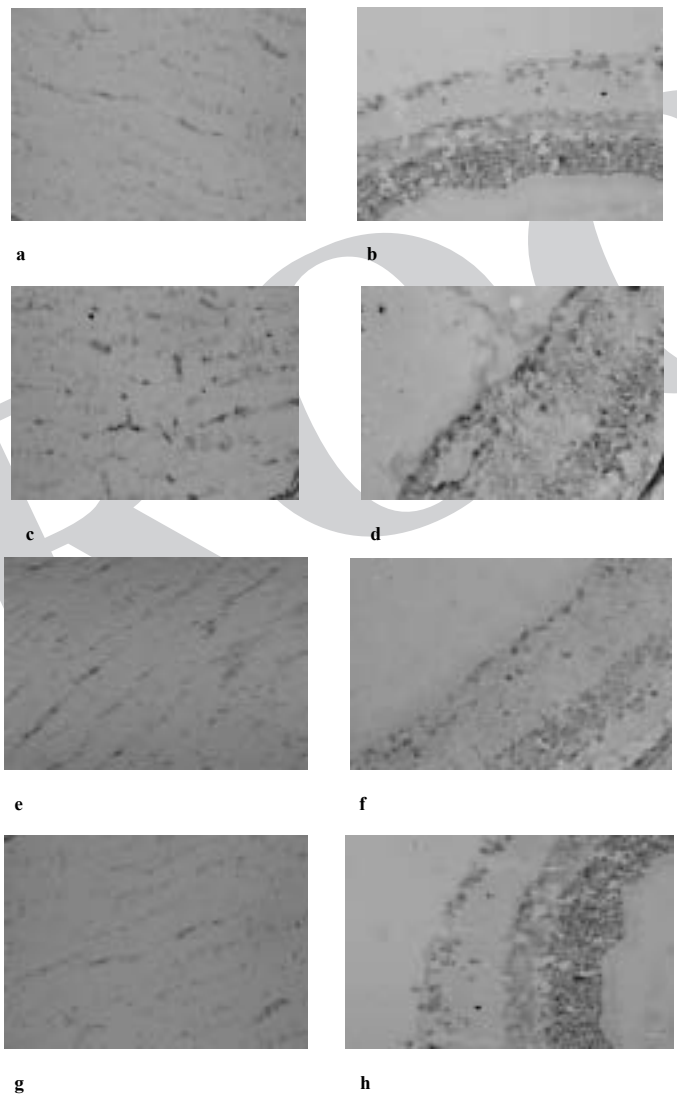

Fig. 4. *Caspase-3 immunoreactivity.* ***a)*** *Section of optic nerve from control rats (500X).* ***b)*** *Section of retina from control rats (500X).* ***c)*** *Section of optic nerve from 5 mM mildronate-treated rats (500X).* ***d)*** *Section of retina from 5 mM mildronate-treated rats (500X).* ***e)*** *Section of optic nerve from 2% MTC-treated rats (500X).* ***f)*** *Section of retina from 2% MTC-treated rats (500X).* ***g)*** *Section of optic nerve from 2 mM mildronate + 0.6 mM L-carnitine-treated rats (500X).* ***h)*** *Section of retina from 2 mM mildronate + 0.6 mM L-carnitine-treated rats (500X).*

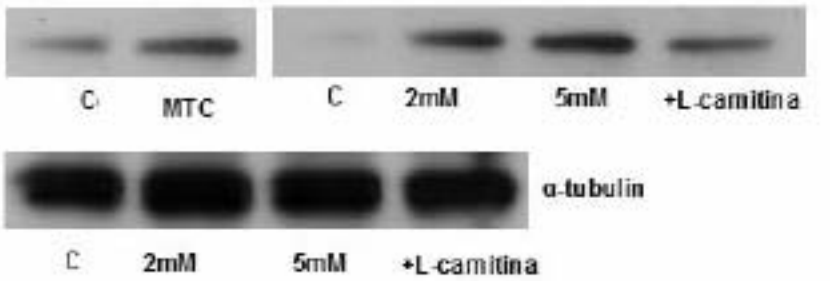

Fig. 5. *Caspase-3 of retina Western blot analysis. C control; MTC: treated with meticellulosa; 2Mm: treated with 2 mM mildronate; 5mM: treated with 5 mM mildronate; +L-carnitine: treated with 2 mM mildronate + 0.6 mM carnitine; α tubulin: standardization of Western blot with tubulin.*

mediated by high induction of iNOS.

In specimens from MTC-treated rats, there were high levels of iNOS both in glial retinal cells (Fig. 2e) and astrocytes of optic nerve (Fig. 2f), similarly to 5 mM mildronate-treated specimens but in this case the oxidative stress was induced by hypoxia (11-13). Mildronate+L-carnitine treatment decreases iNOS expression (Fig. 2g/h), possibly because of the well-known cytoprotective properties of carnitine (11-13, 17-19). Data were confirmed by Western blot analysis of total protein extracts of retina (Fig. 3).

Caspase-3 expression

Caspase 3 immunodetection was performed to verify whether apoptosis had played a role in the cell death observed by TUNEL assay.

We tested specimens from both 5 mM and 2 mM mildronate, MTC-treated, and 5 mM mildronate + L-carnitine- treated animals. In fact, we wanted to investigate whether co-administration of L-carnitine and mildronate can enhance retinal ganglionic cells and astrocyte survival by modulating caspase-3 activity (18-20).

Both in astrocytes and neuronal retinal cells from 5 mM mildronate-treated eyes as well as MTC-treated eyes, the high caspase-3 levels suggest an apoptotic program activation via mitochondrial pathway. Two mM mildronate-treated eyes showed a mild decrease of positivity both in optic nerve and retina (Fig. 4). In specimens treated with mildronate + L-carnitine the staining pattern was quite similar to that found in controls (Fig. 4a and b). Data were confirmed by Western blot analysis of total protein extracts of retina (Fig. 5). The results were homogenous for each group and all rats showed the same aspects.

DISCUSSION

In this study, we firstly analyzed the effects of mildronate both in retina and optic nerve, and we focused on its possible involvement in cell death.

Both retinal cells and optic nerve cells (mainly astrocytes) appeared to be very sensitive to mildronate and showed apoptosis marchers 24 h after treatment.

Optic nerve head astrocytes probably release cytokines that induce apoptosis in retinal ganglion cells and activate microglia that, in turn, leads to increased levels of nitric oxide (NO) (21-24). Treatment with mildronate increases NO levels, and our iNOS immunolocalization in glial retinal cells and astrocytes of optic nerve and Western blot data are in agreement with the pertinent literature (8, 18). Conversely, we have no data to suggest that mildronate can induce ischemia. Experimental data suggest that NO is able to lower IOP, as NO donor drugs are an emerging class of compounds in glaucoma treatment. L-carnitine is a natural substance known for its metabotropic role at cellular level (25) that has a protective capability against the mitochondrial membrane, probably due to its role in the fatty acid transport (26). The simultaneous administration of both carnitine and mildronate was able to reduce the cytotoxic effects that were apparent with the single intraocular administration of mildronate. Differently, high levels of iNOS in MTC-treated rats are explained by mechanical compression on the retinal blood vessels secondary

to IOP increase or cytotoxic compound released by optic nerve astrocytes or by crushed nerve fibers at level of cribriform plate.

This study shows that depletion of carnitine is able to trigger apoptosis and the neuroprotective effects of carnitine result, at least partially, from anti-neurodegenerative (anti-apoptotic) and anti-inflammatory mechanisms. It is suggested that the molecular conformation of carnitine can facilitate its easy binding to mitochondria, and regulate the expression of different signal molecules, hence maintaining normal cellular signaling and survival by modulating caspase-3 activity. Conversely, mildronate could be adopted as an anti-proliferative drug in advanced stages of proliferative ocular diseases.

ACKNOWLEDGEMENTS

This research was supported by grants from Sigma-Tau, Italy.

REFERENCES

1. Rebouche CJ. Kinetics, pharmacokinetics, and regulation of L-carnitine and acetyl-L-carnitine metabolism. Ann N Y Acad Sci 2004; 1033:30-41.
2. Gülçin I. Antioxidant and antiradical activities of L-carnitine. Life Sci 2006; 78:803-11.
3. Chen HH, Sue YM, Chen CH, et al. Peroxisome proliferator-activated receptor alpha plays a crucial role in L-carnitine anti-apoptosis effect in renal tubular cells. Nephrol Dial Transplant 2009; 24:3042-49.
4. Hu ML, Chen YK, Lin YF. The antioxidant and pro-oxidant activity of some B vitamins and vitamin-like compounds. Chem Biol Interact 1995; 97:63-73.
5. Georges B, Le Borgne F, Galland S, et al. Carnitine transport into muscular cells. Inhibition of transport and cell growth by mildronate. Biochem Pharmacol 2000; 59:1357-63.
6. Bremer J. Carnitine-metabolism and functions. Physiol Rev 1983; 63:1420-80.
7. Dambrova M, Liepinsh E, Kalvinsh I. Mildronate: cardioprotective action through carnitine-lowering effect. Trends Cardiovasc Med 2002; 12:275-79.
8. Wang JY, Wen LL, Huang YN, Chen YT, Ku MC. Dual effects of antioxidants in neurodegeneration: direct neuroprotection against oxidative stress and direct protection via suppression of glia-mediated inflammation. Curr Pharm Des 2006; 12:3521-33.
9. Leoni S, Brambilla D, Risuleo G, De Feo G, Scarsella G. Effect of different whole body hyperthermic sessions on the heat shock response in mice liver and brain. Mol Cell Biochem 2000; 204:41-47.
10. Bresin A, Iacoangeli A, Risuleo G, Scarsella G. Ubiquitin dependent proteolysis is activated in apoptotic fibroblasts in culture. Mol Cell Biochem 2001; 220:57-60.
11. Pillich RT, Scarsella G, Risuleo G. Reduction of apoptosis through the mitochondrial pathway by the administration of acetyl-L-carnitine to mouse fibroblast in culture. Exp Cell Res 2005; 306:1-8.
12. Pescosolido N, Del Bianco G, De Feo G, Madia F, Risuleo G, Scarsella G. Induced acute ocular hypertension: mode of retinal cell degeneration. Acta Ophthalmol Scand 1998; 76(S):227:20-21.
13. Scarsella G, Nebbioso M, Stefanini S, Librando A, Pescosolido N. Degenerative effects in rat eyes after experimental ocular hypertension. Eur J Histochem 2012; 56:e42:265-71.
14. Pescosolido N, Cavallotti C, Rusciano D, Nebbioso M. Trabecular meshwork in normal and pathological eyes. Ultrastruct Pathol 2012; 36(2):102-7.
15. Drize JH, Woodard G, Calvery HO. Methods for the study of irritation and toxicity of substances applied topically to the skin and mucous membranes. J Pharm Exp Ther 1944; 82:377-90.
16. Zhu MD, Cai FY. Development of experimental chronic intraocular hypertension in the rabbit. Austl Nw Z J Ophthalmol 1992; 20:225-34.
17. Wenzel U, Nickel A, Daniel H. Increased carnitine-dependent fatty acid uptake into mitochondria of human colon cancer cells induces apoptosis. J Nutr 2005; 135:1510-14.
18. Mutomba MC, Yuan M, Adachi S, Yokoyama CB, Esser V, McGrarry JD, Babior BM, Gottileb RA. Regulation of the activity of caspase by L-carnitine and palmitoylcarnitine. FEBS Lett 2000; 478:19-25.
19. Di Marzio L, Alesse E, Roncatoli P, et al. Influence of L-carnitine on CD95 cross-linking-induced apoptosis and ceramide generation in human cell lines: correlation with its effects on purified acidic and neutral sphingomyelinase *in vitro*. Proc Assoc Am

Physicians 1997; 109:154-63.
20. Cifone MG, Alesse E, Di Marzio L, et al. Effect of L-carnitine treatment *in vivo* on apoptosis and ceramide generation in peripheral blood lymphocytes from AIDS patients. Proc Assoc Physicians 1997; 109:146-53.
21. Ridet JL, Malhotra SK, Privat A. Reactive astrocytes: cellular and molecular cues to biologic function. Trends Neurosci 1997; 12:570-77.
22. Hernandez MR, Pena JD. The optic nerve head in glaucomatous optic neuropathy. Arch Ophthalmol 1997; 115:389-95.
23. Neufeld AH. Nitric oxide: a potential mediator of retinal ganglion cell damage in glaucoma. Surv Ophthalmol 1999; 43(S):129-35.
24. Nebbioso M, Scarsella G, Tafani M, Pescosolido N. Mechanisms of ocular neuroprotection by antioxidant molecole in animal models. J Biol Regul Homeost Agents 2013; 27(1):197-209.
25. Borum PR. Carnitine. Annu Rev Nutr 1983; 3 233-59.
26. Liedtke AJ, Nellis SH. Effects of carnitine in ischemic and fatty acid supplemented swine heart. J Clin Invest 1979; 64:440-44.

MELANOMA AND IFN GAMMA: POTENTIAL ADJUVANT THERAPY

U. BOTTONI[1], R. CLERICO[2], G. PAOLINO[2], P. CORSETTI[2], M. AMBRIFI[2], A. BRACHINI[2], A. RICHETTA[2], S. NISTICÒ[1], G. PRANTEDA[3] and S. CALVIERI[2]

[1]*Department of Health Sciences, University Magna Graecia, Viale Europa, Germaneto, Catanzaro, Italy;* [2]*Unit of Dermatology, Umberto I Polyclinic, La Sapienza University, Via del Policlinico, Rome, Italy;* [3]*Dermatology Unit, NESMOS Department, II School of Medicine, Sapienza University Rome, S. Andrea Hospital, Via Grottarossa, Rome, Italy*

Received March 9, 2014 – Accepted March 24, 2014

Interferon α (IFNα) is the most used adjuvant treatment in clinical practice for melanoma (MEL) high-medium risk patients; however, the use of IFNα has yielded conflicting data on Overall Survival (OS) and disease free survival (DFS) rates. Starting from these considerations, we carried out an analysis on our MEL patients who received adjuvant IFNα therapy, in order to identify possible predictors for their outcome. A total of 140 patients were included in our analysis. Patients with Breslow thickness ≤ 2.00 mm presented a significantly longer mean DFS than patients with Breslow ≥2.01 mm (p = 0.01). Using non- parametric Spearman's Coefficient test we found association between DFS and Breslow thickness (p < 0.001) and between DFS and ulceration (p = 0.03). Performing Multiple Regression test, Breslow thickness (p < 0.001) remained the only statistically significant predictor. From the OS analysis we found that patients with lower Breslow values ≤ 2.00 mm (p < 0.0001), and absence of ulceration (p < 0.004) showed a significantly better long-term survival. From the current analysis we found that the use of low dose IFNα is justified only for cutaneous melanoma ≤ 4.01 mm that was not ulcerated; patients with Breslow ≥ 4.01 mm, in our opinion, should not carry out adjuvant treatment with low dose IFNα, because its side effects could be higher than the its benefits.

The therapeutic management of malignant melanoma (MEL) is one of the most problematic issues for oncologists (1). Among solid tumors, it is one of the most refractory to medical therapy as well as radiotherapy, therefore surgical intervention still remains the most effective treatment for MEL, but only if performed at a very early stage. In fact, the 10-year overall survival (OS) is 93% for stage IA, while for stage IIC it is only 39% (2).

The agent currently most used as adjuvant therapy after radical surgery for such patients at risk of progressing to stage IV is interferon alpha (IFNα), which is a type of IFN mainly produced endogenously by macrophages.

First schedules of adjuvant treatment for MEL patients were based on administration of IFNα at dosage of 3 million international units (MIU) for periods ranging from one to three years (3, 4). However, to date, the most considered schedule of adjuvant treatment for MEL patients is that proposed by Kirkwood et al, that considers high dosages of IFN (0-10 M IU/m2 i.v and s.c) given for one

Key words: low dose interferon alpha, adjuvant therapy, malignant melanoma, thyroidal dysfunction, predictors, metastases

Mailing address:
Prof. Steven Paul Nisticò,
Dept of Health Sciences,
University Magna Graecia,
V.le Europa,
88100 Catanzaro, Italy
e-mail: steven.nistico@gmail.com

0393-974X (2014)

DISCLOSURE: ALL AUTHORS REPORT NO CONFLICTS OF INTEREST RELEVANT TO THIS ARTICLE.

year to MEL patients at stage II (3-5). However, more recently some authors have revalued the administration of adjuvant IFNα at low dosages (6).

Although different authors have previously performed randomized controlled trials and meta-analyses on the use of IFNα as adjuvant treatment in MEL patients, their studies have yielded conflicting data on the effect on overall survival rate (OS) and disease free survival rate (DFS) (7-10). At the same time, some papers tried to characterize possible predictors, that may identify patients who would or would not benefit from this treatment (11-13). In those studies, the main purpose was to restrict the adjuvant treatment with IFNα to only the patients with high susceptibility to respond to the therapy.

Taking these facts into consideration, we carried out an analysis on our MEL patients who had received adjuvant IFNα therapy, to identify possible predictors for their outcome.

MATERIALS AND METHODS

Patients and interferon therapy

We computer-searched the clinical records of all our patients registered in our twenty-year malignant melanoma (MEL) database, from January 1st 1993 to December 31st 2012, to identify patients who had received low-dose Interferon-alpha-2b (IFNα) therapy, as adjuvant treatment. All patients had localized cutaneous MEL with a Breslow thickness ≥ 1.01 mm and had previously undergone surgical removal of the primary cutaneous lesion according to standard surgical criteria (14) and sentinel lymph node procedure.

At the first visit to our Department, all the patients had a WHO performance status of 0 and underwent a general visit to exclude the possible presence of an autoimmune disease (such as lupus).

The following parameters were registered: demographics, anatomical localization and histological characteristics of the primary melanoma. After starting therapy the following parameters were registered: adverse events including thyroidal dysfunction, time interval between diagnosis of primary melanoma and the first metastatic event (DFS), date of death and/or last follow-up (OS).

The clinical controls and the instrumental analyses, were carried out every 4-12 months according to our scheduled follow-up (15). During clinical controls, the following laboratory parameters were registered: complete blood count, glycaemia, creatinine, urea, cholesterol, albumin, bilirubin, lactic dehydrogenase, liver function tests, thyroid function tests and S-100.

IFNα was administered at the dose of 3 million IU (MIU) with sub cutis (s.c.) route 3 times weekly for 6 cycles of 6 months with 1-month intervals between cycles (36-41 months).

In case of adverse events, the dose could be reduced or suspended. If necessary, antipyretics were employed to control fever and/or malaise subsequent to the administration of IFNα.

Thyroidal evaluation

For all patients exclusion criteria for starting IFN therapy was the presence of a thyroidal dysfunction. However, in all patients after starting therapy free three-iodo-thyronine (fT3), free tetra-iodo-thyronine (fT4), TSH, anti-thyreoperoxidase antibodies (anti-TPO) and anti-thyroglobulin (anti-TG) serum levels were evaluated every 3 months during follow-up.

Hyperthyroidism was defined as having TSH < 0.1mU/l, either fT4 level > 26.0 and/or fT3 > 5.5 pmol/l. Hypothyroidism was defined as having TSH level > 4 mlU/l with normal or low fT4 levels.

After the occurrence of a thyroidal dysfunction during the IFN treatment, the therapy was always discontinued and the patient was referred to the endocrinal specialist, to evaluate possible continuation of the therapy.

Statistical analysis

We calculated the incidence rate (IR), free survival (DFS) and overall survival (OS) in the whole group of patients and separated them into subgroups according to the parameters most studied in the literature.

The incidence rate (IR) was considered as the ratio between the observed MM patients with progression and the ones without metastatic progression.

DFS was calculated from diagnosis of primary tumor to the first metastatic progression. Assuming that the effects of the predictor variables are constant over time, we used the Spearmen's coefficient between DFS and the predictive factors analyzed including thyroidal function. The following predictors were evaluated: gender, age (≤60 or ≥61 years), anatomical location of the primary tumor (axial or peripheral), Breslow thickness (1.01-2 mm or > 2 mm), ulceration (presence or absence) and thyroidal dysfunction (presence or absence). The first four parameters are those used by Balch (2). Subsequently, the independent predictors were assessed by Multiple Regression.

To estimate OS, the Kaplan-Meier product was used, and the log-rank test was used to evaluate differences between the survival curves. Patients who were still alive at the time of last follow-up were dismissed at the date of their last follow-up.

A p value < 0.05 was considered statistically significant.

RESULTS

A total of 140 patients [76 male (54.28%) and 64 (45.72 %) female; 87 aged ≤60 years, and 53 aged ≥61 years] were included in our study (Table I). Seventy patients had melanoma (MEL) on the trunk, 3 patients on head and neck, 27 patients on superior limbs and 40 on inferior limbs. We divided the anatomical sites in axial (trunk + head/neck = 73 patients) and peripheral (upper and lower limbs = 67 patients).

Regarding Breslow thickness, 83 patients showed a Breslow thickness between 1.01-2.00 mm, 48 between 2.01-4.00 mm and 9 a ≥ 4.01mm thickness. The ulceration of the primary tumor was found in 23 patients (16.42%), while it was absent in 117 patients (83.58 %) (Fig. 1 A and B).

Analyzing AJCC stage at diagnosis, 60 patients were in stage IB, while 44 patients were in stage IIA, 21 patients in stages IIB and 15 patients in stage IIC. Among treated patients, 48 (34.28%) developed a metastatic progression (Table I). The first event of progression had appeared during the follow-up, the most frequent types of metastases being lymph-nodal or in transit (n= 32) followed by (distant) dermal ones (n = 2), lung (n= 8) and brain metastases (n= 6).

Table I. *Characteristics of melanoma patients who underwent IFNα therapy.*

Gender	Male	76
	Female	64
Age (yrs)	≥ 61	53
	≤ 60	87
Anatomical Sites	Central	73
	(Trunk – Head/neck)	(70 – 3)
	Periferal	67
	(Superior Limbs - Inferior Limbs)	(27-40)
Breslow thickness	T2 (1.01-2.00 mm)	83
	T3 (2.01- 4.00mm)	48
	T4 (> 4.01mm)	9
Clark level	II	2
	III	55
	IV	75
	V	8
Ulceration	Presence	23
	Absence	117
AJCC classification	IB	60
	IIA	44
	IIB	21
	IIC	15
Disease Progression	Presence	48
	Absence	92
First metastatic site	Lymph nodal and in transit	32
	Dermal (distant)	2
	Lung	8
	Brain	6
Thyroidal dysfunction	Presence	10
	Absence	130

yrs: years.

Table II. *Types of metastases and 5-year and 10-year OS of patients under treatment with IFNα according to initial melanoma stage.*

STAGE	#pts	#pts met	regional lymph node and in transit met	distal skin	lung	brain	5-year-OS (our casisitics)	10-year-OS (our casistics)	5-year-OS (AJCC casisitics)	10-year-OS (AJCC casistics)
IB	60	8	5	1	2	-	98	95	89.8	81.1
IIA	44	13	6	1	3	3	85	78	78.2	64.1
IIB	21	16	12	-	2	2	80	65	65.2	52.4
IIC	15	11	9	-	1	1	50	25	45.1	32.3

#pts: number of patients; met: metastases. Comparison of our casistics with those of Balch et al. (16).

Table III. *DFS and OS in patients under treatment with IFNα according to the first event of progression (metastasis).*

Metastases	n	DFS (median months)	OS (median months)
Lymph Node and in transit	32	30	117
Dermal (distant)	2	20	72
Lung	8	27	48
Brain	6	40	44

N: number of patients; DFS: disease free survival; OS: overall survival

After starting IFNα adjuvant therapy, 10 (7.14%) patients (9 female and 1 male) showed thyroid dysfunction. Thyroid abnormality had occurred within a median time of 4.2 months after the first IFNα administration. Eight patients developed hypo-thyroidism, while two patients developed hyperthyroidism. Generally, elevation or suppression of TSH level was the main sign of thyroid dysfunction. In 8 patients specific antibodies anti-thyroperoxidase and/or anti-thyroglobulin were found. Anti-microsomial DNA antibodies in one patient and ANA in two patients were also detected. Autoimmune diseases other than autoimmune thyroiditis, such as lupus erythematosus, were not observed. In all the patients who developed thyroidal dysfunction, these alterations were not present prior to starting IFNα therapy. After registering thyroidal dysfunction, IFNα-therapy was temporarily suspended in 1 patient while in 2 patients IFN was reduced from 3 to 2 or 1 administration per week.

Dividing the patients according to clinical stage, the incidence rate (IR) of recurrences was 1:7 in stage IB patients, 1:2.5 for stage IIA patients, 1:1 for stage IIB patients and 2:1 for IIC stage patients.

To identify possible predictor factors for MEL progression after adjuvant treatment with IFNα, we statistically analyzed the correlation between DFS and some characteristics of melanoma tumors and patients. Female patients showed a better DFS than male (46 years *vs* 27 years), although not reaching the statistical significance ($p = 0.3$). Patients aged $\geq$ 61 years had median DFS of 23 months while younger patients had median DFS of 32 months ($p = 0.7$); while for patients with an axial primary localization the median DFS was 27 months, while it was 31 months for peripheral localization ($p = 0.3$). Patients with Breslow thickness ≤ 2.00 mm presented a significant longer median DFS than patients

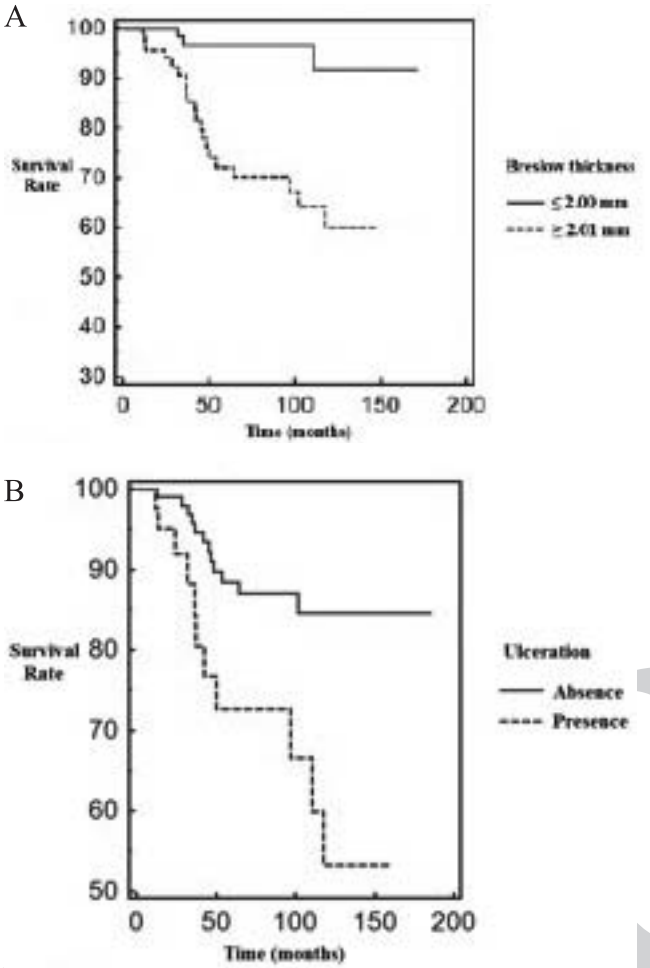

Fig. 1. ***A****) Overall survival of melanoma patients treated with IFNα adjuvant therapy according to Breslow thickness (≤ 2.00 mm or ≥ 2.01mm).* ***B****) Overall survival of melanoma patients treated with IFNα adjuvant therapy (presence or absence of ulceration in primary cutaneous melanoma)*

with Breslow ≥2.01 mm (p = 0.01); Patients with ulcerations showed median DFS of 21 months while it was 44 months for patients without ulceration (p = 0.2). In patients with thyroidal dysfunction median DFS was 44.5 months while for patients without a thyroidal dysfunction it was 24 months (p = 0.3).

Using non-parametric Spearman's Coefficient test between DFS and the single variables, we found association only between DFS and Breslow thickness (p < 0.001; Spearman's coefficient = 0.409) and between DFS and ulceration (p = 0.03; Spearman's coefficient = 0.284). Performing Multiple Regression

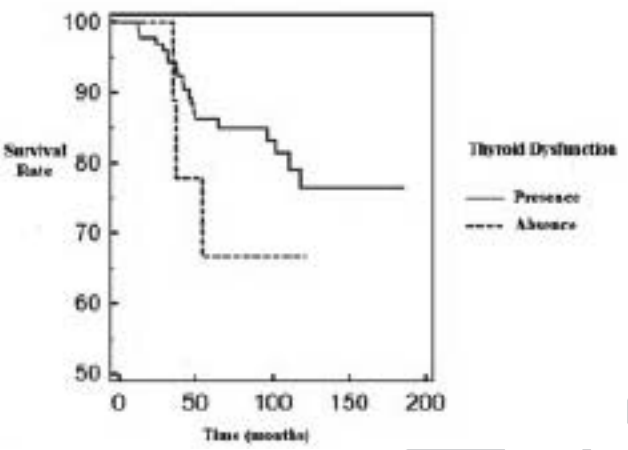

Fig. 2. *Overall survival of melanoma patients treated with IFNα adjuvant therapy (presence or absence of a thyroidal dysfunction that arose during the therapeutic treatment).*

test, Breslow thickness (p < 0.001) remained the only statistically significant predictor.

Subsequently, we analyzed OS of the patients using Kaplan-Meier product and log-rank test according to variables previously described: gender, age, sites of primary tumor, Breslow thickness, ulceration, thyroid dysfunction. From the OS analysis we found that patients with lower Breslow values ≤ 2.00 mm (p < 0.0001), and absence of ulceration (p < 0.004) showed a significantly better long-term survival. Regarding OS in patients with and without thyroid dysfunction, during the first 2 years of follow-up Kaplan-Meier curves showed the same behavior, while the longer follow-up patients with thyroidal dysfunction showed better OS, however without reaching statistical significance: 71 months *vs* 64.4 months with p = 0.2 (Fig. 2).

Subsequently, we analyzed the number and type of melanoma metastases according to the initial AJCC stages (IB; IIA; IIB and IIC) to better evaluate the predictive activity of disease staging. We found a higher incidence of metastases in 38 stage II patients, divided as follow: 12 patients in stage IIA, 14 in stage IIB and 12 in stage IIC. More precisely, patients in stage IIC developed lymph node or in-transit metastases in 9/15 cases, lung metastases in 1/15 case, and brain metastases in 1/15 cases, while only in 4 patients the melanoma did not progress (Table II). Another important finding was the presence of lung metastases also in patients with

low-intermediate stages (IB and IIA) (Table II).

Regarding 5-year-OS and 10-year-OS (Table II), dividing the patients according to stage, we found 98% for stage IB 5-year-OS, and 95% 10-year-OS. With regard to stage IIA, 85% was 5-year-OS and 78% was 10-year-OS. For stage IIB, 80% was 5-year-OS and 65% was 10-year-OS, while for stage IIC 50% was 5-year-OS and 25% was 10-year-OS. Confronting these data with the data from Balch et al. (16) regarding patients at the same stages of disease, we found that for our patients in stage IB IIA and IIB the 5-year-OS and 10-year-OS were better than those reported by Balch et al. (16) while for stage IIC the data were similar or worse (Table II).

Finally, we analyzed DFS and OS of our patients regarding the first type of melanoma metastasis. We found that patients with lymph nodal and in transit metastases had a median DFS of 30 months and a median OS of 117 months while patients with distant dermal metastases had a median DFS of 20 months and a median OS of 72 months, lung metastases showed a median DFS of 27 months and a median OS of 48 months and brain metastases a median DFS of 40 months and a median OS of 44 months (Table III).

DISCUSSION

Among the available treatment options for malignant melanoma (MEL), surgical resection, with or without regional lymph node excision, represents the standard care and allows regional control of the disease and improves survival (8).

However, for patients with high risk (stage IIIB and resectable stage IV M1a and M1b) and also with intermediate risk (stage IB- II and IIIA), adjuvant treatment seems advisable. For this purpose most international trials have used Interferon–alpha 2b (IFNα) as adjuvant treatment.

However, the use of IFNα has yielded conflicting data on the effect on Overall Survival (OS) and disease-free survival (DFS). In fact, in a recent meta-analysis, Mocellin et al. registering inappropriate statistical models and contrasting results among different studies with IFNα as adjuvant treatment, concluded that more efforts are necessary to identify patients who could have benefit from IFNα adjuvant therapy (6, 17).

With this in mind, (6) we carried out this retrospective study. Participating in a spontaneous Italian multicenter protocol, IFNα at 3 million international units (MIU) 3 times per week for 6 cycles of 6 months each was administered as adjuvant treatment to our melanoma patients with Breslow's depth > 1 mm. MEL at stage III received other adjuvant treatment with dacarbazine with or without IL-2, and in some cases IFNα at higher doses as suggested by Kirkwood et al. (3-5).

To highlight any characteristics of patients or MEL useful to identify people more susceptible to adjuvant treatment with IFN, first we analyzed DFS and OS of our patients according to the same prognostic factors as the ones studied by Balch et al. to establish melanoma staging (2). These parameters were: gender, age, anatomical site of first melanoma lesion, Breslow thickness, ulceration. Using the readapted log-rank test for DFS (Table I), the only significant predictors were Breslow thickness ($p = 0.01$) and ulceration ($p < 0.03$). Performing Spearman's test, again low Breslow thickness ($p < 0.001$) and absence of tumor ulceration ($p = 0.03$) resulted the principal and significant values, while in the multiple logistic regression, Breslow thickness ($p < 0.0001$) remained the main predictor. Our results were similar to those reported in other studies (18-20).

Regarding OS analysis compared to the same prognostic factors, we observed that low Breslow ($p <0.0001$) and absence of ulceration ($p < 0.004$), were the principal statistical values to determine a better long-term OS. Ulceration is indeed a marker of an increased propensity for hematogenous dissemination and extracellular matrix invasion independently of tumor thickness (21-22).

However, if these data confirm that our groups of patients are similar to other groups reported in the literature, namely the ones used by Balch et al. (2) to establish AJCC classification for MEL, they do not help us to identify patients more susceptible to receiving adjuvant treatment with IFNα. Therefore, according to some literature data, we analyzed the outcome of MEL patients with thyroid dysfunction induced by IFNα. This event is regarded as a direct immune modulatory action of the drug on the patient immune system. We must highlight that according to our protocol all the patients were analyzed before

starting adjuvant treatment with IFNα to exclude a pre-existing thyroid dysfunction. Thus, our patients who developed thyroid dysfunction after starting IFNα therapy must be regarded as the ones with an immuno-responsivity to IFNα administration. Interestingly patients who developed a thyroidal dysfunction showed DFS values better than the ones without thyroid dysfunction but the statistical significance was not reached (p= 0.3). In fact, in patients with thyroidal dysfunction, median DFS was 44.5 months - about twice the median DFS (24 months) observed in patients without thyroidal dysfunction. Regarding OS and thyroid dysfunction, we observed that during the first 2-3 years it was not important while in the following years subjects with thyroid dysfunction presented better results than the those without. On considering that most patients with thyroid dysfunction were affected by autoimmune thyroiditis, we highlight that, in literature, autoimmune disorders, spontaneous or induced by IFNα, have been associated with improved prognosis in MEL and no-MEL patients (such as patients with hepatitis C)(23). However, conflicting data are still reported and the predictive value of autoimmunity still needs to be elucidated; in fact, while autoimmunity remains a strong independent prognostic marker it is not considered in the EORTC panel.

Again these results do not help to identify patients who could achieve more benefit from IFN therapy. We therefore critically revised the number and type of metastases for each MEL stage and for each one we verified 5-year-OS and 10-year-OS, similarly to what had been reported by Balch et al. establishing AJCC staging for MEL (16). Stressing on 5- and 10-year OS, dividing patients according to the relative AJCC stages, we found better OS in IB patients compared with larger but similar data reported by Balch et al. (16). This increased OS was maintained also for IIA stage, but was stable or decreased for stages IIB-IIC. At the same time, we registered a high percentage of lymph node metastases in stage IIB-IIC. This fact confirms the hypothesis, forwarded by some authors, that in this class of patients (pT3a-pT4b) a lymphadenectomy, regardless of the sentinel lymph node status, should be taken into account. In this way, an elective lymphadenectomy could replace IFNα treatment, which in the current study, as in other studies, did not find significant improvements (24-30).

Finally, we analyzed DFS and OS according to the type of first metastasis. The numberd for each group are not large but they suggest that in these patients loco-regional metastases are not rare, are more early than brain metastases but they often permit a better prognosis for OS, while brain metastases, as we reported in another study, are more late but they do not permit a long OS.

Summarizing, from the current analysis four principal points arise: i) the use of low dose IFN is justified only for non-ulcerated cutaneous melanoma $\leq$ 4.01mm; ii) although there is a better DFS and OS in patients with thyroidal dysfunction, a statistical significance is not reached; iii) patients with Breslow $\geq$ 4.01 mm should not carry out adjuvant treatment with low dose IFNα, because side effects could be higher than the benefits; iv) a radical lymphadenectomy can be considered standard procedure for melanoma patients at stage $\geq$ pT3a.

REFERENCES

1. Tsao H, Kiirkwood JM. Management of metastatic melanoma. Semin Oncol 2007; 34:532-45.
2. Balch CM, Gershenwald JE, Soong SJ, et al. Final version of 2009 AJCC melanoma staging and classification. J Clin Oncol 2009; 27:6199-206.
3. Kirkwood JM, Strawderman MH, Emstoff MS, Smith TJ, Borden EC, Blum RH. Interferon alfa-2b adjuvant therapy of high risk resected cutaneous melanoma: ECOG trial EST 1684. J Clin Oncol 2006; 14:7-17.
4. Kirkwood JM, Ibrahim JG, Sondak VK, et al. High and low dose interferon alpha-2b in high risk melanoma: First analysis of Intergroup trial E1690/S911C9190. J Clin Oncol 2000; 18:2444-58.
5. Kirkwood JM, Ibrahim JG, Sosman JA, et al. High-doses interferon alfa-2b significantly prolongs relapse-free and overall survival compared with the GM2-KLH/QS-21 vaccine in patients with resected stage IIB-III melanoma: results of the intergroup trial E1694/S9512/C509801. J Clin Oncol 2001; 19:2370-80.
6. Haushild A, Weichenthal M, Rass K, et al. Efficacy of low-dose interferon alpha 2a versus 60 months of treatment in patients with primary melanoma of

> 1.5mm tumor thickness: results of a randomized phase III DeCOG trial. J Clin Oncol 2010; 28:841-46.
7. Pietra G, Manzini C, Rivara S, et al. Melanoma cells inhibit natural killer cell function by modulating the expression of activating receptors and cytolytic activity. Cancer Res 2012; 72:1407-15.
8. Hackshaw MD, Krishna A, Mauro DJ. Retrospective US database analysis of drug utilization patterns, health care resource use, and costs associated with adjuvant interferon alfa-2b therapy for treatment of malignant melanoma following surgery. Clinicoecon Outcomes 2012; 4:169-76.
9. Garbe C, Eigentler TK, Keilholz U, Hauschild A, Kirkwood JM. Systematic review of medical treatment in melanoma: current status and future prospects. Oncologist 2011; 16:5-24.
10. Shah GD, Chapman PB. Adjuvant therapy of melanoma. Cancer J 2007; 13:217-22.
11. Bouwhuis MG, Den Hagen TL, Eggermontm AM. Immunologic functions as prognostic indicators in melanoma. Molecula Oncology 2011; 5:183-89.
12. Satzger I, Meier A, Schenck F, Kapp A, Hauschild A, Gutzmer R. Autoimmunity as a prognostic factor in melanoma patients treated with adjuvant low-dose interferon alpha. Int J Cancer 2007; 121:25626-6.
13. Gogas H, Ioannovich J, Dafni U, et al. Prognostic significance of autoimmunity during treatment of melanoma with interferon. N Engl J Med 2006; 354:709-18.
14. Greenstein DS, Rogers GS. Management of stage I malignant melanoma. Dermatol Surg 1995; 21:927-37.
15. Quaglino P, Borgognini L, Bottoni U. Linee guida e follow-up del melanoma cutaneo stadio I-II. G Ital Dermatol Venereol 2007; 142:41-7.
16. Balch C, Buzaid AC, Soong SJ, et al. Final version of the American joint committee staging system for cutaneous melanoma. J Clin Oncol 2001; 19:3635-48.
17. Cascinelli N, Belli F, MacKie RM, Santinami M, Bufalino R, Morabito A. Effect of long-term adjuvant therapy with interferon alpha-2a in patients with regional node metastases from cutaneous melanoma: A randomised trial. Lancet 2001; 358:866-69.
18. Mocellin S, Pasquali S, Rossi CR, Nitti D. Interferon Alpha adjuvant therapy in patients with high risk melanoma: a systemic review and meta-analysis. J Natl Cancer Inst 2010; 102:493-501.
19. Ascierto PA, Kirkwood JM. Adjuvant therapy of melanoma with interferon: lessons of the past decade. J Transl Med 2008; 6:62.
20. Mohr P, Hauschild A, Enk A. Intermittent high-dose intravenous interferon alpha 2b (IFNa2b) for adjuvant treatment of stage III malignant melanoma: an interim analysis of a randomized phase III study (NCT00226408). J Clin Oncol (ASCO Meeting Abstracts) 2008; 26:9040.
21. Zakrzewski J, Geraghty LN, Rose AE, et al. Clinical variables and primary tumor characteristics predictive of the development of melanoma brain metastases and post-brain metastases survival. Cancer 2011; 117:1711-20.
22. Bottoni U, Clerico R, Paolino G, et al. Predictors and survival in patients with melanoma brain metastases. Med Oncol 2013; 30:466.
23. Tran HA, Reeves G, Jones TL. The natural history of interferon-a2b-induced thyroiditisand its exclusivity in a cohort of patients with chronic hepatitis C infection. Q J Med 2009; 102:117-22.
24. Specchio F, Saraceno R, Chimenti S, Nisticò S. Management of non-melanoma skin cancer in solid organ transplant recipients. Int J Immunopath Pharmacol 2014; 27(1):5-9.
25. Muscoli C, Lauro F, Nisticò S, et al. Olea Europea-derived phenolic products attenuate antinociceptive morphine tolerance: an innovative strategic approach to treat cancer pain. J Biol Reg Homeost Ag 2014; 28(1):117-28.
26. Specchio F, Carboni I, Chimenti S, Tamburi F, Nisticò S. Cutaneous manifestations in patients with chronic renal failure on hemodialysis Int J Immunopath Pharmacol 2014; 27(1):1-4.
27. Chiricozzi A, Pitocco R, Saraceno R, Nistico SP, Giunta A, Chimenti S. New topical treatments for psoriasis. Exp Op Pharmacother 2014; 15(4):461-70.
28. Nisticò SP, Saraceno R, Chiricozzi A, Giunta A, Di Stefani A, Zerbinati N. UVA-1 Laser in the treatment of palmoplantar pustular psoriasis. Photomed Laser Surg 2013; 31:434-38.
29. Chiricozzi A, Zhang S, Dattola A, Gabellini M, Chimenti S, Nisticò S. Role of Th17 in the

pathogenesis of cutaneous inflammatory diseases J Biol Regul Homeost Agents 2012; 26(3):313-18.
30. Chiricozzi A, Zhang S, Dattola A, Cannizzaro M.V, Gabellini M, Chimenti S, Nisticò S. New insights in the pathogenesis of cutaneous autoimmune disorders. J Biol Regul Homeost Agents 2012; 26(2):165-70.

FLAKE SIZE-DEPENDENT CYTO AND GENOTOXIC EVALUATION OF GRAPHENE OXIDE ON *IN VITRO* A549, CaCo2 AND VERO CELL LINES

L. DE MARZI[1], L. OTTAVIANO[2], F. PERROZZI[2], M. NARDONE[2], S. SANTUCCI[2], J. DE LAPUENTE[3], M. BORRAS[3], E. TREOSSI[4], V. PALERMO[4] and A. POMA[1]

[1]Department of Life, Health and Environmental Sciences, University of L'Aquila, L'Aquila, Italy; [2]Department of Physical and Chemical Sciences, University of L'Aquila, L'Aquila, Italy; [3]Unit of Experimental Toxicology and Ecotoxicology CERETOX, Barcelona Science Park, Barcelona, Spain; [4]CNR-ISOF, Bologna, Italy

Received January 10, 2014 – Accepted April 14, 2014

This study was carried out by varying both graphene oxide (GO) concentration (10 µg/mL, 50 µg/mL, 100 µg/mL) and flakes sizes of 1320 nm and 130 nm. Characterization by scanning electron microscopy and Raman spectroscopy demonstrate that the area of GO flakes varies of one order of magnitude but their chemical structure remains unmodified. A 24-h cytotoxicity test showed, for A549, a loss in the viability, while the test exhibits overall a positive increase in the viability for CaCo2 and Vero. A 24-h comet assay shows a marked GO genotoxicity: for micrometer-sized GO flakes the genotoxicity is in positive correlation with the concentration, while for nanometer-sized GO flakes there was a high degree of genotoxicity at the lowest concentration tested.

Graphene Oxide (GO), the oxidized form of graphene (a two-dimensional material), has been the subject, in recent years, of an increasing interest in biomedical applications (1). This is due to many specifically appealing features, such as its simple way of production in single layer flakes via chemical routes (2, 3), its hydrosolubility, its availability in flakes with tunable lateral dimensions (from few nm up to hundreds of microns) and, last but not least, its ease to be surface functionalized with different chemical moieties (4, 5). Hence, the use of GO and nano-sized GO has been proposed in various applications including diagnostic tools such as bio-sensors for bacterial diseases (6), disease diagnostic tools (7, 8), in therapy as bactericidal (9, 10), carriers in drug delivery (11, 12), cancer targeting (12) and photo thermal therapy (13) or in tissue engineering (14-16). Such applications raise issues concerning the GO interaction with cells, considering that there are only few and recent *in vitro* and *in vivo* studies focused on GO toxicity issues.

Chang et al. performed both *in vivo* and *in vitro* analyses demonstrating how GO produced a slight loss of cell viability on A549 (human alveolar adenocarcinoma cell line, CCL-185) cells after 72 h of treatment (17). They also highlight a high level of reactive oxygen species (ROS) (well-known toxic oxygen radicals in living system) after the exposure period (17). Another interesting work was published by Wang et al. (18), in which they analyzed the effect of GO both on *in vitro* fibroblast cell line (HDF cell lines) and in mice following an intravenous injection. The results showed the *in vitro* toxic effect of GO at

Key words: Graphene oxide (GO), cytotoxicity, genotoxicity, in vitro assays, A549, CaCo2, Vero, cell lines

Mailing address: Dr Anna Poma,
Department of Life, Health and Environmental Sciences,
University of L'Aquila,
Via Vetoio 1, Coppito I-67100
L'Aquila, Italy
Tel: +39 862 433275 Fax: +39 862 433273
e-mail: annamaria.poma@univaq.it

0393-974X (2014)

concentration values exceeding 50 μg/mL. Further analysis proves GO internalization into the HDF cells by a vesicle-mediated mechanism, which leads to the presence of GO into lysosomes, mitochondria, endoplasm, and the cell nucleus.

GO internalization (19) is very likely related to its chemistry and dimensions and the common results obtained to date show that it can actively interact with living organisms leading to the increase in ROS level (20-22). Another important aspect, especially for a better understanding of the toxic potential of GO, is the strict correlation of GO size and its internalization in cells (23).

The above-mentioned studies on the use of GO as a template material for cell growth have demonstrated its ability to promote the differentiation of stem cells (12). Other studies regard a faster growth of pre-osteoblast on GO rather than on chitosan (13) and the excellent neurite extensions that exist in neurons of the mouse hippocampal cell model on GO rather than on the normal tissue culture polystyrene (14). In this latter work, the authors studied the expression of the GAP-43 protein and demonstrated a great enhancement on its expression compared to the control group, highlighting and suggesting how GO could possibly alter the gene expressions.

To date, very little work has been carried out on the genotoxic potential of GO. Akhavan et al. have pioneered this field by studying the genotoxicity of GO on human mesenchymal stem cells (hMSCs) (24, 25). Considering the high level of ROS found in the hMSCs, they hypothesized and correlated the presence of ROS with the cytotoxic and genotoxic results. Their findings indicate that toxicity is very much dependent on the nanomaterial lateral dimension.

In this study we analyzed for the first time the cyto- and genotoxic effects of chemically pristine GO on different cell lines: A549- human lung carcinoma, CaCo2- human colon carcinoma and Vero-monkey kidney cells. Our study was designed to clearly assess the effect of pristine GO by varying the GO flake sizes without altering its surface chemistry and to evaluate their cyto- and genotoxic effect on cells.

The results obtained via cytotoxicity studies performed with 3-(4,5-Dimethylthiazol-2-yl)-2,5-diphenyltetrazolium bromide test (MTT assay), confirmed the slight cytotoxicity of GO on A549 previously found in a previous study (17), while demonstrating, on the other hand, an overall positive increase of the cell viability for Vero, and in particular CaCo2 upon exposure to GO. The genotoxicity study, carried out with a Comet assay, showed and underscored the size-dependent effect on the three cell lines. Micron-sized flakes of GO induced a genotoxic effect which increased with concentration (10 μg/mL < 50 μg/mL <100 μg/mL) while nano-sized GO flakes at the same concentration values showed a saturated high genotoxic response.

MATERIALS AND METHODS

GO synthesis and characterization

Pristine GO flakes (micro-GO) with a maximum lateral size of 140 μm were prepared in water solution using a modified Hummers method, as described by Treossi et al. (2). Part of the solution was then submitted to 26-h sonication to induce controlled fragmentation of the GO flakes (nano-GO). The sonication was performed with an Elmasonic S10H bath (operating frequency 37 kHz - effective power 30 W). The GO characterization was performed by scanning electron microscopy (SEM) and Raman spectroscopy (RS). The SEM images were obtained using a Zeiss-Gemini LEO 1530 system without sputter coating the samples. RS was performed with a Horiba-JobinYvon LABRAM system (λ=633 nm, 1 μm spatial resolution, and ~2 cm^{-1} spectral resolution). In all cases, samples were prepared by spin coating (at room temperature and in dry air) 10 μL of a 0.5 mg/mL water dispersed GO (either sonicated or not) at 3,000 rpm for 1 min on 100 nm SiO_2/Si(100). The RS data were acquired in air. The statistical analysis of the GO flakes size was carried out on the SEM images with ImageJ software. The size and the area of the GO flakes was determined with a pixel counting procedure. The total number of flakes counted for the analysis ranged between 1000 and 2000. More details on the preparation, characterization and analysis of the same GO solutions are reported by Russier et al. (28).

Cell culture maintenance

A549 (human alveolar adenocarcinoma cell line, CCL-185), CaCo2 (human colorectal adenocarcinoma cell lines, HTB-37) and Vero (kidney epithelial cell line from an African green monkey, CCL-81) were used for the *in vitro* assays. The cells were cultured in a Dulbecco's modified eagle medium (DMEM) completed with 10% of heat-inactivated fetal bovine serum (FBS-HyClone), 2% L-glutamine (Sigma-Aldrich) and 0.5% of

penicillin/streptomycin (Sigma-Aldrich) and maintained in controlled atmosphere (37°C, 5% CO_2). Three *in vitro* culture passages were performed before starting each experiment. Each assay was carried out three times in the same experimental conditions.

MTT assay

The 24-h MTT assay was performed on the three different cell lines: A549, CaCo2 and Vero. A preliminary evaluation to highlight the possible interaction between GO and MTT was carried out, demonstrating no impedance at the wavelength used. The cells were seeded in a 96-well plate (Nunc) with DMEM colture medium ($4x10^3$ cells in 200 µL/each well). After 24 h, pristine GO and sonicated GO solutions (called micro-GO and nano-GO hereafter) were used with the following concentrations: 10 µg/mL, 50 µg/mL, and 100 µg/mL, plus sodium dodecyl sulphate (SDS) as positive control. The cells were exposed to GO for 24 h in order to evaluate the acute toxicity. MTT solution was freshly prepared using MTT powder (5 mg of MTT powder in 1 mL of PBS; Sigma-Aldrich). After an exposition of 24 h, 20 µL of MTT (= 4 µL of 5mg/1mL in PBS + 16 µL of medium) were added to each well and, after 2 h of incubation, the medium containing the MTT was removed, the plate was washed twice with PBS and 130 µL desorb solution was added (96% of 2-propanol and 0.7% of SDS). The signal detection was performed at a wavelength of 540 nm with a spectrophotometer (Bio-TekInstruments, Power Wave X).

Comet assay

The comet assay was performed on A549, CaCo2 and Vero cell lines. The cells were seeded into a 96-well plate with complete medium (10^4 cells in 100 µL/each well). The day after seeding, micro GO and nano GO solutions were added to the culture medium in order to obtain the final GO concentrations of 10 µg/mL, 50 µg/mL and 100 µg/mL, plus negative control. A 24-h exposure treatment was carried out. At the end of the exposure period, the cells were recollected by trypsinization and centrifuged at 1,100 rpm. After centrifugation, the supernatant was eliminated and the pellet was re-suspended in 140 µL of 0.9% agarose in milliQ water, previously prepared (low-melting point agarose – Sigma Aldrich). The suspensions of cells in agarose were then drop-casted onto microscope slides with an agarose layer (agarose electrophoresis grade – Invitrogen prepared with a 1% concentration in milliQ water) put in a freezer for 10 min and then layered in the lysis buffer for 1 h. The lysis buffer was freshly prepared with NaCl 2.5 M, Na_2EDTA 100 mM, Tris 10 mM in milliQ water and the final pH value was then adjusted to 10. The buffer solution was prepared at 4°C and the lysis timing was performed at the same temperature. After the lysis exposure, the samples were left for 30 min in the electrophoretic buffer and then the electrophoresis was performed for 40 min. The electrophoresis buffer was prepared with Na_2EDTA 1 mM and NaOH 300 mM in milliQ water at 4°C. At the end of the electrophoretic run, the samples were put in a neutralizing buffer (Tris 1M with a 7.5 pH in milliQ water) for three times (5 min each). The samples were then stained with 4',6-diamidino-2-phenylindole (DAPI) and analysed with a fluorescence microscope (Nikon Eclipse E600 with super high pressure mercury lamp). Sixty randomly selected cells from each concentration were scored using Comet IV image analysis software. The fluorescence microscope used was a Nikon Eclipse E600. The analysis was performed measuring the tail moment (tail length × fraction of DNA in the tail) and comparing the treated samples versus the not-treated ones (water, solvent control).

Statistical treatment of the data

The means and standard deviations (SD) were calculated for descriptive statistical documentation. The data are the means ± SD, calculated for the three replicates performed for each experimental point. SPSS software was used for analytical statistics.

RESULTS

In Fig. 1 we show two typical SEM images showing homogeneous distributions of individual GO flakes deposited by spin coating on a 100 nm SiO_2/Si(100) substrate. Panel (a) in Fig.1 refers to pristine micro-GO, while panel (b) refers to nano-GO. Flakes of GO can be clearly observed in the two images. At variance with Akhavan et al. (24, 25), the size (defined as the square root of the estimated area) distribution functions were determined using SEM, which combines high lateral resolution and much larger (in comparison to AFM) scan area size. This allows a more accurate determination of the size distributions. The assignment to single layer GO flakes was performed with quantitative contrast analysis procedures as reported (26, 27). The pristine micro-GO and the nano-GO were characterized by an average flake size of 1.32 µm and 130 nm, respectively. The flake size distributions follow a log-normal model, which typically occurs in random fragmentation phenomena (a typical occurrence after GO preparation and sonication) (28). Moreover, as reported in the supplementary material of Bianco et al. (29), from the statistical analysis it was possible to

determine the amount of flakes having size < 100 nm in both the GO solutions. This amount is 0.0001% w/w for micro-GO and 10% w/w for nano-GO.

Panel (c) in Fig. 1 reports the RS analysis of the GO flakes. Data are reported in the case of pristine GO. The spectrum is very much typical of pristine GO as one can state by direct comparison with the supplementary RS investigation reported previously (26). In particular, the intensity ratio of 1.4 between the D (at 1320 cm^{-1}) and the G peak (at 1600 cm^{-1}) is typical of pristine GO (30).

Sonicated and non-sonicated GO have been characterized also by X-ray photoemission spectroscopy (XPS) as reported previously (26). The XPS analysis shows that no substantial variations were found between the micro- and nano-GO spectra.

The substantial chemical identity is not surprising, considering the quantitative arguments elaborated in the following. The flake size reduction (for example induced by sonication) leads to an increase of the edge/surface atom ratio and, consequently, it may lead to a relative increase of the XPS spectral weight of edge functional groups.

Fig. 2 shows the calculated edge/surface atom ratio as a function of the lateral size of a hexagonal shaped graphene flake. The edge/surface atom ratio monotonically decreases with increasing the flakes size, and is greater than 1% (a typical threshold limit value for XPS detection of a chemical species) only for flakes with lateral dimension below 50 nm. In the case of nano-GO, the relative concentration of such flakes is ~0.8% and consequently the increase of the XPS spectral weight of components assigned to edge functional groups (observed instead by Akhavan in (25) for 10 nm average GO flake size as a significant increase of the spectral weight of the carbonyl groups (C=O, 288.0 eV), and carboxyl groups (C=O(OH)) was not observed. The choice of using a nano-GO with a negligible amount of flakes smaller than 50 nm was thus deliberately made in order to not introduce significant chemical differences with respect to the pristine GO in addition to the morphological ones.

The SEM, XPS, and RS characterizations reported above and by Russier et al. (26) allowed to state (from XPS) the chemical identity of pristine micro-GO and nano-GO and their fully non-reduced state (XPS and RS) while, considering dimensions from SEM, the ratio between the average flake area in the two cases

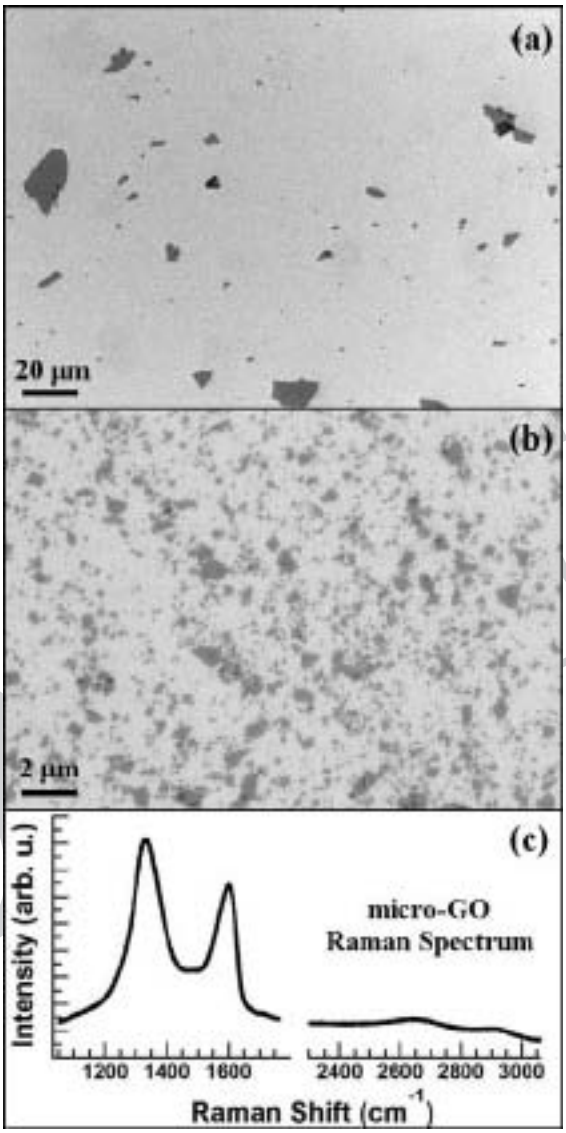

Fig. 1. *SEM images of: (**a**) pristine micro-GO flakes spin coated on 100 nm SiO2/Si(100), (**b**) 26-h sonicated GO flakes (same substrate). **c**) Raman spectrum of single layer micro-GO.*

varies of one order of magnitude. This allowed us to perform a purely size-dependent cyto- and genotoxic study of GO which, to the best of our knowledge, has never been performed previously.

Fig. 3 reports the results of the 24-h exposure MTT assay with solvent control (10% of water), positive control (SDS treatment), pristine GO and nano GO solutions. All the results obtained with the treatments were compared to the solvent control

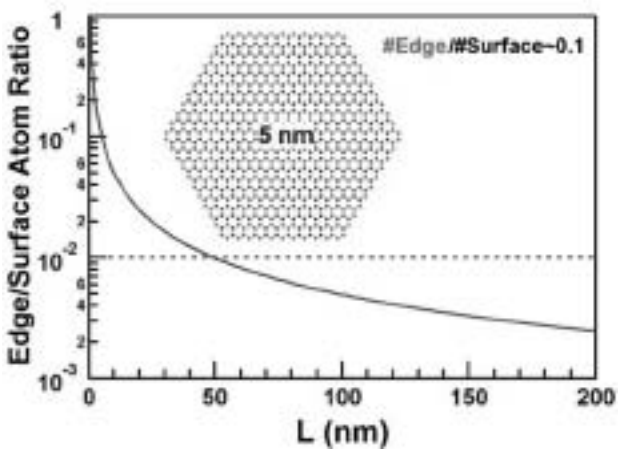

Fig. 2. *Calculated edge/surface atom ratio in graphene flakes as a function of their lateral dimension. The inset shows a flake with a lateral dimension of 5 nm and with an edge/surface atom ratio of ~0.1.*

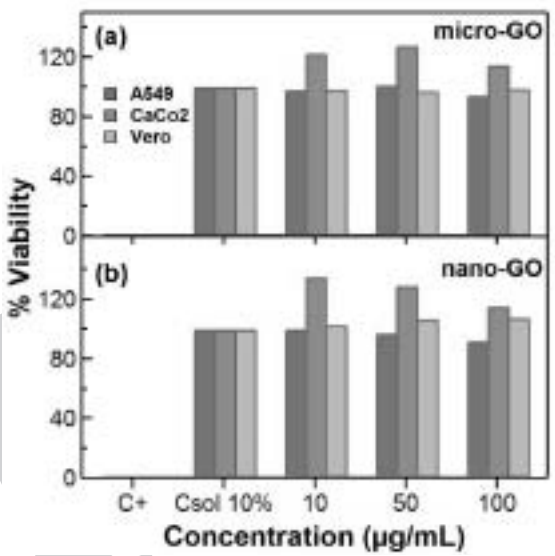

Fig. 3. *24-h MTT assay for the biocompatibility evaluation of both (**a**) pristine micro-GO and (**b**) nano-GO on A549, CaCo2, and Vero. The results are expressed as % of viability compared to the solvent control (10% of water). The data are calculated for at least three independent experiments for each set point. The error bars in the graph are below 1% and are thus not reported.*

(10% of water, a well-known standard in biological assays). Differing from the SDS treatment that shows a 0% of viability, the test demonstrates that, for pristine GO, A549 exhibit a 90% of viability only at the highest concentration used of 100 µg/mL. This result, relative to micro-GO, is in line with the one observed by Chang et al. under identical experimental conditions on A549 (17). The responses to micro-GO of Vero cell line does not deviate from the control results for all the GO concentration range under investigation. Conversely, the CaCo2 cells treated with micro-GO exhibit a marked positive increase in the viability in comparison to the solvent control that can consider evidence of cell proliferation and cell biocompatibility to micro-GO.

Upon exposure to nano-GO (Fig. 3 panel b) the A549 cell line exhibited a cytotoxic response that agreed quantitatively with the results reported by Chang et al. (17) for the interaction with GO with comparable lateral size. Vero cells exhibited 100% viability at the concentration of 10µg/mL but the viability slightly increased at the concentrations of 50µg/mL and 100µg/mL. Again, CaCo2 cells exhibited a positive increase of the viability, with a decreasing trend with increasing nano-GO concentration. Overall, the results showed that

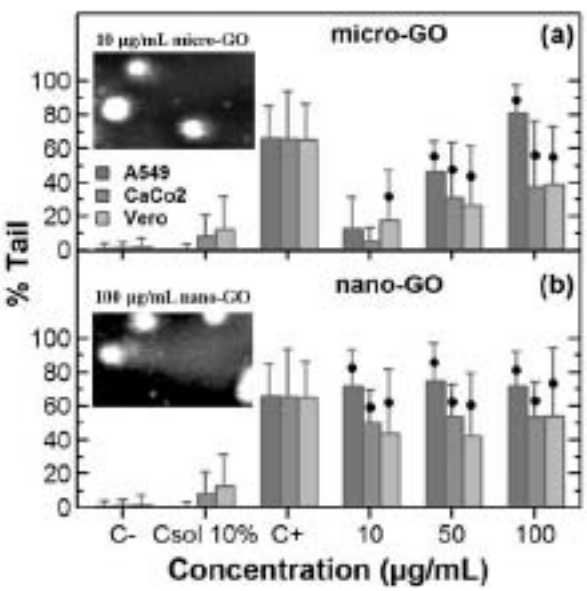

Fig. 4. *24-h Comet assay on A549, CaCo2 and Vero. All the results at the various concentrations tested were compared to the negative control. Panel (**a**): responses to micro-GO. Panel (**b**): response to nano-GO. The inset in the two panels report representative qualitative images of few A549 cells after exposure to 10 µg/mL and 100 µg/mL, respectively, of GO (upper inset) and nano-GO (lower inset). The data are calculated for at least three independent experiments for each set point.*

the interaction of sonicated GO with the cell lines under consideration altered significantly the viability response (either positively or negatively)in respect to the control case. Noteworthy, large GO flakes seemed to increase the viability of CaCo2 cells.

Fig. 4 summarizes the results of the genotoxic response to micro GO and nano GO at 10, 50, and 100μg/mL on the three studied cell lines. Results were compared to the solvent control cells. Moreover, methyl methanesulfonate (MMS) as positive control was used at the concentration of 400 μM. The % of tail obtained with such treatment was 66±20 for the three used cell lines.

In the case of treatment with pristine micro-GO flakes (Fig. 4 panel a) the genotoxic response was moderate (overall less than 20% of the tail) at 10 μg/mL, while it definitely increased at higher GO concentrations (50, and 100 μg/mL), reaching % tail values, at 100 μg/mL pristine micro-GO exposure, exceeding 80% and 60% for A549 and, respectively, Vero and CaCo2.

The results obtained upon treatment with sonicated nano-GO demonstrate a remarkable genotoxic response with % tail values ranging from 60 to 80% for Vero and CaCo2, and A549, respectively. Such tail values did not vary with the concentration of nano-GO.

DISCUSSION

Various possible mechanisms of GO interactions with cells and with the culture medium have to be taken into account to discuss the cytotoxic effect. Already Chang et al. (17), have carefully demonstrated that the cytotoxic effect on A549 is not trivially related to GO depletion of nutrients from the culture medium. This occurrence can thus be ruled out. A positive cells viability increase was, indeed, a clear sign of the GO ability to trigger faster duplication rates of the cells. This was in line with the observed increase of the proliferation of stem, pre-osteoblast, and hippocampal cells (12-14).

The increase of the viability observed in the MTT test could be explained assuming a positive interaction of GO with cell proliferation and survival. A possible molecular and metabolic interaction was not analyzed in-depth but different ways of GO metabolic and molecular activation cannot be excluded as GO can act as a trigger as well as an inhibitor for specific enzymatic pathways involved in the cell growth. To analyze a field still unknown and undefined, a possible direct interaction of GO with genetic materials, with the further and consequent generation of alterations and damage in human differentiated cells, was explored. For this purpose, DNA damage was determined quantitatively in the micro-GO and nano-GO (10 μg/mL, 50 μg/mL, 100 μg/mL) -treated cells using a standard Comet genotoxicity assay.

The Comet assay results indicated a saturated genotoxic response at the nano-GO concentrations used. As a general remark, it was evident that, for both micro-GO and nano-GO, the cell line exhibiting the highest genotoxic response was the A549. We compared this result with the genotoxicity studies carried out to date on GO (24-25). Although the used cell lines were different, there was a quantitative agreement with the Comet test results reported by Akhavan and co-workers, for a 24-h Comet test on stem cells using GO with flake size of 91±37 nm [see Fig. 6 of ref. (24)]. On the other hand, if comparison was made with the potential genotoxicity of other nanostructured materials (such as inorganic nanoparticles) values of the % tail reported here, and reaching 80%, were observed only in the case of CuO nanoparticles (31).

As a general remark, the Comet assay results gave a clear demonstration of a size-dependent genotoxic response to GO of the three cell lines considered in this work.

The discussion of the genotoxic effect can be elaborated focusing on: the size-dependent mechanism of GO interaction with the cell membrane, its size dependent internalization, and the possible chemical triggering of biochemical reactions leading to genotoxic agents (indirect genotoxicity). Even if a detailed understanding of all such mechanisms was beyond the scope of this work, nevertheless, a general scenario can be depicted with the help of previous careful studies reported in the literature.

The study of Yue et al. reporting a “first-principles” molecular dynamic investigation of GO with lipid bilayers, stressed that the passive penetration of a generic double layer lipidic structure (that can represent both plasma membrane and nuclear membrane) by GO flakes upon a mechanism

of "surface-landing" and subsequent internalization, was linearly flake-size-dependent (32). On the other hand, once GO has landed on the cell surface and adheres to it due to its remarkable hydrophilic nature, the internalization energy barrier can be strongly reduced if an edge-mediated internalization occurs, as proposed recently by Ottaviano et al. (28). Independently of the specific internalization mechanism of GO (which deserves further investigations) various studies have confirmed the ability of GO to enter the cell, and that the internalization is size-dependent (19-23). Damage that likely occurs upon internalization can be related to interactions of the GO functional groups with the cell itself leading to production of reactive oxygen species (ROS), that are well-known mediators of damage to all cell structures, including nucleic acids, lipids and proteins (21). Most importantly, oxidative damage is the first step involved in mutagenesis, carcinogenesis and aging. Indirect, ROS induced, DNA damage upon GO exposure cannot therefore, in principle, be ruled out (19). The internalization in the nuclei has been directly demonstrated only by Akhavan with fluorescence in the case of reduced GO nanoribbons with 100 nm lateral size and of few μm typical lengths (25). Given that these GNR with 100 nm lateral size are internalized in the nuclei, further investigations are requested also for GO flakes with lateral dimensions below 100 nm.

Overall, the results presented in this work demonstrate a very strong genotoxic response of the cell lines under investigation once GO flakes with 100 nm average lateral size were considered. If we assume 100 nm as a reasonable threshold value to consider an object truly nanoscopic, we can quantify the concentration of sub-100 nm flakes in pristine micro-GO, taking advantage of the accurate modeling and estimate of the flake-size distribution reported by Russier et al. (26).

In micro-GO the estimate of the mass fraction of flakes with size below 100 nm is $5x10^{-6}$. This corresponds (in the case of 100 μg/mL see Fig. 4 panel a) to an effective concentration of about $5x10^{-4}$ μg/mL of the flakes with sub-100 nm size. However, the amount of sub-100 nm size GO is higher for the nano-GO in respect to the micro-GO. The higher impact on genotoxicity could therefore be related to the higher actual concentration of these sub-100 nm-size flakes in the nano-GO. Thus, the experiments point to the evidence of a high genotoxic response of A549, Vero, and CaCo2 at concentrations of GO with lateral size around 100 nm (and below) at nano-GO concentration values that are almost two orders of magnitude lower that the lowest values reported for the genotoxic investigation of GO by Akhavan in (24).

Summarizing the obtained data, a report on the interaction (cyto- and genotoxic response) of pristine micro-GO and sonicated nano-GO on A549, Vero, and Caco2 cells is reported. A 24-h biocompatibility evaluation by MTT assay was performed to compare the data available in literature (17) for the A549 case, and to evaluate the response to Vero, and CaCo2 cells. MTT showed remarkably, an overall increase of the viability of Vero, and CaCo2 upon exposure to GO. The 24-h comet assay data obtained showed a high genotoxic response for all the three cell lines. The response was saturated (not concentration dependent considering the range from 10 to 100 μg/mL) for nano-GO, and was directly increasing with the concentrations used for micro-GO. The results clearly indicated a size-dependent genotoxic response. GO flakes with sub 100 nm were highly genotoxic even at a relative concentration that can be estimated at $5x10^{-4}$μg/mL.

REFERENCES

1. Novoselov KS, Fal'ko VI, Colombo L, Gellert PR, Schwab MG, Kim K. A roadmap for graphene. Nature 2012; 490:192-200.
2. Treossi E, Melucci M, Liscio A, Gazzano M, Samori P, Palermo V. High-contrast visualization of graphene oxide on dye-sensitized glass, quartz, and silicon by fluorescence quenching. J Am Chem Soc 2009; 131:15576-7.
3. Liscio A, Veronese GP, Treossi E, et al. Charge transport in graphene-polythiophene blends as studied by Kelvin Probe Force Microscopy and transistor characterization. J Mater Chem2011; 21:2924.
4. Melucci M, Durso M, Zambianchi M, et al. Graphene–organic hybrids as processable, tunable platforms for pH-dependent photoemission, obtained by a new modular approach. J Mater Chem 2012; 22:18237.

5. Melucci M, Treossi E, Ortolani L, et al. Facile covalent functionalization of graphene oxide using microwaves: bottom-up development of functional graphitic materials. J Mater Chem 2010; 20:9052-60.
6. Huang YX, Dong XC, Liu YX, Li LJ, Chen P. Graphene-based biosensors for detection of bacteria and their metabolic activities. J Mater Chem 2011; 21:12358-62.
7. Li J, Chen J, Zhang XL, Lu CH, Yang HH. A novel sensitive detection platform for antitumor herbal drug aloe-emodin based on the graphene modified electrode. Talanta 2010; 83:553-8.
8. Qui Y, Qu X, Dong J, Ai S, Han R. Electrochemical detection of DNA damage induced by acrylamide and its metabolite at the graphene-ionic liquid-Nafion modified pyrolytic graphite electrode. J Hazard Mater 2011; 190:480-85.
9. Akhavan O, Ghaderi E. Toxicity of graphene and graphene oxide nano walls against bacteria. ACS Nano 2010; 4(10):5731-6.
10. Santos CM, Tria MCR, Vergara RAMV, Ahmed RC, Rodrigues DF. Antimicrobial graphene polymer (PVK-GO) nanocomposite films. Chem Commun 2011; 47:8892-4.
11. Tian B, Wang C, Zhang S, Feng L, Liu Z. Photothermally enhanced photodynamic therapy delivered by nano-graphene oxide. ACS Nano 2011; 5:7000-9.
12. Feng L, Chen Y, Ren J, Qu X. A graphene functionalized electrochemical aptasensor for selective label-free detection of cancer cells. Biomaterials 2011; 32:2930-7.
13. Huang P, Xu C, Lin J, et al. Folic acid-conjugated graphene oxide loaded with photosensitizers for targeting photodynamic therapy. Theranostics 2011; 1:240-50.
14. Cheng GY, Pang DW, Hwang SM, Tuan HY, Hu YC. A graphene-based platform for induced pluripotent stem cells culture and differentiation. Biomaterials 2012; 33:418-27.
15. Depan D, Girase B, Shah JS, Misra RD. Structure-process-property relationship of the polar graphene oxide-mediated cellular response and stimulated growth of osteoblasts on hybrid chitosan network structure nanocomposite scaffolds. ACTA Biomater 2011; 7:3432-45.
16. Li N, Zhang X, Song Q, et al. The promotion of neurite sprouting and outgrowth of mouse hippocampal cells in culture by graphene substrates. Biomaterials 2011; 32:9374-82.
17. Chang Y, Yang ST, Liu JH, Dong E, Wang Y, Cao A, Liu Y, Wang H. *In vitro* toxicity evaluation of graphene oxide on A549 cells. Toxicol Lett 2011; 200:201-10.
18. Wang K, Ruan J, Song H, Zhang J, Wo Y, Guo S, Cui D. Biocompatibility of graphene oxide nanoscale. Res Lett 2011; 6:8.
19. Gollavelli GG, Ling YC. Multi-functional graphene as an *in vitro* and *in vivo* imaging probe. Biomaterials 2012; 33(8):2532-45.
20. Kryston TB, Georgiev AB, Pissis P, Georgakilas AG. Role of oxidative stress and DNA damage in human carcinogenesis. Mutat Res 2011; 711(1-2):193-201.
21. Valko M, Leibfritz D, Moncol J, Cronin MTD, Mazura M, Telser J. Free radicals and antioxidants in normal physiological functions and human disease. IJBCB 2007; 39:44-84.
22. Waris G, Ahsan H. Reactive oxygen species: role in the development of cancer and various chronic conditions. J Carcinogen 2006; 5:14.
23. Hong BJ, Compton OC, An Z, Eryazici I, Nguyen SBT. Successful stabilization of graphene oxide in electrolyte solutions: enhancement of biofunctionalization and cellular uptake. ACS Nano 2012; 6(1):63-73.
24. Akhavan O, Ghaderi E, Akhavan A. Size-dependent genotoxicity of graphene nanoplatelets in human stem cells. Biomaterial 2012; 33:8017-25.
25. Akhavan O, Ghaderi E, Emamy H, Akhavan F. Genotoxicity of graphene nanoribbons in human mesenchymal stem cells. Carbon 2013; 54:419-31.
26. Russier J, Treossi E, Scarsi A, et al. Evidencing the mask effect of graphene oxide: a comparative study on primary human and murine phagocytic cells. Nanoscale 2013; 5:11234.
27. Perrozzi F, Prezioso S, Donarelli M, et al. Use of optical contrast to estimate the degree of reduction of graphene oxide. J Phys Chem 2013; 117:620-5.
28. Ottaviano L, Filipponi A, Di Cicco A. Supercooling of liquid metal droplets by means of x-ray absorption

investigations. Phys Rev 1994; 49:11749-58.
29. Bianco A. Graphene: Safe or toxic? The two faces of the medal. Angewandte Chemie International Edition 2013; 52(19):4986-87.
30. Nair RR, Wu HA, Jayaram PN, Grigorieva IV, Geim AK. Unimpeded permeation of water through helium-leak-tight graphene-based membranes. Science 2012; 335:442-4.
31. Kumar V, Kumari A, Gulera P, Yadan SK. Evaluating the toxicity of selected types of nanochemicals. Rev Environ Contam Toxicol 2012; 215:39-121.
32. Yue H, Wei W, Yue Z, et al. The role of the lateral dimension of graphene oxide in the regulation of cellular responses. Biomaterials 2012; 33:4013-21.

SALIVARY STEROID HORMONE RESPONSE TO WHOLE-BODY CRYOTHERAPY IN ELITE RUGBY PLAYERS

D. GRASSO[1], P. LANTERI[1], C. DI BERNARDO[1], C. MAURI[2], S. PORCELLI[3], A. COLOMBINI[1], V. ZANI[4], F.G. BONOMI[4,5], G. MELEGATI[2], G. BANFI[1,6] and G. LOMBARDI[1]

[1]Laboratory of Experimental Biochemistry & Molecular Biology, I.R.C.C.S. Istituto Ortopedico Galeazzi, Milan, Italy; [2]Department of Multifunctional Rehabilitation, I.R.C.C.S. Istituto Ortopedico Galeazzi, Milan, Italy; [3]Institute of Bioimaging and Molecular Physiology, National Research Council, Segrate, Italy; [4]Centre of Systemic Cryotherapy, Poliambulatorio Bongi, Orzinuovi, Italy; [5]Cardiovascular Department, O.U. Cardiology, Humanitas Gavazzeni, Bergamo, Italy; [6]Department of Biomedical Sciences for Health, University of Milan, Milan, Italy

Received March 8, 2013 – Accepted April 22, 2014

Saliva represents a low stress, not-invasively collected matrix that allows steroid hormone monitoring in athletes by reflecting type, intensity and duration of exercise. Whole body cryotherapy (WBC) consists of short whole-body exposures to extremely cold air (-110° to -140°C) which, despite being initially used to treat inflammatory diseases, is currently acquiring increasing popularity in sports medicine. Cryostimulation practice is now widely accepted as an effective treatment to accelerate muscle recovery in rugby players. The aim of this work was to study the changes of steroid hormones in saliva of rugby players after both 2 and 14 consecutive WBC sessions, in order to investigate the effects of the treatment on their salivary steroid hormonal profile. Twenty-five professional rugby players, belonging to the Italian National Team, underwent a 7-day cryotherapy protocol consisting of 2 daily sessions. Saliva samples were taken in the morning prior to the start of the WBC, in the evening after the end of the second WBC, and in the morning of the day after the last WBC session. The samples were analyzed for cortisol, DHEA, testosterone and estradiol using competitive enzyme-linked immunosorbent assays. Cortisol and DHEA showed a reduction already after the 2 WBC sessions of the first day; after 14 consecutive WBC sessions cortisol, DHEA, and estradiol levels decreased, while testosterone increased as did the testosterone to cortisol ratio. These results were confirmed by the fact that the majority of subjects showed variations exceeding the critical difference (CD). In conclusion, we found that WBC acutely affects the salivary steroid hormone profile, and the results are evident already after only one twice-daily session. Most significantly, after one-week of consecutive twice-daily WBC sessions, all the hormones were modified. This is the first experimental report that links changes in the hormonal asset to WBC.

Many reports have been recently published on the possible use of saliva specimens in order to monitor the steroid hormone asset both in health and disease. Saliva represents a low stress, non-invasively collected matrix that allows the monitoring of many different parameters in athletes over a variety of

Key words: saliva, steroid hormones, cryostimulation, rugby

Mailing address: Giovanni Lombardi, PhD
Laboratory of Experimental Biochemistry & Molecular Biology, I.R.C.C.S. Istituto Ortopedico Galeazzi,
Via R. Galeazzi, 4,
20161 - Milano, Italy
Tel.: +39 0266214068 Fax: +39 0266214060
e-mail: giovanni.lombardi@grupposandonato.it

0393-974X (2014)

DISCLOSURE: ALL AUTHORS REPORT NO CONFLICTS OF INTEREST RELEVANT TO THIS ARTICLE.

training conditions and environments, enabling numerous and serial controls during an observation period, and ensuring compliance in an elite group (1). Salivary concentrations of steroid hormones are reliable and are highly correlated with those measured in serum, also reflecting type, duration and intensity of exercise. However, salivary hormones are more responsive to the physiological stressors of exercise than the corresponding blood counterparts (2-4). Furthermore, salivary hormone levels reflect the free plasma fractions and the bioactive component of steroid hormones that is potentially able to act in the target tissue (5): salivary testosterone concentrations, for example, represent the fraction available to interact with the androgen receptor, which directly modulates the responses. Parallel measurement of salivary cortisol has been found to be an excellent indicator of the free serum cortisol, reporting a close correspondence with serum in circadian fluctuations (3, 6, 7), as demonstrated also for testosterone and estradiol (2).

Cold therapy is commonly applied as a useful procedure to relieve symptoms of inflammatory diseases such as ankylosing spondylitis, fibromyalgia, arthritis and osteoarthritis; moreover, it is also used to improve lung functions in asthmatics or to alleviate pain consequent to trauma resulting from injuries or overuse, as practiced in sports medicine (8-10). Whole body cryotherapy (WBC) is a form of cold-based therapy, introduced about 30 years ago in clinical practice, for the symptomatic treatment of rheumatoid arthritis. It consists of short (2-3 minutes) whole-body exposures to extremely cold air (-110°C to -140°C) in a cryochamber, while subjects are minimally dressed (11).

There is evidence of the positive effects of WBC in enhancing pro- and anti-inflammatory balance (12), cardiovascular function (9, 13) and oxidative status (14), improving both muscular recovery and activation (15), and reducing the sport-induced haemolysis (11, 16). Following demonstration of its benefits, WBC has acquired increasing popularity in sports medicine (in this instance WBC is more accurately defined as whole body cryostimulation). However, WBC has been claimed as a practice potentially enhancing the performance. High workload for training and psychophysical stress, due to competitions, could modify homeostasis in athletes thought to be physically normal and healthy, even inducing apparently pathological values (17). Studying a feasible improvement of the recovery following injuries or physical fatigue due to overtraining is crucial for athletes in order to consider the real benefits, or the eventual limitations, of WBC; however, the reported general effects of WBC suggest that this treatment may be beneficial to sportsmen (9, 11, 18). Although there is a growing number of papers concerning the hormonal response to heavy physical exercise through the measurement of salivary hormones (19, 20), to our knowledge, there are no reports concerning the effects of WBC on salivary hormone asset in rugby players. For these reasons, the aim of the present work was to investigate the changes in salivary levels of steroid hormones (cortisol, dehydroepiandrosterone (DHEA), testosterone and 17β-estradiol) after two and fourteen consecutive WBC sessions in male professional rugby players in order to investigate the effects of the treatment on their physiological response, considering rugby as a sport often leading to a very high imbalance between exercise exhaustion and recovery.

MATERIALS AND METHODS

Study population

The study population consisted of 27 male professional rugby players from the Italian National Rugby Team, all of whom were participating in the 2012 summer training camp held at the end of the competitive season. Two subjects were excluded because of insufficient sample collection. The final analysis was, thus, carried out on 25 subjects. The mean age was 25.6±3.7 years; the mean weight was 85.9±9.2 kg; the mean body mass index (BMI) (weight in kilograms divided by the square of the height in meters) was 26.2±1.8 kg/m^2.

The study was approved by the Reference Ethics Committee (ASL Milano 1) and consent was obtained from each athlete after a full explanation of the purpose and nature of all procedures.

Cryostimulation protocol

The WBC treatment protocol consisted of 2 daily sessions for 7 consecutive days: the first in the morning after the morning training session,

and the second in the evening after the afternoon training session. During the procedure, subjects were protected from frostbite with shorts (bathing suit), surgical mask, socks, clogs or shoes, gloves, and a cap (or headband) covering the ears; moreover, the subjects were instructed to keep walking while inside the cryochamber, to wriggle their fingers and to not hold their breath. Safety personnel and medical doctors were always on hand. Any sweat was dried before the subject entered the cryochamber, where the air was clear and dry. Each cold-room session consisted of 30-second preconditioning at -60°C and the following 3-min exposure -140°C in a special temperature-controlled cryochamber.

All of the players were naïve to WBC, except for 3 subjects who had been submitted to WBC about five years previously.

Diet and training protocol

Diet regimen was strictly defined by the team physicians and it was kept the same for the whole camp. The athletes trained daily for a total of 4 hours: morning anaerobic training in the gym and afternoon high-intensity discontinuous training on the field. Diet and training programs during the camp were similar to those of the previous 2 weeks. Particularly, no supplements or medications were administered during the camp or the 2 previous weeks. Only one subject was treated with salicylic acid (1 g/die for 2 days) during the first part of the camp to relieve flu symptoms.

Saliva sampling

Unstimulated saliva samples were collected three times during the whole observation: the first (T0) collection was in the morning (08:00 a.m.) prior to the start of the training camp and the WBC session, the second (T1) sampling was performed within 10 minutes from the end of the first WBC session of the afternoon (the second of the first day) and the third (T2) was performed in the morning (08:00 a.m.) of the day after the last WBC session. At T1, all samples were collected in a period of 1 hour (6:30-7:30 p.m.), because athletes entered the cryochamber in groups of 3 for each treatment. Thus, collection of samples from different groups was carried out every 5 minutes during this period. The athletes had to spit in polypropylene low-steroid absorbing tubes (Sali-tubes, DRG® Instruments GmbH, Marburg, Germany), and immediately after the collection, the samples were stored at -20°C until assayed.

Saliva steroid hormones measurement

Each saliva sample, prior to the assay, was centrifuged once (5 min, 3000xg) to sediment the particulate materials. Saliva samples were analyzed for cortisol, DHEA, testosterone, and 17β-estradiol using competitive enzyme-linked immunosorbent assays specifically designed to detect salivary hormone measurements (ELISAs, DRG® Instruments GmbH, Marburg, Germany). The assays were based on the use of either monoclonal (testosterone and cortisol) or polyclonal (17β-estradiol, DHEA) antibodies directed against the specific hormone. The assays were carried out following the manufacturer's instructions.

Sensitivity, intra-assay (CV_w%) and inter-assay (CV_b%) variation ranges were, respectively: 1.9 pg/mL, 6.2-13.8% (CV_w%) and 5.5-9.6 % (CV_b%) for testosterone; 0.4 pg/mL, 2.6-6.9% (CV_w%) and 2.1-4.3% (CV_b%) for 17β-estradiol; 2.2 pg/mL, 2.3-8% (CV_w%) and 3.4-4.7% (CV_b%) for DHEA; 0.537 ng/mL, 1.47%-4.52% (CV_w%) and 5.82-7.47% (CV_b%) for cortisol.

Statistical analysis

Statistical analysis was performed with GraphPad Prism v5.0 software (GraphPad Software Inc., LaJolla, CA, USA). Non-Gaussian distribution of values was assayed by Kolmogorov-Smirnov normality test, and all values in the descriptive analysis were expressed as the median and the range (5^{th} – 95^{th} percentile). Two-tailed paired *t*-test (Wilcoxon's signed rank test) was used to compare basal values (T0) with either T1 or T2 values. Correlation analyses were performed by the means of the two-tailed Spearman's rank correlation coefficient test. The significance level was set at 0.05. In order to understand whether the magnitude of change in serial measurements, from an individual, can be considered statistically significantly ($p< 0.05$), either as a result of the applied treatment or simply due to the additive effects of the within-subject variability and the analytical variability, the calculation of the critical difference (CD) was applied to each couple of comparisons, for each analyte. The CD was

calculated as follows (21): $2.77 \cdot \sqrt{(CV_a^2 + CV_i^2)}$

RESULTS

Acute effects after a single twice-daily WBC session

A double session of WBC, during the same day, had significant effects on the steroid hormonal asset. Salivary cortisol was significantly reduced from 2.425 (1.287–6.153) ng/mL at T0, to 2.105 (1.462–4.781) ng/mL at T1 ($p< 0.05$). Although there was a very wide inter-individual variability, salivary DHEA also showed a significant reduction from 224.8 (40.4–889.2) pg/mL to 138.9 (31.2–927.5) pg/mL ($p< 0.05$). No significant variations were, however, found in testosterone and 17β-estradiol, the testosterone being attested at 46.7 (30.3–101.2) pg/mL at T0 and 47.0 (17.0–65.5) pg/mL at T1, and the 17β-estradiol at 2.3 (0.5–14.9) pg/mL at T0 and 1.6 (0.4–10.8) pg/mL at T1. Nor did the testosterone to cortisol ratio show any significant variation (T0: 18.01 (10.36–33.45); T1: 15.37(6.71–33.40)) (Fig. 1).

The Spearman's analysis showed a direct correlation between DHEA and cortisol ($r= 0.40$; $p< 0.01$) and more weakly between testosterone and cortisol ($r= 0.32$; $p< 0.05$). Testosterone was also correlated with DHEA ($r= 0.46$; $p< 0.01$) and 17β-estradiol ($r= 0.41$; $p< 0.01$).

Effects of one-week consecutive twice-daily WBC sessions

After 14 consecutive WBC sessions, over one week, we found significant variations in the whole salivary steroid hormone profile. Salivary cortisol was significantly reduced from 2.425 (1.287–6.153) ng/mL, at T0, to 1.37 (0.52–2.228) ng/mL at T2 ($p< 0.001$). DHEA was significantly reduced from 224.8 (40.4–889.2) pg/mL to 57.1 (13.4–163.8) pg/mL ($p< 0.001$). Interestingly, over one week, testosterone was significantly increased from 46.7 (30.3–101.2) pg/mL to 68.8 (28.3–109.5) pg/mL ($p< 0.01$). On the other hand, 17β-estradiol was significantly modified, being reduced from 2.3 (0.5–14.9) pg/mL to 1.7 (0.8–4.4) pg/mL ($p< 0.05$). Even in the case of the testosterone to cortisol ratio the longer treatment had significant effects shown by the increase from 18.01 (10.36–33.45) to 48.28 (24.2–85.71) ($p< 0.001$) (Fig. 2).

Table I. *Within-subject variability, the analytical variability and the critical differences calculated for the steroid salivary hormones.*

	CV_i (%)	CV_a (%)	CD (%)
Cortisol	20.9	4.5	59.17
DHEA	5.6	2.3	16.77
Testosterone	17.3	7.1	51.80
17β-estradiol	22.6	3.8	63.48

Table II. *Single-subject variations analyzed for CD.*

	T0 *vs* T1 (n=25)	T0 *vs* T2 (n=25)
Cortisol	2	10
DHEA	18	20
Testosterone	8	7
17β-estradiol	15	17

Number of subjects whose variations of salivary steroid hormone concentration exceed the CD for the paired comparisons.

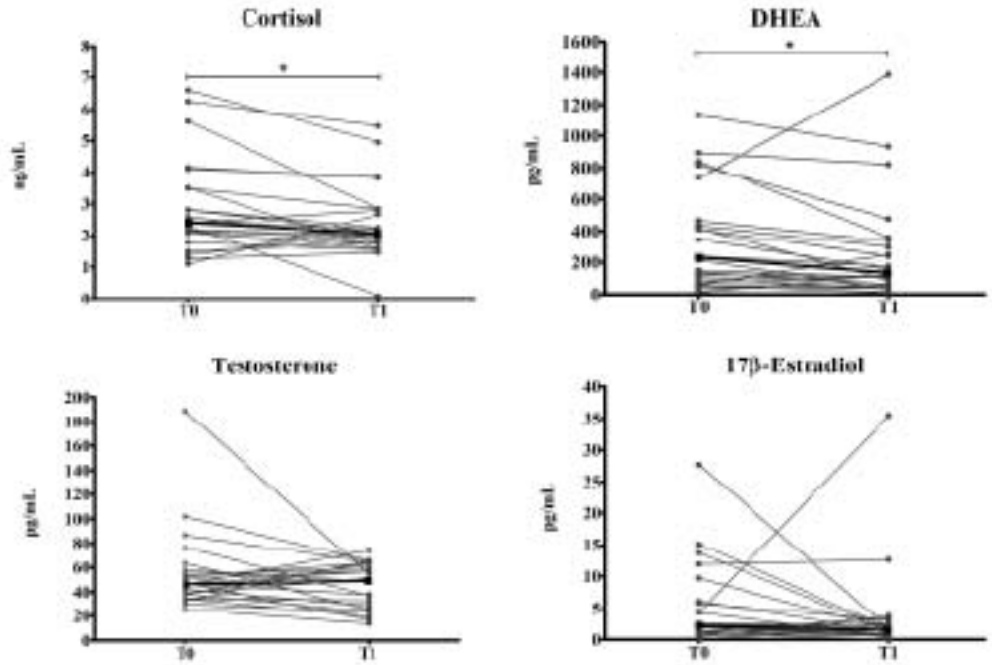

Fig. 1. *Effects of a single twice-daily WBC session. Gray spots indicate values of each athlete before (T0) and after (T1) two sessions of WBC, over the same day. Black squares indicate the median values. The asterisk indicates a statistical significance (*: p< 0.05)*

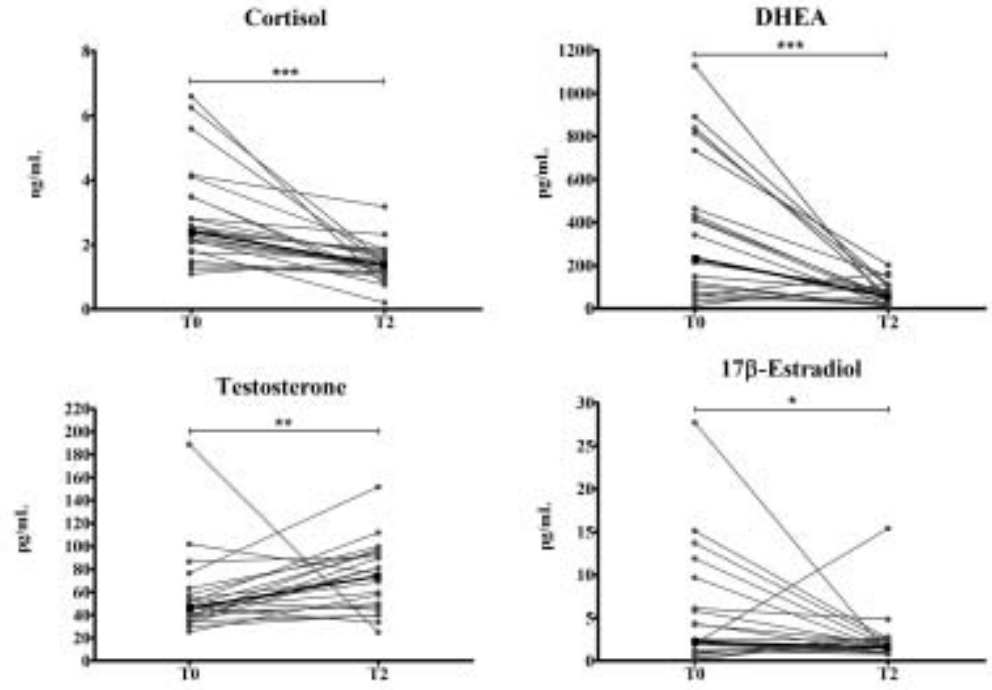

Fig. 2. *Effects of one-week consecutive twice-daily WBC sessions. Gray spots indicate values of each athlete before (T0) and after (T2) fourteen sessions of WBC, over 7 days. Black squares indicate the median values. The asterisks indicate a statistical significance (*: p< 0.05; **: p< 0.01; ***: p< 0.001)*

A good direct correlation was evidenced between DHEA and cortisol ($r= 0.52$; $p< 0.001$) and, more weakly, between estradiol and cortisol ($r= 0.34$; $p< 0.05$), DHEA ($r= 0.30$; $p< 0.05$) and testosterone ($r= 0.36$; $p< 0.05$).

WBC induced-hormonal changes vs critical difference

The within-subject variability, the analytical variability and the critical differences calculated for the steroid hormones are reported in Table I [CV_i are from Ricòs et al. (22)].

Besides the statistical significance reported in the paragraph above, when single-subject variations were analyzed for CD, we observed, as expected, that changes exceeding the CD were mostly evident when T0 and T2 were compared. In particular, while cortisol and testosterone showed weak variations (in 8% and 32% of the subjects between T0 and T1, respectively; in 40% and 28% between T0 and T2, respectively), we observed substantial decreases in DHEA and estradiol evaluating both T0 *vs* T1 (in 72% and 60% of the subjects, respectively) and T0 *vs* T2 (in 80% and 68% of the subjects, respectively). These results are summarized in Table II.

Table I shows the percentage within-subject variability (CV_i), the percentage analytical variability (CV_a) and the calculated critical difference of each analyte. The CV_i are from Ricòs et al. (22); in the case of the CV_a, supplied by the manufacturer, we considered the more adequate CV for a specific concentration range (see the "Materials and Methods" section). CV_i (%) values of cortisol, DHEA and 17β-estradiol refer to serum samples, while CV_i (%) value of testosterone refers to saliva samples.

DISCUSSION

Saliva represents a non-invasive, stress-free alternative to serum, allowing an effective serial monitoring for hormone profiling, not only after or before sports activity but also during training. In the last few years, saliva analysis has become a useful method of choice to access hormonal changes during physical activity, including different training conditions and environments. It is also known that hormones with catabolic or anabolic properties, such as cortisol and testosterone, change in relation to the intensity and the duration of exercise (2, 3). However, the number of analytes that could be assayed on saliva samples is limited owing to different factors, namely: i) systemic conditions that directly or indirectly influence the salivary glands, modifying their activity; ii) direct production, by salivary glands, of molecules usually present in the circulation; iii) local oral acute or chronic conditions that could affect the production and the levels of analytes (23). The passage of macromolecules from the circulation to saliva can occur by passive diffusion (lipophilic steroid hormones), active transport (IgA) or ultrafiltration (sulfated hormones). With regard to the passive diffusion, capillaries surrounding the salivary glands are permeable to small molecules, but the subsequent passages towards the gland cells are facilitated only in the case of apolar compounds (23). Despite salivary unbound steroids showing a linear correlation with their serum free form counterparts, their relative concentrations in saliva are not always the same as those present in the blood because they are partly metabolized in the salivary glands (2). Moreover, it has been shown that changes of cortisol after exercise are more pronounced in saliva compared to blood (24). Correlations have been demonstrated between saliva and serum concentrations of testosterone and cortisol at rest; furthermore, salivary hormone concentrations, reflecting more accurately blood free levels, give valuable data consistent with the biologically active fractions (5). Indeed, most of the circulating testosterone, for example, is bound to albumin and sex-binding globulins (95–98%) while only a small amount (2–5%) remains free, unbound, in the circulation (1).

Physical activity could indirectly, through the induction of plasma volume variations (i.e., hemoconcentration and hemodilution), and directly affect both the binding protein concentrations (sex hormone binding globulin – ShBG, albumin) and the dissociation rates from them (25-27); thus, the possibility to measure only the free hormone fraction is of particular interest in athletes during activity.

Recovery from muscle injury after WBC seems to be particularly effective in endurance and resistance athletes, and it is currently debated whether it can be considered a potentially performance-enhancing practice (17). Recently, WBC has been implemented

in medical protocols to improve recovery from muscle injury, one of the primary concerns of sport activities. However, descriptions of the physiological response to this recovery technique are very few and are mainly addressed to evaluate its effects on the hematological profile and the cardiovascular functions (11). Even though literature on the effects of exercise on salivary concentration of steroid hormones is growing, to our knowledge this is the first report that evaluates the effects of WBC on salivary hormones in rugby players. Salivary measures of steroid hormones can give useful information about how steroid hormones are modified in response to exercise and training. In particular, while, to our knowledge, no data about estradiol and DHEA exist, it is well documented that rugby training induces decreased concentrations of salivary testosterone and increased concentrations of salivary cortisol, besides resulting in a decrease of the testosterone to cortisol ratio, generally considered as an index of stress and tiredness (2). However, literature data demonstrated that DHEA is modified after short-term physical exercise. DHEA increased after exercise, depending on the level of performance and the intensity of the exercise (28), together with the finding of a significant correlation between its serum and salivary concentrations, before and after resistance exercise, in both trained and untrained males (29). Moreover, salivary DHEA and testosterone concentrations were found to be positively related before and after an handball match (30).

In the current study we have demonstrated that the association of WBC and training, in rugby players, affects the salivary steroid hormonal profile asset. We considered two different sets of evaluations: the acute effects of two WBC sessions, during the same day, and the effects of WBC after prolonged treatment (fourteen sessions over seven days). By evaluating the short-term effects, we found a significant decrease in salivary cortisol and DHEA, while testosterone, estradiol and the testosterone to cortisol ratio were not modified. Both cortisol and DHEA showed a decrease at the end of the first day of treatment, after 4 hours of training and two WBC sessions. Even if the changes were statistically significant, a great inter-individual variability was evident, mainly in the case of cortisol and DHEA, as demonstrated by the reported ranges. Despite this variability, the trends were concordant in all the subjects for all the parameters, with only a few discrepant changes: 3 out of 25 subjects for cortisol and 4 out of 25 for DHEA showed an increase. A more heterogeneous situation was evident for testosterone and estradiol. Although acute exercise is known to induce an increase in both cortisol and DHEA (2), the significant decrease we found is consistent with the circadian rhythm of these hormones: higher concentrations in the morning and lower in the evening (31). The appreciable number of subjects who experienced changes in DHEA exceeding the CD (n=18) indicates that the WBC effects are greater than those dependent on the exercise, the biological variability (and, thus, the effects of the diurnal changes) and the analytical variability (characteristic of the method of measurement used). This is not true for cortisol, whereby only 2 subjects esperienced variations exceeding the CD. After 1 week of treatment, cortisol, DHEA, and estradiol decreased whilst testosterone increased, as did the testosterone to cortisol ratio. These changes were associated to the appreciable number of subjects whose variations were higher than the CDs. The coherence of the effects of WBC on the hormonal asset is demonstrated by the highly concordant trends of cortisol and DHEA, over both two and fourteen sessions of WBC, as reflected by the correlation analysis. The changes in testosterone and cortisol could have an important feedback on the recovery, as suggested by Crewther and colleagues (32) who demonstrated that midweek-training salivary concentrations of testosterone, and partially those of cortisol, both pooled from a rugby team, were associated with the game outcomes. This finding indicates that testosterone responsiveness to physical challenges could predict team readiness to competition (32). Thus, our findings, and particularly the increase in testosterone and the associated decrease in cortisol following multiple WBC sessions, could be intended as an index of a preparatory improvement in view of a competition.

CD indicates that, for one subject, the difference between two consecutive measurements is statistically significant and, thus, it is not likely attributable to fluctuations due to the biological variability and/or the analytical variability. Generally, a difference of more than ±95% will probably indicate a true

change, consequent to the application of an external factor (training, therapy, or other) (33). Our findings, relative to the high level of inter-individual variability, account for the need for further studies aimed to better clarify the physiology of steroid hormones in saliva. In this view, the use of the critical difference, in order to highlight "real changes", other than the statistically significant changes, is fundamental, even though, to our knowledge, this is the first time that such an assessment has been applied to the study of salivary hormones. Finally, in our opinion, the modifications in DHEA and testosterone induced by the WBC practice should be taken into account when an athlete's biological passport (ABP) for steroids is introduced (34) into the anti-doping setting. Indeed, many of the changes we found exceeded the CD, possibly leading to the overcoming of the reference limits. If so, it would be more appropriate to consider WBC as a recovery methodology to be used only in a therapeutic setting to treat muscle injury.

The main limitation of this study is the lack of a control group which would make it possible to discriminate between WBC- and training-specific effects on the hormonal asset. This limit is, however, unsolvable when considering elite athletes who are all grouped together for the training camp and who are all submitted to the same interventions. In this regard, it must be considered that previous studies analyzing comparable populations (9, 16, 17) were structured in the same way. Another limitation is represented by the possible usefulness of additional saliva collections over the same period allowing a more serial monitoring of the hormonal profile as a function of the WBC treatment. Future efforts will be addressed in this direction.

In conclusion, the relevance of the hormones, reported in the present study, lies in their importance in giving an index of the psychophysical stress induced by training in sportsmen (2). Although WBC is believed to improve a series of physiological parameters and, thus, recovery, this is the first experimental report that links the beneficial effects of WBC to the changes in the hormonal asset. In other words, the improvement in muscular recovery induced by WBC could be, at least in part, due to the modification in the hormonal asset, and particularly in cortisol and testosterone (35). Our data demonstrate that WBC induces changes in salivary hormone concentrations, overcoming those induced by training, and synchronizing them with their circadian rhythms.

REFERENCES

1. Papacosta E, Nassis GP. Saliva as a tool for monitoring steroid, peptide and immune markers in sport and exercise science. J Sci Med Sport 2011; 14:424-34.
2. Gatti R, De Palo EF. An update: salivary hormones and physical exercise. Scand J Med Sci Sports 2011; 21:157-69.
3. Beaven CM, Cook CJ, Gill ND. Significant strength gains observed in rugby players after specific resistance exercise protocols based on individual salivary testosterone responses. J Strength Cond Res 2008; 22:419-25.
4. Grasso D, Corsetti R, Lanteri P, Di Bernardo C, Colombini A, Graziani R, Banfi G, Lombardi G. Bone-muscle unit activity, salivary steroid hormones profile, and physical effort over a 3-week stage race. Scand J Med Sci Sports 2013; doi: 10.1111/sms.12147.
5. Arregger AL, Contreras LN, Tumilasci OR, Aquilano DR, Cardoso EM. Salivary testosterone: a reliable approach to the diagnosis of male hypogonadism. Clin Endocrinol (Oxf) 2007; 67:656-62.
6. Kraemer WJ, Ratamess NA. Hormonal responses and adaptations to resistance exercise and training. Sports Med 2005; 35:339-61.
7. Hansen AM, Garde AH, Persson R. Sources of biological and methodological variation in salivary cortisol and their impact on measurement among healthy adults: a review. Scand J Clin Lab Invest 2008; 68:448-58.
8. Smolander J, Leppaluoto J, Westerlund T, Oksa J, Dugue B, Mikkelsson M, Ruokonen A. Effects of repeated whole-body cold exposures on serum concentrations of growth hormone, thyrotropin, prolactin and thyroid hormones in healthy women. Cryobiology 2009; 58:275-8.
9. Banfi G, Melegati G, Barassi A, d'Eril GM. Effects of the whole-body cryotherapy on NTproBNP, hsCRP and troponin I in athletes. J Sci Med Sport

2009; 12:609-10.
10. Smolander J, Westerlund T, Uusitalo A, Dugue B, Oksa J, Mikkelsson M. Lung function after acute and repeated exposures to extremely cold air (-110 degrees C) during whole-body cryotherapy. Clin Physiol Funct Imaging 2006; 26:232-4.
11. Banfi G, Lombardi G, Colombini A, Melegati G. Whole-body cryotherapy in athletes. Sports Med 2010; 40:509-17.
12. Pournot H, Bieuzen F, Louis J, Mounier R, Fillard JR, Barbiche E, Hausswirth C. Time-course of changes in inflammatory response after whole-body cryotherapy multi exposures following severe exercise. PloS one 2011; 6:e22748.
13. Lubkowska A, Szygula Z. Changes in blood pressure with compensatory heart rate decrease and in the level of aerobic capacity in response to repeated whole-body cryostimulation in normotensive, young and physically active men. Int J Occup Med Environ Health 2010; 23:367-75.
14. Lubkowska A, Szygula Z, Klimek AJ, Torii M. Do sessions of cryostimulation have influence on white blood cell count, level of IL6 and total oxidative and antioxidative status in healthy men? Eur J Applied Physiol 2010; 109:67-72.
15. Hausswirth C, Louis J, Bieuzen F, Pournot H, Fournier J, Filliard JR, Brisswalter J. Effects of whole-body cryotherapy vs. far-infrared vs. passive modalities on recovery from exercise-induced muscle damage in highly-trained runners. PloS one 2011; 6:e27749.
16. Banfi G, Krajewska M, Melegati G, Patacchini M. Effects of whole-body cryotherapy on haematological values in athletes. Br J Sports Med 2008; 42:858.
17. Lombardi G, Lanteri P, Porcelli S, et al. Hematological profile and martial status in rugby players during whole body cryostimulation. PLoS One 2013; 8:e55803.
18. Galliera E, Dogliotti G, Melegati G, Corsi Romanelli MM, Cabitza P, Banfi G. Bone remodelling biomarkers after whole body cryotherapy (WBC) in elite rugby players. Injury 2012; 44:1117-21.
19. Maso F, Lac G, Filaire E, Michaux O, Robert A. Salivary testosterone and cortisol in rugby players: correlation with psychological overtraining items. Br J Sports Med 2004; 38:260-3.
20. Beaven CM, Gill ND, Cook CJ. Salivary testosterone and cortisol responses in professional rugby players after four resistance exercise protocols. J Strength Cond Res 2008; 22:426-32.
21. Costongs GM, Janson PC, Bas BM, Hermans J, van Wersch JW, Brombacher PJ. Short-term and long-term intra-individual variations and critical differences of clinical chemical laboratory parameters. J Clin Chem Clin Biochem 1985; 23:7-16.
22. Ricos C, Iglesias N, Garcia-Lario JV, et al. Within-subject biological variation in disease: collated data and clinical consequences. Ann Clin Biochem 2007; 44:343-52.
23. Pfaffe T, Cooper-White J, Beyerlein P, Kostner K, Punyadeera C. Diagnostic potential of saliva: current state and future applications. Clin Chem 2011; 57:675-87.
24. Obminski Z, Stupnicki R. Comparison of the testosterone-to-cortisol ratio values obtained from hormonal assays in saliva and serum. J Sports Med Phys Fitness 1997; 37:50-5.
25. Bonifazi M, Lupo C. Differential effects of exercise on sex hormone-binding globulin and non-sex hormone-binding globulin-bound testosterone. Eur J Appl Physiol Occup Physiol 1996; 72:425-9.
26. Obminski Z, Stupnicki R. Effect of temperature and pH on the magnitude of the free fraction of cortisol in serum. Exp Clin Endocrinol Diabetes 1996; 104:350-2.
27. Obminski Z. Changes in the free (unbound) fraction of testosterone in serum *in vitro* as affected by pH and temperature. Exp Clin Endocrinol Diabetes 1998; 106:85-8.
28. Tremblay MS, Copeland JL, Van Helder W. Effect of training status and exercise mode on endogenous steroid hormones in men. J Appl Physiol 2004; 96:531-9.
29. Cadore E, Lhullier F, Brentano M, Silva E, Ambrosini M, Spinelli R, Silva R, Kruel L. Correlations between serum and salivary hormonal concentrations in response to resistance exercise. J Sports Sci 2008; 26:1067-72.
30. Filaire E, Lac G. Dehydroepiandrosterone (DHEA) rather than testosterone shows saliva androgen responses to exercise in elite female handball players. Int J Sports Med 2000; 21:17-20.
31. Ghiciuc CM, Cozma-Dima CL, Pasquali V, Renzi P,

Simeoni S, Lupusoru CE, Patacchioli FR. Awakening responses and diurnal fluctuations of salivary cortisol, DHEA-S and alpha-amylase in healthy male subjects. Neuro Endocrinol Lett 2011; 32:475-80.

32. Crewther BT, Sanctuary CE, Kilduff LP, Carruthers JS, Gaviglio CM, Cook CJ. The workout responses of salivary-free testosterone and cortisol concentrations and their association with the subsequent competition outcomes in professional rugby league. J Strength Cond Res 2013; 27:471-6.
33. Lombardi G, Colombini A, Lanteri P, Banfi G. Reticulocytes in sports medicine: an update. Adv Clin Chem 2013; 59:125-53.
34. Van Renterghem P, Van Eenoo P, Sottas PE, Saugy M, Delbeke F. Subject-based steroid profiling and the determination of novel biomarkers for DHT and DHEA misuse in sports. Drug Test Anal 2010; 2:582-8.
35. Zofkova I. Hormonal aspects of the muscle-bone unit. Physiol Res 2008; 57(S):159-69.

BIOCHEMICAL ASSESSMENT OF GROWTH FACTORS AND CIRCULATION OF BLOOD COMPONENTS CONTAINED IN THE DIFFERENT FRACTIONS OBTAINED BY CENTRIFUGATION OF VENOUS BLOOD

M. CORIGIANO[1], G. CIOBANU[2], E. BALDONI[3] and G. POMPA[2]

[1]Private practice, Rome, Italy; [2]Department of Odontostomatological and Maxillofacial Sciences, Prosthodontics Unit, "Sapienza", University of Rome, Rome, Italy; [3]Department of Clinical and Odontostomatological Sciences, Dental Materials Unit,University of Sassari, Sassari, Italy

Received March 21, 2013 – Accepted February 17, 2014

The aim of this study was to evaluate a biochemical marker with different elements of a normal blood serum and centrifuged blood serum after a different rotation system. For this technique, we used five fractions of a blood Concentrated Growth Factors system (bCGF) and a particular device for the different rotation program. Blood samples were collected from 10 volunteers aged between 35 and 55 in the Operative Unit of the "Sapienza" University of Rome with only a fraction of different biochemical elements. Through an individual blood phase separator tube of venous blood, active factions of serum and 4 fractions of red buffy coat were taken. The biochemical markers with 14 elements were examined at times: P1-11 minutes, P2-12minutes, P3-15 minutes. Exclusively biological materials which are normally applied in the regeneration techniques for different defects and lesions were used with this technique. After specific rotation programs, a different result was obtained for each cycle: P1, P2, P3. In test tubes obtained by separated blood, we observed a higher concentration of proteins, ions, and other antigens compared to normal blood plasma. Examining the biochemical results of different elements, we observed an increase (P≤0,01). Since each person's DNA is different, we could not have the same results in 5 fractions of blood concentration, we did, however, find a good increase in only a fraction of proteins, immunoglobulin and different ions. We obtained five fractions after centrifugation, and we had an increase in different biochemical elements compared to normal blood (P≤0,01) which is significant at different times. These biochemical elements were stimulated by different growth factors, which are used by the immune system, and they induced the formation of hard and soft tissues and good regeneration.

The ultimate goal of regenerative medicine is the ability to obtain the regeneration of tissues through certain important cells such as stem cells (CS). Stem cells hold great promise for the future of regenerative medicine, tissue repair, and gene therapy, and such cell therapy could be employed in the repair of damaged non-hematopoietic tissue. These cells could spontaneously repopulate different organs such as muscle, bone, tendon, adipose, cartilage, marrow stoma, liver or heart and generate differentiated cells in response to acute or chronic organ damage. A more secure and optimal stimulation method to induce tissue regeneration without antigenic complications is the use of biological materials and

Key words: serum, plasma, blood concentration growth factors, protein, biological materials, biochemical element

Mailing address: Giorgio Pompa, MD, DDS,
Department of Odontostomatological,
and Maxillofacial Sciences,
"Sapienza", University of Rome,
Via Caserta, 6 00161 Rome, Italy
Tel.: +39 06 49976619 Fax: +39 06 49976619
e-mail: giorgio.pompa@uniroma1.it

0393-974X (2014)

growth factors in combination with physical devices for the modulation and induction of regenerative stimuli of the treated tissues.

For more than a decade, scientists have learned that our body is a potential source of therapeutically active proteins such as mitogenic, chemotactic, adhesive, angiogenic and anti-angiogenic proteins and neurothrophic factors as well as promising scaffold-like materials such as fibrin. In fact, there is a promising field known as "endogenous regenerative medicine", in which the patient's own plasma and platelet-derived cytokines and biologically active factors are used to stimulate wound healing and tissue regeneration (1, 2).

In research, we can find a different technique of biological material with different growth factors, such as Platelet Rich Plasma (PRP) (3), Plasma Rich in Growth Factors (PRGF) (4), Platelet Rich Fibrin (PRF) (5), blood Concentration Growth Factors (bCGF) (6, 7) which are based on the delivery of growth factors and bioactive proteins to localized sites to trigger healing and regenerative processes. In this technique, the most important finding is an intracellular storage pool of proteins vital to wound healing, which includes:

- Platelets:

(PDGF-AA, PDGF-AB, PDGF-BB-, -CC, and DD-isomes,PDGF receptors alfa and beta) (8).

- Growth factors:

Transforming growth factors (TGF-alfa, TGF-beta1,TGF-beta-2, TGF-beta-3) (9).

Fibroblast growth factors (FGFs-1,FGFs-18).

Insulin-like growth factors (IGF-I,IGF-II).

Vascular endothelial growth factor (VEGF).

Hepato growth factors (HGF).

- Cytokines and chemokines:

IL-1beta, IL-4, IL-6 ,TFN).

Growth factors are polypeptides that act as tools for intercellular communication and to control cell fate. In fact, they mediate many of the cellular functions including cell migration, proliferation, differentiation, metabolism and apoptosis (10). In both processes, precursor cells, growth factors and bone morphogenetic proteins are important elements.

Growth factors are soluble, diffusible, polypeptidic macromolecules which are produced by a great variety of cells. They have potent specific actions on the growth, differentiation and the genotype of numerous cell types, including condrocytes (11). These techniques are used in different branches of medicine such as: orthopaedics (sports medicine, including the repair of chronic tendinitis, repair of circulate ligament, knee osteoarthritis) (12-17); ophthalmology (dry eye symptoms, corneal epithelial defect) (18-19); neurosurgery (nerve regeneration) (17, 20); gastroenterology: (gastric ulcer healing) (21, 22); maxillary surgery: bone regeneration: (sinus lifting, atrophy edentulous bridges, in different defects of bone: cystic, tumors and different periodontal diseases), bone integration implant, revitalization of tooth with necrotic pulp (23-32); endocrinology (diabetic ulcer treatment) (33-36); plastic maxillofacial surgery: (facial plastic, eye plastic, cosmetic surgery) (37-40); consequences of BRONJ in hard and soft tissues (41-43); cardiovascular system; (angina myocardial, infarction myocardial) (44, 45); dermatology: (cosmetic treatment, hair growth) (46), oto-rhino-larynx (tympanic plastic) (47) (Table I).

These techniques are promising treatments within the different branches, but only our technique has a different preparation. Many studies examined the immunological and histological aspects, but did not apply a biochemical analysis. For this study we collected blood vessels and analysed biochemical samples from separators obtained from volunteers versus normal blood plasma, and reported the biochemical marker findings.

Blood concentration

Our study describes 5 fractions of blood, Vlad 3|10, (Fig. 1):

- The upper phase (fr. I) is represented by serum (blood plasma without fibrinogen and coagulation factors). This phase is used for fine interventions in immunotherapy, analgesic and anti-inflammatory. After a bio-chemical examination of this serum, more elements, proteins, albumins, ions (Magnesium, Iron, Calcium, Zinc and Phosphorous), immune-globulins, and Amylase were found (48).
- The next fraction (fr. II) was composed of a block of polymerized fibrin (a clot); very large and dense (white fibrin buffy coat-cloud). Within this clot, we found a rich source of Growth Factor (49). This clot could be used to help fill wounds; as a vehicle for active substances or drugs; placed around

implants. It could be mixed with synthetic material; heterologous material; as autologous material to create different products; and also as a biological membrane (Carpet).

- The next fraction (fr. III) was the red fibrin buffy coat and mixed red and white cells. This contained Fibrin, which after 5 days changed to Growth Fibroblasts. CD34+ was also found within this fraction which may indicate the presence of stem cells. This fraction was mixed with antilogous, autologous, heterologous or synthetic bone to give better regeneration.
- The next fraction (fr. IV) was a viscous red clot which was dense and rich in erythrocytes and platelets. It is also called red buffy coat. There were growth factors within the fraction, which means that it is very useful in regeneration; however, it could be used as filler in large wounds.
- The final fraction (fr. V) red substance was a clot rich in different proteins and metal ions (iron, calcium, magnesium etc.). This fraction is mixed with autologous, heterologous or synthetic bone in the edentulous atrophy jaws to give better regeneration.

The purpose of this study was to collect and analyze biochemical samples obtained from the venous vessels which used five fractions in regenerative medicine.

MATERIALS AND METHODS

We collected blood samples for biochemical examination from 10 volunteers (5 males and 5 females), aged between 35 and 50 years (Table I), 5 non-smokers and 5 smokers. We examined the biochemical markers of normal blood compared with centrifuged blood (separator Vlad 3/10). The reason for this exam between normal blood and centrifuged blood was to monitor elements which could be used as a remedy in regenerative medicine. Blood samples were treated by a Vlad 3\10 blood separator (Vlad 3\10, HTB Italy) according to the manufacturer's instructions.

In this experiment, we examined 5 fractions which were obtained in the blood separator, comparing them to the biochemical elements of normal blood. The main factors studied in this procedure and the main means of growth factors are: protein, amylase, albumin, IgG, IgM, IgA, calcium, Fe, potassium, Na, Cl, Mg, Pho, creatine. The results showed an incredible growth in albumin, immunoglobulin, proteins, amylase and calcium. All 5 fractions were examined at 3 different time-points: 1: 11 min of separation (P1) (Table IIIa); 2: 12 min of separation (P2) (Table IIIb); 3: 15 min of separation (P3) (Table IIIc).

Preparation and examination of centrifuged and normal blood

From each volunteer, we collected 7 tubes of intravenous blood, 6 tubes without anticoagulant in 9 ml (Vacuette® greiner bio-one) glass-coated plastic tubes at 2G capacity. These tubes were placed in a Vlad 3/10 blood separator, and 1 tube with 6 ml capacity was taken from venous blood as a control of normal blood (plasma). Different time-points were used for each tube and cycle. The first cycle was 11 min, the second cycle was 12 min and the last cycle was 15 min. At the same time, 5 fractions were examined, and a biochemical comparison was made to normal blood (Table IV). In all fractions obtained, we examined 14 elements: protein, amylase, Na, potassium, chlorine, calcium, Mg, Pho, Fe, IgM, IgA, IgG, albumin, creatine (Table IV).

In all, sixty tubes of blood samples were collected, which were used for the preparation of bCGF.

After the blood separation, we obtained 5 fractions with a different consistency for each time (Fig 1). For each patient on the same day, we examined 2 tubes (Vacuette®) at 11 min, another 2 tubes (Vacuette®) at 12 min, another 2 tubes (Vacuette®) at 15 min, and one tube 6 ml BD Vacutainer® (LH 102 LU,UK) with a blood normal.

Each fraction was cut from tubes and put into kit bCGF, and then put into small tubes. These tubes were then sent to the biochemistry laboratory of the Polyclinic Operative Unit of the Sapienza University of Rome for examination of 14 markers. We observed the biochemical marker immediately using the Roche Hitachi Cobas 60000 in the first and second fraction.

We were not able to read the other 3 fractions (Fr. III, Fr. IV, Fr.V) because we did not have a good clot condensation. Therefore, we put the 3 fractions in special 5-ml tubes (BD Vacutainer, SST® II Activator, UK) and centrifuged for 4 min. After centrifuge, we obtained plasma from these 3 fractions. The five fractions were obtained at 11 min, 12 min, and 15 min together with tubes of normal blood plasma and examined14 biochemical markers in the Roche Hitachi and obtained a different result. These 7 tubes were collected immediately and kept at a constant temperature of 37°C.

The 2 groups of patients were matched by age, gender, dominance growth factor of blood concentration versus normal blood, mass index $p \geq 0.01$. The experimental results (Table IIIa-c) were correlated using student's *t*-tests. These tests were performed for 5 fractions, which were different at the various time. We observed the biochemical findings in the clinical research, and we found that the procedure was well balanced and comparable within the

group. The VAS score was found to be significant in the blood concentration of growth factors at the time sof P1, P2, P3 and normal blood.

A group of 10 people were examined at 11 minutes (P1)

Each experiment was repeated with 6 samples, for each person, resulting in 56 samples per group ($p \leq 0.01$, student *t*-test). All fractions were compared to each other and normal blood (Table IV).

Calcium level serum in (fr. I) was significantly different than (fr. III) GFs, (fr. IV) red clot, (fr. V) red substance; and (fr. II) white clot was significantly different to (fr. III) GFs, (fr. IV) red clot, and for (fr. III) GFs, (fr. IV) red clot, (fr. V) red substance than normal blood.

Magnesium levels (fr. I) serum and (fr. II) white clot were significantly different to (fr. III) GFs,(fr. IV) red clot, (fr. V) red substance where the biggest difference was p=0.034. Phosphate levels for (fr. I) serum was statistically lower than (fr. IV) red clot. Iron levels in (fr. I) serum were significantly different to (fr. III) GFs, (fr. IV) red clot, (fr. V) red substance.

IgG levels (fr. I) serum were statistically lower than (fr. II) white clot, (fr. III) Gfs, (fr. V) red substance; (fr. III) GFs. They were significantly different to (fr. V) red substance and the (fr. V) red substance was statistically lower p=0.01 than normal blood.

IgA levels in (fr.II) white clot were significantly different to (fr.IV) red clot p=0.03 and (fr.V) red substance than normal blood (p=0.01). IgM levels in (fr.III) GFs were lower than (fr.IV) red clot, (fr.IV) red clot than (fr.V) red substance but in (fr.V) red substance was statistical lower than normal blood.

These immune-globulins have a very important role and they were found to be above the membrane of lymphocytes seen in the (fr. V) red substance. Creatine level in (fr. III) GFs were statistically different than normal blood. Albumin levels of (fr.III) GFs are the highest significant differences with (fr.V) red substance.

There were no significant differences in protein. There was a slight increase of Amylase in (fr. V) red substance, (fr. II) white clot and (fr .IV) red clot was statistically lower than (fr. V) red substance. Phosphorus levels in (fr. I) serum were significantly different to (fr. IV) red clot, and (fr. III) GFs was significantly statistically lower than normal blood (Table IV). Sodium, chlorine, and creatine were not statistically different. These elements are significant in blood plasma (Fig. 2).

A group of 10 people were examined at 12 minutes (P2)

The mean Vas score was significantly higher than the plasma normal blood at P2 (time 12 min) where the blood concentration was $p \leq 0.01$. At P2 (time 12 min.), we obtained growth biochemical markers in the ions of Ca, Mg, Phosphate, Iron, and in a better concentration than normal blood (Fig. 2).

Calcium level in (fr. I) serum and (fr. I) white clot were significantly different than (fr. III) GFs, (fr. IV) red clot; and (fr. III) GFs was significantly different to (fr. V) red substance and normal blood and (fr. IV) red clot than (fr. V) red substance and normal blood.

With magnesium we only had significant differences in (fr. III) GFs p=0.044 than normal blood. Phosphate in (fr. I) serum and (fr. II) white clot was significantly lower than (fr. III) GFs and (fr. III) GFs than (fr. V) red substance. There was a small difference in iron between all the fractions p=0.04.

We obtained good IgG levels in (fr. I) serum and (fr. I) white clot where it was significantly different to (fr. V) red substance. In (fr. II) white clot was significantly lower than normal blood. The biochemical elements IgM in (fr. IV) red clot was significantly different to (fr. V) red substance, and (fr. IV) red clot was statistically lower than normal blood concentration p=0.044. Creatine levels in (fr. I) serum and (fr. II) white clot were statistically different to (fr. III) GFs, (fr. IV) red clot, (fr. V) red substance; and (fr. IV) red clot was statistically lower than normal blood. Albumin levels in (fr. I) serum, (fr. II) white clot, were significantly different to (fr. III) GFs, (fr. IV) red clot, (fr. V) red substance, but (fr. III) GFs and (fr. IV) red clot was statistically lower than normal blood.

At P2 time, the protein was statistically lower than P1 time. For example, (fr. II) white clot was significantly different to (fr. V) red substance, but Amylase levels in (fr. II) white clot were statistically lower than normal blood.

Sodium levels in (fr. II) white clot, (fr. III) GFs, (fr. V) red substance were statistically lower than normal blood. Potassium levels in (fr. I) serum and (fr. II) white clot were statistically lower than (fr. III) GFs; (fr. III) GFs (fr. IV) red clot were significantly different to normal blood p=0.02. Chorine levels in (fr. I) serum were significantly lower than (fr. V) red substance p=0.034 (Table IV, Fig. 2).

A group of 10 people were examined at 15 minutes (P3)

The biochemical results at P3 time showed better growth of protein than P1 time and P2 time. There were highly significant differences in (fr. I) serum, (fr. II) white clot, (fr. III) GFs, and (fr. III) GFs, (fr. IV) red clot, (fr. V) red substance was significantly lower than other fractions and normal blood maxim.

Amylase levels in (fr. I) serum were significantly different to (fr. IV) red clot p=0.03. For (fr. II) white clot, and (fr. V) red substance, it was statistically lower than normal blood p=0.02, whose marker characterizes pancreas (50), and the high levels found in the fraction I, III, IV, V (Fig. 2) are statistically significant in respect to

normal blood.

Sodium levels in (fr. I) serum were significantly different to (fr. V) red substance and (fr. II) white clot. Sodium levels in (fr. III) GFs were statistically lower than normal blood. Potassium levels in (fr. I) serum, (fr. II) white clot, (fr. III) GFs were significantly different to (fr. III) GFs, (fr. V) red substance and normal blood. Chlorine levels in (fr. I) serum, (fr. II) white clot, (fr. IV) red clot were significantly different to (fr. III) GFs, (fr. IV) red clot, (fr. V) red substance and normal blood. Albumin levels in (fr. I) serum, (fr. II) white clot, were significantly different to (fr. III) Gfs, (fr. IV) red clot and (fr. III) GFs, (fr. IV) red clot statistically lower than normal blood. IgM levels in (fr. I) serum, (fr. II) white clot were significantly different to (fr. III) GFs, (fr. IV) red clot, (fr. V) red substance, and the red clot (fr. IV) was statistically lower than normal blood p=0.04 (Table IV, Fig. 2). IgA levels in (fr. I) serum, (fr. II) white clot, were statistically significant than (fr. III)

Table I. *Application of blood has been extended to many different fields.*

Application
Orthopaedics 1. Repair of chronic tendinitis 2. Repair of circulate ligament 3. Sport medicine 4. Osteoarthritis knee
Ophthalmology 1. Dry eye symptoms 2.Cornial epithelial defect
Oto -rhino-laryngologist Tympanoplasty
Neurosurgery Nerve regeneration
Gastroenterology Gastric ulcer healing
Bone regeneration 1. Sinus lifting 2. Atrophy edentulous bridges. In different bone defects (cystic, tumour and different periodontal diseases). 3. Osseointegration implant
Revitalization of tooth with necrotic pulp
Endocrinology Diabetic ulcer treatment
Plastic Maxillofacial surgery 1. Facial plastic 2. Eye plastic 3. Cosmetic surgery
Consequences of BRONJ in hard and soft tissues
Cardiovascular System 1. Angina myocardia 2. Infarction miocardic
Dermatology 1. Cosmetic treatment 2. Hair growth

Table II. *Baseline characteristics of patients. Table shows gender, number of patients, the age of the patients and smoking habit (smoking or non smoking).*

Patient	Gender	AGE	Smoking Habit
1	M	35	non
2	F	50	smoking
3	F	57	non
4	F	44	smoking
5	M	39	non
6	M	48	smoking
7	M	55	non
8	F	38	smoking
9	F	45	non
10	M	37	smoking
		44.8±7.656	

GFs, (fr. IV) red clot and normal blood. Red clout (fr. IV) was statistically lower than normal blood p=0.033. IgA levels in (fr. II) white clout were statistically different to normal blood p=0.01.

In the fraction GFs, red clot and red substance, we found a higher concentration of immunoglobulin than the other fractions and normal blood (Fig. 2). Phosphate levels in serum (fr. I) and white clot (fr. II) were significantly different to GFs (fr. III). Magnesium levels in serum, white clot, GFs were significantly lower than red buffy clot. Iron levels in (fr. II) white clot, (fr. III) GFs, (fr. IV) red clot were significantly lower than (fr. III) GFs, additionally, there were statistical differences in magnesium levels in (fr. IV) red clot, (fr. V) red substance and (fr. IV) red clot compared to normal blood p=0.031.

Concentration of calcium levels in serum (fr. I) and white clot (fr. II) were significantly different to GFs (fr. III), but the white clot (fr. II) was statistically lower than red buffy clot (fr. IV). Concentration of calcium levels in serum (fr. I) and white clot (fr. II) were significantly different to GFs (fr. III), but the white clot (fr. II) was statistically lower than red buffy clot (fr. IV). Concentration of calcium in (fr. III) GFs and (fr. IV) red clot was significantly different to normal blood, and these elements play a role in skeletal bone (Table IV).

Normal blood was compared to every type of centrifuged fraction at P1.The main biochemical components were Ca, IgG, IgM, IgA, creatine, and sodium ($p \leq 0.01$). We obtained a good concentration of biochemical markers in different fractions and different P2 and P3 time in Ca, Mg, Fe, IgM, IgG, IgA, creatinine, albumin, amylase, sodium and potassium where there were significant differences compared to normal blood (Table IV).

RESULTS

The biochemical elements of bCGF and normal blood markers (Table II), with student's *t*-test were examined and calculated. We obtained a significant difference between serum (fr. I), white clot (fr. II) and GFs (fr. III), red buffy clot (IV), red substance (fr. V) and all fractions were compared to one another. The values obtained in bCGF in the different fractions and normal blood varied from sample to sample. A student's *t*-test revealed the differences to be statistically significant ($p \leq 0.01$). After follow-up, we obtained results in the concentration of biochemical components in fraction III-serum, fraction IV-red clot, fraction V-red substance.

The differences between the three groups were significant (student's *t*-test). At P1time (11 min, $p \leq 0{,}01$) there were the most significant ion elements: sodium, potassium, chlorine, calcium ,magnesium, phosphate, IgG, IgA, IgM and creatine characteristics for fraction III, fraction IV, fraction V, but in fraction II there was a significant IgA and Cl. At P1 time, protein, amylase and iron elements did not statistically decrease significantly compared to bCGF among the 5 fractions.

At P2 time (12 min, $p \leq 0{,}01$) a statistically significant biochemical marker was phosphate, but within a significant range there were IgG, IgA, IgM, albumin creatine, iron, magnesium, calcium, potassium, sodium, amylase, and protein characteristic for (fr. III) GFs, (fr. IV) red clot, (fr. V) red substance. In fraction II sodium, potassium, IgM and albumin were statistically significant (p=0.04). At P3 time (15 min) not significant ($p<0.01$) in IgM biochemical marker, but in the(fr. III)-GFs, (fr. IV)-red clot and (fr. V)-red substance with all significant components (Table IV), in the fraction II albumin, magnesium, calcium were significant.

We achieved significant results at P1 time (11 min), P2 time (12 min), and P3 time (15 min), but we had a greater significance in P1 (p=0.061) (fr. IV)-red clot), in P2 (p=0.042), (fr.IV)-red clot and (fr.V)-red substance, in P3 (p=0.047), (fr.III)-GFs and (fr. IV)-red clot. After calculating results at different

Table IIIa. *Mean of 14 biochemical markers in different types of fractions in comparison with normal blood (n=10).*

	Normal Blood	P(1) 11min				
		FR.I	FR.II	FR.III	FR.IV	FR.V
	Mean±SD	Mean±SD	Mean±SD	Mean±SD	Mean±SD	Mean±SD
Protein(g/dL)	7.12±0.239	6.97±0.427	7.021±0.3	7.073±0.335	7.329±0.721	7.1±0.309
T-Amylasy(U/L)	63.5±21.46	62±23.18	63.4±22.23	62.201±22.46	61.8±22.72	63.59±23.48
Sodium(mmol/L)	138.3±3.02	133.5±9.3	135.4±5.87	133.8±5.977	131.99±14.45	137.4±3.339
Potassium(mmol/L)	4.136±0.605	3.848±0.386	3.945±0.432	4.436±0.818	4.658±0.886	4.202±0.598
Chlorine(mmol/L)	101.81±4.187	98.26±9.299	99.59±6.524	99.33±6.332	95.04±14.63	102.7±6.486
Calcium(mmol/L)	2.306±0.125	2.333±0.11	2.388±0.161	2.51±0.155	2.631±0.408	2.424±0.097
Magnesium(mmol/L)	0.683±0.208	0.734±0.049	0.738±0.06	0.767±0.094	0.798±0.131	0.793±0.082
Phosphate(mmol/L)	1.178±0.144	1.132±0.163	1.128±0.165	1.24±0.11	1.296±0.332	1.189±0.156
Iron(umol/L)	15.565±5.279	14.046±5.025	14.612±4.516	14.972±5.145	15.309±4.847	15.246±5.127
IgG(g/L)	10.637±1.169	10.498±1.43	10.759±1.347	10.637±1.294	10.12±2.43	10.986±1.176
IgA(g/L)	1.698±0.415	1.773±0.549	1.753±0.471	1.725±0.585	1.632±0.532	1.738±0.407
IgM(g/L)	1.255±0.541	1.193±0.475	1.149±0.545	1.358±0.477	1.194±0.599	1.306±0.568
Creatine(mg/dL)	0.754±0.147	0.708±0.13	0.748±0.127	0.706±0.162	0.692±0.218	0.732±0.153
Albumin(g/L)	45.62±1.954	45.38±2.172	46.76±2.434	44.91±2.161	46.011±2.295	46.46±2.778

Table IIIb. *Mean of 14 biochemical markers in different typse of fractions in comparison with normal blood (n=10).*

	Normal Blood	P(2) 12 min				
		FR.I	FR.II	FR.III	FR.IV	FR.V
	Mean±SD	Mean±SD	Mean±SD	Mean±SD	Mean±SD	Mean±SD
Protein(g/dL)	7.12±0.239	6.84±0.236	6.72±0.342	6.89±0.375	6.94±0.313	7.02±0.244
Amylasy(U/L)	63.5±21.46	61.2±22.29	60.3±20.28	61.7±23.17	58.9±23.9	60.8±21.31
Sodium(mmol/L)	138.3±3.02	136.3±7.818	133.9±7.752	134.8±6.014	132.5±10.11	135.9±5.839
Potassium(mmol/L)	4.136±0.605	4.135±0.43	4.091±0.455	4.762±0.996	4.639±1.144	4.338±0.759
Chlorine(mmol/L)	101.81±4.18	99.3±6.139	98.34±6.628	100.83±7.11	99.45±6.853	101.67±5.33
Calcium(mmol/L)	2.306±0.125	2.37±0.235	2.363±0.131	2.562±0.359	2.486±0.111	2.348±0.144
Magnesium(mmol/L)	0.683±0.208	0.717±0.092	0.73±0.082	0.713±0.225	0.707±0.223	0.734±0.057
Phosphate(mmol/L)	1.178±0.144	1.146±0.169	1.119±0.211	1.274±0.126	1.222±0.189	1.049±0.314
Iron(umol/L)	15.565±5.27	16.76±6.118	17.068±5.24	18.175±7.55	19.805±7.971	17.41±6.615
IgG(g/L)	10.637±1.16	10.468±1.219	10.482±1.47	10.121±1.59	10.055±1.422	10.71±1.307
IgA(g/L)	1.698±0.415	1.69±0.433	1.629±0.425	1.637±0.451	1.675±0.424	1.74±0.44
IgM(g/L)	1.255±0.541	1.136±0.526	1.134±0.543	1.213±0.588	1.211±0.58	1.282±0.544
Creatine(mg/dL)	0.754±0.147	0.75±0.162	0.723±0.175	0.66±0.244	0.677±0.185	0.745±0.153
Albumin(g/L)	45.62±1.954	45.7±1.252	44.988±2.32	42.422±5.92	44.161±2.375	46.561±2.34

times, centrifugation obtained error bars in IgA, IgG, IgM, albumin, iron, amylase, calcium potassium, phosphate, creatine, magnesium represent mean ± SD for 14 biochemical elements $p \leq 0,01$ and a substantial difference between the fractions, normal blood, and time (Fig. 2). We found that the separation of blood at different times, obtained with particular separator, all of the fractions were significant ($p \leq 0.01$) versus

Table IIIc. *Mean of 14 biochemical markers in different types of fractions in comparison with normal blood (n=10).*

	Normal Blood	P(3) 15 min				
		FR.I	FR.II	FR.III	FR.IV	FR.V
	Mean±SD	Mean±SD	Mean±SD	Mean±SD	Mean±SD	Mean±SD
Protein(g/dL)	7.12±0.239	6.96±0.201	6.74±0.313	7.05±0.25	7.01±0.317	7.12±0.348
Amylasy(U/L)	63.5±21.46	67.8±29.58	61.85±19.94	63.051±22.48	58.206±23.08	63.729±21.92
Sodium(mmol/L)	138.3±3.02	138.2±5.159	134.8±9.271	137.2±8.337	131.6±9.743	137.1±4.724
Potassium(mmol/L)	4.136±0.605	4.035±0.442	4.001±0.514	5.023±0.989	5.108±2.869	4.408±0.53
Chlorine(mmol/L)	101.81±4.187	101.07±6.195	97.18±7.271	100.34±7.591	96.45±6.459	100.781±4.462
Calcium(mmol/L)	2.306±0.125	2.324±0.109	2.366±0.089	2.503±0.128	2.597±0.22	2.416±0.129
Magnesium(mmol/L)	0.683±0.208	0.672±0.206	0.674±0.203	0.673±0.235	0.751±0.244	0.738±0.059
Phosphate(mmol/L)	1.178±0.144	1.173±0.143	1.153±0.154	1.288±0.117	1.229±0.16	1.137±0.203
Iron(umol/L)	15.565±5.279	15.914±4.008	15.216±5.367	16.252±5.403	18.134±6.632	15.662±4.936
IgG(g/L)	10.637±1.169	10.41±1.132	10.44±1.358	10.823±1.422	10.129±1.553	10.46±1.31
IgA(g/L)	1.698±0.415	1.703±0.405	1.77±0.564	1.73±0.515	1.703±0.563	1.728±0.403
IgM(g/L)	1.255±0.541	1.266±0.56	1.265±0.627	1.323±0.631	1.19±0.596	1.331±0.618
Creatine(mg/dL)	0.754±0.147	0.738±0.137	0.697±0.157	0.72±0.165	0.682±0.192	0.732±0.151
Albumin(g/L)	45.62±1.954	46.31±1.707	45.061±2.673	46.5±2.692	44.591±2.113	45.69±3.75

Table IV. *The evaluations represent the average of the concentration values obtained by analyzing the venous blood of ten patients.*

a		Protein (g/dl)					Amylasy(U/L)					Sodium(U/L)					Potassium(mmol/L)				
		Fr(I)	Fr(II)	Fr(III)	Fr(IV)	Fr(V)	Fr(I)	Fr(II)	Fr(III)	Fr(IV)	Fr(V)	Fr(I)	Fr(II)	Fr(III)	Fr(IV)	Fr(V)	Fr(I)	Fr(II)	Fr(III)	Fr(IV)	Fr(V)
P(I) Time 11 min	Fr(I)	-	-	-	-	-	-	-	-	-	-	-	-	-	-	-	-	-	-	-	-
	Fr(II)	-	-	-	-	-	-	-	-	-	-	-	-	-	-	-	0.042	-	-	-	-
	Fr(III)	-	-	-	-	-	-	-	-	-	-	-	-	-	-	-	0.016	0.015	-	-	-
	Fr(IV)	-	-	-	-	-	-	0.029	-	-	-	-	-	-	-	-	-	0.010	-	-	-
	Fr(V)	-	-	-	-	-	-	-	-	0.020	-	--	-	0.018	-	-	0.0-21	0.023	0.038	0.025	-
	Normal blood	-	-	-	-	-	-	-	-	-	-	-	-	0.033	-	-	-	-	0.023	0.022	-
P(II) Time 12min	Fr(I)	-	-	-	-	-	-	-	-	-	-	-	-	-	-	-	-	-	-	-	-
	Fr(II)	-	-	-	-	-	-	-	-	-	-	0.044	-	-	-	-	-	-	-	-	-
	Fr(III)	-	0.037	-	-	-	-	-	-	-	-	-	-	-	-	-	0.010	-	-	-	-
	Fr(IV)	-		-	-	-	-	-	-	-	-	-	-	-	-	-	-	-	-	-	-
	Fr(V)	-	0.010	-	-	-	-	-	-	-	-	-	-	-	-	-	-	-	-	-	-
	Normal blood	-	-	0.044	-	-	-	0.022	-	-	0.028	-	0.044	0.047	-	0.036	-	-	0.022	0.026	-
P(III) Time 15min	Fr(I)	-	-	-	-	-	-	-	-	-	-	-	-	-	-	-	-	-	-	-	-
	Fr(II)	-	-	-	-	-	-	-	-	-	-	-	-	-	-	-	-	-	-	-	-
	Fr(III)	0.041	-	-	-	-	-	-	-	-	-	-	-	-	-	-	-	-	-	-	-
	Fr(IV)		0.034	-	-	-	0.036	-	-	-	-	0.037	-	-	-	-	-	-	-	-	-
	Fr(V)	0.029	-	-	-	-	-	-	-	-	-	-	-	-	-	-	0.017	0.022	-	-	-
	Normal blood	-	-	0.044	-	-	-	0.022	-	-	0.028	-	0.044	0.047	-	0.036	-	-	0.022	0.026	-

normal blood. Regardless of time of centrifuge, all 14 items were highly significant ($p \leq 0.01$) in (fr. III) GFs, (fr. IV) red clot, (fr. V) red substance, but significantly lower in normal blood ($p \leq 0.01$).

DISCUSSION

The analysis of our results makes it possible to form significant working hypotheses concerning the

b

		Chlorine(mmol/L)					Calcium (mmol/L)					Magnesium (mmol/L)					Phosphate (mmol/L)				
		Fr(I)	Fr(II)	Fr(III)	Fr(IV)	Fr(V)	Fr(I)	Fr(II)	Fr(III)	Fr(IV)	Fr(V)	Fr(I)	Fr(II)	Fr(III)	Fr(IV)	Fr(V)	Fr(I)	Fr(II)	Fr(III)	Fr(IV)	Fr(V)
P(I) Time 11 min	Fr(I)	-	-	-	-	-	-	-		-	-	-	-	-	-	-	-	-	-	-	-
	Fr(II)	-	-	--	-	-	-	-	-	-	-	-	-	-	-	-	-	-	-	-	-
	Fr(III)	-	-	-	-	-	-	-	-	-	-	-	-	-	-	-	-	-	-	-	-
	Fr(IV)	-	-	-	-	-	0.012	0.042	-	-	-	0.037	-	-	-	-	-	-	-	-	-
	Fr(V)	0.041	0.041	0.026	0.041	-	0.014	-	0.029	0.061	-	0.034	0.040	-	--	--	-	-	-	-	-
	Normal blood	-	-	-	-	-	-	-	-	-	-	-	-	-	-	--	-	-	-	-	-
P(II) Time 12 min	Fr(I)	-	-	-	-	-	-	-	-	-	-	-	-	-	-	-	-	-	-	-	-
	Fr(II)	-	-	-	-	-	-	-	-	-	-	-	--	-	-	-	-	-	-	-	-
	Fr(III)	-	-	-	-	-	-	0.021	-	-	-	-	-	-	-	-	-	-	-	-	-
	Fr(IV)	-	-	-	-	-	0.036	0.002	-	-	-	-	-	-	-	-	-	-	-	-	-
	Fr(V)	0.034	-	-	-	-	-	-	0.046	-	-	-	-	-	-	-	-	-	0.032	-	-
	Normal blood	-	-	-	-	-	-	-	0.031	-	-	-	-	0.045	-	-	-	-	-	-	-
P(III) Time 15 min	Fr(I)	-	-	-	-	-	-	-	-	-	--	-	-	-	-	-	-	-	-	-	-
	Fr(II)	0.025	-	-	-	-	0.011	-	-	-	-	-	-	-	-	-	-	-	-	-	-
	Fr(III)	-	0.041	-	-	-	-	-	-	-	-	-	-	-	-	-	-	-	-	-	-
	Fr(IV)	0.027	-	-	-	-	-	-	0.017	-	-	-	-	0.022	-	-	-	-	-	-	-
	Fr(V)	-	-	-	0.034	-	0.047	-	0.023	-	-	-	-	-	-	-	-	-	-	-	-
	Normal blood	-	-	-	-	-	-	-	0.031	-	-	-	-	0.045	-	-	-	-	-	-	-

c

		Iron (umol/L)					IgG (g/L)					IgA (g/L)					IgM (g/L)				
		Fr(I)	Fr(II)	Fr(III)	Fr(IV)	Fr(V)	Fr(I)	Fr(II)	Fr(III)	Fr(IV)	Fr(V)	Fr(I)	Fr(II)	Fr(III)	Fr(IV)	Fr(V)	Fr(I)	Fr(II)	Fr(III)	Fr(IV)	Fr(V)
P(I) Time 11 min	Fr(I)	-	-	-	-	-	-	-	-	-	-	-	-	-	-	-	-	-	-	-	-
	Fr(II)	-	-	-	-	-	0.022	-	-	-	-	-	-	-	-	-	-	--	-	-	-
	Fr(III)	-	-	-	-	-	0.033	-	-	--	-	-	-	-	-	-	-	-	-	-	-
	Fr(IV)	-	--	-	-	-	-	-	-	-	-	-	0.031	-	-	-	-	-	0.018	-	-
	Fr(V)	-	--	-	-	-	-	0.033	-	0.040	-	-	-	-	0.031	-	-	-	-	0.023	-
	Normal blood	-	-	-	-	-	-	-	-	-	0.015	-	-	-	-	0.018	-	-	-	-	-
P(II) Time 12 min	Fr(I)	-	-	-	-	-	-	-	-	-	-	-	-	-	-	-	-	-	-	-	-
	Fr(II)	-	-	--	-	-	-	-	-	-	--	0.044	-	-	-	-	-	-	-	-	-
	Fr(III)	-	-	-	-	-	-	-	-	-	-	-	-	-	-	-	-	-	-	-	-
	Fr(IV)	0.026	-	0.021	-	-	-	-	-	-	-	-	-	-	-	-	-	-	-	-	-
	Fr(V)	-	-	-	0.041	-	0.013	-	-	0.025	-	-	-	0.027	0.010	-	-	-	-	-	-
	Normal blood	-	-	-	0.031	-	-	-	-	0.033	-	-	0.011	-	-	-	-	-	-	0.045	-
P(III) Time 15 min	Fr(I)	-	-	-	-	-	-	-	-	-	-	-	-	-	-	-	-	-	-	-	-
	Fr(II)	-	-	-	-	-	-	-	-	-	-	-	-	-	-	-	-	-	-	-	-
	Fr(III)	-	0.027	-	-	-	-	0.047	-	-	-	-	-	-	-	-	-	0.016	-	-	-
	Fr(IV)	-	0.034	--		-	-	-	0.021	-	-	-	-	-	-	-	0.029	-	0.020	-	-
	Fr(V)	-	-	0.012	0.044	-	-	-	-	-	-	-	-	-	-	-	0.028	-	-	-	-
	Normal blood	-	-	-	0.031	-	-	-	-	0.033	-	-	0.011	-	-	-	-	-	-	0.045	-

d

		Creatine(mg/dL)					Albumin(g/L)				
		Fr(I)	Fr(-II)	Fr(III)	Fr(IV)	Fr(V)	Fr(I)	Fr(II)	Fr(III)	Fr(IV)	Fr(V)
P(I) Time 11 min	Fr(I)	-	-	-	-	-	-	-	-	-	-
	Fr(II)	-	-	-	--	-	0.032	-	-	-	-
	Fr(III)	-	0.015	-	-	-	-	0.022	-	-	-
	Fr(IV)	-	-	-	-	-	-	-	0.039	-	-
	Fr(V)	-	-	0.019	-	-	-	-	-	-	-
	Normal blood	-	-	-	-	-	-	-	-	-	0.015
P(II) Time 12 min	Fr(I)	-	-	-	-	-	-	-	-	-	-
	Fr(II)	-	-	-	-	-	-	-	-	-	-
	Fr(III)	0.040	-	-	-	-	-	-	-	-	-
	Fr(IV)	-	-	-	-	-	-	-	-	-	-
	Fr(V)	-	0.045	-	-	-	-	0.043	0.028	-	-
	Normal blood	-	-	-	-	-	-	-	0.042	0.036	-
P(III) Time 15 min	Fr(I)	-	-	-	-	-	-	-	-	-	-
	Fr(II)	-	-	-	-	-	-		-	-	-
	Fr(III)	-	0.038	-	-	-	-	0.049	-	-	-
	Fr(IV)	0.026	-	--	-	-	-	-	-	-	-
	Fr(V)	-	0.016	-	-	-	-	-	-	-	-
	Normal blood	-							0.042	0.036	

Values expressed by the significant difference in the concentration of total protein in the different phases of the bCGF. Comparisons were also made between same parameters of concentration in different phases The exam parameters were compared to untreated venous blood. All data is shown in the table. Concentration of 14 biochemical elements, in different time and fraction $p \leq 0.01$

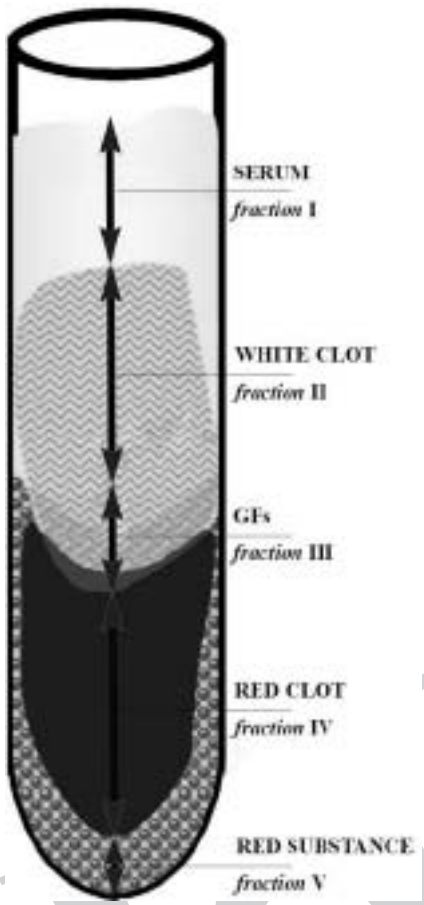

Fig. 1. *Schematic representation of the 5-fraction centrifugation obtained after bCGF.*

biological concentration of growth factors in blood. After comparing our results with those obtained by other authors and a vast range of PRP protocols (3), PRGF (4), PRF (2), we found that we could use the 5 fractions of blood without anticoagulants in regenerative medicine with the bCGF technique. Each fraction has a certain concentration of markers which are used in medicine, which have anti-inflammatory, anti-hemorrhagic, regenerative, and pain-killing properties.

Each fraction was centrifuged at different times which can be distinguished by:

- Amount of fractions obtained in tubes
- Density
- Degree of polymerization.
- Biochemical characteristic markers (Table III)

Current research under discussion identifies 3 types of therapeutic concepts: Platelet rich plasma (PRP), Platelet rich growth factors (PRGF), Platelet rich fibrin (PRF), for examination. These are 3 fractions, but our protocols suggested that the production of markers were found in (fr. III) serum, (fr. IV) red clot, (fr. V) red substance, such as immunoglobulin, protein, albumin, calcium, amylase, iron, potassium, phosphate, magnesium, creatine. There were cells found in branches of platelets which suggest a positive influence on the migration and proliferation of a number of cell types. Bioactive growth factors and chemokine may trigger platelet activation including Transforming Growth Factors (TGF-β1 and β1), Platelet-Derived Growth Factors (PDGF-AA, AB, BB), Vascular Endothelial Growth Factors (VEGF-A and C), Insulin Like Growth Factor (IGF-1) which is found in pancreatic amylase in (fr. III) GFs, (fr. IV) red clot, (fr. V) red substance, Epidermal Growth Factors (EGF) and Hepatic Growth Factors (HGF). These promote local angiogenesis, stem cell homing, cell migration, proliferation and differentiation and deposition of proteins which play a key role in the restoration of hard and soft tissues. But most important, we have α-granules in platelets. These α-granules, found in thrombin (red buffy coat), are united by a membrane within which many vital proteins are found such as PDGF, IGF-β, IGF-I. These form a good biological stat.

Recent studies in lymphocytes demonstrate that some cells can divide and reproduce a new cell (51). Attendant lymphocytes, immunoglobulins are found above the membrane. Also, in red substance and red clot, we found many immunoglobulins, proteins, and calcium. We can demonstrate that the last three fractions (fr. III, fr. IV, fr. V) had a concentration of major elements which are important factors in regenerative medicine. In regenerative medicine, proteins have an important role. They stimulate the growth and development of new blood vessels (angiogenesis) that contribute to the pathogenesis of several diseases (i.e. cancer, atherosclerosis) normal wound healing, development in the hard and soft tissues (52), and these proteins stop bone resorption, as well as trigger rapid maturation of collagen in early wound healing.

In the current research, the only biochemical marker (immunoglobulin), protein, albumin,

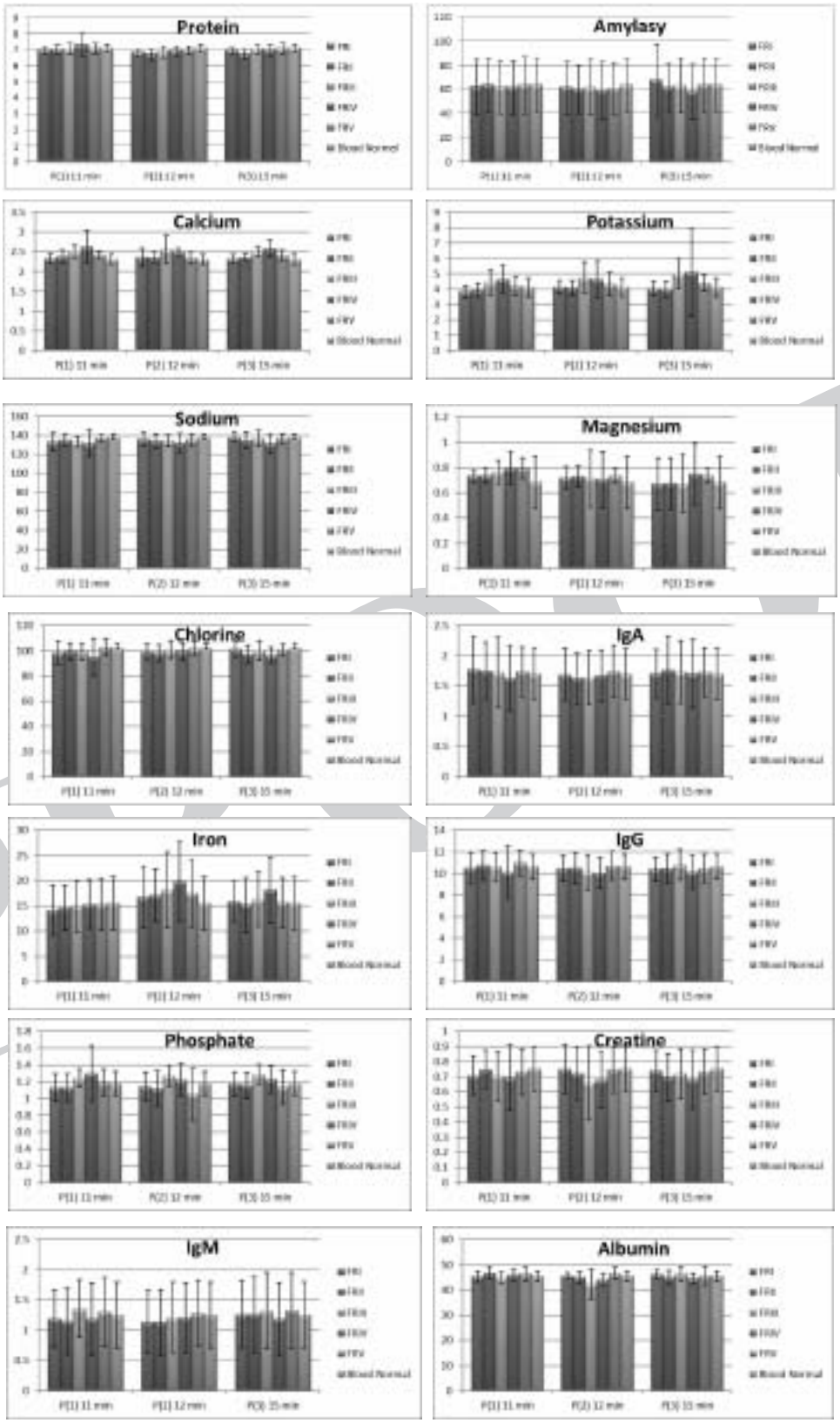

Fig. 2. *Total amount of biochemical elements from bCGF at different time points. Total amount of growth factors released. Error bars represent mean ± SD for n=14. P<0.01.*

calcium, amylase, iron, potassium, phosphate, magnesium, creatine differed significantly between the three groups at different times of centrifuged blood versus normal blood. After a times of (P1)11 min and (P2)12 min, to separate the blood, these fractions can be used as an injection serum form (sample I), membranes "carpet" white buffy coat (sample II),biomaterial GFs (sample III), only red clot can be mixed with natural bone or artificial substance (sampleIV), and red substance can be mixed with natural bone or artificial bone substance (sample V) and can be used in different treatments.

At time P3 (15 min) the sample was well concentrated in the (fr. III) GFs, (fr. IV) red clot, and (fr. V) red substance, and these biomaterials can be used in different patients with a metabolic dysfunction (i.e. cardiovascular diseases, hepatic diseases, hematopoietic). This biomaterial carries the opposite charge to growth factors, and thus forms ionic complex with them. The release of the growth factors can be retarded and controlled depending on the strength of the biochemical interaction (53).

Results obtained with the separators, where biochemical markers did not exceed the normal biochemical level, can be used for different types of treatment such as: sinus lifting procedure, right augmentations, soked preservation, alveolar cleft palate repair, oral/nasal fistula repair, intra-bone defects, jaw reconstruction surgeries, soft tissue procedures like-gingival grafts, periodontal plastic surgery with successful protocols. They also have anti-inflammatory, analgesic, haemostatic and immune stimulated properties to increase soft and hard tissue healing (54).

Within the limits of this study, we noticed that when blood becomes polymerized, it forms a high concentration of growth factors from which five fractions can be obtained. A concentration of the 14 items were found in sample I serum, sample II white clot, but more significant in sample III GFs, sample IV red clot and sample V red substance versus normal blood. A further procedure would include more studies and follows-ups in order to implement this therapeutic protocol with a histological examination.

REFERENCES

1. Hu Y, Liao L, Wang Q, Ma G, Jiang X. Isolation and identification of mesenchymal stem cells from human fetal pancreas. J Lab Clin Med 2003; 141:342-9.
2. Koch TG, Heerkens T, Thomson PD. Isolation of mesenchymal stem cells from equine umbilical cord blood. BMC Biotechnol 2007; 7:26.
3. Tayapongsak P, O'Brien DA, Monteiro CB, Arceo-Diaz LY. Autologous fibrin adhesive in mandibular reconstruction with particulate cancellous bone and marrow. J Oral Maxillofac Surg 1994; 52:161-5.
4. Anitua E. Plasma rich in growth factors: preliminary results of use in the preparation of sites for implants, Int J Oral Maxillo Fac Implants1999; 14:529-53.
5. Dohan D, Choukroun J, Diss A, Dohan S, Dohan A, Mouhyi J, Gogly B. Platelet-rich fibrin (PRF): A second-generation platelet concentrate. Part I: Technological concepts and evolution. Surg Oral Med Oral Pathol Oral Radiol Endod 2006;101:e37-44.
6. Corigliano M, Sacco L, Baldoni E. "CGF una proposta terapeutica". Odontoiatria 2010; 1.
7. Corigliano M, Cipollina A, Crescentini F, Sacco L, Baldoni E. Concentrated Growth Factors (CGFs) in the restorative Tissue Techniques; IADR 88th General session Barcellona; abs 4961:233
8. Lynch S, Niwon J, Colvin R, Antonaides H N. Role of platelet-derived growth factor in wound healing: synergistic effects with other growth factors, Proc Natl Acad Sci USA 84 1987; 7696-700.
9. Gassling VL, Açil Y, Springer IN, Hubert N, Wiltfang J. Platelet-rich plasma and platelet-rich fibrin in human cell culture. Oral Surg Oral Med Oral Pathol Oral Radiol Endod 2009; 108(1):48-55.
10. Helding CH, Westemark B. Platelet-derived growth factors: a family of forms that bind to two distinct receptors. Br Med Bull 1989; 45:453-64.
11. Urist MR. Bone: formation by auto induction. Science 1965; 150:893-9.
12. Randelli P, Arrigoni P, Ragone V, Aliprandi A, Gabitza P. Platelets rich plasma in arthroscopic rotator cuff repair: a prospective RCT study, 2-year follow-up. J Shoulder Elbow Surg 2011; 20(4):518-28.
13. Gobbi A, Karnatzikos G, Mihajan V, Malchira S. Platelet-rich plasma treatment in symptomatic patients with knee osteoarthritis: preliminary results in a group of active patients. Sport Health 2012; 4(2):162-72.

14. Murray MM, Spindler KP, Abreu E. Collagen platelet rich plasma hydrogel enhances primary repair of the porcine anterior crucateligament. Orthop Res 2007; 25(1):81-91.
15. Anitua E, Sanchez M, Dela Fuente M, Zalduendo MM, Orive G. Plasma rich in growth factors (PRGF-endoret) stimulate tendon and synovial fibroblasts migration and improves the biological properties of hyaluronic acid. Knee Surg Sports Traumatol arthrosc 2012; 20(9):1657-65.
16. Wang-Saegusa A, Cugat R, Ares O, Seijas R, Cuscó X, Garcia-Balletbó M. Infiltration of plasma rich in growth factors for osteoarthritis of the knee short-term effects on function and quality of life. Arch Orthop Trauma Surg 2011; 131:311-7.
17. Gobbi A, Karnatzikos G, Mihajan V, Malchira S .Platelet-rich plasma treatment in symptomatic patients with knee osteoarthritis: preliminary results in a group of active patients. Sport Health 2012; 4(2):162-72.
18. Kyoung MK, Young TS, Hong KK. Effect of autologous platelet-rich plasma on persistent corneal epithelial defect after infectious keratitis. J Ophthamol 2012; 56:544-50.
19. Lopez Plandolit S, Morales MC, Freire V, Etxebarria J, Duran JA Plasma rich in growth factors as a therapeutic agent for persistent corneal epithelial defects. Cornea 2010; 29(8):843-8.
20. Yu W, Wang W, Yin J. Platelet-rich plasma: a promising product for treatment of peripheral nerve regeneration after nerve injury. Int J Neurosci 2011; 121:176-80.
21. John L, Dicay M, McKnight W, Dudar G. Platelets accelerate gastric ulcer healing through presentation of vascular endothelial growth factor B. J Pharmacol 2006; 148:274-8.
22. Wallace JL, Dicay M, McKnight W, Dudar GK. Platelets accelerate gastric ulcer healing through presentation of vascular endothelial growth factor. Br J Pharmacol 2006; 148:274-8.
23. Galinto-Moreno P, Avila G, Fernandez-Barbero JE, Aquilar M, Sanchez-Fernandez E, Cutando A, Wang HL. Evaluation of sinus floor elevation using a composite bone graft mixture. Clin Oral Implants Res 2007; 18(3):376-82
24. Simonpieri A, Choukroun J, Del Corso M, Sammartino G, Dohan Ehrenfest DM. Simultaneous Sinus-Lift and Implantation Using Micro-threaded Implants and Leukocyte- and Platelet-Rich Fibrin as Sole Grafting Material: A Six-Year Experience. Implant Dent 2011; 20(1):2-12.
25. Choukroun J, Diss A, Simonpieri A, et al. Platelet-rich fibrin (PRF): a second-generation platelet concentrate. Part V: histologic evaluation of PRF effect on bone allograft maturation in sinus lift. Oral Surg Oral Med Oral Pathol Oral Radiol Endod 2006; 101(3):299-303.
26. Nikolidakis D, Van Den Dolder J, Wolke J, Jansen J. Effect of platelet-rich plasma on the early bone formation around Ca-P coated and coated oral implants in cortical bone. Clin Oral Implants Res 2008; 19(2):207-13.
27. Behnia H, Khojasteh A, Kiani MT, Khoshzaban A, Mashhadi Abbas F, Bashtar M, Dashti SG. Bone regeneration with a combination of nanocrystalline hydroxyapatite silica gel, platelet-rich growth factor, and mesenchymal stem cells: a histologic study in rabbit calvarias. Oral Surg Oral Med Oral Pathol Oral Radiol 2013;115(2):e7-15.
28. Anitua E, Orive G, Pla R, Roman P, Serrano V, Andia I. The effects of PRGF on bone regeneration and on titanium implant osseo-integration in goats: A histologic and histomorphometric study. Wiley Periodicals, Inc. J Biomed Mater Res 2009; 91(A):158-65.
29. Jang ES, Park JW, Kweon H, Lee KG, Kang SW, Baek DH, Choi JY, Kim SG. Restoration of peri-implant defects in immediate implant installations by Choukroun platelet-rich fibrin and silk fibroin powder combination graft. Oral Surg Oral Med Oral Pathol Oral Radiol Endod 2010; 109:831-6.
30. Torabinejad M, Turman M. Revitalization of tooth with necrotic pulp and open apex by using platelet-rich plasma: a case report. J Endod 2011; 37(2):265-8.
31. Choukroun J, Diss A, Simonpieri A, Girard MO, Schoeffler C, Dohan AJ, Mouhyi J, Dohan DM. Platelet-rich fibrin (PRF): A second-generation platelet concentrate. Part IV: Clinical effects on tissue healing Oral Surg Oral Med Oral Pathol Oral Radiol Endod 2006;101:e56-60.
32. Shivashankar VY, Johns DA, Vidyanath S, Kumar

MR. Platelet Rich Fibrin in the revitalization of tooth with necrotic pulp and open apex. J Conserv Dent 2012; 15(4):395-8.

33. Sakata J, Sasaki S, Handa K, et al. A retrospective, longitudinal study to evaluate healing lower extremity wounds in patients with diabetes mellitus and ischemia using standard protocols of care and platelet-rich plasma gel in a Japanese wound care program. Ostomy Wound Manage 2012; 58(4):36-49.
34. Orcajo B, Muruzabal F, Isasmendi MC, Gutierrez N, Sánchez M, Orive G, Anitua E. The use of plasma rich in growth factors (PRGF-Endoret) in the treatment of a severe mal perforant ulcer on the foot of a person with diabetes. Diabetes Res Clin Pract 2011; 93(2):e65-7.
35. Anitua E, Aguirre JJ, Algorta J, Ayerdi E, Cabezas AI, Orive G, Andia I. Effectiveness of autologous preparation rich in growth factors for the treatment of chronic cutaneous ulcers. J Biomed Mater Res B Appl Biomater 2008; 84(2):415-21
36. Villela DL, Santos VL. Evidence on the use of platelet-rich plasma for diabetic ulcer: a systematic review. Growth Factors 2010; 28:111-6.
37. Cervelli V, Nicoli F, Spaloni D, Verardi S, Sorge R, Nicoli M, Balzani A. Treatment of traumatic scars using fat grafts mixed with platelet-rich plasma and resurfacing of skin with the 1540 nm non ablative laser. C and Exp Dermatology 2012; 37(1):55-61.
38. Cervelli V, Gentile P, Scioli MG, Grimaldi M, Casciani CU, Spagnoli LG, Orlandi A. Application of platelet-rich plasma in plastic surgery: clinical and *in-vitro* evaluation. Tissue Eng Part C Meth 2009; 15:625-34.
39. Redaelli A, Romano D, Marciano A. Face and neck revitalization with platelet-rich plasma(PRP): clinical outcome in a series of 23 consecutively treated patients. J Drugs Dermatol 2010; 9(5):466-72.
40. Cervelli V, Palla L, Pascali M, De Angelis B, Cucio BC, Gentile P. Autologous platelet-rich plasma mixed with purified fat graft in aesthetic plastic surgery. Aesthet Plast Surg 2009; 33:716-21.
41. Martins MA, Martins MD, Lascala CA, Curi MM, Migliorati CA, Tenis CA, Margues MM. Association of laser phototherapy with PRP improves healing of bisphosphonate-related osteonecrosis of the jaws in cancer patients: a preliminary study. Oral Oncol 2012; 48(1):79-84.
42 Curi MM, Cossolin GS, Koga DH, Zardetto C, Christianino S, Feher O, Cardoso CL, dos Santos MO. Bisphosphonate-related osteonecrosis of the jaws-an initial case series report of treatment combining partial bone resection and autologous platelet-rich plasma. J Oral Maxillo fac Surg 2011; 69(9):2465-72.
43. Mozzati M, Arata V, Gallesio G. Tooth extraction in patients on zoledronic acid therapy. Oral Oncology 2012; 48:817-21.
44. Li XH, Zhou X, Zeng S, Ye F, Yun JL, Huang TG, Li H, Li YM. Effects of intramyocardial injection of platelet-rich plasma on the healing process after myocardial infarction. Coron Artery Dis 2008; 19:363-70.
45. Wehberg KE, Answini G, Wood D, Todd J, Julian J, Ogburn N, Allen KB. Intramyocardial injection of autologous platelet-rich plasma combined with transmyocardial revascularization. Cell Transplant 2009; 18 353-9
46. Takikawa M, Nakamura S, Nakamura S, et al. Enhanced effect of platelet-rich plasma containing a new carrier on hair growth. Dermatol Surg 2011; 7(12):1721-9.
47. Choukroun JI, Braccini F, Diss A, Giordano G, Doglioli P, Dohan DM. Influence of platelet rich fibrin (PRF) on proliferation of human preadipocytes and tympanic keratinocites: A new opportunity in facial lipostructure and tympanoplasty. Laryngol Otol Rhinol 2007; 128(1,2):27-32.
48. Dohan DM, Choukroun J, Diss A, Dohan SL, Dohan AJ, Mouhyi J, GoglyB. Platelet rich fibrin (PRF): a second generation platelet concentrate. Part-II: platelet-related biologic features. Oral Surg Oral Med Oral Pathol Oral Radiol Endod 2006; 101(3):e45 50.
49. Schilephake H. Bone growth factors in maxillofacial skeletal reconstruction. Int J Oral Maxillofac Surg 2002; 31:469-84.
50. Cope O, Kapnick I, Lambert A, Pratt D, Verlot M. Endocrine function and amylase activity. Enddocr 2013; 25(2):248-256.
51. Maximow A. The Lymphocyte as a stem cell common to different blood elements in embryonic development and during the post-fetal life of

mammals. Cell Ther Transplant 2009; 1:e.000032.01.
52. Nugent MA, IozzoRV. Fibroblast growth factor-2. Int J Biochem Cell Biol 2000; 32(2):115-20.
53. White JG, Krumwiede M. Further studies of the secretory pathway in thrombin-stimulated human platelets. Blood 1987; 69(4):1196-203.
54. Gassiling V, Douglas T, Warneke PH, Acil Y, Wiltfang J, Becker ST. Platelet-rich fibrin membranes as scaffolds for periosteal tissue engineering. Clin Oral Implants Res 2010; 21(5):543-9.

LETTER TO THE EDITOR

TRANSFORMING GROWTH FACTOR-β AND MATRIX METALLOPROTEINASE SECRETION IN CELL CULTURE FROM *EX-VIVO* PBMC AFTER EXPOSURE TO UV RADIATION

P.L. FALCÃO[1], E.M. CUPERSCHMID[2], B.M. TRINDADE[1] and T.P.R. CAMPOS[1]

[1]Programa de Ciências Técnicas Nucleares, PCA 1, Anexo Engenharia, Universidade Federal de Minas Gerais, Belo Horizonte, MG, Brazil; [2]CEMEMOR, Centro de Memórias da Faculdade de Medicina, Universidade Federal de Minas Gerais, Belo Horizonte, MG, Brazil

Received September 21, 2012 – Accepted March 18, 2014

Transforming Growth Factor-β (TGF-β) and Matrix metalloproteinases (MMPs) especially MMP-2 and MMP-9, secreted by a pool of cells from dermic-epidermic tissue, might be associated with a poor prognosis of cancer. We examined the effect of solar radiation on the secretion of TGF-β, MMP-2 and MMP-9 by *ex vivo* PBMC and dermic-epidermic cell pool. The two pools of cells in culture were photo tested using a solar simulator which reproduces the natural light source. The cells were incubated in serum-free medium in the absence and presence of PHA. After two 5 and 45 min exposure times, the supernatant of the cultures was removed at 24 and 48 h and analyzed for TGF-β, and disrupted cell samples for MMP-2 and MMP-9 by RT-PCR. The data obtained by Optical Density by ELISA showed significant differences in the production of TGF-β to the exposed cultures compared to control at 24 and 48 h, respectively. The increases in the MMP-2 and MMP-9 concentrations depending on the exposure time were observed. In conclusion, the UV radiation emitted by the solar simulator was able to stimulate the cells from extracellular matrix in *in vitro* culture to TGF-β production, MMP-2 and MMP-9 expressions and their mRNAs. Since such MMPs and TGF are related to the evolution of cancer and its pathogenesis, these findings confirm that UV radiation can contribute to the prognosis of such diseases based on the MMP and TGF-β secretion.

The maintenance of human health is associated with the ability of the immune system to respond efficiently to endogenous and exogenous agents. Considering that solar ultraviolet (UV) radiation is an important environmental factor that leads to immune suppression, inflammation, photo aging and skin carcinogenesis, studies have been proposed to investigate the pathways and transcription factors involved in the cellular response to UV-irradiation and in a variety of physiological and biological effects, including immune suppression, cellular aging, DNA damage and initiation of cellular apoptosis (1-3). Solar UV radiation is the main cause of human skin cancers, such as cutaneous malignant melanomas and non-melanoma tumors that include basal cell carcinomas and squamous cell carcinomas (3, 4). The hypothesis is that UV wavelength-specific "action spectrum" is stemmed from distinct direct damage to various biomolecules, inorganic molecules of conjugated bonds, ring or linear repeated structures absorbing UV shortwave radiation (200–300 nm). Considering the exposure

Key words: culture cells, UV radiation, TGF-β, metalloproteinases

Mailing address: Dr Patrícia Lima Falcão
Av. Antônio Carlos, 6627,
CEP 31.270-901, Belo Horizonte,
MG, Brazil
Tel: +553134096691
Fax: +553134096660
e-mail: patricialfalcao@gmail.com

0393-974X (2014)

of mammalian cells to UV light, cytokines produced in excess in response to cell injury could activate an enzyme cascade, inducing many target genes. A previous study showed that exposure to UV light or to osmotic shock induced the clustering and the internalization of cell surface receptors for epidermal growth factor (EGF), tumor necrosis factor (TNF), and interleukin(IL) -1 (5). Activation of the EGF and TNF receptors were also detected biochemically (5). Physical stress may also alter the cell surface or receptor conformation, thereby subverting signaling pathways normally used by growth factors and cytokines (6).

Other studies have suggested a relationship between the exacerbated production of proinflammatory cytokines and enzymes and a poor immune response of patients suffering from dysplasia and neoplasia (7, 8). The possible role has been investigated of co-factors excreted by cancerous cells themselves on the induction of uncontrolled replication, leading to unwanted DNA repair that suffered from environmental damage. It is worth mentioning that the evidence of the role of any particular metalloproteinase in a pathological process is provided by the findings of the presence of metalloproteinase mRNA in lesional cells.

The matrix metalloproteinases (MMPs) are produced by monocytes, endothelial cells, and smooth muscle cells, whose function is to break down numerous components of the ExtraCellular Matrix (ECM) as well as other proteins. MMP activity has been related to a number of relevant diseases such as joint destruction in rheumatoid arthritis, osteoarthritis, abdominal aortic aneurysm, acute myocardial infarction and cancer (9). Furthermore, studies have shown that neoplasic cell activity is regulated on transcription and post translation through interactions with specific inhibitors (enzymes). A number of growth factors, cytokines, thrombin, and hormones increase the transcription of these enzymes, while heparin, TGF-β and corticoids inhibit it (10, 11). However, how these cytokines could act by stimulating or modulating the production of other MMPs, as alternative route for cell replication in an attempt to repair tissue, is still unclear (12). Recent studies have shown that the MMPs have raised an extraordinary interest in cancer research because of their potential role in basal membrane and extracellular matrix degradation, consequently allowing tumor invasion and the spread of metastases. Tumors with high expression of collagenases were significantly associated with a higher probability of biochemical recurrence, suggesting that the expression of MMPs and Tissue Inhibitors of MetalloProteinases (TIMPs) seems to have an important role in the molecular biology of prostate carcinomas (13).

Somehow, an imbalance in the production of some specific MMPs might be associated with a poor prognosis of cancer, thus pro- and anti-inflammatory cytokines may be also associated with enzymes that start gene transcriptions encoding MMPs. It is worth speculating whether the production of inflammatory cytokines and the possible modulation by anti-inflammatory cytokines are involved in the genesis of an unsuccessful control response, with tumor cell growth. Considering the complex network of exogenous attacks that a human being receives daily, it is worth mentioning that these attacks include ionizing radiation as a factor of great impact, offering serious risk to the health of exposed individuals.

UVB and UVC are potentially dangerous. Exposure time affects the danger levels and a relatively short exposure time may be able to produce lesions, depending on the age of the individual and of the power source. Within the context of the human skin acting as a barrier against a series of attacks produced by the external environment, one can understand that the cells that make it up show different responses according to the type of aggression and the degree of exposure of the same.

Thus, it is worth mentioning that pro-inflammatory cytokines, produced and activated and cellular enzymes induced by radiation exposure, become valuable objects of study. Therefore, a step forward in understanding the effects of UV radiation can be taken through the investigation of the expression of MMPs and TGF-β from *ex vivo* cells exposed by UV radiation.

MATERIALS AND METHODS

Subjects

Fifteen healthy volunteers who were not on medication and had no past or present history of photodermatosis or skin cancer were included in the study. The experimental

study was approved by the Ethics Committee of the Odilon Behrens Hospital, in Belo Horizonte, Minas Gerais State. The cell samples were obtained from biopsies at the dermo-epidemis in the distal forearm.

Sampling

The cells were collected using a 2 mm punch. The cell pool from biopsy consisted mainly of a population of keratinocytes, fybroblasts, lymphocytes and epithelioid cells together with macrophages or dendritic cells, named here as dermo-epidermis pool cell.

Dermo-epidermis cell culture growth

Cells were grown in RPMI 1640 medium supplemented with 10% NHS (Normal Human Serum), penicillin (100 units.mL^{-1} and streptomycin (100 µg.mL^{-1}) in 24-well tissue culture plates. The cells were plated at a density of 1x10^{6} cells.mL^{-1} and maintained in a humidified atmosphere of 5% CO_2 in air at 37°C until confluence. Serum-supplemented medium was removed and cell monolayer was washed twice with serum-free media. Thus, the cells were incubated in 0.5 mL of serum-free medium with presence of mitogen. The supernatant medium from each well was collected separately, pooled, and centrifuged at 4°C for 10 min at 3,000 *rpm* to remove cells and cell debris.

PBMC culture growth

The PBMC cells were cultured in RPMI-1640 supplemented medium, and the populations were separated by Fycoll gradient. Part of the obtained cells was stimulated in culture with nonspecific mitogenic factor (PHA) for cell viability monitoring. The wells containing cells were phototested using a solar simulator. A set of wells were taken as control samples.

Exposure procedure

The wells containing cells were phototested using the LS1000 Solar Simulator accurately replicating full spectrum sunlight which meets the latest standards for Solar Simulators. Two filters were used: one to deliverer whole spectrum radiation (i.e. UVA, UVB and visible light) and another filter, which delivered UVA. Two exposition periods were carried out: 5 min which provides an intensity of 60 J.cm^{-2}, and 45 min which provides 550 J.cm^{-2}, after determining the thermopile output and the time for delivery. The infrared radiation was excluded using a liquid filter of 0.1% $CuSO_4$.

Exposed and control samples

A set of wells was taken as control samples for the dermo-epidermis pool of cells and PBMC (no irradiation cells - NIC). The exposed samples were identified as dermo-epidermis cells with 5 min exposure and with 45 min exposure; PBMC – with 5 min exposure and with 45 min exposure.

Supernatant collection

The PBMC supernatants were collected from cultures exposed for 5 and 45 min respectively, at 24 and 48 h in the presence and absence of PHA. The supernatant medium from each well was collected separately, pooled and centrifuged at 4°C for 10 min at 1,400 *rpm* to remove cells and debris. The supernatants of the cultures were then adjusted for salt content (0.14 *M* sodium chloride and 0.01 *M* sodium phosphate) and pH (7.4), for the determination of TGF-β.

TGF-β assay

The concentrations of cytokines in the supernatants of the control and exposed cultures were measured using sandwich ELISAs with matched antibody pairs (R&D Systems).

MMP-2 and MMP-9 RT-PCR assay

The dermo-epidermis and PBMC cells were tested by matrix metalloproteinases. The total RNA was obtained from disrupting cells in an RNAse free environment, based on TRIZOL RNA isolation protocol. The cDNA was obtained by adding in 500 µL tubes, 1 µL of random priming (75 ng), 2 µL of RNAse inhibitor (20 units), 1 µL of 1% gelatin; 1-5 mg total RNA and supplemented to 12 µL with DEPC-treated water and incubated at 70°C for 10 min and cooled to 4°C. The following reagents were added: 5 µL of 5X First Strand Buffer ® (250 mmol.L^{-1}Tris-HCl pH 8.3, 375 mmol.L^{-1} KCl, $MgCl_2$ 15 mmol.L^{-1}), 2 µL of 0.1 mol.L^{-1} DTT, and 1 µL of a 10 mmol.L^{-1} dNTP. After incubation at 42°C for 2 min, the following reagent was added: 20 units of reverse transcriptase (SuperScript II®, Gibco Brl®, Life Technologies) and stirred. The reaction medium was then incubated at 25°C for 5 min, 42°C for 50 min, 70°C for 15 min and cooled to 4°C. The PCR amplification of MMPs genes was performed in a total volume of 25 µL containing 3 µL of the cDNA obtained above, 2.5 µL buffer® PCR buffer (200 mmol.L^{-1}TRIS-HCl pH 8.4, 500 mmol.L^{-1} KCl) and 100 mmol.L^{-1} dNTP, 1.5 mmol.L^{-1} $MgCl_2$, 0.6 mmol.L^{-1} of each primer, 4% DMSO, 1.25 units Taq DNA polymerase (Gibco Brl®) and completed by reaction with water treated with DEPC. Thus, they were placed in tubes with one drop of mineral oil. The amplification cycles were 94°C for 4 min followed by 34 cycles of 94°C for 1 min, 42°C for 1 min and 72°C for 1.5 min. Two pairs of oligonucleotides primers were prepared for human MMP-2 specific sequences sense: 5'-GGCCCTGTCACTCCTGAGAT3' and antisense 5'-GGCATCCAGGTTATCGGGGA-3' and to MMP-9

(sense: 5′ CGCAGACATCGTCATCCAGT 3′, antisense: 5′ GGATTGGC CTTGGAAGATGA 3′) (Biosource International, Camarillo, CA). The gels were stained with Ethidium Bromide and were further processed in GelDoc 1000/2000 system (BioRad), Multi-Analyst PC version 1.2 and Mitsubishi Video Printer P91.

Statistical analysis

The group data were presented as arithmetic average and standard deviation. Results were expressed as arithmetic average and standard deviation. Kruskal-Wallis test was applied for analysis of variance (ANOVA). The Mann-Whitney test was used to compare both groups. The relations between variables were studied using Spearman's correlation coefficients. Data were analyzed by StatSoft statistical software package version 5.

RESULTS

The Optical Density (OD) from ELISAs showed significant differences ($p < 0.005$) in the production of Transforming Growth Factor (TGF-β) of the supernatants at 24 and 48 h from the PBMC and

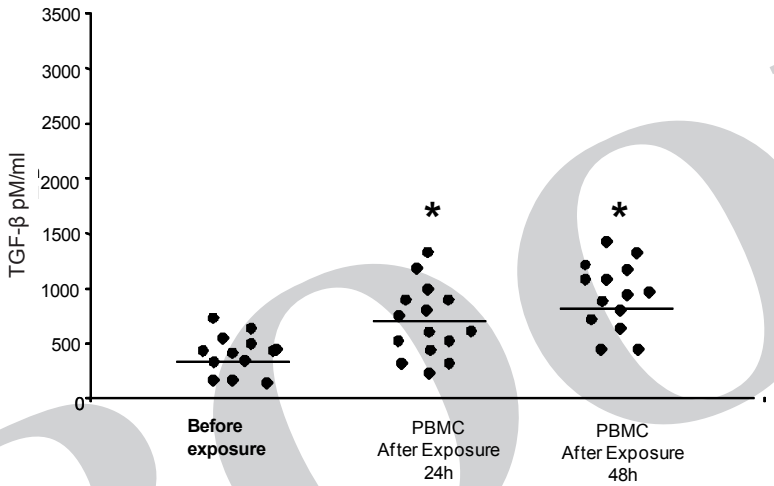

Fig. 1. *Detection of circulating TGF-β from ex-vivo PBMC cell culture before and after exposure to solar simulation, measured at 24 and 48 h after exposition with addition of Phytohemaglutinin. The cytokine was measured using sandwich ELISA specific for TGF-β. Results are shown as individual sample values and median (horizontal line) for 15 samples (p<0.05 and **p<0.001, exposed samples (Mann-Whitney U test).*

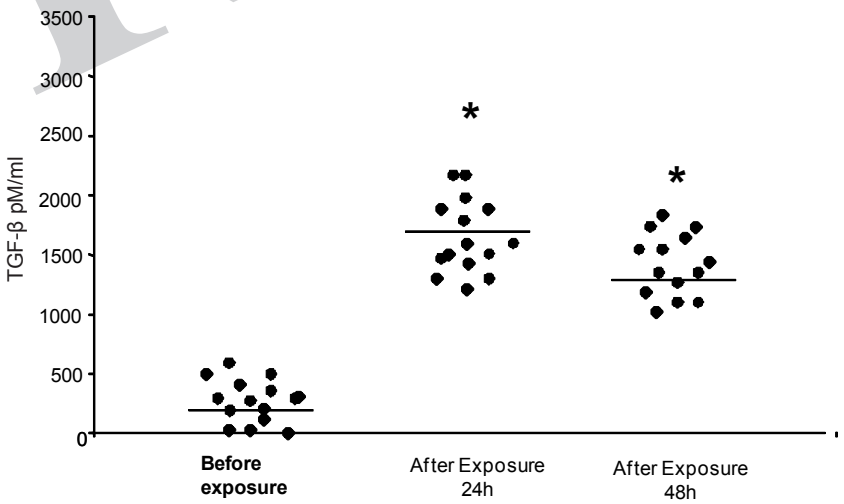

Fig. 2. *Detection of TGF-β from ex-vivo cell culture supernatant (fibroblasts and keratinocytes from dermo-epidermis junction) before and after exposure to solar simulation, measured at 24 and 48 h after exposition. The cytokine was measured using sandwich ELISA specific for TGF-β. Results are shown as individual sample values and median (horizontal line) for 15 samples (p<0.05 and **p<0.001, exposed samples (Mann-Whitney U test).*

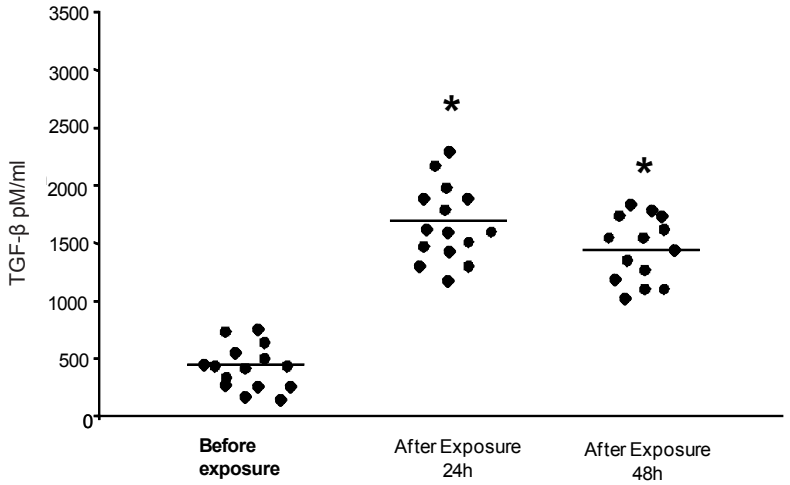

Fig. 3. *Detection of circulating TGF-β from ex-vivo cell culture (fibroblasts and keratinocytes from dermo-epidermis junction) before and after exposure to solar simulation, measured at 24 and 48 h after exposition with addition of PHA (Phytohemaglutinin). The cytokine was measured using sandwich ELISA specific for TGF-β. Results are shown as individual sample values and median (horizontal line) for 15 samples ($p<0.05$ and $**p<0.001$, exposed samples (Mann-Whitney U test).*

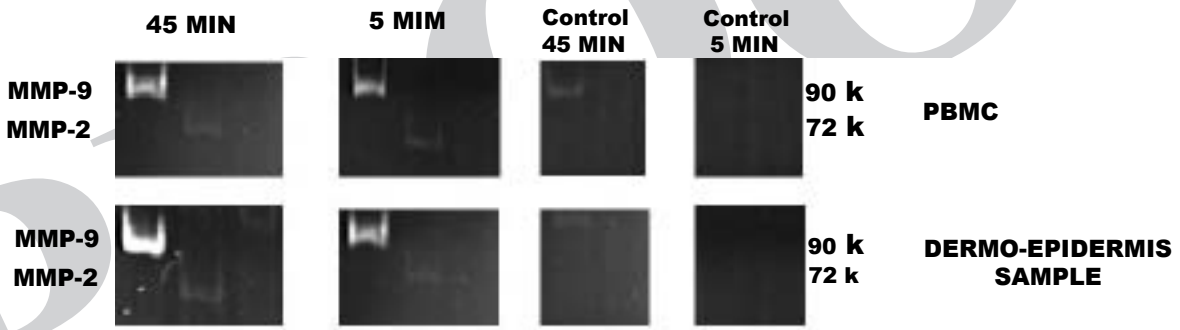

Fig. 4. *10% Polyacrilamine gel analysis of human recombinant MMP-2 and MMP-9 mRNA from an individual before and after exposure to solar simulator. The profiles were obtained from ex-vivo cells submitted to 5 and 45 min exposure times. Peripheral Blood Mononuclear Cells (PBMC) at 45 min and 5 min exposure, fibroblasts and keratinocytes from dermo-epidermis junction were obtained from biopsy from the same individual 45 min and 5 min exposure and control cells to PBMC and dermo-epidermis cells obtained from biopsy from the same individual, respectively.*

dermo-epidermis cultures exposed to the simulator compared to control, respectively, as shown in Figs. 1, 2 and 3. The TGF-β detection on supernatants was higher at 24 h than in 48 h, showing the rapid effect of radiation on the induction of this cytokine production. Indeed, there were significant differences in the concentrations of TGF-β ($p < 0.001$) on supernatant of culture samples exposed to UV radiation and control, as shown in Fig. 1. It is worth mentioning that the results obtained for cell cultures not exposed to solar simulator showed no statistically significant differences in the presence of mitogenic effect of phytohemagglutinn (PHA) for detection of TGF-β.

Concerning the cultures exposed to both 5 and 45 min periods, there was a slight increase in the levels of TGF-β. However, there were no significant differences when the two filters were used in the detection of this cytokine. Therefore, results from

presence of mitogen were grouped together.

In our study it is interesting to observe that the exposed cultures that had the highest detection levels for TGF-β also showed the mRNA for matrix of metalloproteinases. The results obtained by RT-PCR performed in 10% polyacrylamide gel showed bands of high intensity to MMP-2 mRNA apparently greater in the irradiated culture than the control group as shown in two samples in Fig. 4. Concerning the MMP-9, the polyacrylamide gel in the same concentration also reveals increased activity of MMP-9 for all samples from cultures exposed to radiation for 45 min, while weak bands were observed for those cultures exposed to radiation for 5 min. None of the PBMC exposed cultures showed both bands for MMP-9 and MMP-2 (Fig. 4).

DISCUSSION

In our study, it is interesting to note that the UV-exposed cultures which provided a high detection level for TGF-β also showed the mRNA for matrix of metalloproteinases. Interestingly, our data seem to agree with the literature, since the UV effects on human skin had also been studied previously. Indeed, the involvement of proteolytic enzymes in the group of MMPs had been demonstrated in 1998 (14). Other studies showed an association between cytokines, including MMPs, with inducer function in ovarian and cervical cancer (15, 16). The concentrations of three matrix metalloproteinases which are proteolytic enzymes were involved in degradation of collagen molecules (15, 16). In other types of tissues, such as mucosal, the increased MMP-2 and 9 and the expression of tissue inhibitor of matrix metalloproteinase-2 were associated with the progression from vulvar intraepithelial neoplasia to invasive carcinoma. In this study, the population consisted of 68 patients with vulvar neoplasia (13 VIN I, 5 VIN II, 6 VIN III and 4 squamous cell carcinoma) with samples examined by immunohistochemistry (12).

From our study, when we compared the levels of MMP-2 obtained from the *ex-vivo* dermo-epidermis pool of cells with the levels detected for the MMPs obtained from cultures of PBMCs, we observed significantly higher levels ($p < 0.01$) for the cell pool, which is known to include the fibroblasts (16). It is worth mentioning that this cell line is responsible for collagen synthesis and is known to be highly sensitive to degradation by proteolytic action of MMPs. In contrast, there were significantly greater concentrations of the TGF in the culture exposed to solar irradiation, when compared with non-exposed ones (Fig. 1).

These results suggest that multiple exposures to ultraviolet irradiation could lead to permanent elevations of matrix of metalloproteinases, contributing to cellular damage and also for the development of carcinomas (16). However, our findings do not seem consistent with the literature regarding the kinetics of exposure, since the time of 5 min appears to be sufficient for the initial saturation of circulating TGF-β, and the results showed that the difference in detection of this cytokine reported on the time of 45 min was not statistically significant ($p > 0.05$).

In contrast, the RT-PCR performed in 10% gel polyacrylamide point out an increased activity of MMP-9 for all samples from cultures exposed to radiation for 45 min, while weak bands were observed for those cultures exposed to radiation for 5 min. RT-PCR of cells in two periods of exposure suggests that the expression of MMP-9 is dose-dependent, since the exposure time led to greater expression of RNA. However, kinetics with various exposure times will be required to confirm this finding. High levels of MMP-9 observed for cultures taken from biopsies can be explained by the presence of macrophages in culture. Whereas the expression and activity of MMP-9 in the extracellular matrix (ECM) is mainly associated with macrophages which are in great amount in the cell pool. However, this does not occur in PBMC cultures. MMPs degrade various components of the extracellular matrix (ECM), including collagen, laminin, fibronectin, elastin and proteoglycans. Since MMPs play a critical role in cancer invasion, migration metastases and tumorigenesis, blocking tumor cell expression of MMPs can significantly reduce tumor invasion and metastases (17-19). Concerning the concentrations of both MMP-9 and MMP-2, no statistically significant differences were found for either of the filters used in solar simulator.

Although some studies have already shown the role of this cytokine in regulating enzymes, the activity of MMPs is regulated at the transcriptional,

translational and post-translational level by endogenous extracellular signals (cytokines, hormones, and a variety of peptide growth factors) (20-22) and by specific inhibitors and regulators (TIMPs) (23-25). The activity of MMP-2, MMP-7 and TIMP-1-4 increases while MMP-9 decreases with age, since the MMPs level is also under hormonal control. Female sex steroids inhibit MMPs, although MMPs are markedly stimulated by epithelial cell in supplemented medium (26). This stimulation can be prevented by antibodies against interleukin 1 alpha (IL-1 alpha). Ovarian steroids inhibit MMP-1 production by IL-1 alpha-stimulated fibroblasts *in vitro* (25, 27). A link between noradrenaline and MMP-2 is also recognized. Such study assessed the relationship between catecholamines and active MMPs *in vivo* in patients with severe congestive heart failure (CHF) and *in vitro* in human cardiac fibroblasts (28).

In conclusion, our results show that the radiation emitted by the solar simulator was able to stimulate the cells from extracellular matrix in the *in vitro* culture to produce TGF-β, MMP-2 and MMP-9 expression and their mRNAs. It suggests that the effects of UV radiation can contribute to the prognosis of serious diseases such as cancer and its pathogenesis, since MMPs and TGF-β play a critical role in cancer invasion, migration metastasis and tumor genesis, since these enzymes can be secreted in response to external aggression and to an escape mechanism to maintain the viability of the damaged cell.

REFERENCES

1. López-Camarillo C, Campo EAO, Casamichana ML, Plasencia CP, Álvarez-Sánchez E, Marchat L. Protein kinases and transcription factors activation in response to UV-radiation of skin: implications for carcinogenesis. Int J Mol Sci 2012; 13(1):142-72.
2. Epstein JH. Photocarcinogenesis, skin cancer, and aging. J Am Acad Dermatol 1983; 9:487-502.
3. De Gruijl FR, Van Kranen HJ, Mullenders LH. UV-induced DNA damage, repair, mutations and oncogenic pathways in skin cancer. J Photochem Photobiol 2001; B63:19-27.
4. Armstrong BK, Kricker A. The epidemiology of UV induced skin cancer. J Photochem. Photobiol 2001; B63:8-18.
5. Ravanat JL, Douki T, Cadet J. Direct and indirect effects of UV radiation on DNA and its components. J Photochem Photobiolm 2001; B63:88-102.
6. Rosette C, Karin M. Ultraviolet light and osmotic stress: Activation of the JNK cascade through multiple growth factor and cytokine receptors. Science 1996; 274:1194-97.
7. Escaff S, Fernández JM, González LO, Suárez A, González-Reyes S, González JM, Vizoso FJ. Study of matrix metalloproteinases and their inhibitors in prostate cancer. Br J Cancer 2010; 102(5):922-9.
8. Määttä M, Santala M, Soini Y, Turpeenniemi-Hujanen T, Talvensaari-Mattila A. Increased matrix metalloproteinases 2 and 9 and tissue inhibitor of matrix metalloproteinase 2 expression is associated with progression from vulvar intraepithelial neoplasia to invasive carcinoma. Acta Obstet Gynecol Scan 2010; 89(3):380-4.
9. Ye S. Polymorphism in matrix metalloproteinase gene promoters: implication in regulation of gene expression and susceptibility of various diseases. Matrix Biol 2000; 19:623-9.
10. Unemori EN, Lark MW. Cytokine-stimulated human vascular smooth muscle cells synthesize a complement of enzymes required for extracellular matrix digestion. Circ Res 1994; 75:181-9.
11. Galis ZS, Kranzhofer R, Fenton JW 2nd, Libby P. Thrombin promotes activation of matrix metalloproteinase-2 produced by cultured vascular smooth muscle cells. Arterioscler ThrombVasc Biol 1997; 17:483-9.
12. Subramaniam V, Chakrabarti R, Prudhomme GJ, Jothy S. Tranilast inhibits cell proliferation and migration and promotes apoptosis in murine breast cancer. Anticancer Drugs 2010; 21(4):351-61.
13. Azeh L, Mader M, Smirnov A, Beuche W, Nau R, Weber F. Experimental pneumococcal meningitis in rabbits: the increase of matrix metalloproteinase-9 in cerebrospinal fluid correlates with leucocyte invasion. Neurosci Lett 1998; 256:127-30.
14. Lumpkin CKJR., McClung JK, Pereira-Smith OM, Smith-JR. Existence of high abundance anti proliferative mRNA's in senescenthuman diploid fibroblasts. Science 1986; 232:393-5.
15. Roomi MW, Monterrey JC, Kalinovsky T, Rath M, Niedzwieki A. *In vitro* modulation of MMP-2 and

MMP-9 in human cervical and ovarian cancer cell lines by cytokines, inducers and inhibitors. Oncol Rep 2010; 23(3):605-14.
16. Braverman IM, Fonferko E. Studies in cutaneous aging: I. The elastic fiber network. J Invest Dermatol 1982; 78(5):434-43.
17. Liotta LA, Tryggvason K, Garbisa A, Hart I, Foltz CM and Shafie S. Metastatic potential correlates with enzymatic degradation of basement membrane collagen. Nature 1980; 284:67-68.
18. Stetler-Stevenson WG. Type IV collagenases in tumor invasion and metastasis. Cancer Metastasis Rev 1990; 9:289-303.
19. Stetler-Stevenson WG. The role of matrix metalloproteinases in tumor invasion, metastasis and angiogenesis. Surg Oncol Clin N Am 2001; 10:383-92.
20. MacNaul KL, Chartrain N, Lark M, Tocci MJ, Hutchinson NI. Discoordinate expression of stromelysin, collagenase, and tissue inhibitor of metalloproteinases-1 in rheumatoid human synovial fibroblasts. Synergistic effects of interleukin-1 and tumor necrosis factor alpha on stromelysin expression. J Biol Chem 1990; 265(28):17238-45.
21. Woessner JF Jr. Matrix metalloproteinases and their inhibitors in connective tissue remodeling. FASEB J. 1991; 5(8):2145-54.
22. Ries C, Petrides PE. Cytokine regulation of matrix metalloproteinase activity and its regulatory dysfunction in disease. Biol Chem Hoppe Seyler 1995; 376(6):345-55.
23. Dittmann KH, Lottspeich F, Ries C, Petrides PE. Leukemic cells (HL-60) produce a novel extracellular matrix-degrading proteinase that is not inhibited by tissue inhibitors of matrix metalloproteinases (TIMPs). Exp Hematol 1995; 23(2):155-60.
24. Tyagi SC, Kumar SG, Banks J, Fortson W. Co-expression of tissue inhibitor and matrix metalloproteinase in myocardium. J Mol Cell Cardiol 1995; 27(10):2177-89.
25. Kähäri VM, Saarialho-Kere U. Matrix metalloproteinases and their inhibitors in tumour growth and invasion. Ann Med 1999; 31(1):34-45.
26. Bonnema DD, Webb CS, Pennington WR, et al. Effects of age on plasma matrix metalloproteinases (MMPs) and tissue inhibitor of metalloproteinases (TIMPs). J Card Fail 2007; 13(7):530-40.
27. Singer, CF, Marbaix E, Kokorine I, Lemoine P, Donnez J, EeckhoutY, Courtoy PJ. The matrix metalloproteinase-1 (MMP-1) expression in the human endometrium is inversely regulated by interleukin-1 alpha and sex steroids. CeskaGynekol 2000; 65(4):211-5.
28. Banfi C, Cavalca V, Veglia F, et al. Neurohormonal activation is associated with increased levels of plasma matrix metalloproteinase-2 in human heart failure. Eur Heart J 2005; 26(5):481-8.

LETTER TO THE EDITOR

MAGNETIC RESONANCE IMAGING FEATURES OF CEREBELLAR VERMIS MEDULLOBLASTOMA IN AN ADULT CANINE PATIENT

M. PATSIKAS[1], S. JAKOVLJEVIC[2], P. PAPADOPOULOU[1], Z. POLIZOPOULOU[1], G. KAZAKOS[1], D. TONTIS[3], C. SOULTANI[1], A. CHARITANTI[4], I. CHRISSOGONIDIS[4] and I. TSIFOUNTOUDIS[5]

[1]Department of Clinical Sciences, School of Veterinary Medicine, Aristotle University of Thessaloniki, Greece; [2]Department of Diagnostic Imaging, Dick White Referrals LtD, New Market, UK; [3]Department of Pathology, School of Veterinary Medicine, University of Thessaly, Greece; [4]Department of Radiology, School of Medicine, Aristotle University of Thessaloniki, Greece; [5]Department of Radiology, 424 Hellenic Military Hospital, Thessaloniki, Greece

Received January 22, 2014 – Accepted March 28, 2014

A seven-year-old, not-castrated male, Airedale Terrier presented with a history of ataxia and intention tremor of the head of three-week duration. Neurologic examination demonstrated severe hypermetria, intention tremor of the head and a bilateral menace response deficit. Magnetic resonance imaging revealed a well demarcated cerebellar vermis mass, hypointense on T1-weighted images, hyperintense on T2-weighted images, with multiple small foci of high signal similar to that of CSF. Foci dispersed in the mass creating a speckled appearance. Homogeneous faint, wispy post-contrast enhancement of the mass was noted; as a result the tumor became isointense to gray matter and was not clearly evident in post contrast images. The histopathological diagnosis of the excised tumor was cerebellar medulloblastoma.

Embryonal or primitive neuroectodermal tumors (PNETs) are neoplasms composed of primitive, poorly differentiated, round cells. The PNETs group includes medulloblastoma, to separate this from ependymoblastoma, neuroblastoma, ganglioneuroblastoma, medulloepithelioma, and pineoblastoma. Medulloblastoma, a malignant tumor occurring within the cerebellum, is the most common posterior fossa tumor in children, accounting for one-third of childhood pediatric tumors (1). In animals, medulloblastomas have been reported in dogs, cats, cattle, pigs, rats, a baboon and a kowari (2). The diagnosis is based on clinical manifestations and imaging findings using computed tomography (CT) and magnetic resonance imaging (MRI), which is considered the best imaging modality. In humans, the MRI features of cerebellar medulloblastoma have been described in detail. By contrast, only a few reports have been published in veterinary medicine (3-5). This report describes the clinical and MRI findings in an adult Airedale Terrier with a cerebellar vermis medulloblastoma confirmed histopathologically.

Case history

A seven-year-old not-castrated male Airedale Terrier was referred to the University Veterinary Hospital with a history of ataxia and intention

Key words: medulloblastoma, cerebellum, magnetic resonance imaging

Mailing address:
Michail N. Patsikas MD, DVM, PhD, Dipl ECVDI
St Voutyra 11 str,
54627, Thessaloniki, Greece
e-mail: patsikm@vet.auth.gr

0393-974X (2014)

tremor of the head during the previous 3 weeks. The onset of neurological abnormalities was acute and the dog had been treated with prednisolone (Prezolon, Nycomed Hellas, Greece) (0.5 mg/kg *q* 12 hr) with no clinical improvement. Physical and clinicopathological examination (complete blood cell count and serum chemistry profile) were normal. The neurologic examination revealed severe hypermetria and hypertonus (spasticity) mainly involving the thoracic limbs. The dog exhibited a swaying posture, wide-based stance and had exaggerated postural reactions (hopping, wheelbarrowing, hemistanding, proprioceptive positioning). Dysmetria of the head (manifested as intention tremor) and a bilateral menace response deficit were also noted. Fundic examination and vision were considered normal.

A tentative diagnosis of cerebellar disease was made and MRI of the brain was advised. Imaging was performed with the dog under general anesthesia and in ventral recumbency using a 0.5 T MRI scanner (Elscint Privilege, Haifa, Israel) and a quadrature human head coil, with slice thickness of 3-5 mm. T2-weighted images, T1-weighted images and contrast enhanced T1-weighted images [0.1 mmol/kg gadolinium, GdTA Omniscan (Amersham Health AS, Oslo, Norway) IV, injected manually] in the sagittal, dorsal and transverse planes were performed. MRI images revealed a 2.2 x 2.1 x 1.5 cm (W x H x L) well demarcated mass with convex margins, located in the cerebellar vermis, extending from the ventral to the dorsal surface of the cerebellum, causing mass effect and displacing the cerebellar hemispheres laterally. On T1-weighted images the mass was hypointense relative to grey matter and isointense relative to white matter and muscle (Fig. 1). On T2-weighted images the mass was heterogeneous, slightly hyperintense to gray matter and markedly hyperintense to white matter and muscle. The heterogenecity was due to multiple small foci of high signal, similar to that of CSF, dispersed in the mass, creating a speckled appearance (Fig. 2). After intravenous contrast medium administration, homogeneous faint, wispy contrast enhancement of the mass was noted, with poor delineation of the tumor margins, because the mass not clearly evident (Fig. 3, A and B). The ventricular system was mildly dilated; however, perilesional edema was not seen. Differential diagnosis for this intra-axial mass included neoplasia and granuloma.

Euthanasia was performed after the owner denied further treatment due to poor prognosis. At necropsy a well-defined intraparenchymal white mass was visible, located on the midline of the cerebellum, and displacing the cerebellar hemispheres. In gross pathologic examination the tumor had a homogeneous firm cut surface. Imprint cytology of the biopsy tissue indicated small to medium sized round cells individualized or in groups, most with scanty cytoplasm, the majority with hyperchromatic nuclei and some displaying nuclear molding (Fig. 4). Histopathology of excised tissue revealed that the tumor was well demarcated, composed of highly cellular sheets and short stems and bands of uniform small cells with round, oval or elongated basophilic nuclei, scant cytoplasm and inconspicuous nucleoli. Occasionally neoplastic cells palisade along vessels and form pseudorosettes (Fig. 5). The stroma was delicate with numerous thin-walled blood vessels, mainly centrally, while in the periphery the vascular net was not well formed. Mitotic figures were limited. Small foci of tumor necrosis were also noted. Immunohistochemically, the neoplastic cells were variably positive for GFAP, NSE, NFP and S-100 and negative for Vimentin, CK, CD3, and CD79. Based on the above findings a diagnosis of cerebellar medulloblastoma was made.

DISCUSSION

The anatomic localization of lesions of the central nervous system is determined by neurological examination (6, 7). In humans, cerebellar disorders are usually manifested by an ataxic gait and signs of obstructive hydrocephalus (8). Typical cerebellar symptoms in animals include intention tremors, dysmetria, truncal ataxia, and broad-based stance, which were all present in our case (6, 7).

Although neurological examination allows localization of a lesion within the brain and, in most cases, to determine approximately the structures involved, inaccuracies in the neurolocalization of lesions can occur with some large intracranial masses (4). Therefore, diagnostic imaging is required to determine the nature of the lesion, the exact location, and the extension and relationship to the surrounding structures. This information is critical in planning

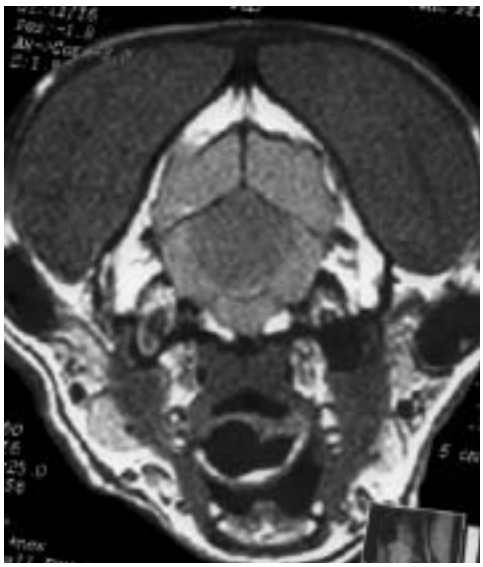

Fig. 1. *Transverse pre-contrast T1-weighted image of the cerebellum with a hypointense well-demarcated midline cerebellar mass, displacing the cerebellar hemispheres laterally.*

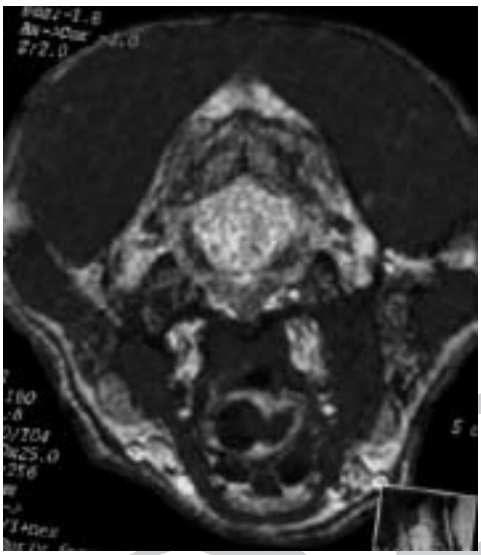

Fig. 2. *Transverse T2-weighted image of the cerebellum with a heterogeneously hyperintense, well-demarcated midline mass. Multiple small foci isointense to CSF are dispersed throughout the mass, creating a speckled appearance.*

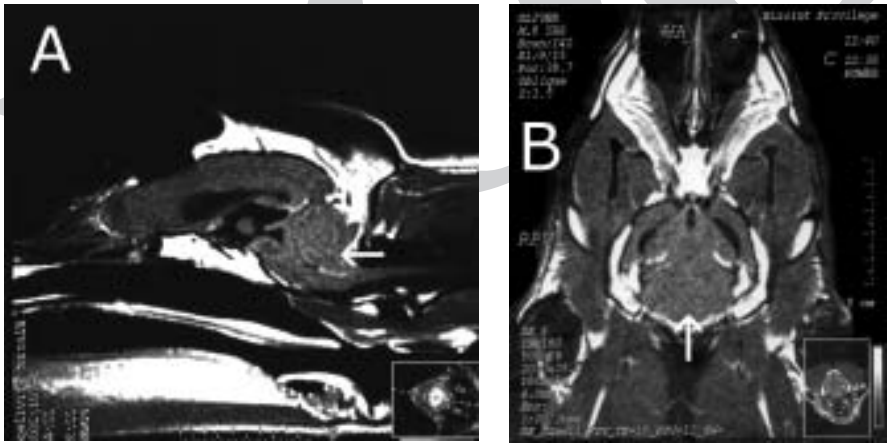

Fig. 3. *Sagittal midline (**A**) and dorsal (**B**) T1-weighted image of the brain after intravenous contrast medium administration. The mass is isointense to the surrounding cerebellar tissue and not clearly demarcated due to faint, wispy post-contrast enhancement. (arrows demonstrate the site of the cerebellar mass seen in pre-contrast images). Mild dilatation of the ventricular system is also seen.*

therapeutic strategies. Multi-detector row CT and MRI are the two most important and commonly used imaging modalities (9).

In the present case, medulloblastoma appeared mildly hypointense to gray matter on T1-weighted images, slightly hyperintense to gray matter on T2-weighted images, and faintly enhanced after intravenous contrast agent administration. These findings appeared similar to those described for medulloblastoma in humans and animals (3-5, 10, 11) Cerebellar medulloblastoma was predominately isointense to gray matter on T1-weighted images and mildly hyperintense to gray matter on T2-weighted images in one dog (4). Hypointense on T1-weighted

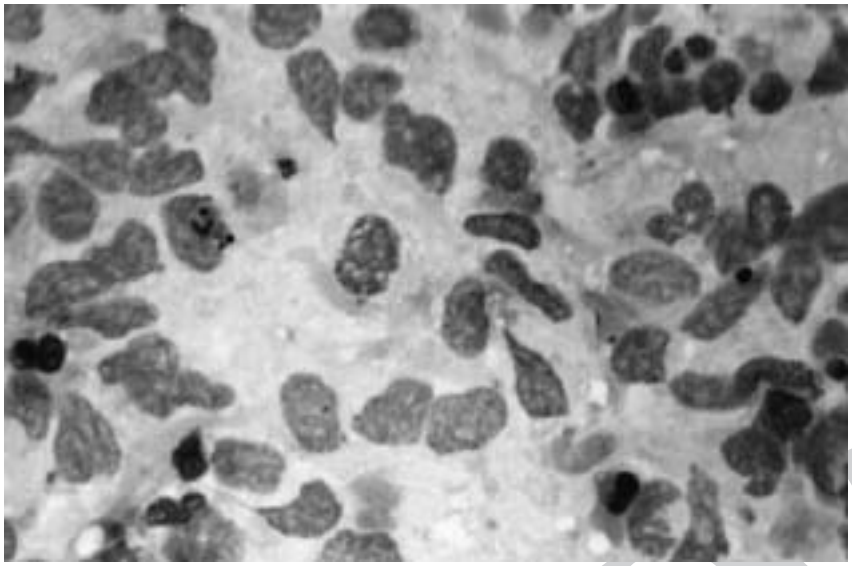

Fig. 4. *Imprint cytology of biopsy tissue, showing clusters of neoplastic cells, some in a pseudo-rossete arrangement (left bottom) and few cells displaying nuclear molding. (Diff-quick staining, magnification x1000)*

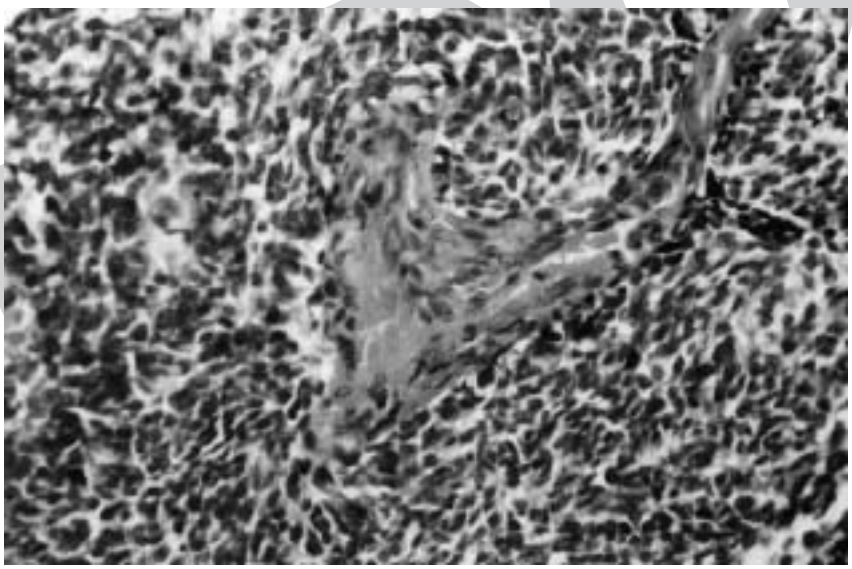

Fig. 5. *Histopathology of the tumor, showing highly cellular sheets of neoplastic cells in a delicated stroma. (Hematoxylin and eosin stain, magnification x400)*

images and iso- and hyperintense on T2-weighted images was reported a cerebellar medulloblastoma in a cat (5). In both adults and children, cerebellar medulloblastomas are most commonly hypo- or isointense to gray matter on T1-weighted images and hyperintense to gray matter or with mixed signal on T2-weighted images (1). They also appear hyperintense on fluid-attenuation inversion recovery sequences (FLAIR) and show a marked signal intensity on diffusion-weighted images (DWI), reflecting the dense nature of the tumor which restricts extracellular diffusion of water protons, and the high nuclear-to-cytoplasmic ratio of these neoplastic cell which limits intracellular motion (11). FLAIR and DWI image sequences were not available in our study.

Small foci with intensity similar to that of CSF on T2-weighted images observed in this case may correspond to small intratumoral necrotic foci seen on histopathological examination. Hyperintense foci responsible for signal heterogeneity on T2-weighted images were also reported in cerebellar meduloblastomas in humans and dogs and may correspond to cysts, necrosis, clump-like calcification and hemorrhage (1, 4, 10). However, this finding is not specific for medulloblastomas, since hyperintense foci can be seen in other types of tumors (12).

In the case presented in this report, post-contrast MRI showed a homogeneous, faint contrast enhancement of the mass; as a result, the tumor became isointense to gray matter, poorly marginated and therefore not clearly evident. To the authors consideration this is a unique finding. This type of enhancement is probably due to not well formed vascular net in the periphery of the mass as this was indicated by histopathologic examination. The effect of time delay between contrast agent administration and imaging, and the effect that manual administration of the agent might have on the degree and pattern of tumor enhancement are not known. In other canine cerebellar medulloblastomas, disseminated patches of mild enhancement in one dog and faint enhancement of the entire mass in another dog were reported (3, 4). Enhancement of cerebellar medulloblastoma was reported in the post contrast images in a cat (5). In humans, post-contrast MRI images of the cerebellar medulloblastoma usually show intermediate to strong enhancement, although mild or intermediate degrees of enhancement have been reported (1, 10).

In our case, MRI revealed a mass in the cerebellar vermis. The differential diagnosis of a cerebellar mass includes neoplasia, cerebrovascular infarct, focal granulomatous meningoencephalitis, and rarely epidermoid cyst or teratomas (13). Cystic lesions appear as thin-walled fluid-filled structures, hyperintense on T2-weighted images with similar or higher intensity to that of CSF, usually with a thin peripheral enhancing rim, unlike the more solid appearance of most medulloblastomas (14, 15). Cerebrovascular infarctions are significantly smaller than tumors, and may have a wedge shape lesion usually within the region supplied by the rostral cerebellar artery or one of its main branches (16-18). However, an overlap in MRI findings of tumors and infarctions can occur and a misdiagnosis of cerebrovascular infarction as tumor is not rare (19). Cerebellar focal granulomatous meningoencephalitis (GME) may show isointensity on T1- and T2-weighted images and severe edema formation that may extend to the opposite side, signs useful for their differentiation from brain tumors (20). However, in most cases the MRI findings of focal GME could not be considered disease specific and both GME and tumors carry a variety of different potential findings, making the differentiation difficult (12).

The differential diagnosis of caudal fossa tumors in dogs includes meningioma, glioma, medulloblastoma, choroid plexus tumor, hemangiosarcoma and metastatic lesions (21). Metastatic neoplasia, the most common posterior fossa tumor in adult humans, is uncommon in dogs (22, 23). Meningiomas show iso- or hypointensity on T1-weighted images and iso- or hyperintensity on the T2-weighted images and are enhanced homogeneously by contrast medium (5, 14, 24, 25). Choroid plexus tumors usually show hypo- or isointensity on T1-weighted images and hyperintensity on the T2-weighted images and are also enhanced homogeneously by contrast medium (5, 26). Gliomas show hypo- or mixed-intensity on T1-weighted images, hyper- or mixed-intensity on T2-weighted images and enhance variously after contrast medium administration. Glioma is usually a differential diagnosis for medulloblastoma (27, 28). MRI findings of cerebellar hemangiosarcoma are not reported in dogs; however, in humans cerebellar hemangiosarcoma shows hypointensity on T1-weighted images and hyperintensity on T2-weighted images (10). As in the case presented in this report, medulloblastomas in dogs appeared usually hypointense to gray matter on T1-weighted images, mildly hyperintense to gray matter on T2-weighted images, and faintly or mildly enhanced after intravenous contrast agent administration (3, 4). There is an overlap between imaging findings of different neoplasms, with most neoplasia being T1-hypointense and T2-hyperintense with varying degrees of contrast enhancement. In certain cases FLAIR and DWI sequences may provide useful data and help in the process of tumor characterization, however, histopathologic examination is considered necessary in tumor differentiation.

Medulloblastoma in adult humans most commonly involve the cerebellar hemispheres (23, 29). The tumors commonly extend to the surface of the brain and may be contiguous with the brain surface adjacent to the tentorium or cerebellopontine angle, giving the appearance of an extra-axial tumor, with meningioma considered as a differential diagnosis (23). In children, classic cerebellar medulloblastomas have a midline location, as in the adult dog of this report, and arise from the anterior portion of the vermis in the mid-and inferior zones (1, 29). In dogs, however, there are not enough reports to establish the effect of age on the distribution of cerebellar medulloblastomas.

The MRI appearance of cerebellar medulloblastoma in the dog of this report is similar to that described for cerebellar medulloblastoma in dogs and humans. An intra-axial cerebellar mass, heterogeneous hyperintense on T2-weighted images, hypointense relative to grey matter on T1-weighted images, with homogeneous faint, wispy contrast enhancement should raise the index of suspicion for vermis medulloblastoma.

ACKNOWLEDGEMENTS

The authors would like to thank the students Georgia M. Ilia and Tatiana M. Ilia for assistance with handling this case.

REFERENCES

1. Meyers SP, Kemp SS, Tarr RW. MR imaging features of medulloblastomas. AJR Am J Roentgenol 1992; 158:859-65.
2. Steinberg H, Galbraith EJ. Cerebellar medulloblastoma with multiple differentiation in a dog. Vet Pathol 1998; 35:543-46.
3. MacKillop E, Thrall DE, Ranck RS, Linder KE, Munana KR. Imaging diagnosis-synchronous primary brain tumors in a dog. Vet Radiol Ultrasound 2007; 48(6):550-53.
4. McConnell JF, Platt S, Smith KC. Magnetic resonance imaging findings of an intracranial medulloblastoma in a polish lowland sheepdog. Vet Radiol Ultrasound 2004; 45(1):17-22.
5. Kitagawa M, Koie H, Kanayama K, Sakai T. Medulloblastoma in a cat: Clinical and MRI findings. J Small Anim Pract 2003; 44:139-42.
6. Oakley RA, Patterson JS. Tumors of the central and peripheral nervous system. In Textbook of Small Animal Surgery. D. Slatter, ed. 3rd ed. Saunders, Philadelphia, 2003; 2405-25.
7. Talarico LR, Dewey CW. Intracranial neoplasia. In Veterinary Surgery Small Animal. K.M. Tobias, S.A. Johnston, eds. Elsevier Saunders, St Louis, 2012; 511-16.
8. Bouffet E, Doz F, Demaille MC, et al. Improving survival in recurrent medulloblastoma: Earlier detection, better treatment or still an impasse? Br J Cancer 1998; 77:1321-26.
9. Drevelegas A. Imaging modalities in brain tumor. In Imaging of brain tumors with histological correlations A. Drevelegas, ed. Springer, Berlin, 2002; 11-25.
10. Drevelegas A. Embryonal tumors. In Imaging of brain tumors with histological correlations A. Drevelegas, ed. Springer, Berlin, 2002; 147-54.
11. Kotsenas AL, Roth TC, Mannes WK, Faeber EN. Abnormal diffusion-weighted MRI in medulloblastoma: does it reflect small cell histology. Pediatr Radiol 1999; 29:524-26.
12. Bentley RT, Ober CP, Anderson KL, et al. Canine intracranial gliomas: relationship between magnetic resonance imaging criteria and tumor type and grade. Vet J 2013; 198:463-71.
13. Summers BA, Cummings JF, de Lahunta A. Tumors of the central nervous system. In Veterinary neuropathology B.A. Summers J.F. Cummings, A. de Lahunta eds. Mosby, St. Louis, 1995;3 79-80.
14. De Decker S, Davies E, Benigni L, Wilson H, Pelligand L, Rayner EL, Shihab N, Volk HA. Surgical treatment of an intracranial epidermoid cyst in a dog. Vet Surg 2012; 41:766-71.
15. Bagley RS, Silver GM, Gavin PR. Cerebellar cystic meningioma in a dog. J Am Anim Hosp Assoc 2000; 36:413-15.
16. McConnell JF, Garosi L, Platt SR. Magnetic resonance imaging findings of presumed cerebellar cerebrovascular accident in twelve dogs. Vet Radiol Ultrasound 2005; 46(1):1-10.
17. Irwin JC, Dewey CW, Stefanacci JD. Suspected cerebellar infarcts in 4 dogs. J Vet Emerg Critical Care 2007; 17(3):268-74.

18. Garosi LS, McConnell JF, Platt SR, Barone G, Baron JC, De Lahunta AM, Schatzberg SJ. Clinical and topographic magnetic resonance characteristics of suspected brain infarction in 40 dogs. J Vet Intern Med 2006; 20(2):311-21.
19. Cervera V, May W, Vite CH, Johnson V, Dayrell-Hart B. Comparative magnetic resonance imaging findings between gliomas and presumed cerebrovascular accidents in dogs. Vet Radiol Ultrasound 2011, 52(1): 33-40.
20. Kitagawa M, Kanayama K, Satoh T, Sakai T. Cerebellar focal granulomatous meningoencephalitis in a dog: Clinical findings and MR imaging. J Vet Med A Physiol Pathol Clin Med 2004; 51:277-79.
21. Kraft SL, Gavin PR, De Haan C, Michael M, Wendling LR, Leathers CW. Retrospective review of 50 canine intracranial tumors evaluated by magnetic resonance imaging. J Vet Intern Med 1997; 4:218-25.
22. Braund KC. Neoplasia of the nervous system. Comp Cont Educ Pract Vet 1984; 6:717-22.
23. Koci TM, Chiang F, Mehringer CM, Yuh WT, Mayr NA, Itabashi H, Pribram HF. Adult cerebellar medulloblastoma: imaging features with emphasis on MR findings. Am J Neuroradiol 1993; 14:929-39.
24. Gearhart MA, DeLahunta A, Summers BA. Cerebellar mass in a dog due to granulomatous meningoencephalitis. J Am Anim Hosp Assoc 1986; 22:683-86.
25. Ryan K, Marks SI, Kerwin SC. Granulomatous meningoencephalitis in dogs. Comp Cont Educ Pract Vet 2001; 23:644-51.
26. Pastorello A, Constantino CF, Archer J. Choroid plexus carcinoma cells in the cerebrospinal fluid of a Staffordshire Bull Terrier. Vet Clin Pathol 2010; 39(4):505-10.
27. Young BD, Levine JM, Porter BF, et al. Magnetic resonance imaging features of intracranial astrocytomas and oligodendrogliomas in dogs. Vet Radiol Ultrasound 2011; 52(2):132-41.
28. Fukuoka H, Sasaki J, Kamishina H, et al. Gliomatosis cerebelli in a Saint Bernard Dog. J Comp Path 2012; 147:37-41.
29. Barr JD, McNamara KP, Barr MS. Neuroradiology case of the day. Am J Radiol 1994; 162:1476-77.

LETTER TO THE EDITOR

CARDIAC MYXOMA ORIGINATING FROM AREAS OF VENTRICULAR AKINESIA

D. DE VITI[1], A. STRAGAPEDE[1], G. RICCIONI[2], V. BUCCIARELLI[3], T. BUCCIARELLI[4] and C.D. MEMMOLA[1]

[1]Cardiology Unit, Casa di Cura Santa Maria, Bari, Italy; [2]Cardiology Unit, San Camillo del Lellis Hospital, Manfredonia, Foggia, Italy; [3]Department of Neuroscience and Imaging, [4]Department of Clinical and Experimental Sciences, University of Chieti, Italy

Received June 10, 2013 – Accepted April 1, 2014

We present a case of large pedunculated myxoma (61×39 mm) in the left ventricular cavity with anterior-septal and anterior free wall akinesia. Angiographic study showed normal coronary arteries, but the clinical signs strongly suggested a previous myocardial infarction. We can not exclude the possibility that the ventricular akinesia results from embolization of tumor fragments. For a time, cardiac myxomas were believed to arise from mural thrombi. In this case the presence of blood stasis or low-velocity blood flow related to wall motion abnormalities may have played a role in improving tumor growth.

A 51-year-old man with a history of diabetes mellitus and cigarette smoking presented with clinical signs of acute heart failure. The electrocardiogram showed a QS complex in V1-V3. Transthoracic echocardiography revealed a large pedunculated mass (61×39 mm in diameter) with an irregular surface in the left ventricular (LV) cavity. A global LV systolic dysfunction with apical, anterior septal and anterior free wall akinesis was found. Angiographic study showed normal coronary arteries.

The tumor was removed surgically with good result. Histologic examination demonstrated a myxoma with a maximal diameter of 6 cm (Figs. 1 and 2). In order to exclude the possibility of myocardial infiltration (a few variations in disease process of ventricular myxoma have been previously reported), and differentiate the cause of the wall motion abnormality, a gadolinium-enhanced cardiovascular magnetic resonance was performed one month after surgical resection (Fig. 3).

The presence of significant risk factors for CAD, Q waves on the ECG and the pattern of subendocardial enhancement strongly suggested the presence of prior infarction (1). The occurrence of coronary recanalization or embolization from minimally stenotic plaque is well documented; we can not exclude the possibility that the ventricular akinesia resulted from

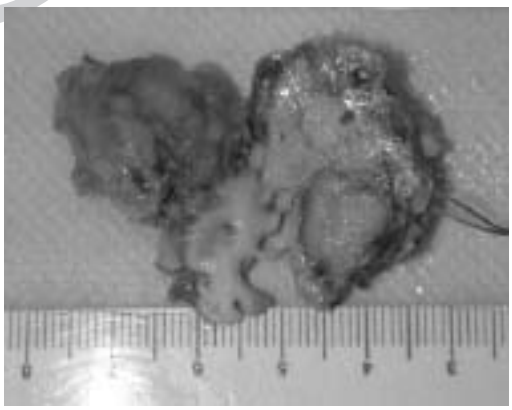

Fig.1. *Photograph of the cut surface of the pedunculated resected myxoma.*

Key words: cardiac myxoma, wall akinesia, mural thrombi

Mailing address: Daniele De Viti, MD
Cardiology Unit,
Casa di Cura Santa Maria,
Via de Ferraris 65,
70124 Bari, Italy
Tel: +39 3284043309, +39 0805040111
e-mail: danieledeviti@tiscali.it

0393-974X (2014)

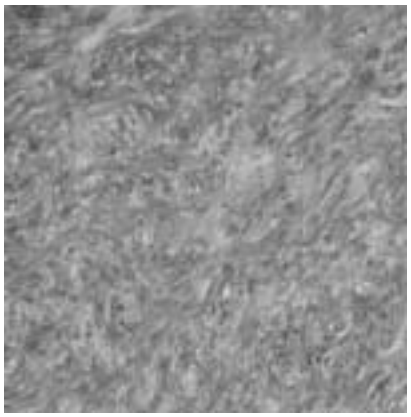

Fig. 2. *Microscopic features of myxoma (hematoxylin-eosin stain) demonstrates heterogeneous lesion with nests of myxoma cells and myxoid matrix. Unusual histologic features of cardiomyocytes around the pedicle were also found.*

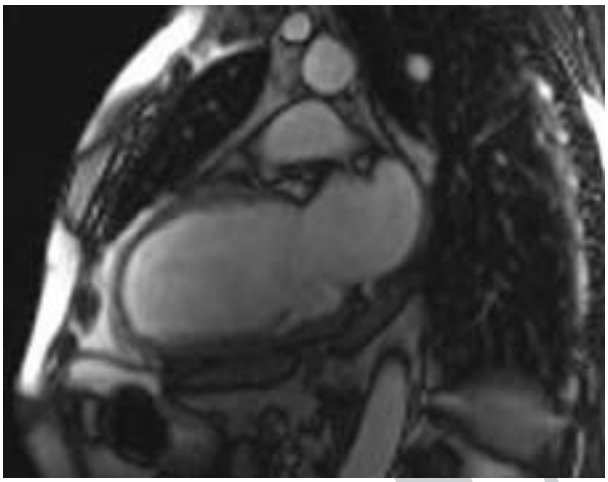

Fig. 3. *Cardiovascular magnetic resonance imaging one month after surgical resection shows the extensive LV involvement with dilation and systolic dysfunction; thinning is clearly seen, especially in the anterior wall.*

embolization of tumor fragments. For a time, cardiac myxomas were believed to arise from mural thrombi. Although the once-held theory that myxoma is a form of organizing thrombus has largely been discarded, in this peculiar case the presence of blood stasis or low-velocity blood flow related to wall motion abnormalities may have played a role in improving tumor growth (2). Nevertheless, we can not exclude the development of the mass in a normal ventricular wall kinesis resulted in wall motion abnormalities promoting blood stasis and a rapid tumor growth.

REFERENCES

1. Mc Crohon JA, Moon JCC, Prasad SK, et al. Differentiation of heart failure related to dilated cardiomyopathy and coronary artery disease using gadolinium-enhanced cardiovascular magnetic resonance. Circulation 2003;108:54.
2. Salyer WR, Salyer DC. Myxoma-like features of organizing thrombi in arteries and veins. Arch Pathol 1975; 99(6):307-11.

LETTER TO THE EDITOR

ATRIAL NATRIURETIC PEPTIDE AND VASOPRESSIN-PRESENCE IN THE CILIARY BODY OF EYE IN THE PIG (*SUS DOMESTICUS*)

B. VALENTINO, A. VALENTINO, L. LIPARI, A. LIPARI and E. FARINA

Department of Experimental Medicine and Clinical Neuroscience (BioNec), University of Palermo, Italy

Received January 31, 2014 – Accepted April 23, 2014

The aqueous humor is produced in the ciliary body, therefore in this study we investigated the Atrial natriuretic peptide (ANP) and vasopressin (VP)-presence in the ciliary body of the pig eye since these peptide are involved in the homeostasis of body fluids. The results show ANP-presence in the epithelial cells and in the endothelial cells of the blood vessels and VP-presence in the epithelial cells, in the endothelium of canal of Schelmm and in the muscle cells of the blood vessels. These peptides might regulate the synthesis and the composition of the aqueous humor and regulate the hydrodynamic flow and haemodynamic flow of the blood.

The eye synthesizes the aqueous humor by the epithelial cells of the ciliary body. The aqueous humor, likely all body fluids, is under the homeostatic control of several hormones. In physiological conditions the blood pressure and the aqueous humor pressure should allow the water-transport from the blood vessels to the posterior chamber of the eye. The intercellular junctions of the non-pigmented epithelium constitute a blood/water barrier which would cause a swelling inside the same epithelium, if the activity of the Na/K pump does not permit the water–transport from the blood vessels to the posterior chamber and, in consequence, inhibiting the epithelial swelling.

It is clear that the homeostasis of the body fluids is insured not only by the NA/K pumps, but also by the action of the hormone vasopressin (VP) and atrial natriuretic peptide (ANP).

Some studies on the eye of different species were carried out to investigate the presence of ANP and VP, which could be involved in the regulation of the electrolyte concentration in the aqueous humor.

In the rat eye, Palm and coll. (1) found that intravenous VP-infusion decreases the intraocular pressure; Gondim and coll. (2) found that intravenous VP-injection causes the reduction of intraocular pressure and pupil size by the stimulation of V(1)-receptors. By contrast, the VP-intracerebroventricular injection elevates the intraocular pressure and does not change the pupil size.

Recent studies on rabbits confirmed that the exogenous VP reduces both the intraocular pressure and orbital venous pressure significantly and that VP is a powerful vasoconstrictor in the choroidal vascular bed (3).

The VP-presence, by immunohistochemistry, was found in the rat retina almost exclusively in the ganglion cell layer (4). Recent studies on rat retina show AVP and V1a-V1b receptors in the ganglion cell layer and in the inner nuclear layer. These results suggest that the retina has an intrinsic AVP-synthesizing and -receiving mechanism that can

Key words: ANP, ciliary body, pig eye

Mailing address: Dr Elvira Farina,
Dipartimento di Medicina Sperimentale
e Scienze Neurologiche (BioNec),
Via del Vespro 129,
90127 Palermo, Italy
Tel.: +39 091 6553585
e-mail: farina.elviravitt@tiscali.it

0393-974X (2014)

operate in a paracrine way through receptors (5). Furthermore, the VP-presence, was found in rat eye in the anterior uvea and retina (6).

In rat eye, ANP was detected by immunohistochemistry in the anterior uvea and retina. The uveal ANP-content was greater than the retina and also more abundant than VP and angiotensin (6). In the human retina, the presence of NPs was revealed by immunohistochemistry in the neural retina, retinal pigment epithelium and within the astrocytes and in their processes enveloping vessels. ANP-binding sites were found in the corneal endothelial cells reversibly bound 125I-ANP with high affinity. Moderate densities of [125I]ANF-binding sites are found in the rat and guinea pig eye (7).

In literature few studies concern ANP-mRNA in the eye. In rat and rabbit (8) the ANP-mRNA was observed in the retina, choroid and ciliary processes. A differential distribution of ANP, BNP and CNP mRNAs was observed in ocular tissues, suggesting that at least part of the natriuretic peptide immunoreactivity detected in the eye arises from the local synthesis of the peptide.

Furthermore, the literature data point out that ANP, BNP and CNP and their receptor transcripts are expressed and are functional in human lens epithelial cells (9). ANP/BNP/CNP were also expressed in the rat neural retina (10), and a strong immunoreactivity has been seen in the outer and inner plexiform layers and on numerous neurons in the inner nuclear layer, while only BNP/CNP immunoreactivity has been seen in some ganglion cells. ANP is expressed also in the rat retinal amacrine cells (11), and in the rat retinal Müller cells (10).

In consideration of the important activity of peptides, VP and ANP, on the regulation of humor aqueous and in consideration that few studies are reported in the literature on the synthesis of VP and ANP in the ciliary body, this immunohistochemical study investigated the presence of both peptides in the ciliary body of the pig eye.

MATERIALS AND METHODS

The eyes of ten pigs, *Sus domesticus*, were removed immediately after sacrifice; the anterior segment of each eye was fixed in Bouin's fluid, dehydrated in graded alcohols and embedded in paraffin. Sections, 7-µm thick, were cut with Leica microtome RM2145, dried overnight at 37°C and then stored at room temperature until use. All samples were obtained with the consent of the local Ethics Committee**.**

Immunohistochemistry

The slides were dewaxed in xylene, rehydrated and transferred into distilled water for 5 min. Immunostaining was performed using the DakoCytomation EnVision + System-HRP (AEC) kit from Dako (Dako, Glostrup, Denmark), sections were covered with Peroxidase block reagent and incubated for 5 min at room temperature. The samples were rinsed once in PBS buffer pH 7.2. The sections were covered with or without rabbit anti-ANP polyclonal antibody (Chemicon, Temecula, CA, USA) and incubated at 4°C overnight. The antibody was diluted in a 0.1% BSA solution at the dilution of 1:800. Samples were rinsed twice in PBS pH 7.2 and then incubated with Peroxidase Labelled Polymer reagent for 30 min. Samples were rinsed twice in PBS pH 7.2, and then incubated with Substrate-Chromogen reagent and immediately observed under a light microscope; the reaction continued until staining appeared (2–10 min). Reaction was stopped by rinsing the slides in distilled water. Negative control sample was treated in the same way, however, without the use of primary antibody. Slides were coverslipped using Dako Cytomation Faramount Aqueous Mounting Medium from Dako (Dako, Glostrup, Denmark). The specimens were observed under a Leica DM1000 light microscope.

RESULTS

The ciliary body (Fig. 1a) extends from the base of the iris to the ora serrata where it is continuous with the choroid. In section the ciliary body is roughly triangular in shape and is composed of a vascular stroma, smooth muscle and covering epithelium, it has anatomically recognizable regions: pars plica and pars plana. The pars plica contains the ciliary processes which are ridges or folds each with a core of stroma and blood vessels and covered by two layers of columnar epithelium: an outer pigmented layer and an inner non-pigmented layer. The inner layer is in contact with the aqueous humor.

The ANP-immunostained sections show that the epithelial columnar cells of the pars plica are ANP-immunopositive and also the pars plana presents ANP-immunopositive cells. The epithelial cells show intense immunopositivity overall in their apical area (Fig. 1b). The endothelial cells of the blood vessels are ANP- immunopositive. (Fig. 1c).

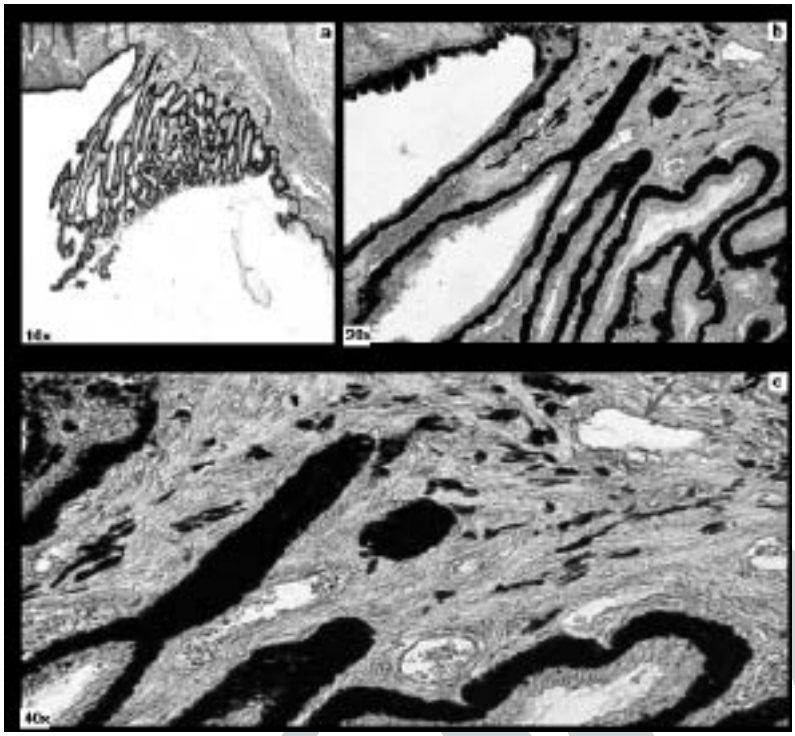

Fig. 1. ***a****) Pig ciliary body. Panoramic view. 10x.* ***b****) ANP-immunopositive epithelial cells. 20x.* ***c****) ANP-immunopositive endothelial cells of canal of Schlemm 40x.*

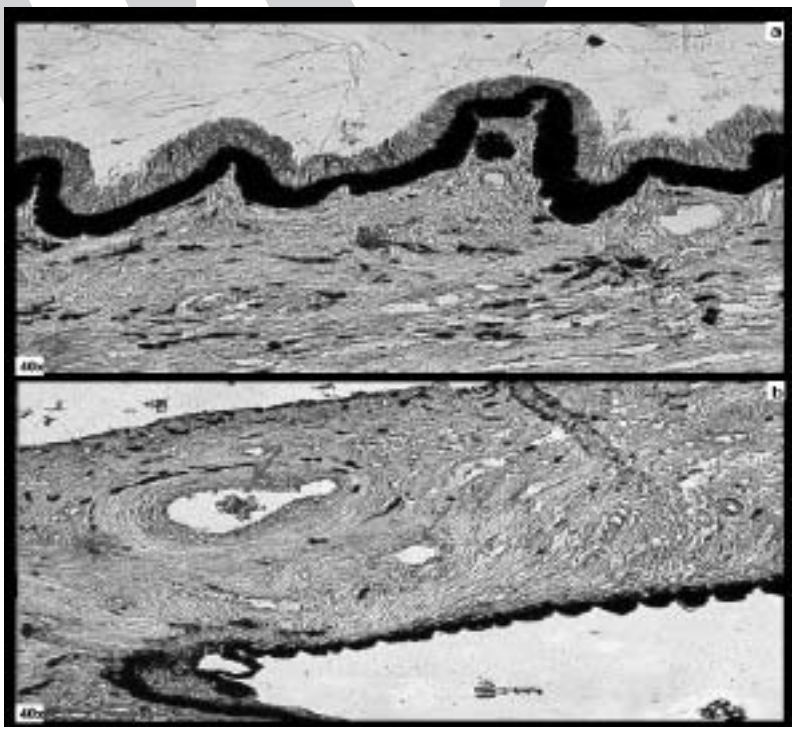

Fig. 2. ***a****) VP-immunopositive epithelial cells. 40x.* ***b****) VP-immunopositive endothelial cells of the aqueous canal (thin arrow). VP-immunopositive endothelial and muscular cells of blood vessel (thick arrow) 40x.*

The VP-immunostained sections show that the epithelium of inner layer of the ciliary body presents nuclei located in different levels and show an intense VP-immunopositivity in the cytoplasm overall in the apical area of the cells. VP-immunopositivity is located also in the pars plana of the ciliary body (Fig. 2a). The endothelium of canal Schlemm and the muscle cells of the wall of the blood vessels show VP-immunopositivity (Fig. 2b). Controls result ANP/VP- immunonegative.

DISCUSSION

The composition of all body fluids is under the control of different hormones such as VP, VIP, ANP, oxytocin NPs, etc.

VP, a nonapeptide, synthesized in the hypothalamic nuclei, plays the peripheral effects in the vasoconstriction and in the renal tubule. ANP is a biologically active peptide mainly synthesized and excreted by the cardiomyocytes, but ANP is not only a cardiac hormone - it plays an important role on the functions of the different organs such as brain (12-14), kidney (15), turbinate (16, 17), lung (18), pleura (19) and pancreas (20, 21), as well as salivary glands (22). ANP plays an important role, likely VP, on the regulation and electrolyte homeostasis of body fluids, also in stress as physical exercise (23, 24).

The aqueous humor synthesized by epithelial cells of the ciliary body, circulates from the posterior chamber through the pupil foramen into the anterior chamber, then filters through a trabecular meshwork lined by endothelium, running around the circumference of the root of the iris, enters the canal of Schlemm which ends in the venous vessels. The synthesis of the aqueous humor, responsible for the intraocular pressure, is regulated constantly by hormone vasopressin, ANP, alarin (25) etc. acting on the ciliary body and blood flow.

In literature are reported the effects which exogenous VP and ANP determine on the intraocular pressure of aqueous humor. Our study on the pig eye investigates the presence of these hormones in the epithelium and blood vessels of the ciliary body in synergy with the hormones, and the Na/K pumps act on the solvated Na+/K+ ions and induce the transport of water through the blood/ciliary water. The immunohistochemical results show that VP is detected in the epithelial cells, in endothelial and muscle cells of blood vessels and in the endothelium of the Schlemm canal, indicating a local VP-synthesis. Furthermore, VP-presence in these sites (epithelial cells, endothelial cells of vessels and of the Schelmm canal indicates its involvement in production and composition of the aqueous humor; while the VP-presence in the muscle cells of the blood vessels indicates its involvement in blood flow regulation. We retain that VP, in agreement with data reported relating to the blood vessels in the different organs, is a factor regulating the haemodynamic flow by a paracrine mechanism.

The immunohistocheminal results for ANP show that in the pig eye ANP is detected in the epithelial cells of the ciliary body and in the endothelial cells. In the epithelial cells ANP is involved in the secretion of aqueous humor by paracrine mechanism, likely VP, and in the endothelial cells, regulates the blood flow in the ciliary body.

In conclusion, we show that the VP and ANP are synthesized in the pig eye as in rodent and human eye (26, 27) and their presence in the ciliary body is involved in the synthesis and the composition of the aqueous humor and on the regulation of the hydrodynamic and haemodynamic flow of the aqueous humor and of the blood.

REFERENCES

1. Palm DE, Shue SG, Keil LC, Balaban CD, Severs WB. Effects of angiotensin, vasopressin and atrial natriuretic peptide on intraocular pressure in anesthetized rats. Neuropeptides 1995; 29:193-203.
2. Gondim EL, Liu JH, Costa VP, Weinreb RN. Exogenous vasopressin influences intraocular pressure via the V(1) receptors. Curr Eye Res 2001; 22:295-303.
3. Bogner B, Tockner B, Runge C, et al. The effect of vasopressin on choroidal blood flow, intraocular pressure, and orbital venous pressure in rabbits. Invest Ophthalmol Vis Sci 2011; 52:7134-40.
4. Djeridane Y. Immunohistochemical evidence for the presence of vasopressin in the rat harderian gland, retina and lacrimal gland. Exp Eye Res 1994; 59:117-20.
5. Moritoh S, Sato K, Okada Y, Koizumi A. Endogenous arginine vasopressin-positive retinal cells in arginine

vasopressin-eGFP transgenic rats identified by immunohistochemistry and reverse transcriptase-polymerase chain reaction. Mol Vis 2011; 17:3254-61.
6. Palm DE, Keil LC, Severs WB. Angiotensin, vasopressin, and atrial natriuretic peptide in the rat eye. Proc Soc Exp Biol Med 1994; 206(4):392-5.
7. Quirion R, Dalpé M, De Lean A, Gutkowska J, Cantin M, Genest J. Atrial natriuretic factor (ANF) binding sites in brain and related structures. Peptides 1984; 5:1167-72.
8. Fernandez-Durango R, Nunez DJ, Brown MJ. Messenger RNAs encoding the natriuretic peptides and their receptors are expressed in the eye. Exp Eye Res 1995; 61:723-9.
9. Cammarata PR, Braun B, Dimitrijevich SD, Pack J. Characterization and functional expression of the natriuretic peptide system in human lens epithelial cells. Mol Vis 2010; 16:630-8.
10. Cao LH, Yu YC, Zhao JW, Yang XL. Expression of natriuretic peptides in rat Müller cells. Neurosci Lett 2004; 365:176-9.
11. Jin Y, Zhong YM, Yang XL. Natriuretic peptides are localized to rat retinal amacrine cells. Neurosci Lett 2007; 421:106-9.
12. Kawata M, NakaoK, Morii N, et al. Atrial natriuretic polypeptide: topographical distribution in the rat brain by radioimmunoassay and immunohistochemistry. Neuroscience 1985; 16:521-46.
13. Farina Lipari E, Lipari D, Dieli F, Valentino B. The ANP secretion during the development of rat hypothalamic supraoptic nucleus. Eur J Histochem 2005; 49:379-84.
14. Farina Lipari E, Lipari A, Dieli F, Valentino B. ANP presence in the hypothalamic suprachiasmatic nucleus of developing rat. It J Anat Embryol 2007; 112:19-25.
15. McKenzie JC, Scott J, Inagami T. Imunohistochemical localization of atrial natriuretic factor in the kidney, adrenal medulla, pituitary and atrium of rat. J Histochem Cytochem 1991; 33:928-32.
16. Valentino B, Lipari D, Restivo F, Speciale R, Gallina S, Farina Lipari E. Localization of the atrial natriuretic factor in the human inferior turbinates. An immunohistochemical study. Acta Otorhinolaryngol Ital 2003; 3:94-97.
17. Incandela S, Incandela C, Farina EV, Lipari L. Atrial natriuretic peptide (ANP)-presence in human inferior turbinate after treatment botulinum toxin type A treatment. Res J Biol Sci 2012; 7:238-39.
18. Valentino B, Lipari D, Dieli F, Leone A, Farina E. Distribution of atrial natriuretic Factor (ANF) in respiratory tract and lung showed by immunohistochemical and PCR methods. Dent Med Probl 2003; 40:17-22.
19. Farina E, Lipari D, Leone A, Dieli F, Valentino B. Localization of atrial natriuretic factor (ANF) in the normal parietal pleura in rabbit. Immunohistochemical studies and PCR analysis. Dent Med Probl 2004; 41:209-212.
20. Chabot JG, Morel G, Kopelman H, Belles-isles M, Heisler S. Atrial natriuretic factor and exocrine pancreas autoradiographic localization of binding sites and ultrastructural evidence for internalization of endogenous ANF. Pancreas 1987; 2:404-13.
21. Valentino B, Lipari D, Peri G, Lipari L, Valentino A, Farina E. ANP and insulin presence in human foetal pancreas. It J Anat Embryol 2009; 114(1):21-26.
22. Lipari L, Farina E, Buscemi M, Gerbino A. Atrial natriuretic peptide presence in parotid gland of human fetus at 13th week of development and in adult man. Folia Histochem Cytobiol 2013; 51:55-58.
23. Farina Lipari E, Lipari D, Valentino B. Modifications of atrial natriuretic peptide and vasopressin peptides in the rat hypothalamic supraoptic nucleus during resistance training. Ital J Anat Embryol 2010; 15:211-7.
24. Farina E, Cappello F, Lipari L, De Felice V, Valentino A, Valentino B. Modifications of oxytocin, atrial natriuretic peptide and vasopressin peptides in rat hypothalamic paraventricular nucleus during resistance training. Anat Histol Embryol 2013; doi: 10.1111/ahe.12051. [Epub ahead of print]
25. Schrödl F, Trost A, Strohmaier C, et al. Distribution of the regulatory peptide alarin in the eye of various species. Exp Eye Res 2013; 106:74-81.
26. Palm DE, Keil LC, Sassani JW, Severs WB. Immunoreactive atrial natriuretic peptide in the retina of rats and rabbits. Brain Res 1989; 504:142-4.
27. Ortego J, Coca-Prados M. Functional expression of components of the natriuretic peptide system in human ocular non pigmented ciliary epithelial cells. Biochem Biophys Res Comm 1999; 258:2.